ANALYSING THE PHYSICAL AND MECHANICAL CHARACTERISTICS OF SOFT CLAY REINFORCED WITH POLYPROPYLENE COLUMNS

MD. IKRAMUL HOQUE

DOCTOR OF PHILOSOPHY

UNIVERSITI MALAYSIA PAHANG
AL-SULTAN ABDULLAH

UNIVERSITI MALAYSIA PAHANG AL-SULTAN ABDULLAH

DECLARATION OF THESIS AND COPYRIGHT

Author's Full Name	:	MD. IKRAMUL HOQUE
Date of Birth	:	25/08/1980
Title	:	ANALYSING THE PHYSICAL AND MECHANICAL CHARACTERISTICS OF SOFT CLAY REINFORCED WITH POLYPROPYLENE COLUMNS
Academic Session	:	SEMESTER II 2023/2024

I declare that this thesis is classified as:

☐	CONFIDENTIAL	(Contains confidential information under the Official Secret Act 1997)*
☐	RESTRICTED	(Contains restricted information as specified by the organization where research was done)*
☒	OPEN ACCESS	I agree that my thesis to be published as online open access (Full Text)

I acknowledge that Universiti Malaysia Pahang Al-Sultan Abdullah reserves the following rights:

1. The Thesis is the Property of Universiti Malaysia Pahang Al-Sultan Abdullah
2. The Library of Universiti Malaysia Pahang Al-Sultan Abdullah has the right to make copies of the thesis for the purpose of research only.
3. The Library has the right to make copies of the thesis for academic exchange.

Certified by:

(Student's Signature)

____
Passport Number
Date: 04 July 2024

(Supervisor's Signature)

ASSOC. PROF. TS. DR. MUZAMIR HASAN
____
Name of Supervisor
Date: 04 July 2024

NOTE : * If the thesis is CONFIDENTIAL or RESTRICTED, please attach a thesis declaration letter.

اونيۏرسيتي مليسيا ڤهڠ السلطان عبدالله
UNIVERSITI MALAYSIA PAHANG
AL-SULTAN ABDULLAH

SUPERVISOR'S DECLARATION

I hereby declare that I have checked this thesis and in my opinion, this thesis is adequate in terms of scope and quality for the award of the degree of Doctor of Philosophy in Civil Engineering.

(Supervisor's Signature)

Full Name : ASSOC. PROF. TS. DR. MUZAMIR HASAN

Position : ASSOCIATE PROFESSOR

Date : 04 JULY 2024

اونيۏرسيتي مليسيا ڤهڠ السلطان عبدالله
UNIVERSITI MALAYSIA PAHANG
AL-SULTAN ABDULLAH

STUDENT'S DECLARATION

I hereby declare that the work in this thesis is based on my original work except for quotations and citations which have been duly acknowledged. I also declare that it has not been previously or concurrently submitted for any other degree at Universiti Malaysia Pahang Al-Sultan Abdullah or any other institutions.

MHoque
____
(Student's Signature)

Full Name : MD. IKRAMUL HOQUE

ID Number : PAG20005

Date : 04 JULY 2024

UMPSA
اونيۏرسيتي مليسيا ڤهڠ السلطان عبدالله
UNIVERSITI MALAYSIA PAHANG
AL-SULTAN ABDULLAH

ANALYSING THE PHYSICAL AND MECHANICAL CHARACTERISTICS OF SOFT CLAY REINFORCED WITH POLYPROPYLENE COLUMNS

MD. IKRAMUL HOQUE

Thesis submitted in fulfillment of the requirements
for the award of the degree of
Doctor of Philosophy

Faculty of Civil Engineering Technology

UNIVERSITI MALAYSIA PAHANG AL-SULTAN ABDULLAH

JULY 2024

ACKNOWLEDGEMENTS

I would like to convey my profound gratitude to the divine entity known as Almighty ALLAH SWT for providing me with the necessary resources to navigate this particular endeavour. Additionally, I want to seize this moment to extend my heartfelt appreciation to all individuals who have played a role in the successful completion of this project. I would like to extend my sincere appreciation to my supervisor, Associate Prof. Dr. Muzamir Hasan, for providing direct oversight, consistent advice, and guidance over the course of this research endeavour, particularly throughout the composition of this thesis.

I also extend my gratitude to the technicians at the Geotechnics Laboratory of Universiti Malaysia Pahang, who graciously offered their support and collaborated in the preparation and execution of the laboratory model experiments.

This research and scholarship received financial support from Universiti Malaysia Pahang and the Ministry of Higher Education Malaysia. The aforementioned contributions are duly appreciated. I would like to extend my sincere gratitude and recognition to my parents, brother, and extended family for their unwavering emotional support and affection. I also would like to express my gratitude to my wife, Asma Sultana Keya, and my two boys, Arshan al Quavi and Arham al Afi, for their support, dedication, and perseverance throughout the completion of this work.

ABSTRAK

Kemajuan infrastruktur di tanah lembut agak mencabar kerana tanah ini berkebolehmampatan tinggi, beban kapasiti yang rendah dan ubah bentuk sisi. Teknik-teknik tiang berbutiran kasar mempunyai keupayaan untuk mengurangkan penempatan di tanah yang lemah dan lembut dengan meningkatkan beban kapasiti, dan mempercepatkan penyelesaian tekanan air yang berlebihan. Selain itu, kekuatan ricih tanah lembut boleh ditingkatkan secara ketara melalui penggunaan tiang pengukuhan dengan menghalang ubah bentuk sisi butiran tanah liat. Matlamat utama penyelidikan ini ialah untuk menyiasat kesan tiang polipropilen kepada ciri-ciri peningkatan kekuatan ricih dan kebolehmampatan tanah liat kaolin lembut yang disusun semula. Kualiti kekuatan ditinjau menggunakan analisis dalam beberapa aspek, seperti nisbah penggantian luas, nisbah tinggi penembusan, dan nisbah penggantian isipadu. Pemeriksaan ini merangkumi kedua-dua tiang polipropilen tunggal dan berkelompok. Selain itu, kesan tekanan terkurung pada sifat kebolehmampatan tanah kaolin diperkuat polipropilen dinilai. Salah satu matlamat kajian ini adalah untuk menyediakan carta reka bentuk yang menghubungkan perbandingan penggantian isipadu dan tekanan purata berkesan normal kepada kekuatan ricih (Su) daripada tiang polipropilen diperkuat dengan tanah kaolin dengan menggunakan kerangka mekanik tanah keadaan kritikal. Sampel kaolin diperkuat dinilai menggunakan Ujikaji Kebolehmampatan Terkurung (UCT) dan Ujikaji Tiga Paksi Terkukuh Tak Tersalir (CU). Diameter dan ketinggian tiang polipropilen serta tekanan terkurung yang berkesan, σ_3, adalah antara faktor penyelidikan. Analisis hasil dijalankan dengan menggunakan kriteria kegagalan Mohr-Coulomb dan kriteria keadaan kritikal. Berdasarkan hasil UCT, ia telah diperhatikan bahawa Su secara amnya bertambah baik kerana nisbah penembusan ketinggian meningkat, bagaimanapun, apabila ia mencapai 100% nisbah penembusan ketinggian, ia mula berkurangan. Perbandingan penggantian luas polipropilen juga mempengaruhi peningkatan Su. Kekuatan ricih sampel tanah tidak berubah walaupun nisbah penggantian luas yang tinggi. Oleh kerana lingkaran sampel tanah lebih kecil daripada yang diperlukan, kekuatan ricih tiang perlu ditingkatkan. Perbandingan meningkat kerana kekuatan meningkat dalam tidak adanya tekanan yang mengehadkan. Walau bagaimanapun, penggantian luas yang berlebihan mengurangkan kekuatan ricih sampel yang diperkuat oleh tiang berkelompok kerana lebar sampel tanah yang tersisa menjadi terlalu sempit untuk menyokong tiang. Dengan menggunakan kriteria kegagalan Mohr-Coulomb daripada penemuan ujikaji CU, sudut geseran yang berkesan kekal relatif tetap selepas memasukkan tiang polipropilen. Walau bagaimanapun, ia membawa kepada peningkatan dalam kekuatan ricih tak tersalir dan kejeleketan tanah liat kaolin. Selain itu, ia telah ditunjukkan bahawa penambahan tiang polipropilen meningkatkan penyelesaian tekanan air liang. Menggunakan rangka kerja mekanik tanah keadaan kritikal, analisis ini membolehkan untuk menentukan parameter kritikal yang unik untuk setiap sampel, yang ialah M, Γ, dan λ. Untuk komposit tanah-polipropilen, majoriti nilai M ditemui jatuh antara 1.18 dan 1.30. Jarak ini sama dengan perubahan dalam sudut geseran keadaan kritikal, yang berkisar dari 30° hingga 35°. Akibatnya, komposit tanah-polipropilen boleh diklasifikasikan ke dalam kategori "campuran batu kasar dan pasir dengan tanah berbutiran halus". Secara amnya, boleh disimpulkan bahawa pemasangan tiang polipropilen mempunyai potensi untuk meningkatkan kekuatan ricih dan ciri-ciri kebolehmampatan tanah liat lembut. Oleh itu, carta reka bentuk telah dibangunkan dengan tujuan sebagai alat reka bentuk, secara khusus untuk mengira jumlah yang diperlukan polipropilen yang diperlukan untuk mewujudkan tiang menegak yang selaras dengan kekuatan ricih yang diperlukan oleh tanah liat yang ditingkatkan.

ABSTRACT

The progression of infrastructure on soft soil is quite challenging due to the soils high compressibility, low bearing capacity and lateral deformation. Granular column techniques have the ability to decrease settlement in weak and soft soil by increasing the bearing capacity, and accelerating the dissipation of excessive pore water pressure. Moreover, soft soil's shear strength can be significantly improved through the employment of reinforcing columns by preventing the lateral deformation of the clay particle. . The main objective of this research is to investigate the impact of polypropylene columns on enhancing the shear strength and compressibility characteristics of soft reconstituted kaolin clay. The strength qualities were examined using the analysis of several aspects, such as the area replacement ratio, height penetration ratio, and volume replacement ratio. This examination encompassed both single and grouped polypropylene columns. Furthermore, the impact of confining pressure on the compressibility properties of polypropylene-reinforced kaolin clay was evaluated. One of the goals of this study is to provide a design chart that links the volume replacement ratio and mean normal effective stress to the undrained shear strength (S_u) of polypropylene columns reinforced with kaolin clay by utilizing the critical state soil mechanics framework. The reinforced kaolin samples were assessed using the Unconfined Compression Test (UCT) and Consolidated Undrained (CU) Triaxial Test. The polypropylene columns' diameter and height as well as the effective confining pressure, σ'_3 , were among the research factors. The analysis of the results was conducted by utilizing the Mohr-Coulomb and critical state failure criteria. Based on the UCT results, it was observed that the Su generally improved as the height penetrating ratio increased, however, once it reached 100% height penetrating ratio, it began to decrease. The area replacement ratio of polypropylene also affected the S_u increment. The shear strength of the soil sample did not change despite its high area replacement ratio. As the soil sample's circumference was smaller than required, the column's shearing strength needed to be increased. The ratio increased as the strength increased in the absence of restricting pressure. Nonetheless, excessive area replacement decreased the shear strength of the sample reinforced by group columns as the remaining width of the soil sample became too narrow to sustain the columns. By using the Mohr-Coulomb failure criterion of the CU test findings, the effective friction angle remained relatively constant after inserting polypropylene columns. However, it did lead to an improvement in undrained shear strength and apparent cohesion of the kaolin clay. Additionally, it was demonstrated that the addition of polypropylene columns increased the pore water pressure's dissipation. Using the critical state soil mechanics framework, the analysis allowed for the determination of unique critical state parameters for each sample, which were M, Γ, and λ. For the soil-polypropylene composite, the majority of M values were found to fall between 1.18 and 1.30. This range is equivalent to a variation in the critical state friction angle, which ranged from 30° to 35°. As a result, the soil-polypropylene composite can be classified under the category of "mixtures of gravel and sand with fine-grained soils". In general, it can be concluded that the installation of polypropylene columns has the potential to improve the shear strength and compressibility characteristics of soft clay. Therefore, a design chart was developed with the purpose of working as a design tool, specifically for calculating the necessary volume of polypropylene that is required to create vertical columns that align with the desired shear strength of the improved clay soil.

TABLE OF CONTENT

DECLARATION

TITLE PAGE

ACKNOWLEDGEMENTS ii

ABSTRAK iii

ABSTRACT iv

TABLE OF CONTENT v

LIST OF TABLES xi

LIST OF FIGURES xiii

LIST OF SYMBOLS xxi

LIST OF ABBREVIATIONS xxiii

LIST OF APPENDICES xxiv

CHAPTER 1 INTRODUCTION 1

1.1 Background of Study 1

1.2 Problem Statement 5

1.3 Objectives of the Study 7

1.4 Scope of the Research 7

1.5 Limitation of Research 10

1.6 Research Significance 10

1.7 Thesis Proposal Organisation 11

CHAPTER 2 LITERATURE REVIEW 13

2.1 Introduction 13

2.2 Clay Soil 13

2.3 Characteristics of Clay 16

2.3.1 Consolidation and Compressibility 18

2.3.2 Undrained Shear Strength 20

2.4 Critical State Theory 21

2.4.1 Definition of State Parameters 21

2.4.2 State Boundary Surface 23

2.4.3 Critical Void Ratio Line 25

2.4.4 Undrained Shear Strength 26

2.4.5 Critical State Parameters of Some Types of Soil 26

2.5 Kaolin Clay 28

2.5.1 Chemical Properties of Kaolin 29

2.5.2 Physical Properties of Kaolin 30

2.5.3 Mechanical Properties of Kaolin 31

2.5.4 Summary 32

2.6 Polypropylene 33

2.6.1 Chemical Properties of Polypropylene 34

2.6.2 Properties of Polypropylene 34

2.6.3 Summary 35

2.7 Soil Reinforcement 36

2.8 Columns in Soil 38

2.8.1 Basic Physical Modelling of Columns in Soil 39

2.8.2 Previous Research on Columns in Soil 41

2.8.3 Failure Mechanisms of Columns in Soil 57

CHAPTER 3 METHODOLOGY **61**

3.1 Introduction 61

3.2 Selection of Material 63

3.3 Collection of Materials 64

3.3.1 Kaolin clay soil 64

3.3.2 Polypropylene 64

3.4 Determination of Properties of Materials and Laboratory Tests Standards 64

3.5 Laboratory Tests for the Assessment of Physical Properties 65

3.5.1 Sieve Analysis Test 66

3.5.2 Relative Density Test 67

3.5.3 Water Absorption Test 68

3.5.4 Specific Gravity Test 68

3.5.5 Hydrometer Test 69

3.5.6 Atterberg Limit Test 71

3.6 Laboratory Tests for the Assessment of Mechanical Properties 72

3.6.1 Falling Head Permeability Test 72

3.6.2 Constant Head Permeability Test 73

3.6.3 Standard Proctor Compaction Test 74

3.6.4 Vane Shear Test 75

3.6.5 Unconfined Compression Test (ASTM D2166) 76

3.6.6 Consolidated Undrained (CU) Triaxial Test 77

3.7 Design of Polypropylene Column Model 79

3.7.1 General 79

3.7.2 Preparation of Kaolin Clay Sample 80

3.7.3 Polypropylene Columns Installation 85

3.7.4 Polypropylene Column Arrangement 87

3.7.5 Details of Laboratory Tests 89

3.8 Consolidated Undrained Triaxial Test 90

3.8.1 System Elements 92

3.8.2 Data Analysis using CU Triaxial Test 95

3.9 Data Analysis and Result Presentation 102

3.10 Laboratory Tests for the Assessment of Morphological Properties 102

CHAPTER 4 RESULTS AND ANALYSIS 104

4.1 Introduction 104

4.2 Basic Properties of Polypropylene and Kaolin 104

4.2.1 Particle Size Distribution 107

4.2.2 Atterberg Limit 108

4.2.3 Relative Density Test 110

4.2.4 Specific Gravity Test 110

4.3 Mechanical Properties 111

4.3.1 Standard Compaction 111

4.3.2 Falling Head Permeability 112

4.3.3 Constant Head Permeability 112

4.3.4 Shear Strength 113

4.4 Morphological Properties 120

4.5 Compressibility 122

4.6 Consolidation Parameters 122

4.7 Controlled Sample 124

4.8 Samples Reinforced with a Single Polypropylene Column 127

4.8.1 Height Penetrating Ratio, H_c/H_s = 0.6 127

4.8.2 Height Penetrating Ratio, H_c/H_s = 0.8 130

4.8.3 Height Penetrating Ratio, H_c/H_s = 1.0 133

4.9 Samples Reinforced with a Group of Polypropylene Columns 136

4.9.1 Height Penetrating Ratio, H_c/H_s = 0.6 136

4.9.2 Height Penetrating Ratio, Hc/Hs = 0.8 139

4.9.3 Height Penetrating Ratio, $H_c/H_s = 1.0$ 142
4.10 Summary of Compressibility Analysis 145
4.11 Unconfined Compression Test 149
4.11.1 Undrained Shear Strength 149
4.11.2 The Effect of Area Replacement Ratio 150
4.11.3 The Effect of Column Penetration Ratio 153
4.11.4 The Effect of Volume Replacement Ratio 156
4.12 Consolidated Undrained Triaxial Test 158
4.12.1 Stress Strain Behaviour 161
4.12.2 Excess Pore Pressure 172
4.12.3 Shear Strength Parameters 174

CHAPTER 5 CRITICAL STATE ANALYSIS 183
5.1 Introduction 183
5.2 Stresses and Void Ratio at Critical State 183
5.3 Controlled Sample 187
5.4 Samples Reinforced with Polypropylene Column 189
5.4.1 Single Column 189
5.4.2 Group Columns 202
5.5 Critical State Line Equations and Critical State Parameters 215
5.6 Variation of M, λ and Γ with Volume Replacement Ratio 217
5.7 Undrained Shear Strength at Critical State 218
5.7.1 Theoretical Correlation between Undrained Shear Strength and Specific Volume at Critical States 220
5.7.2 Variation of Undrained Shear Strength with Specific Volume 224
5.7.3 Effect of Volume Replacement Ratio 227
5.8 Summary of Critical State Analysis 232

CHAPTER 6 CONCLUSION AND RECOMMENDATION **233**

6.1 Introduction 233

6.2 Conclusion 233

6.3 Recommendations for Future Research 237

REFERENCES **238**

APPENDICES **248**

Test Details 279

Specimen Details 279

Conditions at Failure 281

Test Details 282

Specimen Details 282

Conditions at Failure 284

Test Details 285

Specimen Details 285

Conditions at Failure 287

LIST OF TABLES

Table 2.1	Particle sizes of different soil types	15
Table 2.2	Characteristics of clay soil	18
Table 2.3	Categorisation of undrained shear strength of clay soil	20
Table 2.4	Critical state parameters of some soil types	28
Table 2.5	Chemical composition of kaolin	30
Table 2.6	Physical properties of kaolin clay from previous works	31
Table 2.7	Mechanical properties of kaolin from previous works	32
Table 2.8	Properties of polypropylene from previous works	35
Table 2.9	Summary of literature review	50
Table 3.1	Overview of test standards and methods that are used for the determination of properties of selected materials	65
Table 3.2	Sample coding and CU triaxial test programme for unreinforced clay and clay reinforced with polypropylene columns	79
Table 3.3	Moisture content for kaolin specimens	84
Table 3.4	Density of various-sized polypropylene columns set in samples of kaolin	86
Table 3.5	Number of samples to be tested	90
Table 4.1	Properties of polypropylene from manufacturer	105
Table 4.2	Test result found for the properties of polypropylene and kaolin	106
Table 4.3	Comparison of LL, PL and PI with previous researchers	109
Table 4.4	Comparison of specific gravity of kaolin with previous researchers	110
Table 4.5	Comparison of standard compaction result with previous researchers	112
Table 4.6	Comparison of permeability coefficient of kaolin with previous researchers	112
Table 4.7	Statistically analysing shear strength data from vane shear tests	115
Table 4.8	Result of undrained shear strength obtained from the vane shear test	116
Table 4.9	Peak deviator stress and axial strain from UCT	117
Table 4.10	Consolidation parameters	122
Table 4.11	Summary of analysis on unconfined compression test	149
Table 4.12	Effect of area replacement ratio for fully penetrating polypropylene columns on improvement shear strength of kaolin clay	152
Table 4.13	Volume replacement ratio with improvement shear strength	157

Table 4.14	Summary of results from consolidated undrained triaxial test	159
Table 4.15	Summary of results from consolidated undrained triaxial test for shear stress at failure and effective normal stress	175
Table 5.1	Deviator stress, mean normal effective stress, void ratio and specific volume at critical state	184
Table 5.2	Critical state line equations and critical state parameters from CU tests for kaolin reinforced with polypropylene columns	216
Table 5.3	Undrained shear strength and increased in the strength at critical state	219
Table 5.4	Calculated and laboratory values of undrained shear strengths, and specific volumes of samples at critical states	221
Table 5.5	Undrained shear strength at critical state and the corresponding initial specific volume	224

LIST OF FIGURES

Figure 1.1	Location of Titan Petchem (M) Sdn Bhd Plant in Malaysia.	4
Figure 2.1	The soil distribution map in west Malaysia.	14
Figure 2.2	Critical state line and stress pathway for undrained loads on normally consolidated clay	22
Figure 2.3	Plots of triaxial tests results of CU and CD	23
Figure 2.4	The critical state boundary surface	25
Figure 2.5	Chemical structure of Kaolin	29
Figure 2.6	Chemical structure of Polypropylene	34
Figure 2.7	Failure mechanism of single stone columns	58
Figure 2.8	The failure mechanism of group stone columns	59
Figure 3.1	Flow chart for the implementation of the research methodology	62
Figure 3.2	Sieve Analysis Equipment	66
Figure 3.3	Equipment for Relative Density Test	67
Figure 3.4	Small Pycnometer	69
Figure 3.5	Hydrometer test apparatus	70
Figure 3.6	Cone penetration test	71
Figure 3.7	Falling head permeability test	73
Figure 3.8	Constant Head Permeability Test	74
Figure 3.9	Standard Proctor Compaction Test	75
Figure 3.10	Laboratory Vane Shear Test Machine	76
Figure 3.11	Unconfined Compression Test Machine	77
Figure 3.12	Apparatus for the preparation of soft homogenous kaolin specimens	81
Figure 3.13	Kaolin mixed with water poured into the mould	81
Figure 3.14	Customised mould set for 50 mm diameter and 100 mm height specimen	82
Figure 3.15	Kaolin was compressed via pressure to both ends with a customised cap	82
Figure 3.16	Hole was drilled using 10 mm and 16 mm diameter drill bits	83
Figure 3.17	Specimens extruded out of the mould being kept inside the case	84
Figure 3.18	Location of points for moisture content determination	85
Figure 3.19	Installation of polypropylene soft kaolin clay specimen	86
Figure 3.20	Detailed polypropylene column arrangement in clay samples for both single and combined columns	88

Figure 3.21	Completely instaled single and group polypropylene columns in the sample made of soft kaolin clay	89
Figure 3.22	GDS Completely Automatic Triaxial System equipment setup	91
Figure 3.23	Diagram of GDSTAS Hardware elements (www.gdsinstruments.com)	93
Figure 3.24	Cell pressure and back pressure were controlled with an advanced pressure/volume controller	94
Figure 3.25	GDSLAB software	95
Figure 3.26	GDSLAB test plan for consolidated undrained triaxial test	96
Figure 3.27	Setup for Stage 1	97
Figure 3.28	Stage 1 offers several optional test termination criteria	97
Figure 3.29	Setup for Stage 3	98
Figure 3.30	Optional test termination condition for Stage 3	98
Figure 3.31	Setup for Stage 4	99
Figure 3.32	Optional test termination condition for Stage 4	100
Figure 3.33	Setup for Stage 5	101
Figure 3.34	Optional test start condition for Stage 5	102
Figure 3.35	Scanning Electron Microscope Machine	103
Figure 4.1	Polypropylene was acquired from Titan Petchem (M) Sdn. Bhd. (PM201)	105
Figure 4.2	Particle size distribution curve of kaolin and polypropylene	108
Figure 4.3	Plasticity Chart (ASTM D2487)	109
Figure 4.4	Compaction curve for kaolin	111
Figure 4.5	Graph showing normal stress vs shear stress	114
Figure 4.6	Deviator stress and excess pore-water pressure versus axial strain for kaolin clay and kaolin reinforced with polypropylene	118
Figure 4.7	Mohr-Coulomb effective stress failure envelopes for (a) Kaolin clay;	119
Figure 4.8	Top view of polypropylene particle 30 times zoomed and 500 zoomed areas of selected areas	121
Figure 4.9	Side view of polypropylene particle 30 times zoomed and 500 zoomed areas of selected areas.	121
Figure 4.10	Volume change against square root time for consolidation stage of controlled sample	126
Figure 4.11	Pore pressure dissipation against log time for consolidation stage of controlled sample	126
Figure 4.12	Volume change vs square root time for the sample's consolidation stage when it was reinforced by a single column with a diameter of 10 mm and a height penetration ratio of 60%	128

Figure 4.13	Pore pressure dissipation vs logarithmic time during consolidation stage of sample reinforced by a single column 10 mm in diameter and 60% in height.	128
Figure 4.14	Volume change vs square root time for the sample's consolidation stage when it was reinforced by a single column with a diameter of 16 mm and a height penetration ratio of 60%.	129
Figure 4.15	Pore pressure dissipation vs logarithmic time during consolidation stage of sample reinforced by a single column 16 mm in diameter and 60% in height.	130
Figure 4.16	Volume change vs square root time for the sample's consolidation stage when it was reinforced by a single column with a diameter of 10 mm and a height penetration ratio of 80%	131
Figure 4.17	Pore pressure dissipation vs logarithmic time during consolidation stage of sample reinforced by a single column 10 mm in diameter and 80% in height.	131
Figure 4.18	Volume change vs square root time for the sample's consolidation stage when it was reinforced by a single column with a diameter of 16 mm and a height penetration ratio of 80%.	132
Figure 4.19	Pore pressure dissipation vs logarithmic time during consolidation stage of sample reinforced by a single column 16 mm in diameter and 80% in height	133
Figure 4.20	Volume change vs square root time for the sample's consolidation stage when it was reinforced by a single column with a diameter of 10 mm and a height penetration ratio of 100%.	134
Figure 4.21	Pore pressure dissipation vs logarithmic time during consolidation stage of sample reinforced by a single column 10 mm in diameter and 100% in height.	134
Figure 4.22	Volume change vs square root time for the sample's consolidation stage when it was reinforced by a single column with a diameter of 16 mm and a height penetration ratio of 100%	135
Figure 4.23	Pore pressure dissipation vs logarithmic time during consolidation stage of sample reinforced by a single column 16 mm in diameter and 100% in height	136
Figure 4.24	Volume change vs square root time for the sample's consolidation stage when it was reinforced by a group column with a diameter of 10 mm and a height penetration ratio of 60%	137
Figure 4.25	Pore pressure dissipation vs logarithmic time during consolidation stage of sample reinforced by a group column 10 mm in diameter and 60% in height	137
Figure 4.26	Volume change vs square root time for the sample's consolidation stage when it was reinforced by a group column with a diameter of 16 mm and a height penetration ratio of 60%	138

Figure 4.27	Pore pressure dissipation vs logarithmic time during consolidation stage of sample reinforced by a group column 10 mm in diameter and 60% in height	139
Figure 4.28	Volume change vs square root time for the sample's consolidation stage when it was reinforced by a group column with a diameter of 10 mm and a height penetration ratio of 80%	140
Figure 4.29	Pore pressure dissipation vs logarithmic time during consolidation stage of sample reinforced by a group column 10 mm in diameter and 80% in height	140
Figure 4.30	Volume change vs square root time for the sample's consolidation stage when it was reinforced by a group column with a diameter of 16 mm and a height penetration ratio of 80%	141
Figure 4.31	Pore pressure dissipation vs logarithmic time during consolidation stage of sample reinforced by a group column 16 mm in diameter and 80% in height	142
Figure 4.32	Volume change vs square root time for the sample's consolidation stage when it was reinforced by a group column with a diameter of 10 mm and a height penetration ratio of 100%	143
Figure 4.33	Pore pressure dissipation vs logarithmic time during consolidation stage of sample reinforced by a group column 10 mm in diameter and 100% in height	143
Figure 4.34	Volume change vs square root time for the sample’s consolidation stage when it was reinforced by a group column with a diameter of 16 mm and a height penetration ratio of 100%	144
Figure 4.35	Pore pressure dissipation vs logarithmic time during consolidation stage of sample reinforced by a group column 16 mm in diameter and 100% in height	145
Figure 4.36	For (a) single and (b) group polypropylene columns, the time to obtain full consolidation vs effective confining pressure	146
Figure 4.37	Diagram illustrating the impact of different effective confining pressures on smearing and crushing kaolin specimens reinforced with polypropylene columns	148
Figure 4.38	Improvement of shear strength vs area replacement ratio Ac/As (%)	151
Figure 4.39	Undrained shear strength is affected by the column height to diameter ratio	154
Figure 4.40	Improvement of undrained shear strength for both single and group polypropylene columns through the height penetrating ratio	155
Figure 4.41	Schematic illustrations of soft kaolin clay that are reinforced with partially and fully penetrated granular columns and confined by the surrounding soil pressure	156
Figure 4.42	Improved undrained shear strength with an increased volume replacement ratio	158

Figure 4.43	Deviator stress versus axial strain and pore pressure versus axial strain for kaolin specimens reinforced at an effective confining pressure of 50 kPa using a single polypropylene column	162
Figure 4.44	Deviator stress versus axial strain and pore pressure versus axial strain for kaolin specimens reinforced at an effective confining pressure of 100 kPa using a single polypropylene column	164
Figure 4.45	Deviator stress versus axial strain and pore pressure versus axial strain for kaolin specimens reinforced at an effective confining pressure of 200 kPa using a single polypropylene column	166
Figure 4.46	Deviator stress versus axial strain and pore pressure versus axial strain for kaolin specimens reinforced at an effective confining pressure of 50 kPa using a group polypropylene column	168
Figure 4.47	Deviator stress versus axial strain and pore pressure versus axial strain for kaolin specimens reinforced at an effective confining pressure of 100 kPa using a group polypropylene column	170
Figure 4.48	Deviator stress versus axial strain and pore pressure versus axial strain for kaolin specimens reinforced at an effective confining pressure of 200 kPa using a group polypropylene column	172
Figure 4.49	Shear stress failure vs. effective normal stress failure envelopes for single and group column-reinforced kaolin specimens	178
Figure 4.50	Height penetration ratio in relation to effective frictional angle	179
Figure 4.51	Height penetration ratio in relation to apparent cohesion	179
Figure 4.52	Area replacement ratio relatio to apparent cohesion	181
Figure 4.53	Area replacement ratio relation to effective frictional angle	181
Figure 5.1	Effective stress paths for kaolin clay sample reinforced with single and group polypropylene columns	186
Figure 5.2	(a) Stress paths and CSL in q : p' space and (b) CSL in e : p' space for	188
Figure 5.3	Critical state line in v : ln p' space for controlled sample	189
Figure 5.4	Effective stress paths for clay samples reinforced with single polypropylene columns	190
Figure 5.5	(a) Critical state line and stress pathways in q: p' space; (b) Critical state line in e: p' space for a clay sample reinforced at 60% penetration using a 10 mm-diameter single polypropylene column	191
Figure 5.6	Critical state line in v: ln p' space for kaolin clay reinforced with a single polypropylene column with a diameter of 10 mm and 60% penetration	192
Figure 5.7	(a) Critical state line and stress pathways in q: p' space; (b) Critical state line in e: p' space for a clay sample reinforced at 60% penetration using a 16 mm-diameter single polypropylene column	193

Figure 5.8 Critical state line in v: ln p' space for kaolin clay reinforced with a single polypropylene column with a diameter of 16 mm and 60% penetration 194

Figure 5.9 (a) Critical state line and stress pathways in q: p' space; (b) Critical state line in e: p' space for a clay sample reinforced at 80% penetration using a 10 mm-diameter single polypropylene column 195

Figure 5.10 Critical state line in v: ln p' space for kaolin clay reinforced with a single polypropylene column with a diameter of 10 mm and 80% penetration 196

Figure 5.11 (a) Critical state line and stress paths in q : p' space; (b) Critical stale line in e : p' space for a clay sample reinforced at 80% penetration with a single polypropylene column of 16 mm in diameter 197

Figure 5.12 Critical state line in v: ln p' space for kaolin clay reinforced with a single polypropylene column with a diameter of 16 mm and 80% penetration 198

Figure 5.13 (a) Critical state line and stress pathways in q: p' space; (b) Critical state line in e: p' space for a clay sample reinforced at 100% penetration using a 10 mm-diameter single polypropylene column 199

Figure 5.14 Critical state line in v: ln p' space for kaolin clay reinforced with a single polypropylene column with a diameter of 10 mm and 100% penetration 200

Figure 5.15 (a) Critical state line and stress pathways in q: p' space; (b) Critical state line in e: p' space for a clay sample reinforced at 100% penetration using a 16 mm-diameter single polypropylene column 201

Figure 5.16 Critical state line in v: ln p' space for kaolin clay reinforced with a single polypropylene column with a diameter of 16 mm and 100% penetration 202

Figure 5.17 Effective stress pathways for clay sample reinforced with group polypropylene columns 203

Figure 5.18 (a) Critical state line and stress pathways in q: p' space; (b) Critical state line in e: p' space for a clay sample reinforced at 60% penetration using a 10 mm-diameter group polypropylene column 204

Figure 5.19 Critical state line in v: ln p' space for kaolin clay reinforced with a group polypropylene column with a diameter of 10 mm and 60% penetration 205

Figure 5.20 (a) Critical state line and stress pathways in q: p' space; (b) Critical state line in e: p' space for a clay sample reinforced at 60% penetration using a 16 mm-diameter group polypropylene column 206

Figure 5.21 Critical state line in v: ln p' space for kaolin clay reinforced with a group polypropylene column with a diameter of 16 mm and 60% penetration 207

Figure 5.22	(a) Critical state line and stress pathways in q: p' space; (b) Critical state line in e: p' space for a clay sample reinforced at 80% penetration using a 10 mm-diameter group polypropylene column	208
Figure 5.23	Critical state line in v: ln p' space for kaolin clay reinforced with a group polypropylene column with a diameter of 10 mm and 80% penetration	209
Figure 5.24	(a) Critical state line and stress pathways in q: p' space; (b) Critical state line in e: p' space for a clay sample reinforced at 80% penetration using a 16 mm-diameter group polypropylene column	210
Figure 5.25	Critical state line in v: ln p' space for kaolin clay reinforced with a group polypropylene column with a diameter of 16 mm and 80% penetration	211
Figure 5.26	(a) Critical state line and stress pathways in q: p' space; (b) Critical state line in e: p' space for a clay sample reinforced at 100% penetration using a 10 mm-diameter group polypropylene column	212
Figure 5.27	Critical state line in v: ln p' space for kaolin clay reinforced with a group polypropylene column with a diameter of 10 mm and 100% penetration	213
Figure 5.28	(a) Critical state line and stress pathways in q: p' space; (b) Critical state line in e: p' space for a clay sample reinforced at 100% penetration using a 16 mm-diameter group polypropylene column	214
Figure 5.29	Critical state line in v: ln p' space for kaolin clay reinforced with a group polypropylene column with a diameter of 16 mm and 100% penetration	215
Figure 5.30	Variation of (a) M, (b) λ, and (c) Γ with volume replacement ratio for kaolin clay reinforced with polypropylene columns	218
Figure 5.31	Variation of undrained shear strengths with volume replacement ratio for all samples at p'_o = 50 kPa	223
Figure 5.32	Variation of undrained shear strengths with volume replacement ratio for all samples at p'_o = 100 kPa	223
Figure 5.33	Variation of undrained shear strengths with volume replacement ratio for all samples at p'_o = 200 kPa	224
Figure 5.34	Variation of undrained shear strength with specific volume	226
Figure 5.35	Variation of volume replacement ratio with specific volume	227
Figure 5.36	Variation of undrained shear strength with volume replacement ratio	228
Figure 5.37	Variation of the volume replacement ratio-induced increase in undrained shear strength	229
Figure 5.38	Variation of undrained shear strength with volume replacement ratio	230
Figure 5.39	Correlation between a constant A and p'_o	231
Figure 5.40	Correlation between a constant B and p'_o	231

Figure 5.41 Design chart shows the undrained shear strength of kaolin clay reinforced with polypropylene at different volume replacement ratios 232

LIST OF SYMBOLS

A_c	Area of polypropylene column
A_s	Area of kaolin clay specimen
c	Cohesion
c'	Apparent cohesion
D_c	Diameter of polypropylene column
D_s	Diameter of kaolin clay specimen
D_r	Relative density
G_s	Specific gravity
g/cm^3	Gram per centimetre cube
H	The slope of Hvorslev surface on the q-p' plan
H_c	Height of polypropylene column
H_s	Height of kaolin clay specimen
k	Slope of over consolidation (swelling) line
kN	Kilo newton
kN/m^2	Kilo newton per metre square
kPa	Kilo pascal
Γ	Intercept of critical state line on the with the
Γ_C	Specific volume of soil (in compression) on the critical
M	Slope of critical state line in q – p' plane
M_C	Value of M triaxial compression test
Mg	Mega gram
MN	Mega newton
Mg/m^3	Mega gram per metre cube
mm	Millimetre
µm	Micrometre
m/s	Metre per Second
N_{KO}	Specific volume of anisotropically normally
p'_o	Initial mean normal effective stress
A_c	Area of polypropylene column
A_s	Area of kaolin clay specimen
c	Cohesion

e	Void Ratio
p	Mean total normal stress
p'	Mean effective normal stress
q	Deviator stress
q_{max}	Maximum deviator stress
q_u	Unconfined compression stress
R^2	Correlation cohesion
s	Shear strength
s_u	Undrained shear strength
S_d	Standard deviation
Δs_u	Undrained shear strength improvement
V_c	Volume of polypropylene column
V_s	Volume of kaolin clay specimen
w	Moisture content
w_{opt}	Optimum moisture content
ρ_d	Dry density
$\rho_{d(max)}$	Maximum dry density
γ	Unit Weight
γ_{min}	Minimum unit weight
γ_{max}	Maximum unit weight
ϕ	Frictional angle
ϕ'	Effective friction angle
ϕ'_c	Critical internal fiction angle
%	Per cent
^{o}	Degree
σ	Total normal stress
σ'	Effective normal stress
$\sigma_1, \sigma_2, \sigma_3$	Principal total stresses
$\sigma'_1, \sigma'_2, \sigma'_3$	Principal effective stresses
λ	Slope of normal consolidated line with the v : p' space state line consolidated line
ξ	slope of u/p'e versus ε plot
e	Void Ratio

LIST OF ABBREVIATIONS

AASHTO	American Association of State Highway and Transportation Officials
ASTM	American Society for Testing and Materials
BPA	Bisphenol A
BS	British Standard
BSCS	British Soil Classification System
CL	Lean Clay
HCL	Hydrochloric Acid
HDPE	High Density Polyethylene
LDPE	Low-Density Polyethylene
LL	Liquid Limit
PE	Polyethylene
PET	Polyethylene Terephthalate
PI	Plastic Index
PL	Plastic Limit
PS	Polystyrene
PVC	Polyvinyl Chloride
PP	Polypropylene
SPI	Society of the Plastics Industry
TO layer	A Layer of Tetrahedral Sheet with A Layer of Octahedral Sheet
TOT layer	2 Layers of Tetrahedral Sheet with A Layer of Octahedral Sheet
UCT	Unconfined Compression Test
US	United Stated
USCS	Unified Soil Classification System
USDA	United State Department of Agriculture
VOC	Volatile Organic Compounds

AASHTO	American Association of State Highway and Transportation Officials
ASTM	American Society for Testing and Materials
BPA	Bisphenol A
BS	British Standard
BSCS	British Soil Classification System

LIST OF APPENDICES

Appendix A:	Sieve analysis test result	249
Appendix B:	Hydrometer test result	251
Appendix C:	Atterberg limit test result	252
Appendix D:	Relative density test result	254
Appendix E:	Sacrifice gravity test result	254
Appendix F:	Standard compaction test result	255
Appendix G:	Falling head test result	256
Appendix H:	Constant head permeability test result	257
Appendix I:	Unconfined compression test (UCT)	258
Appendix J:	Mohr-Coulomb Failure Criterion	272
Appendix K:	Shear strength by direct shear small shear box	279
Appendix L:	Consolidated Undrained Triaxial Compression Test	288

CHAPTER 1

INTRODUCTION

1.1 Background of Study

The fundamental requisite for the comprehensive progress of any country is the existence of an adequate infrastructure that includes residential buildings, highways, tunnels, bridges, and several other civil engineering projects. In the past, suitable land for construction sites abound, but nowadays, there is a drastic increase in land costs due to the rapid increase in infrastructure development, especially in metropolitan areas. The construction of clay soil has increased in prevalence mostly as a result of the limited availability of suitable land for infrastructure development and other improvements (Chambers et al., 2016). Construction is therefore now also being carried out on sites with extremely poor soil conditions, such as clays, which cover a large region in Malaysia.

Soft soil in Malaysia is often categorised as an quaternary sediment, which encompasses alluvial deposits and organic or peat soils (Kaniraj et al., 2015). According to the Quarterly Geological Map of Malaysia, significant areas of the western and eastern coastlines of Peninsular and East Malaysia are characterised by the presence of soft land; a common feature observed in the coastal plains of the country. The presence of a significant proportion of soft ground inside the country, along with the concentration of economic and social development in coastal areas, necessitates the undertaking of construction projects on these challenging deposits. In the past, several failures have been recorded either locally or internationally due to high soil compressibility and low shear strength, which had caused excessive settlement and structural deformation, such as embankment. The Public Works Department of Malaysia (PWD) has been actively engaged in several roadway and building projects on soft soil, owing to the nation's significant and rapid expansion witnessed over the last few decades. The Public Works Department (PWD) plays a significant role as the primary technical agency for the Government of Malaysia. Its participation in development projects can occur in two main capacities: construction and forensic investigation. The summary of geotechnical forensic investigations conducted by JKR on problematic projects since 2010 is presented. Out of a total of 252 forensic instances, about 72% (182 cases) pertain to the matter of ground settlement. The remaining 28% of cases are attributed to other variables like vibration, erosion, foundation failures, and similar causes (Mohamad et al., 2016). Therefore, it is apparent that the foremost technical obstacle encountered in the construction of soft soil is unquestionably the problem of soil settlement.

There is substantial potential for reusing waste materials to improve soil strength from a geotechnical and soil mechanics standpoint. Solid waste is widely recognised as one of the primary environmental issues in Malaysia, constituting a significant environmental challenge for the entire country. According to a study conducted by Ismail and Ani (2015), it was found that in 2013, the average daily solid waste generation per capita in Malaysia was approximately 800 grams. Only approximately 5% of the waste is recycled, according to Saadi at al. (2016), and the amount of waste created has increased as a result of growth and development. Nevertheless, Malaysia's waste management standards continue to be insufficient in light of the substantial quantity and intricate nature of the trash generated. Engineering firms may utilise waste to create sustainable buildings. For instance, polypropylene is among the waste materials that have been generated for this purpose. Polypropylene (PP), a thermoplastic polymer, possesses the characteristic of reusability. The use of this substance spans over a diverse array of items, encompassing textiles, plastics, food packaging, reusable containers, and tyres. Hence, this study aims to investigate the challenges associated with establishing infrastructure on soft soils and mitigate the scarcity of landfills in Malaysia due to increasing daily waste. It is expected that significant advancements in soil improvement techniques will be made as a result of this research. Furthermore, the utilisation of polypropylene as a waste product can lead to reduced expenses associated with soil improvement. Ideally, the insights derived from the study will provide valuable contributions to the ongoing progress of the field of clay soil development.

In many countries, including Malaysia, there is growing concern over the extensive production of plastic garbage. After putrescible garbage and paper, plastic waste makes up the third-highest volume of municipal solid waste (MSW) in Malaysia. Plastic garbage makes up 24.40% of Kuala Lumpur's MSW by weight in 2000, and the majority of it is disposed of in landfills. The unsuitability of landfills as a disposal method for plastic waste has become apparent due to the inherent characteristics of plastic. In Malaysia, the useful lifetime of landfills is decreasing as a result of a 2% annual rise in waste production. Therefore, attempts are being undertaken to employ degradable plastic or to divert specific plastic trash from landfills.

According to the MPMA (2011), 2 million tonnes of plastic are reportedly manufactured locally annually in Malaysia alone. Plastic remains the third most significant contributor to total waste tonnage, trailing behind putrescible waste and paper. However, the availability of data pertaining to plastic waste and recycling efforts is notably limited, mostly due to the predominant focus on MSW.

Polypropylene is lightweight in nature, having a low density compared to other plastics. It has a relatively low cost and is energy saving in the manufacturing and transportation process. Polypropylene is used as a raw material for the granular column, and its performance is almost the same as the conventional stone column. The effectiveness in improving soil strength is dependent on the properties of polypropylene (Hasan et al., 2015). According to the result obtained by Lee (2016), the maximum shear strength increment by reinforcing kaolin clay with polypropylene column is 91.24%, which proved that polypropylene is a suitable filler to be used in reinforcing soft clay. The two largest companies producing polypropylene are Polypropylene (M) Sdn. Bhd. and Titan Petchem (M) Sdn. Bhd., both with respective outstanding yearly production capabilities of 80,000 and 370,000 metric tons, respectively. The location of Titan Petchem (M) Sdn Bhd.'s plant is shown in Figure 1.1. Polypropylene is simple to process and is lightweight and rigid. It has a high average tensile strength of 330 kg/cm^2, an average density of between 0.855 and 0.946 g/cm^3, and a range of densities.

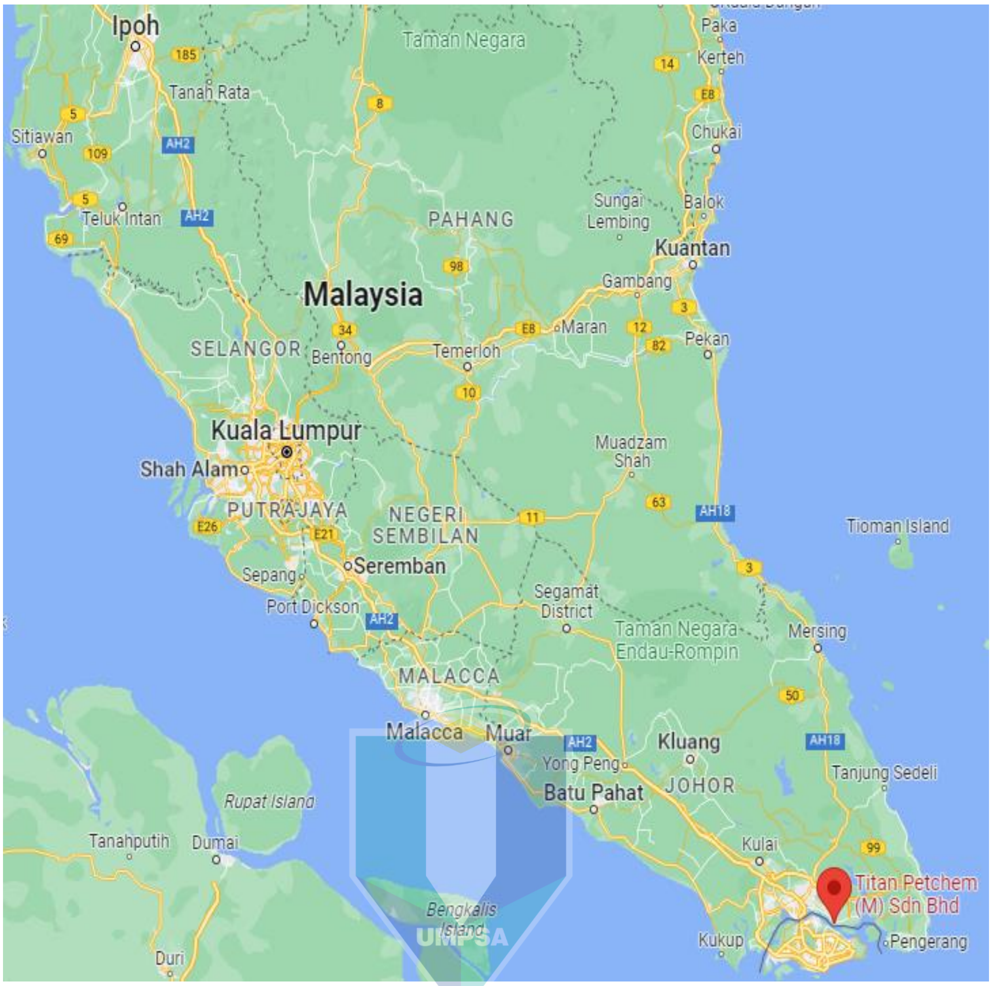

Figure 1.1 Location of Titan Petchem (M) Sdn Bhd Plant in Malaysia.

On the contrary, it is well acknowledged that soft soil has notable compressibility and restricted bearing ability. In order to facilitate building on soft soil, it is imperative to employ a ground improvement approach that may efficiently improve bearing capacity while concurrently reducing settlement and consolidation time. Sand drains, stone columns, prefabricated vertical drains, and many more methods have been selected over the years for this purpose. Choosing the right ground improvement method is essential to guarantee a safe and economical building. The stone column approach has gained significant popularity in recent times as a means to address building challenges encountered in soft soil conditions (Hasan, 2013). The stone column is commonly utilised in cohesive, soft soil to augment its capacity to carry loads, reduce settling, and aid in the dissipation of pore water pressure. Polypropylene exhibits characteristics that are analogous to those of sand, suggesting its potential viability as a substitute material for stone columns. The use of polypropylene as a substitute material in stone columns offers the possibility of reducing both the financial outlay of the project and the necessary space for disposing of any residual polypropylene. According to Hasan and Samadhiya (2016), the utilisation of granular columns in engineering applications has been implemented to improve load-bearing capacity and mitigate settlement issues in soils that possess weak or soft properties. This process is thought to be among the most flexible and economical ways to deal with unstable ground conditions.

Maakaroun at al. (2015) reported that in controlled laboratory studies, the presence of a fully penetrating column within clay samples resulted in a notable 33% enhancement in strength as compared to those without a sand column. Furthermore, the research findings indicated that the observed augmentation in undrained shear strength observed in fully penetrated soil columns ranged from 13% to 19.5%. Moreover, the recorded increase in undrained shear strength showed a variation ranging from 67.5% to 75% when evaluating area replacement ratios of 7.9% and 17.8% respectively. The granular column can increase bearing capacity and provide a shorter drainage path, which can speed up the crucial process of consolidation. Thakur et al. (2021) suggested that the installation of granular material columns offers two distinct benefits. Firstly, due to the inherent stiffness and increased frictional strength of the granular material in comparison to soft clay, these columns function as piles. Consequently, these mechanisms efficiently transfer the applied stress to greater depths by means of both shaft resistance and end bearing. Furthermore, it is important to highlight that the material used for columns has a higher permeability when compared to clay. This results in the drainage channel being shorter, which speeds up the consolidation process and increases the strength overall. A full-scale field test has also revealed this, according to Ling et al. (2019).

1.2 Problem Statement

Soft clay is a soil formation that has low bearing capacity, high compressibility, and a tendency for lateral flow. It causes excessive displacement of structures (Korita et al., 2022). Moreover, the process of disposing of soft soil is both costly and time-intensive. In addition, the establishment of infrastructure on soft soils may necessitate frequent post-construction maintenance activities aimed at decreasing the potential risks of structural problems (Mirzababaei et al., 2018). The characteristics of soft clay make it very undrainable. These circumstances, particularly during the rainy season in

Malaysia, cause serious havoc to structures. Thus, tackling this problem is of significant importance. Due to its effectiveness and positive economic impact, introducing a stone column or vertical column is a widely employed method for treating soft clay soils. The stone columns help reduce settlements, increase the bearing capacity, and accelerate the pre-consolidation of clay soil deposits.

Crushed stones and sand are the primary constituents of the stone column construction (Choudhury et al., 2023). However, the uncontrollable usage of natural resources in granular columns like sand and stone is a matter of concern and calls for the crucial need to search for alternative substitutes for vertical column from renewable materials. To tackle these issues, the utilisation of renewable materials like polypropylene can be a potential solution. A stone column is normally installed in soft, cohesive soil to improve bearing capacity, reduce settlement, and accelerate pore water pressure dissipation (Adriyati et al., 2023). On the other hand, Polypropylene is endowed with better crack resistance and stress absorption capability in comparison to sand (Saberian et al., 2023). Additionally, it can absorb stresses and movements without causing structural damage. The high friction angle value of polypropylene could increase soft clay's bearing capacity, while the high permeability coefficient could accelerate the consolidation. Furthermore, the coefficient of the permeability of polypropylene is higher than that of sand, thus releasing extra pore water pressure from the sample (Wang et al., 2019). Since the other functional attributes of polypropylene are similar to sand, it is anticipated that, using polypropylene as a substitute material in stone columns can replace the use of sand.

Utilising polypropylene can tackle the complex disposal issues of polypropylene manufacturing plants, which is currently a major concern for environment and lanfills. Eventually, such an initiative will reduce the scarcity of daily waste landfills in Malaysia. This led to the idea of introducing a polypropylene column for this study. The implementation of polypropylene columns has the potential to address issues related to disposal and the environment, as well as reduce costs associated with construction projects. Morever, based on available research, using polypropylene for ground improvement instead of granular columns has never been explored. In order to effectively use enhanced soft clay materials, it was necessary to evaluate the effects of the polypropylene column's size and confining pressure on the enhancement of strength and compressibility properties. Analysing critical state soil mechanics will give new insight into the findings.

1.3 Objectives of the Study

The objective of this study is to examine the potential of utilising polypropylene columns as a means to improve the compressibility and shear strength characteristics of soft, normally consolidated clays. The acquired results involve a comparison between the strength characteristics of soft clay that has been reinforced with polypropylene columns and the strength characteristics of both a single polypropylene column and a group of polypropylene columns. Additionally, the effect of confining pressure on the compressibility characteristics was examined. The comparisons above were conducted through the assessment of the area replacement ratio (Ac/As), height penetrating ratio (Hc/Hs), and volume replacement ratio (Vc/Vs). For the purpose of fulfilling the objectives of the research, the study established the following objectives:

1. To determine the physical and mechanical characteristics of kaolin clay and polypropylene.
2. To assess how the strength of the soft soil reinforced with polypropylene columns is affected by the area replacement ratio, height penetration ratio, and volume replacement ratio.
3. To analyse the effect of different sizes and heights of polypropylene columns through Mohr-Coulomb failure criteria and critical state failure criteria.
4. To correlate the volume replacement ratio and mean normal effective stress with the undrained shear strength of kaolin clay reinforced with polypropylene columns.
5. To establish a design chart using the critical state soil mechanics framework.

1.4 Scope of the Research

The research was carried out through controlled experiments on the laboratory scale. The research encompassed the performance of the Unconfined Compression and Consolidated Undrained (CU) Triaxial tests on reconstituted specimens of soft kaolin clay. The specimens underwent modification through the utilisation of single or group polypropylene columns. The polypropylene material was obtained from Titan Petchem (M) Sdn. Bhd., a corporation located in Pasir Gudang, Johor. The granular material utilized in the vertical column consists of particles with diameters ranging from 1.08 millimetres to 3.35 millimetres. The kaolin powder used in this study, referred to as 'S300', was obtained from Kaolin (M) Sdn. Bhd., an enterprise situated in Selangor, Malaysia. This research creates an excellent research scope in the field of column construction in soft soil. Concisely, to achieve the research target the fundamental elements would be investigated as follows.

Polypropylene and kaolin have been subjected to laboratory testing conducted in accordance with the British Standard (BS) and the American Society of Testing Materials (ASTM) to determine their respective characteristics. The physical, mechanical, and morphological characteristics (SEM) of polypropylene have been determined by conducting a number of laboratory experiments:

i) Sieve Analysis Test
ii) Standard Compaction Test
iii) Relative Density Test
iv) Constant Head Permeability Test
v) Scanning Electron Microscopic Test (SEM)
vi) Direct Shear Test
vii) Consolidated Undrained Triaxial Test

The physical and mechanical properties of kaolin were determined from the following laboratory tests:

i) Specific Gravity Test
ii) Hydrometer Test
iii) Sieve Analysis Test
iv) Atterberg Limit Test
v) Falling Head Permeability Test

vi) Standard Compaction Test

vii) Vane Shear Test

viii) Unconfined Compression Test (UCT)

ix) Consolidated Undrained (CU) Test

Customised moulds were utilised to make reconstituted kaolin specimens. The specimens were composed of a pliable clay substance and had dimensions of 50 mm in diameter as well as 100 mm in height. A particular specimen was identified as the "controlled specimen" due to the absence of the polypropylene column installation.

The remaining two samples were characterised by polypropylene columns of heights measuring 60 mm and 80 mm, respectively, which exhibited an acceptable level of penetration (Hasan et al., 2018, 2019; Hoque et al., 2023).

The third sample, on the other hand, had fully penetrating polypropylene columns reaching 100 mm in height. A single column was installed in the sample's centre, and a triangle configuration was selected for a group of columns since it was the easiest to ensure uniform column placement especially with regards to the distance between columns. The determination of column spacing was achieved through the use of the area ratio and the ratio of column area to the total clay area. The polypropylene columns in this research have diameters of 10 and 16 mm, correspondingly. Therefore, the area ratio (Ac/As) for a single column was found to be 4% and 10.24% for the column's area and the specimen's area, respectively. In the context of a group of columns, the observed area ratios (Ac/As) for the column and specimen areas were determined to be 12% and 30.72%, respectively. The height penetration ratios (Hc/Hs) for partially penetrating columns, in which the columns only partially extended through the specimens, were determined to be 0.6 and 0.8. On the other hand, columns that totally penetrated the specimens, extending entirely from top to bottom, had a height penetration ratio of 1.0.

The primary evaluation was carried out by putting the clay sample through a polypropylene column once all necessary evaluations had been completed to ascertain the basic properties of the kaolin clay. The two main tests that have been chosen were the Consolidated Undrained (CU) Triaxial Test and the Unconfined Compression Test (UCT). Determining the soil's shear strength and analysing soil specimen failure were the tests' primary goals. However, the CU test's objective was to assess the extent and rate of settlements. This study's primary goal is to investigate the essential components that affect people's motivation to participate in the test.

1.5 Limitation of Research

Research-grade S300 Kaolin powder was employed as a component for the production of consistent and uniform clay materials. The used kaolin samples were prepared at a density of 1.72 x 10^{-4} gm/mm^3 using 20% water content. The selected particle size of polypropylene for the construction of the vertical column was between 1.18mm to 3.35 mm, which falls within the range of sand particles. The density of the polypropylene column formed by the raining technique was maintained at 0.90 g/cm^3, with a shrinkage value of about 1.4%. Tensile strength of polypropylene was at yield 330kg/cm^3 and elongation at yield 12%.

Three specimens were used to evaluate each combination of the area ratio and the height penetration ratio. The specimens used in the consolidated undrained triaxial test were saturated at first and then subjected to backpressures of 50 kPa, 100 kPa, and 200 kPa. After that, the samples were sheared after completing isotropic consolidation at effective confining pressures of 50 kPa, 100 kPa, and 200 kPa. The specimens exhibited an adequate amount of saturation, as indicated by a B-value ranging from 0.95, indicating complete saturation. The samples underwent an undrained shearing process at a steady strain rate of 9% hourly. When the highest axial strain approached around 20%, the tests came to an end. Because of this, the study's conclusions are restricted to the characteristics of the materials used and the listed limitations.

1.6 Research Significance

Engineers have always found it difficult to complete construction on soft soils. There are many recognised methods for improving soil, and one of them is the use of stone columns. To lessen the reliance on non-renewable materials, a modified approach was developed to substitute natural materials with recyclable, trash, and by-product materials. The use of a polypropylene column not only has substantial importance within the context of the building sector, but also serves as a means for maintaining and upholding sustainability.

Generally, the significance of research are as follows:

i) The study's findings investigate how different polypropylene column diameters affect the soft, reinforced kaolin clay's compressibility and shear strength. This work adds significantly to our understanding of how polypropylene columns behave in the specific setting of soft clay ground improvement.

ii) The use of polypropylene columns is presented in this research study as a way to improve the geotechnical properties of soft clay soils. It is clear that there are significant discrepancies between the suggested methodology and conventional techniques like piling.

iii) The primary objective of this study is to investigate the impact of increased confining pressure exerted by polypropylene columns, together with the effective confining pressure, on the shear strength and compressibility properties of reinforced specimens. The aim of this method is to replicate the surcharge system employed at construction sites.

    The research carried out in this study has led to the development of a design chart that can be utilised as a useful instrument for design applications, specifically in the estimation of the necessary quantity of polypropylene needed to get the appropriate shear strength of the improved clay soil.

1.7 Thesis Proposal Organisation

This investigation incorporates the subsequent chapters:

Chapter 1 provides an exposition of the contextual background, as well as an elucidation of the scope and objectives of the thesis.

Chapter 2 provides an extensive analysis of the existing literature pertaining to the topic matter. This elucidates the theoretical framework and practical implementation of employing polypropylene columns in the stabilisation of soft soils.

Chapter 3 provides a comprehensive account of the operational methodology employed in the reinforcement of soft soil using polypropylene columns. This chapter provides a thorough examination of the research methodology employed to analyse the strength and compressibility characteristics of soft clay improved with polypropylene columns. This methodology encompasses both programmatic and laboratory experimental approaches, specifically focusing on small-scale model tests. This chapter presents a thorough examination of the experimental setup's design, the processing techniques employed for homogeneous clay samples, and the construction procedure involved in fabricating polypropylene columns.

Chapter 4 of the study focuses on the categorisation of the research materials based on their individual traits. This document presents an analysis of the essential properties and categorisation of kaolin and polypropylene, together with their respective density and shear strength values. This chapter additionally addresses the morphological characteristics of polypropylene.

This chapter encompasses an examination of compressibility, which entails an analysis of the consolidation parameters and the duration required for the samples to achieve full consolidation. The utilisation of the Mohr-Column failure criteria was applied for the purpose of analysing the shear strength, which was derived based on the findings obtained from laboratory tests. This chapter presents a comprehensive analysis of the findings and a scholarly discussion on the impact of the area replacement ratio, height penetration ratio, and effective confining pressure.

Chapter 5 of this study utilised a direct approach based on the Cambridge stress field to assess the mechanical resilience of reinforced kaolin clay. The foundation of the framework is the critical state model of soil mechanics, first presented by Schofield and Wroth in 1968. It can be described as a theoretical model. The pertinent graphics were generated utilising data acquired from isotropically typically consolidated undrained triaxial testing. Moreover, a comprehensive examination was performed on the stress pathways of the tissues. A design chart was established with the intention of providing practical advantages to engineers.

In Chapter 6, the research findings were thoroughly analysed, conclusions were drawn, the subsequent outcomes were discussed, the study's contributions were highlighted, and suggestions for further research were offered.

CHAPTER 2

LITERATURE REVIEW

2.1 Introduction

This chapter covers previous research on the behaviour of clay while reinforced with granular materials, the use of the clay improvement system, and the method or procedure used to increase the strength characteristics of clay soil. The objective of this study is to assess the compressibility and strength characteristics of clay, namely the soft reconstituted kaolin clay, and investigate the effect of polypropylene columns on its behaviour. This research is relevant to the construction industry. This chapter also offers a better explanation of the polypropylene columns and their characteristics that affect the stone columns in the soil reinforcement technique in construction areas.

2.2 Clay Soil

The characteristics and attributes of soil are of considerable importance in the process of developing a structure. Soil is a heterogeneous mixture that comprises organic matter, minerals, gasses, liquids, and living creatures, which serves as a natural substrate that encourages and improves plant development. The ecological processes of soils and their dynamic character are impacted by a multitude of elements, including age, location within the landscape, parent material of the soil, presence of animal and plant life, and fluctuations in the environment. Consequently, soils undergo significant shifts as they transition from one location to another. The development of an infrastructure becomes harder when it is built on soft soil. The term "soft soil" applies to a type of soil characterised by its composition of clay or silty clay. This soil is considered as being generally undisturbed and in a condition of equilibrium, mostly due to the force exerted by its own weight. It does not see substantial secondary or delayed consolidation after its initial creation (Das and Sivakugan, 2018).

The main source of soil is the disintegration of the parent rock, which comprises different grain sizes. Rock is weathered into smaller sizes when it is continuously exposed to pressure, heat, and reactions with organisms. The particles in the soil exhibit varying degrees of disintegration and decomposition, resulting in a variety of size distributions. As time goes by, the rock turns from large particles into smaller particles, and this is the process where sediment is formed. When the sediments undergo deposition and cementation, sedimentary rock is formed.

Sedimentary rock can afterwards be categorised into coarse, medium, fine, and very fine classifications, which are determined by the size of the individual grains. The term "clay" is used to refer to soil composed of exceptionally small particles. The finest size among all soil particles is attributed to its formation as the ultimate result of rock weathering. The dissolved clay particles are crystallised in an aqueous environment (Abdel-Aleem et al., 2023), and they deposit mostly in coastal areas. Figure 2.1 illustrates the distribution of soil in West Malaysia, with the grey regions indicating the presence of soft clay.

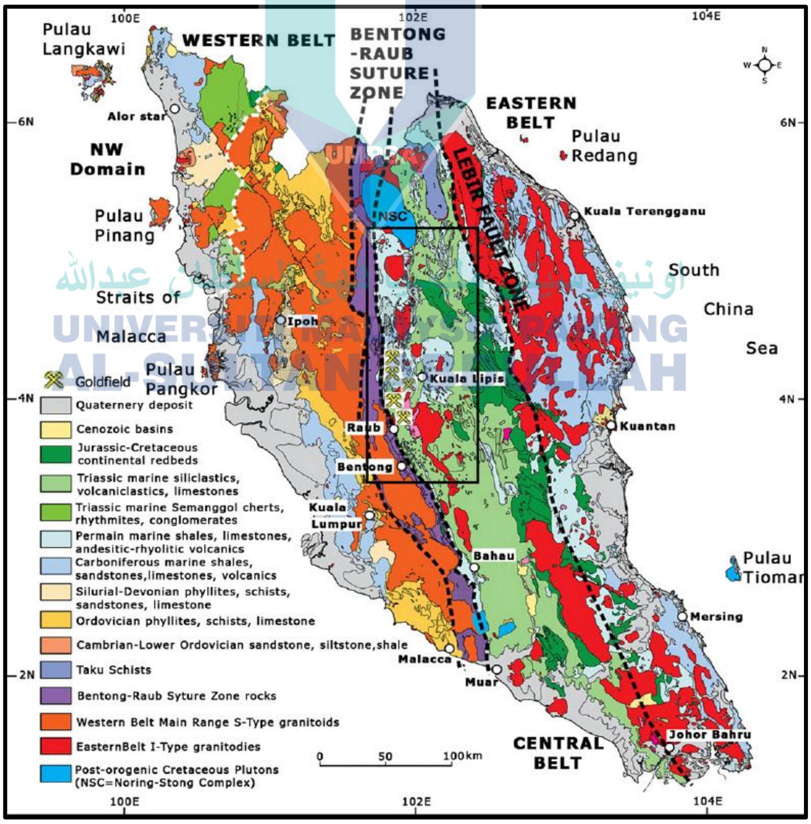

Figure 2.1 The soil distribution map in west Malaysia.
Source: Baioumy et al. (2015)

Clay is a secondary rock that is also regarded as a sedimentary rock, which is created by finely grained natural soil formed by a parent or primary rock like an igneous rock as well as other materials through the procedure of long-term chemical weathering. Particles can be transferred by rivers and deposited thereafter. Clay is a soil variant characterised by its fine-grained texture, including more than 50 percent of soil particles by weight that can pass through the No. 200 sieve. The soil particles are smaller than 2 microns. These particles are transparent to the human eye. The permeability of clay is very poor. The mineralogy and structure of the molecules of a clay particle are extremely unclear and highly complex. Clay is categorised as a cohesive soil in the field of geotechnical engineering, and its strength is known to diminish due to environmental influences or alterations in moisture levels. Table 2.1 illustrates the particle sizes related to various soil types.

Table 2.1 Particle sizes of different soil types

Soil type	**Particle Diameter (mm)**
Very coarse sand	2.0 – 1.0
Coarse sand	1.0 – 0.5
Medium sand	0.5 – 0.25
Fine sand	0.25 – 0.10
Very fine sand	0.10 – 0.05
Silt	0.05 – 0.002
Clay	<0.002

Source: Das and Sivakugan (2018)

The Peninsular Malaysia has a region of 804 km and a total area of 131792 km^2 (Sany et al., 2019), where non-volcanic igneous rock and granite comprised half of the overall area. Approximately 30% of the terrestrial surface is characterised by the presence of various rock formations (Annammala et al., 2018). In other words, clay has deposited 20 percent of the land and is mainly found in coastal regions, including Pahang. Hence, interacting with soft subgrade or clay soil is one of the most critical issues to be discussed (Liu et al., 2021), especially as rapid urbanisation and infrastructure development have led to a significantly higher demand for land space in recent days. This has prompted the construction sector to develop soft soil that is otherwise unsuitable for construction activities.

2.3 Characteristics of Clay

There are numerous varieties of clay soils that rely on clay minerals. The five main varieties of clay minerals identified in clays are chlorite, smectite, sepiolite, kaolinite, and illite. The characteristics of clay soil are given in Table 2.2.

Chlorite is soft and flexible in consistency. It is typically light green to grey in colour. It is made up of silicate minerals. It is strongly observed in hydrothermal ore deposits and has a wide variety of composition, temperature, and pressure situations.

Smectite clay is very rare since its crystal form is capable of interacting with liquids. Its appearance is formed by pink, white, light green, and yellow substances. It has a higher plasticity that readily absorbs moisture and swells.

Sepiolite, with its lightweight and porous structure, originates from the alteration of magnesium-rich minerals and finds applications in absorbents, filtration, and as a drilling mud additive. Sepiolite is a lump of clay with a dull-white deposit. It has no swelling properties due to its hydrous magnesium silicate. The silicate group also creates sepiolite, which is lightweight and porous. Sepiolite-based clays are soluble in high salt concentrations.

On the other hand, Montmorillonite, is a member of the smectite group, exhibits remarkable swelling properties, making it a versatile material in various industries (Kumari and Mohan, 2021). Its ability to absorb water and expand significantly contributes to its applications in drilling fluids, soil amendments, and as a key component in barrier systems for waste containment. The genesis of montmorillonite lies in the alteration of volcanic ash, where the mineral undergoes hydrothermal reactions and cation exchange processes over time. This transformation results in the formation of a layered structure with spaces between the layers that can accommodate water molecules and other ions, leading to its expansive nature.

Specifically, Kaolinite, being a primary component of kaolin clay, is derived from the weathering of aluminum-rich minerals such as feldspar (Kumari and Mohan, 2021). It comprises aluminium silicate material, which gives it a distinctively poor "shrink-swell" capacity. It is a component of white clay. Even then, it is often formed in orange or red while iron oxide is present. It is the most essential mineral to be contained in kaolin, porcelain, or pottery. Halloysite is a type of clay mineral that is chemically similar to kaolinite but has a unique tubular structure (Kumari and Mohan, 2021). It typically forms in low-temperature hydrothermal environments through the alteration of volcanic ash and other silicate minerals. Halloysite is prized for its high surface area and nanotube morphology, making it valuable in applications such as nanotechnology, catalysis, and controlled release of substances in various industries.

Illite is a mineral of white clay with a tightly interlinked molecular structure that makes it a non-swelling clay. It is a natural mineral found in sediments, soils, and metamorphic rocks (Kumari and Mohan, 2021). Illite is a non-swelling clay mineral belonging to the mica group. Illite is formed through the weathering of feldspar-rich rocks and sedimentary processes involving the alteration of micas. Illite presents a contrasting profile to montmorillonite. As a non-swelling clay mineral, illite is valued for its plasticity and stability. Its molecular structure, characterized by tightly interlinked layers, grants it strength and cohesion, making it an ideal material for ceramic products, construction materials, and as a constituent in drilling muds. Illite commonly forms through the alteration of mica minerals such as muscovite and biotite, as well as through the weathering of feldspar-rich rocks. This transformation involves complex chemical reactions under varying temperature and pressure conditions, leading to the development of illite-rich clay deposits in sedimentary environments.

Attapulgite, also known as palygorskite, is a fibrous clay mineral with a needle-like crystal structure (Zhang et al., 2017). It forms in magnesium-rich environments, such as marine sediments and volcanic ash deposits. Attapulgite is renowned for its exceptional adsorption and rheological properties, making it useful in applications such as adsorbents, thickeners, and as a stabilizer in drilling muds. Bentonite is a clay mineral mainly composed of montmorillonite, along with varying amounts of other minerals such as quartz, feldspar, and gypsum (Maxim et al., 2016). It typically forms from the alteration of volcanic ash in the presence of water. Bentonite is well-known for its swelling and adsorption capabilities, making it widely used in industries such as foundry, construction, drilling, and environmental remediation.

Talc is a soft, greasy-feeling mineral composed of magnesium, silicon, and oxygen (Kumari and Mohan, 2021). It forms through the alteration of magnesium-rich rocks such as serpentine and amphibole. Talc is renowned for its lubricating and antistick properties, making it a common ingredient in cosmetics, pharmaceuticals, plastics, and ceramics.

Vermiculite is a hydrated phyllosilicate mineral that undergoes significant expansion when heated, a property known as exfoliation (Rehman et al., 2023). It forms through the weathering of biotite and phlogopite minerals in certain geological environments. Vermiculite is valued for its lightweight, fire-resistant, and insulating properties, making it useful in horticulture, construction materials, and as a component in fireproofing and insulation products.

Table 2.2 Characteristics of clay soil

Parameter	**Values**
Bulk Density (Mg/m^3)	1.50 – 2.15
Dry Density (Mg/m^3)	1.20 – 1.75
Specific Gravity	2.55 – 2.75
Effective Cohesion (kPa)	20 - 200
Liquid Limit (%)	> 25
Plastic Limit (%)	>20

Source: Sharma (2020)

2.3.1 Consolidation and Compressibility

Clays are a type of soil that has lower bearing capacity and greater compressibility (Zaini et al., 2023). Clay deposits are commonly found in a wide variety and provide high compressibility, lower strength, and poor water quality. By definition, clays are of high compressibility and lower strength, most are sensitive, and their strength is reduced by disruptions. Soft soil particle thickness is significantly smaller than particle width and length. The term “soft earth” can be used to describe clay that incorporates aluminium hydro silicate and can be formed by hand.

Soil compressibility refers to the phenomenon wherein the application of a compressive force on soil leads to a change in volume due to the reorganisation of soil particles. Soil compression is generated by (a) water or air dislocation from empty spaces, (b) soil particle deformation, and (c) soil particle dislocation. Consolidation is a mechanism by which saturated soil particles are bundled more tightly together under constant static pressure over a long period of time. Water drains from the spaces between solid particles to carry out this process. The rate of compression and the volume of soil compressibility are required for the consolidation process. The odometer consolidation test is a useful tool for determining poor soil permeability (Cheng et al., 2020). Immediate settlement in clays happen before the elastic deformation of saturated and dry soils without altering the water content. Air is extracted from the void spaces due to the stress caused by the saturated soil. This method is often referred to as an elastic settlement. The primary consolidation settlement occurs when the pore pressure, which is the dominant factor in the void spaces, is released. As a result, the cohesive, saturated soil shifts, causing water to disperse. When the primary consolidation happens, the rate of movement between the particles is highest, and the shear stress will induce the peak resistance to change in volume (Liu et al., 2020). Clay has been identified as providing improved load power combined with a large decrease in settlement. In addition, consolidation settlement is increased and post-construction settlement is decreased in addition to being granular or crushed gravel with easily drained material. (Beyene et al., 2023). The very first phase, described as the preliminary compression or elastic settlement (immediate settlement), is triggered by preloading. The second phase, referred to as primary consolidation, observes an increase in soil volume and the dissipation of excessive water pressure. The third phase, referred to as secondary consolidation, is when the soil particles shift and undergo plastic deformation, causing the excess water pressure to release.

As described by Salimnezhad et al. (2021), clay soils are solid under normal conditions, but when filled with water, they lose their stiffness. The principal factor contributing to the uneven settlement and insufficient carrying capacity is the degradation of clay's strength and stiffness, which poses a potential threat to the structural integrity of the building's foundation. Clay is created when the water content of disturbed cohesive soil exceeds its liquid limit. This kind of soft soil cannot tolerate extreme stress and ends up being troublesome in construction. When working with soil in building materials, there are a variety of soil characteristics that need to be noticed, including internal friction angle, cohesion, capillarity, permeability, and elasticity. Thus, it is important to identify these properties in order to develop a rational approach to solve civil engineering difficulties presented by clay soil.

2.3.2 Undrained Shear Strength

Untapped shear strength serves as a fundamental geotechnical measurement that is utilised to evaluate the stability and load-bearing capacity of foundations in saturated clay soils (Wang et al., 2022). In engineering design, undrained shear strength is a crucial consideration, as instability can happen due to shear failure. A natural soil material with fine grains that contains clay particles is called clay. The engineer has a difficult task since clay is very compressible and has low shear strength. The engineer has a part to play in maintaining the shear strength that can sustain the system and to ensure that there is no unnecessary settlement. There are several ways to assess shear strength, either by lab tests, field experiments, or both. The soil load, or internal resistance of each unit area of the soil mass, is computed using the shear strength test. The strength of clay may be ascertained using a field valve test, a cone penetration test, an unconfined compressive strength test, or a traditional penetration test, as previously discovered (Sun et al., 2023; Wang et al., 2022). If the compressive strength of the clay is less than 50 kPa, it is considered unconfined clay; if it is less than 25 kPa, it is considered very clay. Instances of in situ tests include cone penetration tests, field valves, piezo-cones, and pressure metres, regular penetration tests; triaxial tests; laboratory valves; unconfined compression tests; and direct simple scissors (DSS) tests, which are classified as lab tests. Table 2.3 illustrates the classification of clay soil's undrained shear strength.

Table 2.3 Categorisation of undrained shear strength of clay soil

Solidity	**Undrained Shear Strength (kN/m^2)**
Hard	>400
Very stiff	200-400
Stiff	100 -200
Medium	50-100
Soft	25-50
Very soft	0 – 25

Source: Das and Sobhan (2015)

The repository environment, the backdrop of stress, the materials, frameworks, and physical and mechanical qualities all affect the degree of undrained shear strength (Lyu et al., 2020). Deshpande et al. (2021) reported that soft soil could lead to unnecessary settlement, leading to undrained deterioration of the infrastructure if no appropriate land development is achieved. Some soils are simply not capable of bearing the pressure or force placed on them by the foundation of a house. As a consequence, the foundation would fall into the soft soil.

2.4 Critical State Theory

In 1958, Roscoe, Schofield, and Wroth published a paper on soil yielding that introduced the idea of critical state theory. Several subsequent publications were produced as a result of further investigation, primarily within the Engineering Department at the University of Cambridge, United Kingdom. A theoretical framework known as "critical state theory" explains how applied stress, shear strength, and volume interact with one another in different types of soil, providing a common thread. The manifestation of this concept assumes the structure of a model. It was hypothesised that soils that have been drained and saturated experience compression when subjected to loading, resulting in a reduction in both their volume and water content. Conversely, upon relief from stress, these soils expand and exhibit an increase in both parameters. However, in the absence of drainage, the amount of soil remains constant despite fluctuations in pore water pressure (Duan et al., 2023; Santos et al., 2020). Permeability affects how quickly tissues compress or swell. Sand moves very quickly, whereas clay moves quite slowly. It is extremely difficult to adequately characterise soil behaviour for over-consolidated and undrained soil since the Mohr-Coulomb failure theory ignores volume changes. A critical specific volume and shear stress cause soils to yield and reach their critical state strength. This yielding is therefore thought to occur at a location on the three-dimensional "failure" envelope of the state boundary surface. The material does not expand or contract when sheared or vibrated, which is when the crucial void ratio would occur (Xiao et al., 2016).

2.4.1 Definition of State Parameters

To establish the critical state line, a graph representing the particular volume compared to the effective stress must be constructed in order to reach the desired ratio of voids (Whitlow, 2001). In Figure 2.2, the location in space of the critical state line (CSL) is depicted inside a graph representing the volume-mean normal effective stress. It is seen that the CSL is situated slightly below and parallel to the NCL.

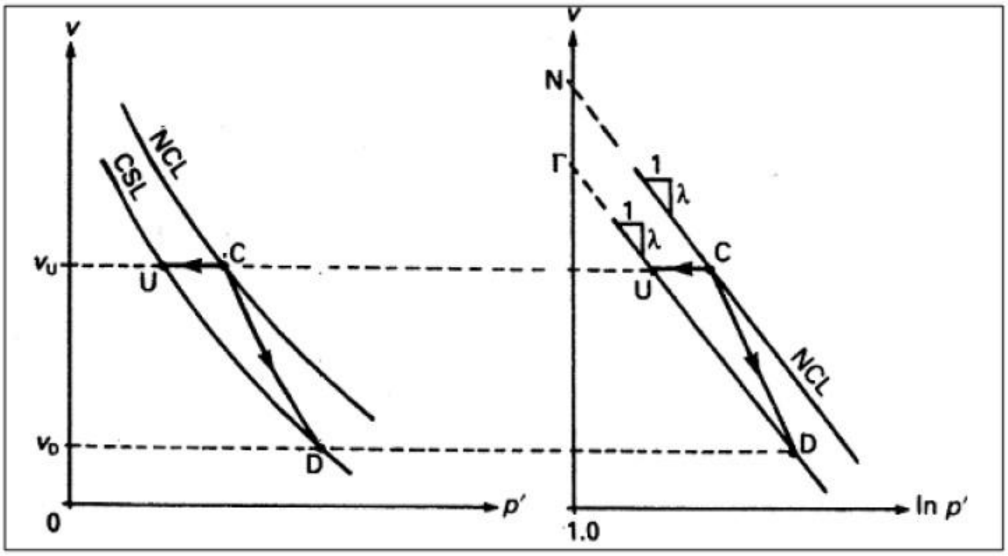

Figure 2.2 Critical state line and stress pathway for undrained loads on normally consolidated clay

Source: Whitlow (2001)

$$q = Mp' \tag{2.1}$$

$$M = \frac{6Sin\phi'_c}{3 - Sin\phi'_c} \tag{2.2}$$

$$v = \Gamma - \lambda \ln p' \tag{2.3}$$

$$\lambda = \frac{C_C}{\ln(10)} = 0.434C_C \tag{2.4}$$

In which:

M = The Slope of Critical State Line on the p'- q' plane

v = Specific Volume = 1+e

e = Void ratio

Γ = Intercept of Critical State Line with the v – axis

The parameters q and p' for the state are defined as:

$$\text{Deviator stress, } q = \sigma'_1 - \sigma'_3 \tag{2.5}$$

$$\text{Mean normal effective stress, } p' = \frac{1}{3}(\sigma'_1 + 2\sigma'_3) \tag{2.6}$$

In which:

σ'_1 = Effective Vertical Stress

σ'_3 = Effective Confining Pressure

2.4.2 State Boundary Surface

Two distinct stress paths, one for drained and one for undrained specimens, are proposed by Whitlow (2001). The stress trajectories for six tests conducted on consolidated drained specimens (CD) and consolidated undrained specimens (CU) within the q: p' area are depicted in Figure 2.3(a). The diagram presented in Figure 2.3(a) demonstrates that both the undrained and drained trials culminate at the same failure envelope, denoted as q=Mp′. The sole differentiation is in the variation of volume during the shearing stages in drained testing, while it remains consistent in undrained tests. The stress pathways CU and CD have a similar shape, as seen in Figure 2.3(b).

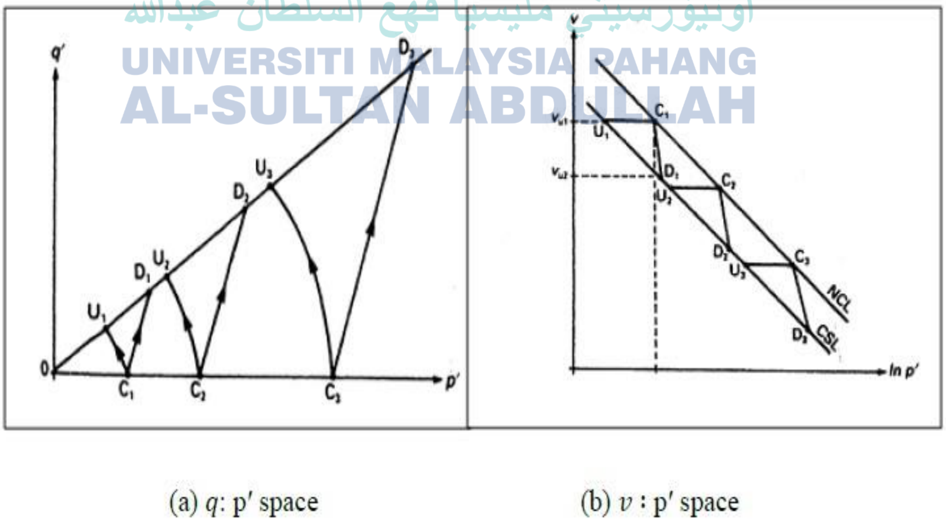

Figure 2.3 Plots of triaxial tests results of CU and CD

Source: Whitlow (2001)

Whitlow (2001) claims that these stress channels travel through the Roscoe surface; a three-dimensional surface whose boundaries are the normal consolidation line

(NCL) and the critical state line (CSL). The Roscoe surface applies when the stress route begins at NCL in typically consolidated soils. The second part of the boundary surface, the Hvorslev surface, controls the amount of severely over-consolidated soil that can be surrendered. The zero tensile stress, or "no tension cut-off," is the third part of the state and is speculated to be the limit for soils (Schofield et al., 1968). The entire soil boundary surface is depicted in Figure 2.4. The following are the boundary surface equations:

$$\text{No tension cut-off}: \ q = 3p' \tag{2.7}$$

$$\text{Hvorselev}: q = Hp' + (M - H)\exp\frac{\Gamma - v}{\lambda} \tag{2.8}$$

$$\text{Roscoe Surface}: q = Mp\left(1 + \frac{\Gamma - v - \lambda \ln p'}{\lambda - K}\right) \tag{2.9}$$

In which:

q : Deviator stress

p' : Mean normal effective stress

H : The Slope of Hvorslev surface on the q-p' plane

v : Specific Volume = 1 + e

Γ : Intercept of Critical State Line on the with the *v* – axis

M : The Slope of Critical State Line on the q – p' plane

λ : The Slope of Normal Consolidated Line with the *v* – p' space

ϕ'_C : Critical Internal Friction Angle

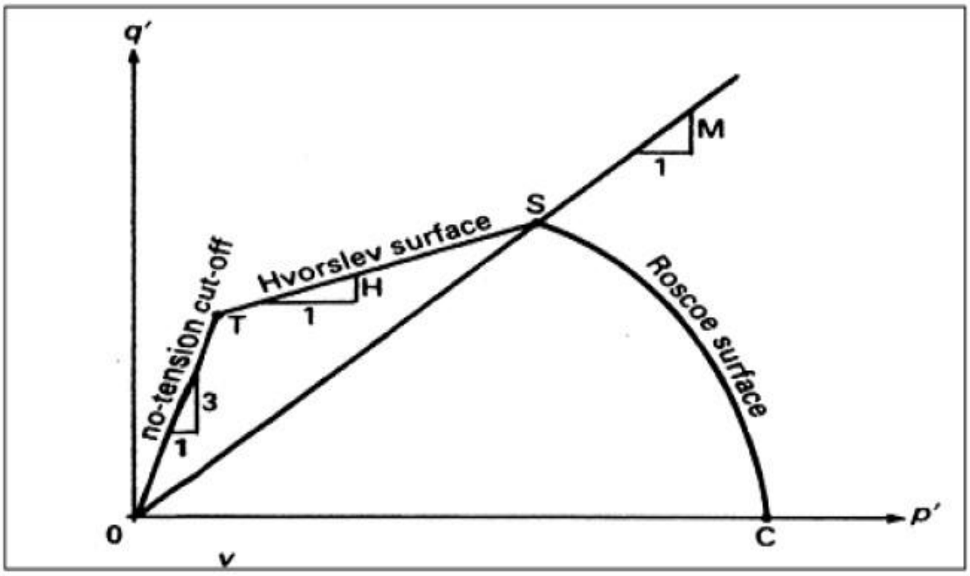

Figure 2.4 The critical state boundary surface
Source: Whitlow (2001)

2.4.3 Critical Void Ratio Line

Whitlow (2001) commonly employed the term "critical void ratio" to denote a specific state of sand. A thorough description of this state is still lacking, even though there are two distinct definitions: one that deals with changes in volume during drained testing (Casagrande, 1938), and another that deals with variations in effective stress and the ensuing changes in strength during undrained tests (Taylor, 1948). The clarity of those formulations may be improved by utilising the idea of loading pathways inside the (p, e, and q) space. For clays, the idea of void ratio holds true as well. In a drained test, the ultimate state of a sample is referred to as the critical void ratio state when additional shear distortion escalation does not change the void ratio. Within a particular set of drained tests, it is possible to predict the expected positions of the crucial void ratio points to lie along a linear route on the drained yield surface During an undrained test, the void ratio of the specimen remains constant while the effective stress experiences variations, ultimately resulting in a critical void ratio that must be maintained throughout the shearing process. After a series of undrained tests, it is anticipated that the set of important void ratio points would lie on or close to a line on the undrained yield surfaces (which may or may not be the same as the line previously specified). According to the results of the drained and undrained trials, every loading path in (p, e, q) space converges to a single, distinct line. The critical void ratio line is the name given to the curve in question. The line representing the critical void ratio will exhibit parallelism to both the drained and undrained yield surfaces. If the two surfaces are indeed identical, the yield surface would be constituted by the shared surface.

2.4.4 Undrained Shear Strength

Equation 2.3 and Equation 2.5, which are the two CSL equations, may be used to find the connection between the parameters Γ, λ, and v and the deviator stress at the critical state:

$$q = M \exp[\frac{\Gamma - v}{\lambda}] \qquad 2.10$$

The undrained shear strength, S_u is q/2, therefore, by using critical state analysis, the soil's undrained shear strength becomes:

$$S_u = \frac{1}{2} M \exp[\frac{\Gamma - v}{\lambda}] \qquad 2.11$$

The critical state parameters M, Γ and λ are unique for the respective type of soils.

2.4.5 Critical State Parameters of Some Types of Soil

Marto (1996) investigated the effects of cyclic undrained loads with periods between drainage rests on isotropically and anisotropically cemented Keuper Marl Silt in order to develop an efficient stress volumetric compression model with an experimental basis. Three phases of undrained two-way cyclic loading were included in the experimental programme, along with monotonic strain-controlled triaxial testing (containing both isotropically and anisotropically consolidated tests). The critical state boundary surface was tested on silt that is often over-consolidated. The plastic silt used in this study exhibits the subsequent characteristics: a specific gravity (Gs) value of 2.66, a liquid limit (w_L) of 36%, a plastic limit (w_P) of 17%, and a plasticity index (I_P) of 19%. A series of four experiments were conducted to determine the critical state border surface and critical state characteristics. These experiments include isotropic consolidation, anisotropic consolidation, monotonic triaxial compression, and monotonic triaxial extension. To determine the characteristic consolidation line, swelling line, and recompression line, the two specimens were exposed to isotropic consolidation, followed by swelling and then recompression. To create the swelling line and K_o-line, two more samples were anisotropically consolidated. Furthermore, the researchers conducted triaxial testing on samples that had undergone anisotropic and isotropic consolidation processes, each subjected to distinct stress histories. The findings of this investigation revealed that the slope of the critical state line, the compression failures envelope, and the normal consolidation line exhibited uniformity among samples that underwent both anisotropic and isotropic compaction. The following are the Keuper Marl Silt critical state parameters as determined by Marto (1996) using the compression test:

$\lambda = 0.08$, $N = 2.062$, $\Gamma_c = 2.026$

$k = 0.02$, $N_{KO} = 2.062$, $Mc = 1.16$

$\xi = 0.0141$, $\Gamma_c = 2.023$, $Mc = 1.04$

In which:

λ = Slope of normal consolidation line

Γ_C = Specific volume of soil (in compression) on the critical state line

k = Slope of over-consolidation (swelling) line

N_{KO} = Specific volume of anisotropically normally consolidated line

M_C = value of M triaxial compression test

ξ = slope of u/p'_e versus ε plot

The critical state point was found to be equal to 0.69 at p'/p'_e axis and 0.8 at q/p'_e axis in the q/p'_e - p'/p'_e plot, with the Hvorslev surface equation obtained as:

$$\frac{q}{p'_e} = 0.26 + 0.78\frac{p'}{p'_e} \qquad 2.12$$

Table 2.4 presents the compilation of critical state characteristics for various soil types, as collected by previous researchers, as documented by Marto (1996).

Table 2.4 Critical state parameters of some soil types

Soil	**λ**	**Γc**	**N**	**M**	ϕ'_c	**k/λ**
			Fine Grained Soils			
London Clay	0.16	2.45	2.68	0.89	23^0	0.39
Kaolin Clay	0.19	2.14	3.26	1.00	25^0	0.26
Glacial Clay	0.09	2.81	1.98	1.18	29^0	0.16
			Coarse Grained Soils			
River Sand	0.16	2.99	3.17	1.28	32^0	0.09
Decomposed Granite	0.09	2.04	2.17	1.59	39^0	0.06
Carbonate Sand	0.34	4.35	4.80	1.65	40^0	0.01

Source: Marto (1996)

2.5 Kaolin Clay

Kaolin, also referred to as China clay, is a pliable white clay material that carries notable importance as an ingredient in the production of porcelain. Additionally, it is widely applied in the creation of paper, rubber, paint, and various other commodities. This clay substance is widely accessible and finds extensive use in various applications such as ceramics, paint extenders, paper coatings, paper fillers, cracking catalysts, rubber fillers, plastic fillers, and cement blocks. Kaolinite is the predominant mineral constituent found in kaolin, a substance that often includes mica and quartz. In rarer instances, kaolin may also contain anatase, haematite, bauxite, zircon, illite, halloysite, kyanite, sillimanite, ilmenite, attapulgite, graphite, montmorillonite, feldspar, and rutile (Adeniyi et al., 2023; Dill, 2020). Kaolin is named after the mountain from which it has been extracted in China for generations (Kao-ling). It is a versatile industrial mineral and is widely used in ceramics, paint, plastics, paper, rubber, ink, catalysts, insecticides, pharmaceutical formulations, and more, as fillers or raw materials. The key properties of kaolin that are vital for commercial use include its distribution of particle form, size, and more (Yahaya et al., 2017). The distinctive qualities of kaolin are its particle size and colour. Kaolin is usually based on a fine mineral aggregate that is almost white in colour and has high plasticity. Most clays involve at least some kaolinite, and some clay beds are completely kaolinite. Kaolinite is found everywhere in stream beds, rocks, soils, and many other locations. In most parts of the globe, kaolinite has a pink-orange-red colour owing to iron oxide, giving it a unique rust hue. China clay or kaolin are the terms for kaolinite-rich rock. Because of its low strength qualities, kaolinite clay is regarded as a weak soil. Kaolinite clay is found in most soil types in Malaysia as a clay mineral, which is why this study focuses mainly on kaolin clay.

2.5.1 Chemical Properties of Kaolin

One component of an industrial mineral that undergoes chemical breakdown and contains $Al_2Si_2O_5(OH)_4$ is kaolin. It is a tier silicate mineral that has one octahedral sheet of aluminium and one tetrahedral sheet joined by oxygen atoms. Kaolin is a mineral with a chemical structure made up of ordered hydrated aluminium silicate arranged in a 1:1 ratio. It possesses a very fine particle size and is composed of one layer of silicon-oxygen (SiO_4) tetrahedra and one layer of aluminium-oxygen/hydroxide ($[Al\ (O, OH)_6]$) octahedra. Alternatively, it can be described as a $[Si_2O_5]^2$ sheet and a [Al2(OH)4]2 sheet, which are interconnected through the exchange of apical oxygen and reciprocal bonding. The conceptual formulation of the compound is $Si_2Al_2O_5(OH)_4$. Other formulations include $Al_2O_3{\bullet}2SiO_2{\bullet}2H_2O$ and $Al_2O_7Si_2{\bullet}2H_2O$. The molecule possesses a molecular mass of 258,071 (Alaba et al., 2015). Figure 2.5 depicts the chemical composition of kaolin.

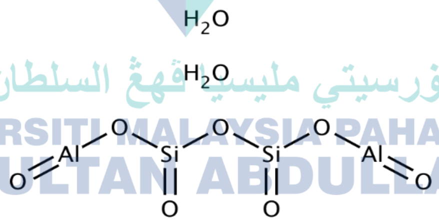

Figure 2.5 Chemical structure of Kaolin

Referring to the results reported by researchers, the main ingredients of kaolin are silica and alumina, as the amounts of silica and alumina are the highest and second-highest among the chemical compositions, respectively. Silica is one of the ingredients of cement and occupies 19%–23% of the cement mass. It is chemically expressed by SiO_2, which is also called silica dioxide. Silica improves the structural integrity of cement. Alumina is also part of the cement composition, which is chemically expressed by Al_2O_3. Cement contains 2%–6% alumina in its mass and adds quick-setting properties. Based on the findings of researchers, it has been observed that kaolin exhibits a substantial proportion of silica and alumina. Thus, it has cementitious and pozzolanic characteristics by itself. Unfortunately, the character is weak, and the situation becomes worse when there are numerous voids and high-water content. Therefore, the admixture is needed to improve the strength of kaolin.

The study conducted by Chigondo et al. (2019) revealed that the percentages of silica and alumina were 58.02% and 20.34%, respectively. The kaolin utilised in this investigation was purchased from Chemtex Corporation, an Indian commercial provider situated in Kolkata. According to the findings of Yahaya et al. (2017), the kaolin sourced from Kaolin (Malaysia) Sdn. Bhd. has around 57.63% silica and 37.77% alumina. According to the study done by Hajkova (2018), the kaolin sample that was examined had an alumina concentration of 41.03% and a silica content of 52.03%. According to Chen et al. (2020), the percentages of alumina and silica are 39.53% and 46.51%, respectively. The chemical composition of kaolin is shown in Table 2.5.

Table 2.5 Chemical composition of kaolin

Chemical Content	**Percentages (wt %)**			
	Chigondo et al. (2019)	**Yahaya et al. (2017)**	**Chen et al. (2020)**	**P. Hazkova (2018)**
SiO_2	58.02	57.63	46.51	52.03
Al_2O_3	20.34	33.77	39.53	41.45
MgO	1.99	0.596	0.023	0.13
CaO	2.29	0.346	0.059	0.15
K_2O	0.71	1.801	0.42	0.79
TiO_2	2.05	0.605	-	1.62
Fe_2O_3	1.35	0.860	0.73	1.05
P_20_5	0.45	0.311	-	0.26
LOI	10.95	-	-	2.52

2.5.2 Physical Properties of Kaolin

Dickite, kaolinite, and halloysite are categories of minerals of kaolin and clay generally found in nature. One distinguishing characteristic of kaolin, as compared to other types of clay, is its controllable particle size, smooth texture, and white colour.

Hasan et al. (2018) used kaolin power grade S300 obtained from Kaolin (M) Sdn. Bhd. in Puchong, Selangor, Malaysia. According to Kaolin (M) Sdn. Bhd. (2011), kaolin clay can be described as a chemically hydrated aluminium silicate that remains functionally unchanged. Slurring untreated clay may create water cleaned with kaolin, and any pollutants can extracted by sieving. Damoerin at al. (2015) examined the physical characteristics of the kaolinite clay used for the triaxial test to mimic realistic circumstances. Zaini and Hasan (2023) used the untreated kaolin specimen in powder form and white colour from the kaolin industry collected from Kaolin (M) Sdn. Bhd., where the materials were examined for physical characteristics in compliance with BS 1377: Part 2: 2022. According to Sasikumar (2016), the soil utilised for this study was kaolinite sourced from English India Clay Limited, Trivandrum. The characteristics of kaolinite employed for the experimental examinations are shown in Table 2.6.

Table 2.6 Physical properties of kaolin clay from previous works

Parameters	Researchers			
	Hasan et al. (2018)	**Damoerin et al. (2015)**	**Sasikumar (2016)**	**Zaini and Hasan (2023)**
Liquid Limit w_L (%)	36.00	77.93	66.00	69.00
Plastic Limit w_P (%)	26.00	39.10	33.00	36.00
Plastic Index I_p (%)	10.00	38.83	33.00	33.00
Specific Gravity G_s (mg/m^3)	2.62	2.59	2.70	2.68

2.5.3 Mechanical Properties of Kaolin

Based on the research directed by Hasan et al. (2018), it was determined that the ideal moisture level for kaolin is approximately 20 percent, while the maximum dry density is measured at 1.55 mg/m^3. The permeability coefficients of kaolin have been determined to be 8.96x10^{-12} m/s. The primary aim of conducting the falling head permeability experiments was to assess the hydraulic conductivity of kaolin, a fine-grained soil material. Furthermore, Das and Soni (2015) conducted an empirical investigation on a kaolinite sample that is commonly employed in industrial applications. The permeability coefficients of kaolin were measured to be 5.00 x 10^{-7} m/s. Comparing the results to Liu et al. (2015), it was discovered that 15% of the sample had the ideal water content and that the maximum dry density for kaolin was

1.70 mg/m^3. Permeability coefficients for kaolin were 5.60 x 10^{-9} m/s. Mousavi and Wong (2016) found that after analysing the properties of kaolin, the best water content was found to be 18.10 percent, and the maximum dry density observed for kaolin was 1.63 mg/m^3. The permeability coefficients of kaolin were determined to be 5.80 x 10^{-10} m/s. Table 2.7 presented herein provides a comprehensive overview of the mechanical properties of kaolin as reported in prior scholarly investigations.

Table 2.7 Mechanical properties of kaolin from previous works

Parameters	**Researchers**			
	Hasan et al. (2018)	**Das and Soni (2015)**	**Mousavi and Wong (2016)**	**Liu et al. (2015)**
Maximum Dry Density, (mg/m^3)	1.55	1.78	1.63	1.70
Maximum Moisture Content (%)	19.40	18.37	18.10	15.00
Permeability, k (m/s)	8.96 x 10^{-12}	5.00 x 10^{-7}	5.80 x 10^{-10}	5.60 x 10^{-9}

2.5.4 Summary

Clay minerals, encompassing a diverse range of types such as montmorillonite, illite, kaolinite, and others, exhibit inherent weaknesses that present challenges in geotechnical engineering and construction activities. These weaknesses, though varying in intensity across different clay types, collectively underscore the need for ground improvement techniques to enhance soil stability and mitigate potential risks. Clay minerals, including montmorillonite, illite, and kaolinite, are known for their high plasticity, which results in significant volume changes in response to changes in moisture content. This plastic behavior can lead to soil instability, settlement issues, and structural damage in buildings and infrastructure. Illite, while less prone to swelling, still presents issues related to its low load-bearing capacity and susceptibility to shear failure. Kaolinite, with its low plasticity, may seem less problematic; however, its poor drainage characteristics and vulnerability to erosion make it susceptible to slope instability and foundation settlement. Despite these variations, common weaknesses persist among clay minerals, including low permeability, which impedes effective drainage and increases the risk of water-related issues such as swelling and shrinkage.

Moreover, the inherent plasticity of clay minerals, regardless of type, can lead to settlement problems and structural damage in buildings and infrastructure.

Addressing these weaknesses requires tailored ground improvement strategies that account for the specific characteristics of the soil and the intended engineering objectives. Techniques such as soil stabilization, compaction, and reinforcement play crucial roles in enhancing soil strength, reducing deformability, and improving overall performance.

2.6 Polypropylene

Polypropylene (PP) is a thermoplastic product that has been commonly used in several industrial applications as a matrix material on account of its flexibility to accommodate various forms of fillers and reinforcements, a wide range of physical properties, a good balance of mechanical properties, good manufacturing properties, and low cost. Because polypropylene has a low specific gravity, it produces the most fibre for a given weight, which ensures that polypropylene provides decent bulk and cover despite being lighter in weight. In automotive and mechanical engineering, the use of polypropylene composites has increased primarily because of their outstanding rigidity, which allows them to be substituted for traditional materials. Plastic is one of the biggest waste products produced by people around the world.

As plastics are now involved in every area of our lives, recycling waste plastics, which is an effective way to handle and treat waste plastics, has become an essential part of the industry at present. In contrast to their virgin products, plastic recycling is an economic and beneficial way of saving 20%–50% from the consumer price point (Ozbakkaloglu at al, 2017). However, many recycled polymeric materials, including polypropylene, are still disposed of in landfills or incinerated during the recycling of waste plastic (Jagadeesh et al., 2022), eventually resulting in secondary contamination or lack of landfill space. In order to lessen the load of the current municipal solid waste disposal programmes, such as open dumping or landfilling, ongoing efforts are also required to identify the best long-term alternative. Faced with the challenges of environmental issues and the recycling of polypropylene waste materials, research experiments have recently started to be carried out to better utilise these items. Using waste material as soil reinforcement can be one of the most effective and sustainable solutions for the environment.

2.6.1 Chemical Properties of Polypropylene

The molecular architecture of porous polypropylene (PP) has a distinctive arrangement of CH_3 groups that are localised on a specific facet of its carbon backbone. This structural feature imparts enhanced rigidity, increased crystallinity, and heightened resistance to deformation under applied mechanical forces compared to polyethylene (PE). The chemical composition of polypropylene is depicted in Figure 2.6.

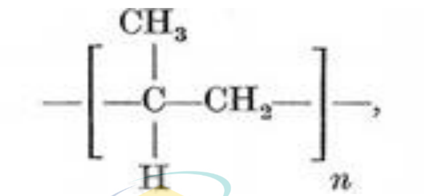

Figure 2.6 Chemical structure of Polypropylene
Source: Maddah (2016).

It is more difficult and obscure to sustain temperatures as high as 160°C (320°F) without softening. These materials have the ability to be repeatedly melted and heated to a specific temperature before they cool and solidify once again. The degree of crystallinity in the material displays a transitional feature that exists between low-density polyethylene (LDPE) and high-density polyethylene (HDPE). The material under examination has a lower strength-to-density ratio when compared to HDPE and LDPE. It encompasses densities that range from 0.90 to 0.92 g/cm^3.

2.6.2 Properties of Polypropylene

Due to its low density, good process ability, great mechanical properties, and chemical resistance, polypropylene (PP), an important polymer in modern society, is extensively prepared and used in our everyday lives (Yin et al., 2015). As polypropylene is essentially plastic with a low water absorption rate, it cannot undergo tests that are conducted in a geotechnical lab that is exclusively dedicated to soil testing and used in our everyday lives (Yin et al., 2015). The characteristics of polypropylene (PP) were reported by Titan Petchem (M) Sdn. Bhd. in a study done by Hasan et al. (2018). The manufacturer's material data table indicates that the polypropylene utilised in Correia et al.'s (2015) research has a density of 905 kg/m^3, tensile strength of 250

N/mm^2, and Young's modulus of 3500–3900 N/mm^2. Kalantari et al. (2015) used polypropylene with 300–440 MPa tensile strength and no water absorption. Table 2.8 presents the characteristics of polypropylene as demonstrated in previous research.

Table 2.8 Properties of polypropylene from previous works

Parameters	**Researchers**		
	Hasan et al. (2018)	**Correia et al. (2015)**	**Kalantari et al. (2015)**
Density (g/cm^3)	0.9	0.905	0.91
Tensile Strength (N/mm^2)	330	250	300-440
Water Absorption (%)	0.002	-	-

2.6.3 Summary

Polypropylene (PP) exhibits a range of characteristics that make it an attractive material for various industrial applications, including ground improvement techniques such as stone column reinforcement. PP is a versatile thermoplastic material known for its flexibility in accommodating fillers and reinforcements, wide range of physical properties, good mechanical strength, and low cost. Its low specific gravity allows it to provide significant bulk and cover despite its lightweight nature, making it an ideal choice for ground improvement applications where both strength and economy are paramount. One key advantage of PP is its chemical composition, which includes a distinctive arrangement of CH_3 groups on its carbon backbone. This molecular structure imparts enhanced rigidity, increased crystallinity, and heightened resistance to deformation under mechanical forces compared to other polymers. Additionally, PP exhibits good processability, mechanical properties, and chemical resistance, making it extensively used in everyday applications. In the context of ground improvement, PP's properties, such as its high tensile strength and low water absorption rate, make it particularly suitable for reinforcing stone columns. Research studies have demonstrated the effectiveness of PP in enhancing the load-bearing capacity and stability of soil when used as a reinforcement material. By utilizing recycled PP materials, such as waste plastics, in ground improvement projects, not only can environmental challenges related to plastic waste disposal be addressed, but also sustainable solutions can be achieved.

Overall, the characteristics of polypropylene, including its chemical properties, mechanical strength, and environmental sustainability, position it as a promising material for ground improvement methods like stone column reinforcement. By leveraging the unique properties of PP, engineers can enhance the performance and longevity of infrastructure projects while promoting environmental stewardship through the utilization of recycled materials.

2.7 Soil Reinforcement

Soil reinforcement is a method employed to improve the mechanical properties of soil to enable it to withstand increased loads and maintain its structural stability. When the soil can handle a large load and the related sedimentation is manageable, top-quality soils are the first choice for building. With increased urbanisation and land use, these locations could not be as readily accessible, necessitating the use of less ideal soils like clay. When a site does not meet the necessary design requirements, it is considered to have poor soil conditions. When the ground can hold a heavy load and the related sedimentation is manageable, quality soils are the best choice for construction. With increased urbanisation and land use, these locations could not be as readily accessible, necessitating the use of less ideal soils like clay.

Engineers must utilise a solution if the recommended location is determined to perform poorly. Several choices exist, including removing the existing, subpar soils by digging them up, abandoning the location, redesigning the building, or improving the soil's properties. First off, lowering the cost of transportation and shipping, resource accessibility, and environmental problems cannot be achieved by excavating in the now unstable soil. Second, abandoning the project is only allowed if a suitable location is available and there is no binding decision to keep the project at that particular location. Thirdly, the structural design can be changed or updated to better fit the soil conditions by driving the shaft deeper into a layer of strata beneath the weak soil that can support more weight. The methods previously stated, however, are only effective for a little time. For long-term growth, improving soil properties is preferred.

There are a few ways to improve soil in order to acquire geotechnical features that are modified without the use of products, including the incorporation of special materials and the provision of reinforcement for the soil. The function of tree roots and other living things in nature provide numerous examples of the old practice of soil reinforcing. These developments are known to have taken place between the fifth and fourth century B.C. This concept is utilised to improve a variety of desired soil qualities, including permeability, shear strength (c and ϕ), bearing capacity, and so on. The concept and principle under consideration were originally formulated by Jones (2013), who conducted a study illustrating the enhanced shear resistance of a soil mass through the incorporation of reinforcement elements. Significant progress has been achieved in soil reinforcing technology in the last several years, leading to its widespread use in a variety of fields. These applications encompass the augmentation of drainage capabilities, filtration efficiency, and load-bearing capacity.

The incorporation of reinforcing inclusions inside a soil mass is a highly efficient and effective way to enhance the engineering qualities of soils. Improving the soil's carrying capacity, stability, and ability to withstand lateral deformation are the main goals of soil reinforcement. Reinforced soils can be achieved through the incorporation of continuous reinforcement inclusions, such as sheets, strips, or bars, in a prescribed arrangement within a soil mass. This method is known as systematically reinforced soils. Numerous scholars have extensively examined conventional techniques for enhancing soil quality and their efficacy over an extended period. These strategies encompass the utilisation of reinforcement elements such as sticks, boards, strips, textiles (Yan et al., 2016), and membranes (Oyegbile and Oyegbile, 2017).

The utilisation of natural materials, including jute (Kumar and Srivastava, 2017; Wang et al., 2017; Zaidi et al., 2016), coir (Subramani and Udayakumar, 2016), sisal and bamboo (Hegde and Sitharam, 2015; Malakar and Sultana, 2021), for soil reinforcement is prevalent in numerous countries. Stone columns and geosynthetic reinforcement are well recognised as prominent ground improvement techniques within the field. However, a number of researchers have done a great deal of studies on how these techniques are applied in various circumstances. Engineers choose these structures because they are straightforward, simple for construction, and often cost-effective as well.

2.8 Columns in Soil

Multiple types of materials have been employed thus far as column materials with the purpose of enhancing soil strength. In addition, numerous methodologies have been implemented to augment the stability of peat soil deposits, including the application of precast stabilised peat columns (Kalantari and Rezazade, 2015), lime columns (Prakash et al., 2022), 2022), and cement-treated soil columns (Namikawa, 2016) among others. It is commonly known that the stone column approach works well to increase the bearing capacity and decrease the consolidation settling of the soil (Shehata et al., 2021; Muneerah et al., 2016; Chen et al., 2022).

The technology of stone column construction was first established in European countries during the early 1960s, which was afterwards used worldwide. Vibrated stone columns have been widely utilised in soil stabilisation projects in Europe, Asia, and the United States over the past three decades. The contemporary utilisation of this method has become more prevalent owing to its ability to provide significant cost reductions and adhere to predetermined schedules, hence surpassing conventional piling techniques in various scenarios. The initial load transfer suggestion, the ultimate bearing capacity evaluation, and the settlement calculation in stone columns were proposed by Sexton et al. (2016). There are two distinct types of stone column collapses found in a weak subsoil layer: bulging (Al-Obaidy et al., 2016) and shear failure (Kumar et al., 2022). According to Etezad et al. (2015), the primary cause of failure in an individual stone column is predominantly associated with bulging. However, failure via general, local, or punctured shear processes may also result from the presence of various stone columns combined with the surrounding soil.

The soil's properties, the columns' shape, and the system's overall design all influence the precise mode of collapse. The geometric properties of the ground, the strength properties of the soft soil, and the stone column are used to determine the reinforced ground failure mechanism. According to Zukri and Nazir (2018), using a stone column in clay increases load power and significantly reduces settling. The consolidation settlement is enhanced as the substance is granular and readily drained. Hence, acceptance tests were carried out on-site and concentrated on either a small group of columns (finite group) or a single column (single-column loading). Stone columns are formed in the form of a vast assemblage, comprising an infinite group.

Stone columns work most efficiently when used to stabilise huge regions of clay soil. Their use in separate communities below the building foundations is constrained and is not used. As a result, broad-loaded regions that implement standardised loading on foundation soils like underwater reservoirs, tank farms, and fillings are a significant field of application.

There are certain disadvantages to using stone columns made of clay. Normally, radial drainage is restricted by the clay particles that seem to be trapped around the stone column (Zukri and Nazir, 2018). Small pads, strips, and extended loads are the three different loading scenarios that are often utilised in as a single column to support point loads (Castro, 2016). Because the stone columns function as a sand drain, they accelerate the consolidation process. Besides, the foundation can be reinforced by replacing the weak soil with high-strength materials.

2.8.1 Basic Physical Modelling of Columns in Soil

Shear strength has been conducted on cohesive specimens (Aslani et al., 2019), and it was noted that adding stone columns improve soft clay substrate's overall stiffness as well as its shear strength. Altering the stone columns' composition, area replacement ratio, and location has also been shown to potentially improve their shear strength. The single-column design has the least improvement in shear strength and stiffness values, while the square arrangement of columns has seen the most significant gain. Vertical drains and providing the soil with the appropriate support are the two main purposes of the stone columns. This allows the subsurface to consolidate fast under any given load. The lateral displacement of the stone during movements causes the hole diameter to frequently be larger than the matching diameter of the housing or probe. This is mostly dependent on the type of soil, the vibrating mechanism's features, the stone's length, its undrained shear strength, and the installation technique. This will determine the diameter of the stone columns by calculating the highest and lowest densities of stone and the compressed volume of material required to fill the hollow to a certain height.

In their work, Lima et al. (2019) conducted an investigation to describe the observed and simulated behaviour of a soft clay deposit that underwent reinforcement using stone columns. Next, in a coal and ore stockyard, the field performance of a soft foundation reinforced by stone columns was compared using numerical analysis. Performance along a 500-operational day was measured for a 130 m wide segment with two rocks stack. The serviceability behaviour of the stabilised region was observed using a sophisticated instrumentation that included 14 sensors. The PLAXIS 2D finite element code, in conjunction with complementary numerical research, enabled precise modelling of the increase in lateral earth pressure caused by the installation of columns. In order to facilitate the numerical investigation, a plane strain methodology was employed to turn the stone columns into equivalent walls. The results of this investigation showed how well the planar strain model could predict the total deformations seen in the reinforced foundation. The empirical observations from the field data were corroborated by the behaviour exhibited in the simulated excess pore pressure curves. These curves demonstrated a consistent decrease during the consolidation phases, followed by a maximum value at the onset of loading.

The implementation of stone columns in coherent soil often entails a load-bearing column of a well-compressed coarse aggregate in the field for many functions, such as for drainage, stabilisation, and densification. Poor sandy soils have an undrained shear strength ranging from 7 to 50 kPa, and the positioning of a stone column is critical. More weight is placed on the land as a result of the stone columns. Soil settling decreases as a result of the stone columns' increased shear strength, complementing the load increase (Basack et al., 2017). Kirsch and Kirsch (2017) found that the stress concentration factors which are primarily influenced by the toughness of the stone columns and the hardness of the soil were the most crucial in determining the structure of the stone columns.

Etezad et al. (2015) looked at a group of stone columns' capacity to support weight in soft soil. The use of tone columns is a strategy to ensure a practical, economical, and environmentally sustainable ground development. Using compacted aggregate materials to build columns is a commonly used method to increase the shear resistance and bearing capacity of weak soil as well as enhance its stability. However, it has been frequently observed that a solitary stone column experiences failure due to the phenomenon of bulging. The geometry of the system, the kind of soil, and the characteristics of the columns are among the elements that may result in perforated shear procedures. These global, local, or other mechanisms cause a collection of stone columns and the surrounding soil to collapse. The geometric properties and strength parameters associated with the soft soil and stone column may be analysed to identify the reinforced ground's failure process. This study presents a theoretical calculation of cohesive soil's improved load-bearing capability in the existence of shear-failure mechanisms and a rigid raft foundation. The limit-equilibrium approach was used in the suggested model, which also integrates the idea of the composite reinforced soil characteristics. Regarding the bearing capacity of foundations on homogenous soil, numerical and experimental investigations presented in the literature offer data in favour of the hypothesis. To facilitate a practical application, a design process and accompanying charts have been made available.

2.8.2 Previous Research on Columns in Soil

Clay soils can be strengthened by mounting stone columns. It has earned widespread success as a recognisable approach to improve bearing ability and reduce soft soil settlements. To assess the existence of the stone columns and, in particular, how they behave when erected in soft soil, several researchers have conducted laboratory studies.

In order to enhance soft soil, Roshan et al. (2023) conducted a numerical analysis of floating bottom ash columns that rest on embankments. In order to prevent major problems with strength, bearing failure, and settlement, the geotechnical engineer must overcome many obstacles while constructing an embankment on soft clay. In such cases, using stone columns can help improve bearing capacity and minimise settlement. The current study used numerical modelling approaches to examine how bottom ash columns behave when they are loaded by an embankment. The Plaxis 3D foundation program was utilised to accurately simulate the behaviour of soft soil reinforced with bottom ash columns underneath an embankment subjected to stresses produced by traffic. The dataset had two columns with lengths of 7.5 and 5 meters, respectively, as well as three distinct area replacement ratios (Ar) of 10%, 15%, and 20%. The variables incorporated in the study were as follows. The results showed that reducing the final settling and consolidation times was significantly impacted by increasing the Ar and column length. When the concentration of Ar gas reached 20%, a 58% reduction in settling was observed at a column depth of 7.5 m. The study proposed the use of bottom ash columns to enhance the geotechnical properties of the problematic soil beneath the embankment.

The installation procedure, behaviour of individual and group columns, and numerical plain-strain modelling of stone columns were documented by Kelesoglu and Durmus (2022). There exist three essential conditions that must be fulfilled in order for columnar stone to effectively mitigate the challenges posed by soft soil. To underscore the difficulty in modelling the behaviour of individual and collective stone columns designed to support soft soils using axisymmetric and plane-strain approaches, the study investigated the collective behaviour of stone columns through the use of two-dimensional plane-strain numerical models. The effects of differences in stiffness, drainage potential, and the presence of soft soils must be taken into account when modelling stone columns under plane-strain circumstances. The study investigated the feasibility of employing the expansion of the column shaft method in combination with two different conversion techniques that rely on comparable plane-strain permeability and stiffness. Numerical models for plane-strain and axisymmetric single-column column groups were built using the available centrifuge test data, which was thoroughly documented and used as a guide. After building the matching plane-strain permeability finite element model, the computed and observed findings were found to correspond well. Hence, the investigation's findings shed light on the plane-strain modelling of a collection of stone columns.

Grizi at al. (2022) conducted a numerical analysis of the settling behaviour of soft soil that was increased by stone columns. The use of columnar forms, such slabs and embankments, is commonly recognised as an effective way to enhance the settling properties and load-carrying ability of soft soil foundations for extensive arrays of columns to support an infinitely broad load. The goal of this study was to ascertain the relative importance of design factors, including footing shape, column spacing, column length, and the existence of a crust layer, in affecting the settlement performance of stone columns supporting shallow foundations. This study made use of a thorough 3D finite element analysis. Precise long-term settlement forecasts comprising drained and undrained evaluations were generated when a soft soil profile was generated and well characterised. Significant effects on the deformational behaviour of the stone columns were seen when the hard crust layer absent in laboratory models was discovered.

The study on soft soil reinforcement with stone columns was conducted by Mokhtari and Kalantari (2022), which found that using stone columns in clays can result in a notable decrease in settling as well as a minor increase in load capacity. While decreasing post-construction settlement, granular and easily draining material enhances consolidation settlement. In soft soils like North Carolina clay, silt, and peat, stone columns that are often installed on a volume displacement system by drilling a hole with a predefined diameter and appropriate depth may serve a particular function.

Thakur at al. (2021) conducted an experimental investigation of ground improvement by employing enclosed stone columns. Using stone columns made soft soils more rigid, increasing their load bearing capacity and speeding up the consolidation process, which reduced settling. The study aimed to ascertain if vertically and horizontally reinforced stone columns can take the place of traditional, unreinforced stone columns. Geotextile was used to reinforce stone columns vertically and was inserted into the columns on a regular basis to provide horizontal support in the form of circular geotextile discs. Three and four sets of unreinforced and reinforced stone columns were the subject of the model experiments on fragile sandy soil. The load-settlement reactions and failure modes of the reinforced and unreinforced groups were investigated. According to new research, stone column clusters with reinforcements have a higher load-bearing capability than clusters without reinforcements. Additionally, the set of four horizontally reinforced stone columns has slightly higher bearing capabilities (1-2%) with a 30 mm settlement than vertically contained stone columns, despite the fact that their bearing capacities are almost equal.

The behaviour of a single stone column wrapped in geotextile in soft soils was investigated by Farah and Nalbantoglu (2020). Stone columns are frequently used to increase the bearing capacity of weak soils. Both enclosed and unencased freestanding stone columns were investigated in this study to see how they fare in soft soils. However, few studies have been conducted on the topic of erecting stone columns on a single-layered dirt basis even though the former has been the subject of a great deal of study. Experimental pilot tests were conducted on a modest scale in this study to compare the performance of soft soil in a single layer with that of soft soil covered by a layer of loose sand. Every time stone columns were used, more and more soft earth was found to be available to support them. The stone columns' effect on the soft soil's capacity to sustain weight was measured using the bearing improvement ratio. Through distributing induced stresses across a greater region, the usage of geotextile increased bearing capacity. The greatest amount of bulging was observed in a stone column not covered by a single layer of soft soil at a depth of 1.5 times the column's initial diameter from the top; however, the largest amount of bulging was shown in an encased stone column in the same layer of soft soil at a depth.

Aslani at al. (2019) looked at the shear strength of a clay base reinforced by stone columns. The initial undrained reaction of a clay bed reinforced with a stone column was evaluated using a large direct shear testing apparatus within the plane measurements of 305 x 305 mm. This inquiry hazardously analysed the impact of significant constraints, including the percentage of zone substitution, the design of the stone section, the average weight value, and the substance of the stone segment. The experiments utilised two distinct materials, namely crushed gravel and fine-grained sand. Additionally, three various replacement ratios were implemented, namely single, square, and triangular stone column designs. In addition, standard pressures of 35, 55, and 75 kPa were used to get the desired result. The findings demonstrated that the installation of the stone column considerably increased the overall rigidity and shear strength of the clay substrate. Research investigations have demonstrated how several components affect the shear strength of stone columns. These factors include the column's material composition, the surrounding area's replacement ratio, and the column's structural characteristics. Square column layouts, on the other hand, were linked to the greatest and lowest increases in shear stiffness and strength values, respectively. Single columns had the reverse impact.

Hasan et al. (2019) conducted a number of experiments to see whether adding a single column of crushed coconut shells (CCS) would improve the clay's shear strength. Since CCS is a waste product, soil improvement expenses might be greatly decreased. The impacts of a single CCS column's height penetration ratio on the mechanical and physical characteristics of kaolin and CCS, as well as the shear strength parameters, were examined in this work. An unconfined compression test (UCT) was performed on four batches of kaolin samples, one of which was used as a control, to ascertain the shear strength. Four samples in total were taken from each batch to get the precise value. The columns constructed from crushed coconut shells had heights of 100 mm, 80 mm, and 60 mm, and their corresponding column penetration ratios were 1.00, 0.80, and 0.60, respectively. These were the experimental variables. The kaolin specimen was put through a series of sixteen unconfined compression tests, with each test using dimensions of 50 mm in diameter and 100 mm in height. As a result, the shear strength of columns reinforced with crushed coconut shells was found to significantly increase. In particular, when a 4% area displacement ratio was used, the shear strength improved by 19.02%, 34.76%, and 24.34% for column penetrating ratios of 0.60, 0.80, and 1.00, respectively. Based on the statistical data, a link had thus been found between the height of the column and the increase in shear strength. The height of the column has a significant impact on this relationship. The "critical column length" argument holds substance in this inquiry as the maximum column height did not provide the strongest results.

Hasan et al. (2018) conducted experimental research to investigate the link between different diameters of group-encapsulated lime bottom ash columns and the undrained shear strength of clay that had been reinforced by these columns. The 10 mm and 16 mm diameters of the lime bottom ash column were used to create small-scale modelling column samples that were 50 mm in diameter and 100 mm in height. Three independent columns, each containing three samples from different length categories, were required for each diameter. The length divisions needed to include measurements of 60, 80, and 100 mm. The test findings show that the soft soil's strength qualities improved as a consequence of using lime bottom ash columns. A number of factors, including the penetration ratio of the surrounding community of encased lime bottom ash columns, the columns' diameter, and their critical length, affect the augmentation of shear strength. The experimental study involved the application of lime bottom ash columns, which had a diameter of 10 mm and an area replacement ratio of 12%. The results of the investigation indicated that the specimens showed a rise in shear strength of 29.00%, 44.17%, and 29.75% when subjected to penetration rates of 0.6%, 0.8%, and 1.0%, correspondingly. The bottom ash columns, which had a diameter of 16 mm and an area replacement ratio of 30.72%, exhibited improvements in shear strength of 1.0%, 3.92%, and 7.33% at the sample penetration rate and Hc/Hs ratios of 0.6, 0.8, and 1.0% respectively.

Moradi et al. (2018) conducted a series of small-scale physical modelling experiments aimed at enhancing the stability of clay and investigating the potential application of a bottom ash column. The primary aim of this research was to examine the bearing capacity properties and failure mechanism of a set of end-bearing bottom ash columns, while also comparing the performance of columns with and without geotextile encasement. The incorporation of bottom ash columns was shown to substantially augment the load-bearing capability of clay. It is noteworthy that a mere fraction of the enhanced area yielded a significant 239 percent rise. The utilisation of a geotextile to encase the bottom ash column was found to result in a transition from bulging deformation to buckling failure as the bearing capacity increases. The study's conclusions were consistent with using bottom ash waste for granular columns in soil development strategies that put the environment's sustainability first.

The effect of soft soils on the placement of stone columns was examined by Ellouze et al. (2017). The numerical simulations in this study focused on the longitudinal expansion of stone material by utilising vibro displacement and replacement techniques. This study investigated the behaviour of reinforced soil upon the placement of stone columns in order to shed light on potential improvements that can be made to the properties of weak soils prior to their ultimate loading. The impact of this augmentation on the predicted increase in soil settling was thus assessed. A numerical investigation was carried out to create predictions for soft soil by comparing the Mohr-Coulomb and hardening soil constitutive laws using the axisymmetric unit cell model (UCM). To predict the settling of reinforced soil, the Mohr-Coulomb structural model for soft clay and the corresponding group of end-bearing column models were employed inside an axisymmetric design. The study was conducted to examine the impact of a higher Young's modulus on the decrease of settling in soft clay using both the single-cell and group of columns models. A considerable decrease in settlement may be anticipated when taking the group of columns model into account.

Hasan et al. (2016) examined the soft clay's undrained shear strength in relation to varying concentrations of lime silica fume. A cost-effective and environmentally advantageous technique for developing numerous infrastructure projects, such as highways, reservoirs, rivers, and embankments, is soil stabilisation. Incorporating binders or byproducts like silica fume and lime can alter the geotechnical characteristics of soil. Using this method, the soil is stabilised chemically. The primary objectives of this study were to determine the physical properties of the soft clay material and its strength when mixed with 6% silica fume and different proportions (3%, 5%, 7%, and 9%) of lime. The objective of this study was to investigate the impact of lime stabilidation with the addition of silica fume on the unconfined compressive strengths of soft clay and soft clay-lime-silica fume mixtures. In order to do this, the samples underwent an unconfined compression test. Based on the results obtained, it can be inferred that all types of soil samples had a modest degree of flexibility. The moisture content at which maximum performance was achieved increased by 23.5%, but the highest density achieved under dry conditions decreased by 5.92% when lime concentration ranged from 0% to 9% and silica fume content was fixed at 6%. A reduction in permeability was seen when comparing the permeability of the combinations with that of the soft clay. The soft clay sample's shear strength increased by 29.83% when 6% silica fume and 5% lime were added. The experimental findings indicated that a proportion of 5% lime to 6% silica fume yielded the highest efficacy in enhancing the shear strength of soft clay. The enhanced unconfined compressive strength of the soft clay was observed with the introduction of lime-silica fumes.

Mohapatra at al. (2016) studied the outcomes of direct shear tests performed on the granular columns coated with geosynthetic material. A great deal of research has been done on how geosynthetic-encased granular columns (EGC) behave under vertical loads. However, reactions of EGCs to lateral strains have not been extensively studied up to this point. This work's primary goal was to measure how encasement affects EGCs' lateral load capability. Granular columns were placed inside a 305 × 305 mm shear box and were subjected to multiple direct shear tests. The standard pressure range used for the tests was 15 kPa to 75 kPa. This study examined two distinct column widths, three different plan configurations, and three different encasement methods. It also examined the durability of envelopes and the enhancement of shear strength resulting from geosynthetic encasement, as evidenced by the test results. Also emphasised were the multiple failures seen in granular columns that were subjected to lateral strain.

Marto et al. (2016) studied the effects of increasing the parameters for clay shear strength while using bottom ash columns (BAC) to reinforce structures. The shear strength values were calculated using pore pressure calculations and consolidated undrained triaxial tests on 39 kaolin samples in total. These, along with column height, diameter, and confining pressure, were test factors. The findings demonstrated that while BAC did not change the friction's producing angle, it did give clay specimens a more cohesive appearance. In general, when partial column penetration was used, the clay seemed to be more cohesive. In the presence of BAC, it has also been shown that the pore water pressure dissipation during consolidation was enhanced.

In their study, Mohanty and Samanta (2015) conducted an investigation of the behaviour of stone columns within stratified soil. This investigation included a combination of experimental and numerical methodologies. The study included a combination of laboratory experiments and computer simulations to assess the reactivity of the ground and investigate the impact of soil layering on the effectiveness of stone columns. A comprehensive parametric investigation was conducted utilising the Plaxis finite element software. The soil and stone columns were evaluated numerically, accounting for drained conditions, using the Mohr-Coulomb failure criterion. The results indicated that the stone column's maximum axial stress stayed consistent in both stacking configurations after it had traversed a distance equal to twice its diameter. Moreover, the thickness of the overlying clay layer affected this stress level. With regards to layering methods, it is crucial to remember that the topmost layer greatly affects the maximum axial stress that the enhanced ground as a whole can bear. This collision reaches four times the diameter of the stone column. How much stiffer the improved ground becomes depends on the thickness of the top layer of soft clay. The highest value is attained in the soft clay to the most significant depth and remains constant at various depths in the stiff clay layer above. For both stacking systems, the vertical bulging rose when the highest layer of soft clay approached twice the diameter of the stone column.

Yusuf (2015) studied the behaviour of soft soil reinforced by a series of crushed polypropylene columns. The work provided empirical evidence to support the hypothesis that the incorporation of group-crushed polypropylene (PP) columns leads to a substantial enhancement in the shear strength of kaolin clay. Several batches of kaolin clay were utilised to evaluate the shear strength of soil, both with and without reinforcement. Polypropylene (PP) columns that had been group-crushed were used to strengthen these batches. A test for unconfined compression was used to conduct the evaluation. The amount of improvement in the shear strength of the clay was contingent upon the replacement ratio of the region and was achieved through the utilisation of group-crushed PP columns. The column penetration ratio also influenced the shear strength. When the column reached a critical length, it was found that there is a greater chance of failure, which causes a large expansion.

The study of deformation for stone columns coated in geotextile was examined by Zhang and Zhao (2015). Using mathematical approaches based on the unit-cell theory, the deformation behaviours of stone columns covered with geotextiles at any depth below the top plane could be predicted. When stone columns were loaded from above, the tops bended axially and typically bulged laterally. The proposed analytical approach immediately incorporated this stone column deformation feature. By employing parametric models, the impact of column spacing, column diameter, and vertically applied stress from the geotextile encasement on the deformation behaviours of the columns was ascertained. The findings suggest that a stiffer geotextile encasement can help prevent column bulging and settlement. The diameter and spacing of the columns should be considered when choosing the geotextile stiffness for encased stone columns, as these factors have a significant effect on reducing settling.

The settling behaviour of stone-column supports was studied by Black et al. (2015). Vibrating stone columns are often utilised to strengthen soft ground situations as they increase bearing capacity and reduce foundation settlement. It is commonly recognised that they function well in terms of bearing capacity. However, a deeper knowledge of their settlement characteristics is also needed, particularly in the context of small-group configurations. The results of testing physical models on triaxial specimens with diameters of 300 mm and heights of 400 mm were published in this publication. A comparison of single versus group design and the ratio of column length to diameter to area replacement were two of the variables examined. The results of the research were as follows. Because of the design's flexibility, settling may be controlled by utilising a shorter column with a higher area replacement ratio or a longer column with a lower ratio. Because of its adaptable design, settling may also be controlled by utilising a shorter column with a higher area replacement ratio or a longer column with a lower area replacement ratio. To reduce settlement, designers recommend a 30–40%

area replacement ratio. The settling performance of a small column group is heavily impacted by foundation interactions and inter-column impacts.

A novel approach to a sustainable and financially sensible environment for the construction sector is the utilisation of waste materials and products from various industries as reinforcing materials for soft soil.

Table 2.9 Summary of literature review

Sl No.	Author and Year	Study Area	Findings
01	Roshan et al. (2023)	The effectiveness of unstable bottom ash columns in enhancing the rigidity of soft soil embankments was investigated analytically and numerically. Stone columns are useful in these situations because they both prevent settling and increase bearing capacity.	The results indicated that the ultimate settlement was notably expedited with increased area replacement ratios and column length, underscoring the significant impact on the consolidation process. The area replacement ratio of 20% with a 7.5 m column depth was found to result in the highest settlement reduction of 58%.
02	Kelesoglu and Durmus (2022)	The stresses exerted by the soil must be taken into account while modelling individual and group stone columns with axisymmetry and plane strain for supporting soft soils. The installation method was described and the extra pore pressures for a single column within axisymmetric circumstances were calculated using a simple method based on column shaft expansion.	The calculated and measured values that were reasonably in agreement when the similar plane-strain permeability was used to generate the finite element model. The primary objective of this study was to enhance comprehension of the utilisation of plane-strain modelling in the context of a collection of stone columns.
03	Grizi et al. (2022)	A well-known method for enhancing the carrying capacity and settling performance of foundations constructed on soft soils is the use of columnar structures like slabs and embankments. This research looked at the effects of important design factors using a comprehensive 3D finite element analysis.	The results suggest that by precisely defining a soft soil profile, it is possible to confidently estimate long-term settling utilising both drained and undrained assessments. Although it is usually disregarded in controlled laboratory studies, the existence of a thick crust layer significantly affects the deformational mode of the stone columns.

Table 2.9 Continued

Sl No.	Author and Year	Study Area	Findings
04	Mokhtari and Kalantari (2022)	Stone columns are often employed in North Carolina's regions with soft soil compositions including peat, silt, and clay. The most common method of utilising a volume displacement device involves drilling a hole of suitable depth and diameter.	The usage of stone columns was linked to a significantly reduced settlement and a minor improvement in load capacity in clay soils. The consolidation settling was enhanced and the post-construction settlement was reduced when the material exhibited effective drainage properties.
05	Chen et al. (2021)	In centrifuge models, several degrees of encasement material stiffness were evaluated to find the ideal stiffness for an embankment supported by a geosynthetic-encased stone column (GESC) on soft clay.	The introduction of enclosed stone columns resulted in a notable reduction in ground settling as they provided support to the embankment. Instead of bulging or breaking, as was seen with normal stone columns, encased stone columns may buckle underneath the weight of the slope.
06	Shehata et al. (2021)	The purpose of this finite element analysis was to determine the impact of setting stone columns in soft soil. The analyses considered many radial excitations to accurately reproduce the construction process.	This research was conducted with the hope of enhancing the functionality of soil-stone columns in the foundations. The natural soil in the area was enhanced, and the cost to remodel the land was drastically cut.
07	Thakur et al. (2021)	This study investigated the potential of using horizontally and vertically reinforced stone columns to replace conventional, unreinforced stone ones. The load-settlement behaviours and failure mechanisms demonstrated by clusters, whether reinforced or unreinforced, were extensively studied.	Stone columns are commonly employed in areas with soft soils to enhance the stiffness of the soil, which improves its load-bearing capacity and expedites the consolidation process, thereby mitigating settlement. The structural integrity of the columns was damaged, resulting in reduced stiffness, strength, and drainage capacities, when adjacent soil infiltrates the columns due to external loading.
08	Farah and Nalbantoglu (2020)	In soft soils, the efficacy of stone columns with and without encasing was examined. This study used small-scale pilot testing in a controlled lab setting to compare the performance of soft soil with and without a coating of loose sand on top.	It has been frequently shown that the use of stone columns in these conditions improves the inferior soil's capacity to support weight. The bearing capacity increased because the geotextiles spread the built-up loads over a larger area.

Table 2.9 Continued

Sl No.	Author and Year	Study Area	Findings
09	Aslani et al. (2019)	An extensive direct shear testing apparatus measuring 305 mm by 305 mm in-plane was utilised to replicate the short-term, undrained behaviour of the clay bed supported by a stone column. In this analysis, the importance of key components was undervalued. These factors included the composition of the stone segments, average weight, zone substitution ratio, and stone section layout.	The results showed how the stone column improved the overall rigidity and shear strength of the clay bed. The structure of the column, the area's replacement ratio, and the stone that was employed had all been enhanced. The results for shear strength and stiffness increased substantially and somewhat for square column arrangements but decreased for single columns.
10	Lima et al. (2019)	This study presented a comparative investigation of the numerical simulation and field behaviour of a soft foundation that has been reinforced with stone columns at a coal and ore stockyard. The stabilised area's serviceability behaviour was observed using a comprehensive instrumentation consisting of 14 sensors.	The plane strain model that was used allowed for accurate prediction of the reinforced foundation's total deformations. The modelled excess pore pressure curves behaved similarly to the field data, reaching a maximum at the time of loading application, and decreased progressively as consolidation continued.
11	Hasan et al. (2019)	The objective of this work was to investigate the potential utilisation of a singularly crushed coconut shell (CCS) column to enhance the shear strength of soft clay.	The internal shear strength of the soft clay was improved by the addition of one single CCS column. The ratio of heights penetrated determined the degree of this enhancement. The results of the investigation support the "critical column length" idea, which maintained that total penetration does not result in the strongest connections.
12	Hasan et al. (2018)	The purpose of this research was to use a laboratory-scale model to investigate the feasibility of increasing the shear strength of lime bottom ash columns within a group structure. The quality of the kaolin was determined by testing seven separate batches.	The study found that adding lime bottom ash columns in groups increased the shear strength of kaolin. Based on the data gathered, it can be inferred that the critical length of the column was around four to eight times its diameter.

Table 2.9 Continued

Sl No.	Author and Year	Study Area	Findings
13	Mohanty et al. (2018)	A combination of small-scale laboratory experiments and numerical studies were conducted to examine the effect of soil layers on ground improvement and the conduct of stone columns. In order to determine how the elevated ground would respond generally to stress, how it would differ from settling loading was applied to the stone column region.	The enhanced ground's increased stiffness improvement factor was a result of the greater top layer of soft clay. The soft clay's entire depth was where it reaches its maximum value, whereas the stiff clay's upper depths stayed constant. It has been observed that for both layering processes, a rise in the thickness of the soft clay top layer caused the vertical extent of bulging to extend, possibly increasing the diameter of the stone column.
14	Moradi et al. (2018)	This study examined the bearing capacity and manner of failure of clay for a series of bottom ash columns intended to support ends with and without geotextile encasing.	The bottom ash column's load-bearing capacity increased when a geotextile was wrapped over it to prevent column bulging and instead caused buckling failure. The research results are consistent with using bottom ash by-products as an effective substrate for granular column applications in soil development strategies that put the environment first.
15	Hasan et al. (2016)	The principal objectives of the study were to determine the physical properties of the soft clay used and its strength in combination with varying concentrations of silica fume (6%) and lime (3%, 5%, 7%, and 9%). The study employed an unconfined compression test to assess the impact of including silica fume and lime for stabilisation on the unconfined compressive strength of both soft clay and combinations of soft clay with lime and silica fume.	According to the findings, there was a moderate level of flexibility present in every soil sample. With a mixture of 6% silica fume and 9% lime, the optimum dry density dropped by 5.92% and the optimal moisture content rose by 23.5%. As compared to the soft clay sample without modifications, the study found a substantial increase in shear strength of 29.83% when the soft clay sample was combined with 6% silica fume and 5% lime.

Table 2.9 Continued

Sl No.	Author and Year	Study Area	Findings
16	Ellouze et al. (2017)	The goal of the study was to demonstrate how improved soft soil qualities may be before applying maximum loads by analysing the behaviour of reinforced soil following the installation of stone columns.	Research was conducted to compare the predictions of the unit cell and group of column models on the decrease in settlement that occurs as Young's modulus of the soft clay increases. The analysis suggests that using the group of columns strategy will likely result in a notable decrease in settling.
17	Barack et al. (2017)	Stone columns are commonly employed as load-bearing elements in cohesive soil, where they provide many functions such as stabilising the soil, facilitating drainage, and enhancing compaction.	The weights integrated into the soil were increased and soil settling was reduced by fortifying the stone columns' shear strength.
18	Demir et al. (2016)	Ten model experiments were carried out on soft soils using materials that were classified as natural aggregate (NA) and recycled concrete aggregate (RCA). The columns were constructed with recycled concrete aggregate, or RCA.	The research findings indicated a significant increase in the carrying capacity ratio between individual and collective columns of RCA and NA in soft soil beds. Additionally, there was a documented increased trend in the undrained shear strength of the soil.
19	Muneerah et al. (2016)	The aim of this study was to increase the strength of soft kaolin clay samples by using replacement and displacement installation techniques. The samples had dimensions of 400 mm in length and 300 mm in diameter. Several granular columns of varying lengths were used to achieve this.	It is possible for the settlement-reduction factor values derived from the displacement strategy to slightly exceed those derived from the replacement method. There was no noticeable difference in settlement between installations using a single 40 mm-diameter column and those using a short floating column (L/D = 5).
20	Rajagopal et al. (2016)	The behaviour of geosynthetic-encased granular columns (EGC) under vertical loads was thoroughly investigated and generally understood. To ascertain the extent to which EGCs' lateral load capability is impacted by encasement.	The results of the study indicated that the utilisation of geosynthetic encasement leads to an enhancement in shear strength. Additionally, the use of strength envelopes facilitates the understanding of the effects caused by the encasement.

Table 2.9 Continued

Sl No.	Author and Year	Study Area	Findings
21	Black et al. (2015)	In this experiment, triaxially oriented, vertically reinforced sand columns were used to reinforce 200 mm high by 100 mm diameter samples of soft kaolin clay. To strengthen the samples, the experiment utilised either three sand columns, each measuring 20 mm in diameter, or a single column with a diameter of 32 mm.	The findings of the study demonstrated that specimens with a single, completely penetrating column for reinforcement showed a 33% increase in strength in comparison to samples without any columns. The findings suggest that clustering columns together might result in less stiffness than a single column when equal area replacement ratios are taken into account.
22	Etezad et al. (2015)	The study presents an analytical approach for estimating the bearing capacity of soft soil below a rigid raft foundation that is reinforced with stone columns. The model employs the limit-equilibrium technique and integrates the composite characteristics of reinforced soil.	An environmentally sound, practical, and cost-effective strategy for improving soil stability is to use stone columns. To enhance the quality of deficient soil and increase its shear resistance and subsequent bearing capacity, the implementation of columns consisting of compacted aggregate was employed.
23	Marto et al. (2015)	To assess the effects of adding bottom ash columns (BAC) individually and collectively while reinforcing clay shear strength characteristics.	The clay sample was supplemented with the bottom ash column (BAC), resulting in a minimal alteration in the productive angle of friction, while the apparent cohesiveness exhibited an increase. The reduction in pore water pressure seen throughout the consolidation process can be attributed to the presence of Biologically Activated Carbon (BAC).
24	Yusuf (2015)	The behaviour of soft soil that has undergone reinforcement by the inclusion of a crushed polypropylene column was studied. The primary objective of this study was to investigate the impact of including group-crushed polypropylene (PP) columns on the shear strength characteristics of kaolin clay.	The shear strength of the clay was improved by using group-crushed precast prestressed (PP) columns; however, the degree of increase depended on the particular local replacement ratio.The importance of considering the column penetration ratio should not be underestimated while aiming to improve shear strength.

Table 2.9 Continued

Sl No.	Author and Year	Study Area	Findings
25	Zhang and Zhao (2015)	The study used parametric analyses to investigate how various parameters, including geotextile encasement, vertical applied stress, and column diameter and spacing, affected the deformation properties of the columns.	The results indicate that adopting a stiffer geotextile encasement efficiently reduces column bulging and settling. The diameter and distance between the columns should be included when calculating the geotextile stiffness for encased stone columns. These factors were found to exert a notable influence on the extent of settlement reduction.

2.8.2.1 Research Gap in Existing Literature

Current literature reviews focused on stone columns, recycled concrete aggregate (RCA), and other columns. However, the specific application of polypropylene columns for soil reinforcement has not been extensively explored in available research works. Consequently, there is an opportunity to close this gap by offering a thorough examination of the mechanical and physical properties of polypropylene columns and how they affect soft clay. The literature research mentions looking at crucial stone column design factors such column spacing, length, and diameter. However, it does not discuss the evaluation of similar parameters for polypropylene columns. Hence, investigating the optimal dimensions and configurations of polypropylene columns, such as penetration depth, spacing, and size, is essential to determine their effectiveness in soil reinforcement.

While some studies have discussed the failure criteria for stone columns, such as the Mohr-Coulomb failure criteria, information on how to apply these requirements to polypropylene columns is lacking. Analysing the failure criteria, both Mohr-Coulomb and critical state failure criteria specifically for polypropylene columns in soft clay, would help in understanding their behaviour and performance under different loading conditions. Moreover, many studies in the literature review mentioned laboratory or numerical testing but do not provide a comprehensive assessment of physical and mechanical characteristics. Hence, a more detailed examination of the laboratory testing procedures and results, as well as their correlation with field performance, is essential for a thorough understanding of polypropylene column behaviour in soft clay. By bridging these information gaps, it is possible to develop sustainable and effective soil reinforcing techniques and get a deeper understanding of the mechanical and physical characteristics of soft clay reinforced with polypropylene columns.

2.8.3 Failure Mechanisms of Columns in Soil

Stone columns can experience multiple failure mechanisms when implemented under compressive loads. According to the findings of Ashour et al. (2022), there would be a failure of some sort in the stone columns due to the parameters' diameter, duration, and arrangement. Abdelhamid et al. (2023) confirmed that three distinct loading patterns are applied to the stone columns. Initially, single columns are employed for minor base loading to support loads in situations when the stone columns' perimeter lateral column restrictions are equal. Second, the column is more restricted in the direction parallel to the strip to facilitate the loading of the strip. In the context of the third scenario, it is imperative to furnish substantial evidence to substantiate extensive loadings. This entails ensuring that the stone columns' periphery experiences uniform lateral confinement, resulting in an increase in the soil's lateral resistance when it settles under significant loads. The stiffness characteristics of the underlying soil and the stone column determine how much pressure is exerted to the granular base or foundation. Higher contact tension is the result of a stiffer stone column.

2.8.3.1 Single Columns in Soil

The primary cause of the distinctive stone columns' failure mechanism is the bulging that has been noticed in these columns. It occurs when the surrounding soil does not include protection from lateral stress. Abdelhamid et al. (2023) suggested that stone columns should be built either as floating columns, where the tips of the columns are inserted in the soft layers, or as the end bearings of the soft soils. The lateral containment allows access to the stone columns by applying horizontal soil pressure to the columns, which relies on load transfer. This makes the pile foundation different from other foundation types as it depends on the tip and the skin's robustness (Kirsch and Kirsch, 2017). As a result of exaggerated lateral stress, soil deformation is caused by column bulges that is caused by increased lateral stress. Abdelhamid et al. (2023) contended that, even in the case of floating or end bearings, the bulging failure mechanism has been established for stone columns larger than critical. According to Kirsch and Kirsch (2017), the collapse of solitary stone columns can occur as a result of the bulging phenomenon observed in long, end-bearing columns. ii. The phenomenon of shearing in short, end-bearing columns. iii. The sinking of short, floating columns due to punching. iv. Bulging occurring in deeper levels. This occurs when the soil's surroundings could not withstand lateral stress, as shown in Figure 2.7 (a). Figure 2.7 (b) demonstrates the shear surface formed through the columns, where the bulging emerges at a depth of up to 4D in homogeneous soils. For a span of less than 4D of short columns of stone, stone columns will be punched. As shown in the pictures, a failure owing to bulging at depths larger than 4D may occur when the stone columns have sufficient thick soil surfaces (more than 2D).

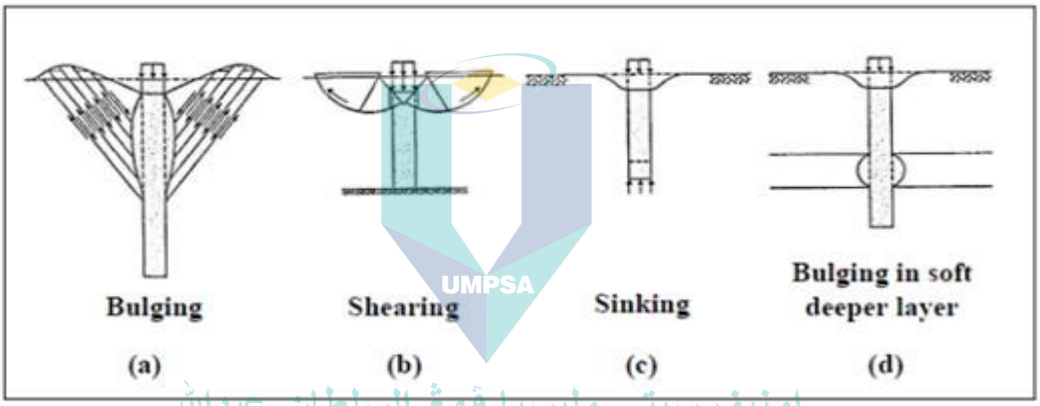

Figure 2.7 Failure mechanism of single stone columns
Source: Kirsch and Kirsch (2017)

2.8.3.2 Group of Columns in Soil

The implementation of a collection of stone columns that mutually support one another can be employed as a method to infer the likelihood of failure mechanisms. It is crucial to emphasise that the matter of bearing capacity exclusively refers to several stone columns situated in close proximity to the surface of the aggregate column. Using a set of centrifuge model tests, Li et al. (2021) examined the process of embankment collapse reinforced by a combination of enclosed and ordinary stone columns. The study's findings showed that the traditional stone columns had noticeable shear effects in the bottom area, inward bending in the central region, and bulging phenomena in the top portion. There was a noticeable decrease in the bulging of the upper section when the stone columns were enclosed with geogrid. However, it was seen that there existed a phenomenon of inward bending. The stone column group generated failure mechanism modes, namely shear failure, bulging, bending (buckling), and punching (Abdelhamid et al., 2023). The utilisation of replacement and displacement techniques presents viable alternatives for the implementation of a stone column within a clay substrate. The procedure of replacement involves the extraction of the deficient soil and subsequent substitution with a column, which is then forcefully inserted into the ground by the process of displacement. Figure 2.8 depicts a collection of stone columns that provide support to inflexible foundations, wherein the likelihood of failure mechanisms has been identified.

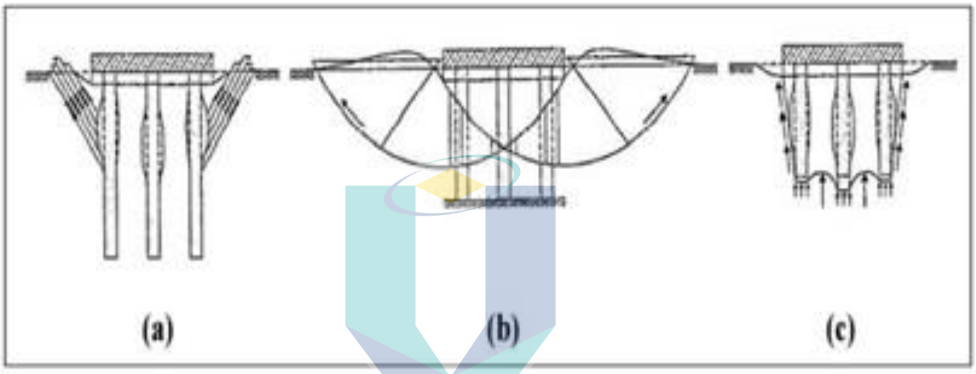

Figure 2.8 The failure mechanism of group stone columns
Source: Kirsch and Kirsch (2017)

2.8.3.3 Critical Column Length

The use of the critical length idea has been suggested based on the findings of a prior study conducted by Abdelhamid et al. (2023), which demonstrated that extending the length of the column does not result in substantial changes to the soil's capacity. Previous research has employed sand columns of different lengths to examine the influence of column penetration on the enhancement of carrying capacity in the specimens. Several academic studies have proposed the idea of a "critical column length", suggesting that the effectiveness of clay would not be enhanced beyond a column that surpasses this particular barrier. The study done by Abdelhamid et al. (2023) showed that clay specimens, when reinforced with both single and group stone columns, experienced failure characterised by lateral bulging. This phenomenon was predominantly observed in the top four to five diameters and the height of the column. The bulging feature was most noticeable in the higher parts of the sand columns. The rate of advancement for fully penetrated columns depends on a number of factors, including the shear strength of the clay soil, the size and design of the sand columns, and the angle of friction displayed by the column material. According to Castro (2017a), the length of the column was important up to a certain length, but as the reinforcement area ratio grew, stiffness and shear strength improved. This suggests that there was no improvement in strength with increasing column length, even though the stiffness could still increase. According to the findings of Castro Castro (2017b), it was determined that the utilisation of lengthier columns yielded advantageous outcomes in terms of settlement control objectives. According to Najjar et al. (2020), it is suggested that achieving optimal load transmission necessitates stone columns with a length roughly 5-8 times greater than their diameter. The research outcomes also suggest that an augmentation in the area ratio may potentially result in an escalation of the crucial time. This can be attributed to a failure mechanism that is compelled to occur at a greater depth under the foundation. The study's findings lend support to the critical column length theory, which postulates that, after a certain point, further increases in undrained shear strength are inconsequential. In most cases, it was found that individual columns showed far more significant strength increases than group columns.

In conclusion, Polypropylene (PP) stands out as the superior choice for column material due to its remarkable characteristics. Its unique chemical composition, characterized by CH_3 groups on its carbon backbone, endows PP with remarkable rigidity, heightened crystallinity, and superior resistance to mechanical deformation, distinguishing it from other polymers. Moreover, PP's favorable combination of properties, including good mechanical strength, chemical resistance, and processability, further enhances its suitability for column fabrication. In particular, its high tensile strength and low water absorption rate make it an ideal choice for reinforcing stone columns, as demonstrated by research studies. Furthermore, PP's affordability and ease of fabrication enhance its attractiveness as a column material. These significant attributes not only ensure the reliability and longevity of the column but also contribute to cost-effectiveness and operational efficiency. Therefore, based on its unparalleled combination of properties, PP emerges as the optimal material for column construction, providing researchers and industries with a dependable and versatile solution for their separation needs.

CHAPTER 3

METHODOLOGY

3.1 Introduction

This chapter presents a comprehensive overview of the experimental procedures employed to achieve the objectives of the research, encompassing laboratory work, calibration techniques, methodology, and plans for data processing. This chapter's main goal is to provide an explanation of every procedure used in the research to make sure all objectives have been satisfied. The project begins with problem recognition in this analysis. The study focuses on whether polypropylene can function as a suitable substitute for granular material in alternative soil reinforcing methods. First, it is necessary to determine the issue so that the goal of the research can be accomplished. Next, recent research on the subject has been closely checked to identify previous attempts to resolve the identified issues. Previous research and sources were compiled from publications, international conference papers, journal articles, and a thesis on soft soil, kaolin clay, soil reinforcement, and polypropylene. Next, the preparation and execution of the project methodology were accompanied by the study of previous experiments. The methodology encompasses a series of laboratory experiments aimed at assessing the mechanical, physical, and strength properties of polypropylene and kaolin clay, as well as the composite material formed by reinforcing kaolin with polypropylene columns. Cylindrical specimens, with a diameter of 50 mm and a height of 100 mm, were produced using kaolin as the clay element, and polypropylene provided the granular component. The studies were conducted at Universiti Malaysia Pahang's Soil and Geotechnical Laboratory. The final selection of laboratory equipment for various tests was dependent on criteria such as suitability and financial considerations. This situation also led to the use of guiding frameworks like the British Standard (BS) and the American Society of Testing Materials (ASTM). This chapter presents a thorough examination of the process of setting up the model test, including the test content and the overall procedures involved. Figure 3.1 is a flow chart that clearly illustrates the implementation of the research approach.

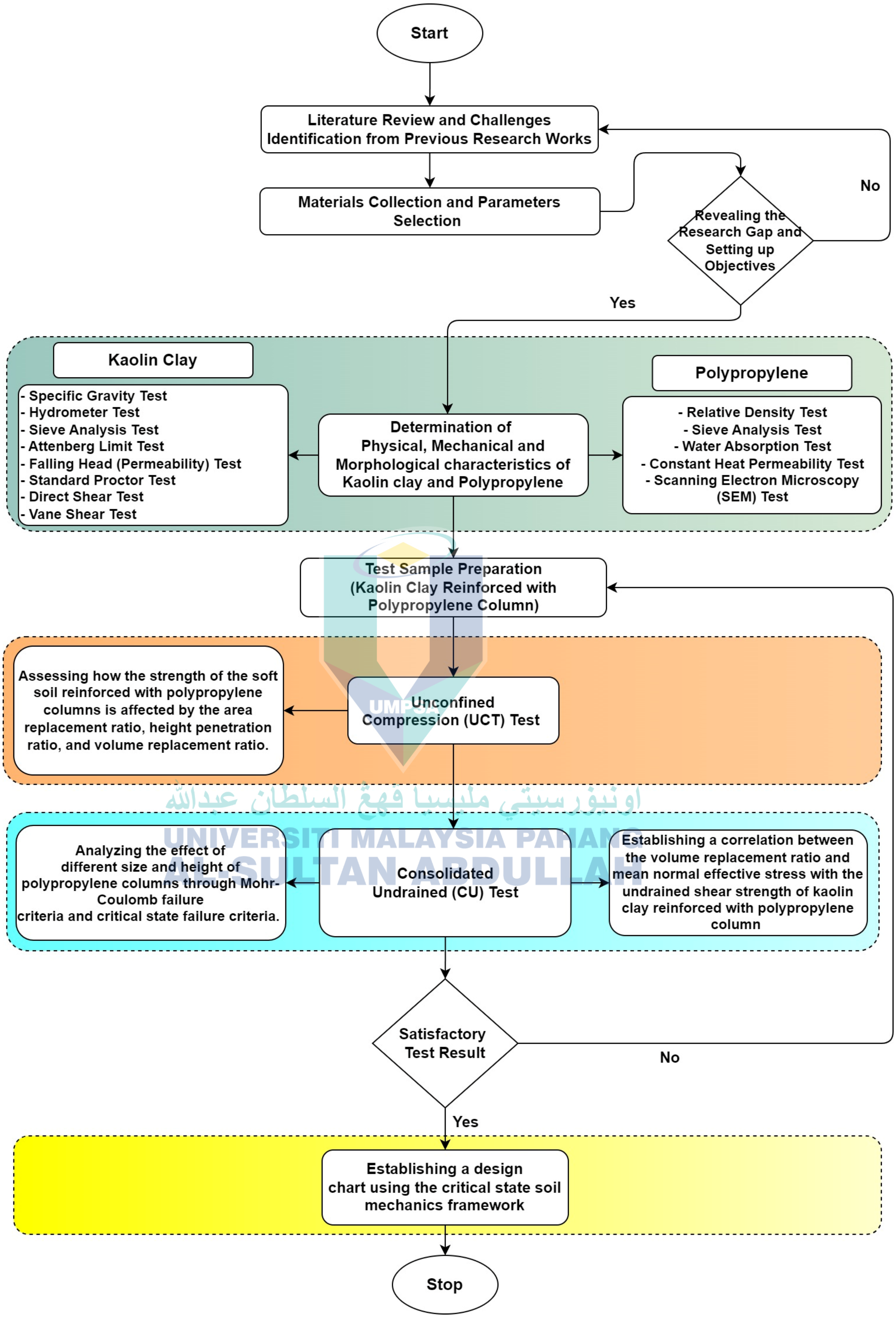

Figure 3.1 Flow chart for the implementation of the research methodology

3.2 Selection of Material

The selection of materials is essential to achieve the goals. The study utilised polypropylene and kaolin clay as its raw components. A number of tests on polypropylene columns in a bed of kaolin clay were included in the experimental program. On unreinforced clay beds, tests were also conducted without the use of polypropylene columns.

In the first instance, polypropylene is ideal for use as a granular material in columns. Polypropylene is now integrated into daily activities. Day after day, the use of plastics has risen dramatically due to their lightweight and durable properties. However, waste plastics are a huge environmental issue internationally. Waste polypropylene is not environmentally friendly; it has populated landfills for a long time, causing difficulties for vegetation and marine ecosystems. Hence, rather than tossing out an excessive amount of uncycled polypropylene, this study suggests a method to save the world by reusing this excessive material to reinforce clay.

The substance known as kaolin power grade S300 was utilized. In order to maintain the uniformity of the data gathered, it is imperative that the clay samples exhibit homogeneity across all research investigations. Apart from the price, kaolin was chosen as it is the most popular clay soil and is simple to acquire. Like kaolinite, it is a clay mineral with a loose consistency and an earthy feel. It can be broken easily without complications, and when saturated, it can be formed or shaped. Kaolinite emerges as the predominant mineral within clay, constituting the primary constituent across all clay deposits.

In this research, kaolin S300 was selected to represent the soft soil as many researchers have also this kind of soft clay in their studies. Haolin clay was also chosen due to its price and its availability in the market. Another name for kaolin clay is China clay, which is named after the place where it was discovered. The kaolin clay utilised in this study was sourced from Selangor, Malaysia.

3.3 Collection of Materials

3.3.1 Kaolin clay soil

The soil sample used in this study was obtained from Kaolin (M) Sdn. Bhd., a company located in Selangor, Malaysia. The study utilised a sample comprising of kaolin powder. The formulation of kaolin clay was achieved by the utilisation of a particular compaction method. The utilisation of Grade S300 Kaolin powder was employed as a constituent in the fabrication of consistent and uniform clay substances. Furthermore, kaolin is the best choice when it comes to cost and usability. Aluminium silicate hydroxide was specifically designated as $Al_2Si_2O_5(OH)_4$ in the chemical composition of the clay mineral kaolinite. It breaks readily, especially when wet. Additionally, it has a hydrophilic composition that resembles a plate, meaning that it will combine or wet with water to make a sludge that will create homogenous clay. Following the removal of plants, the clay's surface was dug up, ground into a powder, and allowed to air dry. The hydrophilic mineral known as kaolin, characterised by its flat structure, is manufactured with the intention of being mixed with water to create a slurry. This slurry can then be utilised to produce a uniform clay material.

3.3.2 Polypropylene

Polypropylene was obtained from different places in Malaysia. As polypropylene is a plastic with a low water absorption rate, it cannot undergo geotechnical lab tests that are specific to soil sampling alone. As a result, the polypropylene properties were obtained by another venture from Titan Petchem (M) Sdn. Bhd. Only a few polypropylene investigations can be carried out, which are the Direct Shear Test, Sieve Analysis Test, Relative Density Test, and Constant Head Permeability Test.

3.4 Determination of Properties of Materials and Laboratory Tests Standards

A comprehensive assessment of the mechanical and physical characteristics of soft kaolin and polypropylene was conducted via a series of experimental experiments. Soft kaolin clay was reinforced with polypropylene columns in a lab test to determine its shear strength. The American Society for Testing and Materials (ASTM) and the British Standard (BS) were frequently used as benchmarks, depending on the testing facilities at hand. The primary aim of this investigation was to comprehensively document all aspects of the experimental procedure, encompassing the equipment used, methodologies employed, and specifics on the undrained strength tests done on soft clay with polypropylene column reinforcements. The next part presents a comprehensive overview of the parameters under investigation, the materials utilised, the experimental setup, and the methods employed for testing. Table 3.1 presents the laboratory testing programme and the procedural criteria.

Table 3.1 Overview of test standards and methods that are used for the determination of properties of selected materials

Material	Tests		Test Standards
Polypropylene	The Relative Density Test		ASTM D4254-16
	Sieve Analysis Test		BS 1377: Part 2: 2022: 9
	Water Absorption Test		ASTM D570-22
	Constant Head Permeability Test		ASTM D2434-19
	Scanning Electron Microscopy (SEM) Test		ASTM E986-04
Kaolin Clay	Specific Gravity Test		BS 1377: Part 2: 2022: 8
	Hydrometer Test		ASTM D7928-21e1
	Sieve Analysis Test		BS 1377: Part 2: 2022: 9
	Atterberg Limit Test	Liquid Limit	BS 1377: Part 2: 2022: 4.3
		Plastic Limit	BS 1377: Part 2: 2022: 5.3
	Falling Head Permeability Test		ASTM D 2434-22
	Standard Proctor Test		BS 1377: Part 4: 2022: 3.3
	Direct Shear Test		ASTM D3080-04
	Vane Shear Test		ASTM D2573-08
Kaolin Clay Reinforced with Polypropylene Columns	Consolidated Undrained Triaxial		BS 1377: Part 7: 2022
	Unconfined Compression Test		ASTM D2166-06

3.5 Laboratory Tests for the Assessment of Physical Properties

The determination of the physical characteristics of interest was carried out in line with the British Standard Soil Test Methods for Civil Engineering Purposes (BS 1377: 2022) and the standards established by the American Society for Testing and

Materials (ASTM). A series of six laboratory experiments were conducted, consisting of two tests specifically designed for polypropylene, namely the Relative Density Test and the Dry Sieving Test. Additionally, four tests were performed on soft kaolin clay, including the Sieve Analysis Test, Atterberg Limit Test, Specific Gravity Test, and Hydrometer Test.

3.5.1 Sieve Analysis Test

Sieve analysis studies are conducted to categorise a collection of soil particles into different size categories and determine the proportional proportions based on dry mass of each size range. Using standardised soil classification to assess the classification of the material, sieve analysis experiments were performed on kaolin and polypropylene. Generally, the sieve arrangement begins with a sieve that has the largest mesh at the peak, followed by a smaller sieve size. To capture the particles that went through the smallest size of the sieve, a container was used at the bottom of the sieve.

Figure 3.2 Sieve Analysis Equipment

The dimensions of the sieve must align with the dimensions of the sieve mesh. Additionally, to mitigate particle loss, a cover was employed atop the sieves during the agitation procedure. The shaker's condition of agitation was present for a length of 10 minutes. The measurements of the samples stored on each sieve were taken. The graphical representation of the particle size distribution curve is depicted. In this experimental study, the dry weight obtained within a specific size range was utilised to classify the particles of the material into distinct groups based on their sizes. The correlation between the percentage of passing material and the size of the sieve or particle is illustrated in a semi-logarithmic graph. Figure 3.2 displays the testing equipment utilised in the sieve analysis test.

3.5.2 Relative Density Test

The procedure for conducting relative density testing typically involves the application of a vibrating table to determine the maximum and lowest dry densities of polypropylene. Four options are provided by Methods 1A, 1B, 2A, and 2B of ASTM D 4254. The method of choice to determine the relative density of polypropylene is 2A, which makes use of oven-dried soils and a vertically vibrating table controlled by an eccentric or cam. The material that would be used for the minimum unit weight was decided. First, the material was placed into moulds of a certain volume; the mass of the substance was then utilised to fill the mould and measured. Excluding the material, the overall unit weight was calculated using the same procedure. With the help of a vibrating table, the material was packed into the mould as densely as possible to cause vibrations. The polypropylene column in the test method was the result of the rinsing technique. At some heights, a predefined height was used to pour the polypropylene into the pre-drilled cavity via free fall. Figure 3.3 shows the apparatus utilised for conducting the relative density test.

Figure 3.3 Equipment for Relative Density Test

The determination of the relative density of the polypropylene material in the vertical column may be accomplished by utilising Equation 3.1, which depends on the dry density of the polypropylene.

$$D_r = \frac{\gamma_{max}(\gamma - \gamma_{min})}{\gamma(\gamma_{max} - \gamma_{min})} \times 100\% \qquad 3.1$$

In which:

D_r = Relative density

γ = Weight in units of the present sample

γ_{max} = Maximum unit weight

γ_{min} = Minimum unit weight

3.5.3 Water Absorption Test

The polypropylene specimens were cooled in a desiccator following their drying in an oven at a temperature and duration specified for the water absorption test. The specimens were immediately weighed after cooling. Next, for 24 hours or until equilibrium, the substance was submerged in water at predetermined temperatures, usually 23°C. After removal and drying with a lint-free cloth, the specimens were weighed.

3.5.4 Specific Gravity Test

The specific gravities of kaolin clay were calculated using a small pycnometer test. The calculation involved computing out the mass of gas-free distilled water at a specific temperature divided by the number of soil particles per unit volume. The specific gravities of kaolin can be measured using a small pycnometer, which is a stoppered bottle with a peak capacity of 50 ml. The mass specimens were mounted within a small pycnometer, where half of the pycnometer was equipped with distilled water. The next move was to position the tiny pycnometer inside the vacuum chamber. The air within the sample containing the purified water and the combination of substances were separated by the vacuum chamber. After leaving the specimens for 24 hours, the distilled water was applied to the small pycnometer until it was complete. The mass of the pycnometer was then determined. Figure 3.4 illustrates the apparatus utilised for conducting the specific gravity test. The determination of the sample's specific gravity was conducted by utilising Equation 3.2.

$$G_S = \frac{(m_2 - m_1)}{(m_4 - m_1) - (m_3 - m_2)} \quad 3.2$$

Where

G_s = specific gravity of soils

m_1 = the mass of empty pycnometer (g)

m_2 = the mass of the pycnometer + dry soil (g)

m_3 =the mass of the pycnometer + soil + water (g)

m_4 = the mass of the pycnometer + water (g)

Figure 3.4 Small Pycnometer

3.5.5 Hydrometer Test

The hydrometer analysis method is commonly employed to assess the particle size distribution of soil components that are finer than the No. 200 sieve, which has a diameter of 0.063 mm. The approach in question establishes an estimated lower limit for particle size at 0.001 mm. Before the hydrometer sedimentation examination for kaolin, any organic matter available had been extracted by chemical treatment. The kaolin was treated with dispersion and thoroughly stimulated to ensure the isolation of the discreet particles.

Figure 3.5 Hydrometer test apparatus

The examination was conducted to examine the distribution of the material's particle size as it passes through the 0.063-mm sieves. The 50 grams of soil that could pass through 0.063-millimeter sieves were all aseptically put into a 1000-millilitre sedimentation cylinder. One thousand millilitres of dispersing solution was added to the second cylinder. They were then placed in a constant-temperature bath at 26°C. A rubber bung was attached to each cylinder for a watertight seal. The cylinder filled with the dispersant solution was extracted and vigorously shaken. It was also constantly replenished in the water bath. Next, the stopwatch was started. The rubber bungalows were withdrawn. The hydrometer was mounted and was permitted to move freely. However, the bottom of the stem was twisted with fingers in a rapid rotation to dissipate the air bubbles. The hydrometer data was taken at 0, 0.5, 1, 2, and 4 minutes. The hydrometer was then extracted and cleaned with deionized water. Next, it was put in a dispersant solvent cylinder. The reading of the hydrometer was then registered. The hydrometer was then returned to the specimen suspension for testing at 8, 15, and 30 minutes, 1, 2, 4, 8 hours, overnight, and, if possible, twice daily. The testing apparatus utilised for the hydrometer test is shown in Figure 3.5.

3.5.6 Atterberg Limit Test

The Atterberg limit test contains three distinct processes, namely the liquid limit test, the plastic limit test, and the shrinkage limit test. The Atterberg limit test is a fundamental procedure employed to evaluate the moisture content of the soil, as the flexibility of soil may be altered by manipulating its moisture content. The constraints of the Atterberg limits test are crucial in ascertaining the composition of fine-grained soils, particularly those consisting predominantly of clay particles.

The assessment of the plasticity thresholds of clay soils may be achieved by the use of the Atterberg limits, as the moisture content of clay soil is regarded as an indicative parameter of its plastic characteristics. The exploration of the plastic limit (PL) and liquid limit (LL) are markers for determining the clay material's stiffness as the main areas of focus in the study. The behaviour of soil with respect to its plasticity index (IP) can be described by the following mathematical expression:

$$PI = LL - PL \tag{3.3}$$

Figure 3.6 Cone penetration test

The cone penetration technique was employed to assess the liquid limit (LL) of five kaolin specimens. Moreover, the liquid limit was ascertained by evaluating the penetration of liquid of a standard cone with a designated mass in the soil. In contrast, the primary aim of conducting the plastic limit (PL) test was to ascertain the minimal moisture content at which a substance meets the criteria for classification as a plastic material. Assessment of the plastic limit for three samples soil and clay can be found in four various states, depending on the amount of moisture present: liquid, semi-solid, plastic, and solid. The plastic limit was assessed according to the specifications outlined in BS 1377: Part 2: 2022: Clause 5.3, utilising a cone penetration method. In a similar manner, the liquid limit test was conducted in accordance with the specifications provided in BS 1377: Part 2: 2022: Clause 4.3. The concept of "plasticity index" (BS 1377: Part 2, 2022: Clause 5.4) refers to the quantitative disparity between the liquid limit and the plastic limit. Meanwhile, the shrinkage limit (SL) test was performed on two (2) samples using a volumetric shrinkage approach. Soils with low plasticity that can profit from this analysis include clay and silty soils. The shrinkage range can be lowered to 20% and unnecessary cracking can be prevented by regulating the moisture content of the positioning in relation to the shrinkage cap. The apparatus for testing the volumetric shrinkage limit is shown in Figure 3.6.

3.6 Laboratory Tests for the Assessment of Mechanical Properties

The primary objective of conducting the four laboratory experiments was to determine and assess the mechanical properties shown by the specimens. The assessment of polypropylene involves two specialised examinations, namely the Standard Compaction Test as well as the Constant Head Permeability Test. Two tests were also conducted to assess the characteristics of soft kaolin: the Standard Compaction Test and the Falling Head Permeability Test.

3.6.1 Falling Head Permeability Test

Soil's capacity to allow liquids to flow through its structure is measured by a property called permeability. There are two different approaches to permeability testing: the falling head permeability test and the constant head permeability test. The permeability test with a falling head is well-suited for finer materials, including clay slits, due to its capacity to assess permeability in soils with medium and low permeability. These soils are characterised by permeability values below 0.0001 m/s. The coefficient of the permeability of kaolin was determined using the falling head measure, following the guidelines specified in the ASTM D 2434 standard. Typically, this technique is important for finer materials. Both the constant head permeability test and the falling head test use the same apparatus. Although the apparatus is much the same, this experiment only employed the burette and the bottom half within the permeability cell rather than a constant head tank. Figure 3.7 illustrates the apparatus employed for conducting falling head permeability tests.

Figure 3.7 Falling head permeability test

3.6.2 Constant Head Permeability Test

The continuous head permeability test is a commonly utilised laboratory technique to assess the permeability of granular soils, namely those composed mostly of sands and gravels with negligible silt content. Testing can be done with this method on granular soil samples that have been disturbed or reconstituted. Water that moves freely but does not remain in the spaces between the granular polypropylene particles is caused by their larger size when compared to silt and clay particles. Consequently, the application of a constant head permeability test was used to determine the permeability of granular polypropylene. Particles up to 5 mm in size can be tested with a constant head and up to 10 mm in size with a test utilising a 114 mm diameter cell or constant head. The flow velocity generated through a hydraulic gradient of uniform may be used to calculate the coefficient of permeability. Several parameters, such as porosity, size, direction, and viscosity, may potentially influence soil water. The experimental setup employed for conducting continuous head permeability testing is illustrated in Figure 3.8.

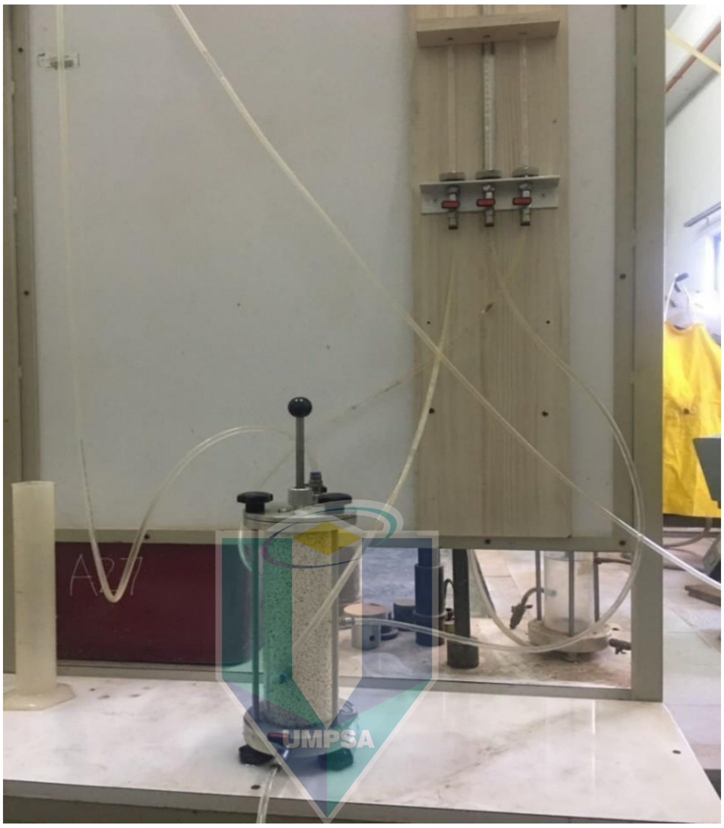

Figure 3.8 Constant Head Permeability Test

3.6.3 Standard Proctor Compaction Test

The standard proctor compaction test is used to determine the optimal moisture content and relative dry density of the material. The dry density of the soil can be increased by the mechanical compression and consolidation of soil particles. The compaction test's main goal is to assess the relationship between density and moisture content. There is an absence of alteration in the dimensions of the soil particles, and no extraction of water occurs. The oven-dry sample, which weighed around 3.4 kg, was measured first. The 4.75-mm sieve was used to filter the gathered material. After adding some water to the mixture, the mixture was mixed to do the analysis. The compaction mould, equipped with a base plate, was measured and recorded. The mould was affixed to the base plate using the collar. Subsequently, a certain amount of damp earth was introduced into the mould. The compaction process involved the successive compaction of three layers, with a 30-centimeter gap between the hammer point and the soil, utilising the free fall method. Different materials were employed for varying levels of moisture content. A chart showing the relationship between the dry weight and moisture content was produced using the data collected for the study. The optimal moisture percentage and total dry weight were calculated. The density of kaolin was measured in relation to its moisture content. The testing apparatus employed in the conventional proctor compaction test is shown in Figure 3.9.

Figure 3.9 Standard Proctor Compaction Test

3.6.4 Vane Shear Test

The vane shear test is employed as a technique to evaluate the sensitivity of fully saturated cohesive soil and for estimating the undrained shear strength in field conditions. The applicability of this testing method is restricted to fine-grained soils that have the capacity to hold water content during the testing procedure. The test requires the soil sample to be completely wet throughout. A vane is put into the test specimen and rotated until the soil reaches its failure point. The analysis of the torque obtained and the diameter of the vane employed may then be performed to determine the undrained shear strength and sensitivity.

To evaluate the uniformity of the produced specimens, laboratory vane shear tests were carried out on the interior portion of reconstituted clay specimens. The necessity arose from the utilisation of the compaction process in the creation of the samples, hence emphasising the importance of ensuring homogeneity and consistent strength in the samples. The laboratory vane shear test done on kaolin specimens is depicted in Figure 3.10.

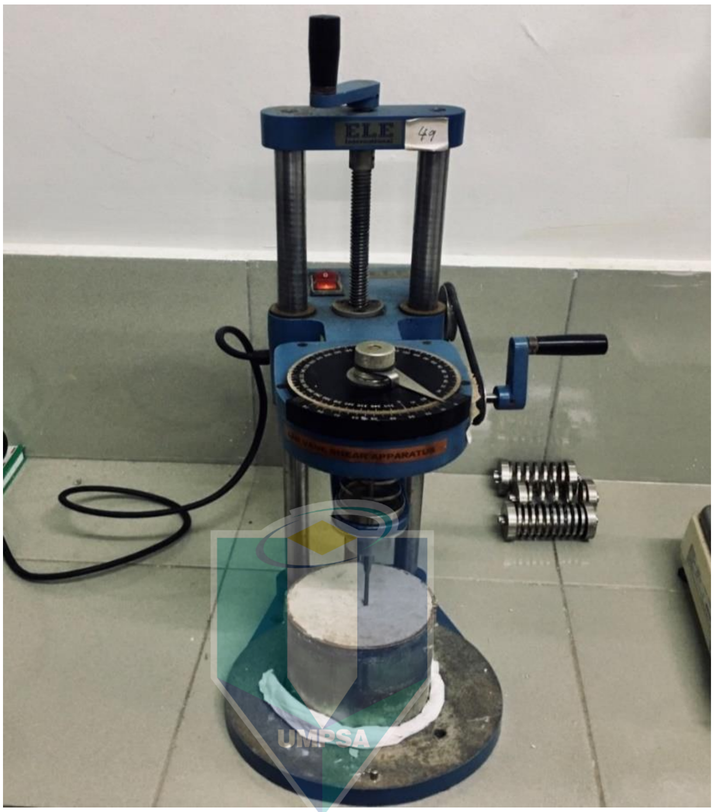

Figure 3.10 Laboratory Vane Shear Test Machine

3.6.5 Unconfined Compression Test (ASTM D2166)

The unconfined compression test is widely recognised as a rapid and uncomplicated technique to evaluate shear strength in soil, making it a commonly employed approach in soil shear analysis. This methodology was utilised for the assessment of stress-strength and unconfined compressive strength in fine-grained soils, specifically kaolin clay. The test is often effective in assessing the mechanical properties of solid sample materials that are either constantly collected or compressed. Unconfined compression testing was thus used to measure the shear strength of polypropylene column-reinforced clay material composites. This method is recognised for its expeditiousness, making it the most efficient option in this context. In this test, the axial strain resulting from the breakdown and the axial load at that point were recorded numerically. The undisturbed sample was prepared, and the specimen was compacted. The specimen was put into the loading system to be focused on the bottom plate. The loading frame was made up of two metal plates. The top plate was stationary and connected to the load-measuring unit. After the soil sample was positioned between the plates, the bottom plate was progressively elevated; the resistance of the stationary top plate was applied to the sample by an axial force. Loads were determined using a calibrated test ring or an electronic load cell. The measurement of vertical deformations was accomplished using a dial scale. This dial gauge was attached to the upper plate and was used to measure the difference in elevation between the upper and lower plates. To determine the form of the stress-strain relationship, the load, deformation, and time data were taken at a constant rate of 20 seconds. To provide further clarification, the specimen was subjected to axial stress in the form of unconfined compression, without any accompanying lateral container strain. This study's evaluation of the undrained shear strength of clay reinforced with 10 mm and 16 mm-diameter polypropylene columns was one of its goals. The testing approach presented in this study demonstrates the anticipated cohesive soil strength outcome in relation to total stress. Figure 3.11 depicts the testing apparatus utilised for conducting the unconfined compression test.

Figure 3.11 Unconfined Compression Test Machine

3.6.6 Consolidated Undrained (CU) Triaxial Test

The purpose of the ensuing consolidated undrained (CU) triaxial test was to determine if adding individual and multiple polypropylene columns to soft kaolin clay increased its shear strength in comparison to unreinforced kaolin. The study also attempted to determine how the pore water pressure created throughout the experiment was affected. Since the triaxial test offers several advantages over the direct shear test, conducting this was advised. The direct shear test includes pressing the failure plane with the device, whereas the triaxial test simulates almost exact circumstances. The tests given for this study at CU were performed with the GDS system. The comprehensive instructions for executing the method may be found in Section 3.9.

In the context of a triaxial test, the minor principle stresses (σ_3) and intermediate principal stresses (σ_2) often arise due to the application of cell pressure. On the other hand, the axial pressure placed on the specimen frequently results in primary principle stress (σ_1). The difference between the main principle stress (σ_1) and the minor principle stress (σ_3) is the mathematical expression for the deviator stress (q). Triaxial testing may be broadly categorised into two main classifications: consolidated undrained (CU) and consolidated drained (CD).

The present study employed the consolidated undrained (CU) test that included three distinct stages: shearing, consolidation, and saturation. The cylindrical specimens employed in this study had a diameter of 50 mm and an overall height of 100 mm. The examination of all these stages may be located in Section 3.7.2. During the whole process of consolidation, the specimen was successfully subjected to confinement by the application of pressure. The consolidation method resulted in a loss of water, which therefore impacted the volume of the specimen. A graph was constructed to depict the variations in volume across the specified time intervals, with the objective of ascertaining the point at which the consolidation process reached its culmination. The specimen appeared to be through the consolidation phase as it was subjected to an axial load that would tear it until it failed when the drainage valve was controlled. The monitoring and recording of particle pressure, deviator stress, and axial deformation were carried out automatically during the shearing process, provided that the speed of shearing was sufficiently mild to ensure the maintenance of pore water pressure equilibrium over the whole specimen. Table 3.2 displays the schedule for triaxial testing of consolidated undrained (CU).

Table 3.2 Sample coding and CU triaxial test programme for unreinforced clay and clay reinforced with polypropylene columns

Sample	Number of Columns	Column Diameter (mm)	Area Ratio, Ac/As (%)	Column Height mm	Column Height Penetration Ratio, Hc/Hs	Column Volume, (mm^3)	Volumn Penetration Ratio, Vc/Vs (%)
Control Sample							
C	0	0	0	0	0	0	0
			Single Column				
S1060	1	10	4	60	0.6	4712.39	2.40
S1080	1	10	4	80	0.8	6283.19	3.20
S10100	1	10	4	60	1.0	7853.98	4.00
S1660	1	16	10.24	60	0.6	12063.72	6.14
S1680	1	16	10.24	80	0.8	16084.95	8.19
S16100	1	16	10.24	60	1.0	20106.19	10.24
			Group Column				
G1060	3	10	12	60	0.6	14137.17	7.20
G1080	3	10	12	80	0.8	18849.57	9.60
G10100	3	10	12	60	1.0	23561.94	12.00
G1660	3	16	30.72	60	0.6	36191.16	18.43
G1680	3	16	30.72	80	0.8	48254.85	24.57
G16100	3	16	30.72	60	1.0	60318.57	30.72

3.7 Design of Polypropylene Column Model

3.7.1 General

The main objective of this research is to examine the compressibility and undrained strength characteristics of clay soil that has been reinforced by the implementation of polypropylene columns. The primary objective of the polypropylene column design is to depict the prevailing conditions seen in the building sector, while concurrently providing support to the earth layer. Because of the liquefaction of the underlying soil layers, this model was not intended to cause soil undulation, tilt, or uneven soil surface subsidence. The clay was designed using a light compaction process, and the reinforcement of the polypropylene column was made of clay using a replacement method. The process of replacement was chosen to extract the clay soil in order to create a void for the installation of the polypropylene column, reduce soil disruption, and prevent the incidence of swelling on the surface of the samples. The process of drilling holes to accommodate the polypropylene column installation was executed by utilising drill bits with the designated diameter, and applying the method of replacement.

3.7.2 Preparation of Kaolin Clay Sample

Figure 3.12 shows the equipment used to prepare soft kaolin specimens. In this study, the moisture content maintained in the reconstituted samples was 20%. This level was chosen as it is the ideal moisture level for kaolin clay, according to a reference from Head (1982). Moreover, the typical dry density range for kaolin clay at 20% MC, based on Proctor compaction, is approximately 1.3 to 1.6 g/cm³. According to Head (1982), the compaction method was used to apply the soil to a defined compaction effort or to get the soil to a given dry density or void ratio. The moist soil was mixed by hand until it was evenly distributed, then poured into the specially designed mould (Figure 3.13) and compacted into three layers. A 3.10 kg steel extruder was used to crush each layer with five free-fall strokes. The kaolin material which consisted of the specifically built mould (see Figure 3.14) underwent compaction to produce a specimen with a diameter of 50 mm and a height of 100 mm (Figure 3.15). Before introducing the soil into the mould, a thin coating of silicone grease was applied to the inside surface of the mould. Furthermore, a smooth polyethylene sheet was strategically positioned over the coated surface to reduce the level of friction that occurs between the soil and the wall of the mould.

Figure 3.12 Apparatus for the preparation of soft homogenous kaolin specimens

Figure 3.13 Kaolin mixed with water poured into the mould

Figure 3.14 Customised mould set for 50 mm diameter and 100 mm height specimen

Figure 3.15 Kaolin was compressed via pressure to both ends with a customised cap

According to initial predictions of negligible mass reductions during the operation, the applied approach effectively preserved the integrity of each specimen. Complete adherence to a roughly equal distribution of soil mass and mould volume allowed for the accomplishment. The "controlled sample" specimens did not have a polypropylene column attachment. For kaolin samples reinforced with polypropylene columns, drill bits with diameters of 10 mm or 16 mm were used to make a hole for the column to reduce the specimen's expansion while it was within the mould (Figure 3.16). The columns were specifically intended to have a height of 100 mm for completely penetrating columns, while partially penetrating columns were created with lengths of 60 mm and 80 mm. The specimen was then taken out of the moulds and placed in an appropriate container. To encourage the stabilisation of pore pressure, the container was left undisturbed for at least 24 hours after that (Figure 3.17). The geographical distribution of the places utilised for measuring the moisture content of the samples is depicted in Figure 3.18, while the moisture content of the kaolin samples is presented in Table 3.3.

Figure 3.16 Hole was drilled using 10 mm and 16 mm diameter drill bits

Figure 3.17 Specimens extruded out of the mould being kept inside the case

Table 3.3 Moisture content for kaolin specimens

		Moisture Content		
		Specimen 1	**Specimen 2**	**Average**
Layer 1	Point 1	19.60	19.20	19.40
	Point 2	20.10	19.40	19.75
	Point 3	19.30	19.76	19.53
	Point 4	20.30	19.10	19.70
	Point 5	19.70	20.50	20.10
Layer 2	Point 1	19.40	19.80	19.60
	Point 2	20.10	19.90	20.00
	Point 3	19.66	19.70	19.68
	Point 4	19.70	19.80	19.75
	Point 5	19.20	20.30	19.74
Layer 3	Point 1	19.44	20.20	19.82
	Point 2	19.90	19.70	19.80
	Point 3	20.25	19.95	20.10
	Point 4	20.70	20.30	20.50
	Point 5	19.80	20.30	20.10

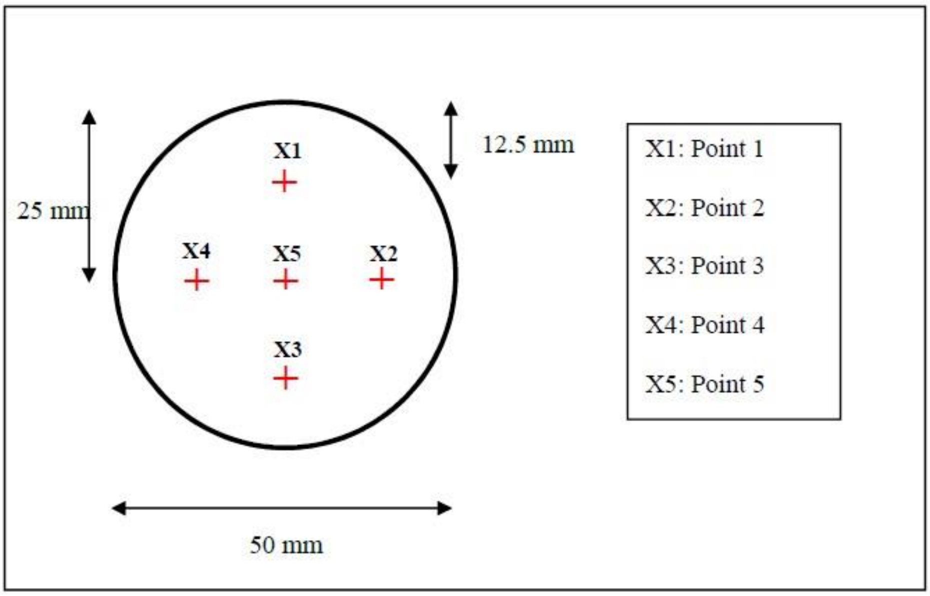

Figure 3.18 Location of points for moisture content determination

3.7.3 Polypropylene Columns Installation

The investigation involved the production of specimens to assess the shear strength of kaolin clay that had been reinforced with polypropylene columns. The control sample consisted of three produced samples, each lacking polypropylene reinforcement and exhibiting a 0-penetration ratio. The provided samples were used to determine the unmodified sample's shear strength. Every individual kaolin sample has a uniform penetration ratio, namely 0.6, 0.8, and 1.0. However, the area replacement ratio differs across specimens. Subsequently, perforations were created with a drill bit with a suitable diameter, while the specimens remained enclosed within the mould to impede any expansion. This was done in preparation for the fabrication of the polypropylene column for the reinforced specimens.

The penetration ratios (Hc/Hs) for each batch of kaolin specimens were consistent, with values of 0.0, 0.6, 0.8, and 1.0. The column diameter was seen to have two distinct measurements, specifically 10 mm and 16 mm. These measurements corresponded to area displacement ratios of 4.00% and 10.24%, respectively, denoted as the column area to sample area ratio (Ac/As). The specimen apertures were subsequently substituted with polypropylene material, as depicted in Figure 3.19. The polypropylene particles possess typical diameters ranging from 1.08 mm to 3.35 mm.

Figure 3.19 Installation of polypropylene soft kaolin clay specimen

The determination and production of the mass of polypropylene necessary to fill each pre-drilled hole were conducted to ensure constant density throughout all polypropylene columns. This was achieved by using the known volume of each hole. The data is presented in Table 3.4. This method enabled the production of an identical entity for each of the polypropylene columns that were used in this study's soft kaolin clay reinforcement.

Table 3.4 Density of various-sized polypropylene columns set in samples of kaolin

Column Diameter (mm)	**Column Length (mm)**	**Volume (mm^3)**	**Density (Mg/m^3)**	**Mass of Polypropylene (g)**
	60	4712.40		2.65
10	80	6283.20		3.53
	100	7853.98	0.562	4.41
	60	12057.60		6.78
16	80	16084.95		9.04
	100	20106.19		11.30

3.7.4 Polypropylene Column Arrangement

A polypropylene column was positioned in the centre of the research to reinforce the specimens. However, a triangle arrangement was used for the column groupings as it made it easier to maintain precise column placement and spacing during development. The columns were placed midway between the kaolin specimen's geometric borders and centres to provide an even weight distribution throughout all of them. The determination of the inter-column distance was achieved by assessing the area ratio, which represents the column area as a fraction of the overall clay area. Figure 3.20 illustrates the organisational configuration of both individual and collective columns. For the purpose of choosing area ratios and designing the column, the research conducted by Black et al. (2015) provided the framework. A picture containing specimens that were reinforced using individual and multiple polypropylene columns is shown in Figure 3.21.

The polypropylene column's diameter (D) and the granular material's particle size (d) were the two key variables that determined the proper column dimension for the model testing. Powrie (2018) suggested that for model testing, it is preferable to have a D/d ratio that closely matches that of the prototype structures. The abbreviation "D/d" was employed throughout the time period spanning from 52 to 83. Stone columns in practice are typically constructed using crushed rock or gravel, which possess average diameters ranging from D = 0.6 to 1 m. The constituent materials of these columns consist of particles with typical sizes falling between 25 and 50 mm. Hence, the ratio D/d has a range spanning from 12 to 40. The experiment utilised polypropylene columns of varying widths, specifically 10 mm and 16 mm. Additionally, particles within the size range of 1.08 mm to 3.35 mm were employed. As a result, throughout the process of model testing, the ratio values of D/d exhibited a range of 4 to 17. Due to the imposition of limitations on the column diameter to mitigate boundary effects, the lower range values of D/d seen in the model experiments were comparatively lower than those encountered in practical applications. Moreover, a lower D/d ratio means the columns interact more closely with fewer particles. This can cause strain localization around the columns and may not perfectly simulate the more distributed strain field expected in prototypes. In addition, the interaction between column material and surrounding soil particles plays a significant role in the shear behavior and load-bearing capacity. A lower D/d ratio could alter the interlocking effects and the shear resistance along the interface, potentially leading to conservative estimates of improvement in shear strength.

The research utilised polypropylene columns of varying widths, specifically 10 mm and 16 mm. These dimensions yielded Ac/As ratios of 4% and 10.24% for each respective column. For the group column, area ratios of 12% and 30.72% were used. The height penetration ratio, denoted as Hc/Hs, shows how the vertical dimensions of the specimen and the column correlate. This study utilised three separate ratios, namely 0.6, 0.8, and 1.0, which corresponded to slightly penetrating columns and fully piercing columns, respectively.

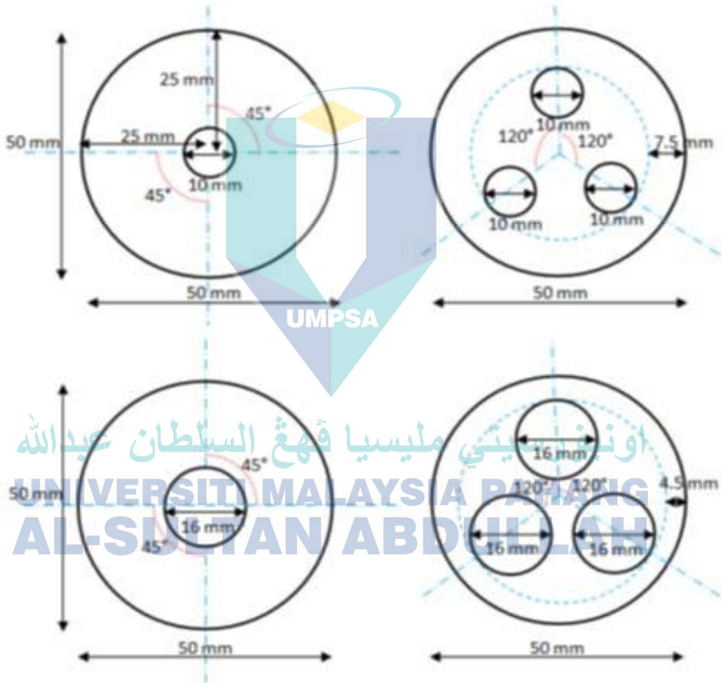

Figure 3.20 Detailed polypropylene column arrangement in clay samples for both single and combined columns

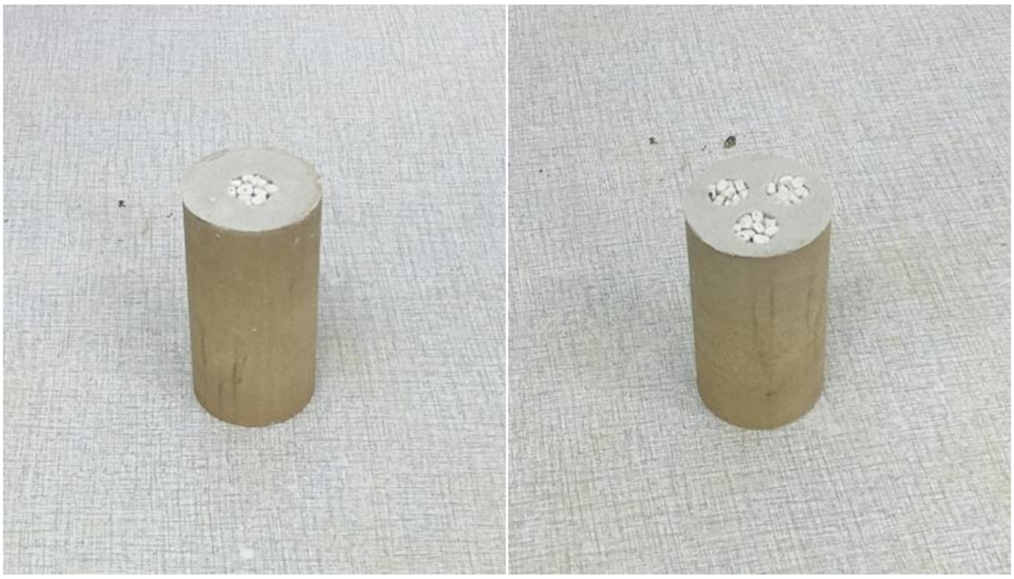

Figure 3.21 Completely instaled single and group polypropylene columns in the sample made of soft kaolin clay

3.7.5 Details of Laboratory Tests

The soil samples were appropriately processed by introducing them into polypropylene columns, followed by conducting CU and UCT tests on the resultant specimens. The sample measured 50 mm in diameter and 100 mm in height. Polypropylene columns with two distinct diameters, specifically 10 mm and 16 mm, were implemented into the sample. The depiction of the layout of the single and group columns can be observed in Figure 3. The experiments involved the utilisation of column heights measuring 60 mm, 80 mm, and 100 mm. This study aims to investigate the variation in a clay sample's shear strength in response to various column heights. Experiments were also done on materials in the absence of polypropylene columns. The aforementioned samples were designated as control specimens. Each unique orientation was examined using three samples. Table 3.5 presents a concise overview of the number of tests to be conducted. The obtained results were examined to distinguish the variations in shear strength between individual columns and columns that are clustered together. The analysis also encompassed an examination of the changes in shear strength across different column diameters and heights. Finally, depending on the results acquired, a design chart was created.

Table 3.5 Number of samples to be tested

Diameter, D and Height, H of kaolin specimen (mm)	Diameter of single and group polypropylene columns (mm)	Length of single and group polypropylene columns (mm)	Number of specimens with single column	Number of specimens with group columns
	Control Specimens	-	3	
D = 50 H = 100	10	60	3	3
		80	3	3
		100	3	3
	16	60	3	3
		80	3	3
		100	3	3
Total			39	

3.8 Consolidated Undrained Triaxial Test

The Consolidated Undrained Triaxial Test was performed by utilising the Automatic Triaxial System apparatus situated at the Geotechnical Laboratories at the Faculty of Civil Engineering Technology, Universiti Malaysia Pahang Al-Sultan Abdullah. The device is depicted in Figure 3.22. The software suite is known as GDSLAB, including of GDSLAB Version 2.8.3.1 and GDSLAB Reports, is also included as part of the system installation.

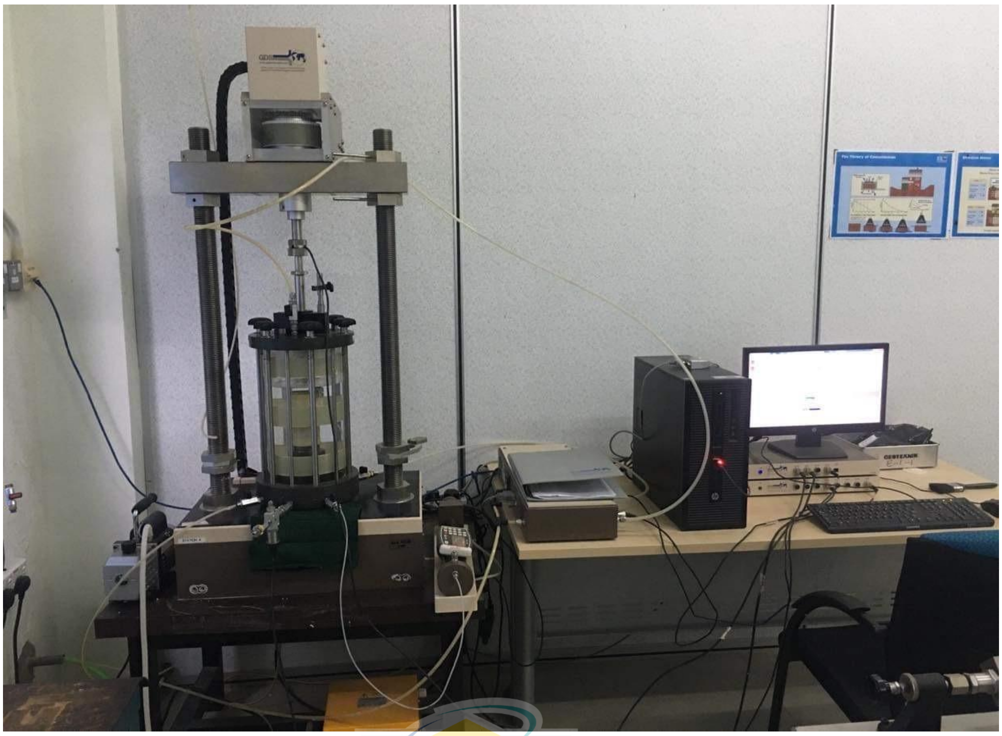

Figure 3.22 GDS Completely Automatic Triaxial System equipment setup

The GDSTAS was developed in accordance with global guidelines for data display and test execution, and it is eligible for national laboratory accreditation programmes. The system was controlled by the user's PC, which ran GDSLAB software and Microsoft Windows operating system.

The selection of the test type was determined by considering factors such as the test menu, test parameters (such as cell pressure, back pressure, testing rates, etc.), and test terminating conditions. The technical specifications of the GDSTAS used were stated as follows:

i) Computer-automated control of testing

ii) GDSLAB, an MS Windows® programme for post-test analysis and test control

iii) Totally independent of both cell pressure and back pressure

iv) Choice of spot-verification

v) Clearly specified methods of calibration with the Budenberg dead weight tester

vi) Adherence to worldwide norms and guidelines.

All test data were automatically saved to a file while the test was run. A block of the most recent live test data was given alongside up to three graphs in the online graphics. Tests were carried out throughout the night and occasionally on weekends and public holidays. The testing rate, back pressure, and cell pressure were all directly managed by the computer. The computer stored the following properties on the PC hard drive: axial displacement, axial load, pore pressure, and volume change. To ensure the precision and dependability of the test results, an annual verification and calibration procedure was implemented on the equipment. The latest calibration was carried out on October 5, 2021, which was before the start of the laboratory test.

3.8.1 System Elements

The fundamental system hardware elements are shown in Figure 3.23. The arrangements were as follows:

i) Enterprise Triaxial Automated System (ELTAS) which was based on 1MPa Enterprise Pressure/Volume Controller (ELDPC).
ii) Standard Triaxial Automated System (STDTAS) which was based on 3MPa Standard Pressure/Volume Controller (STDDPC).
iii) Advanced Triaxial Automated System (ADVTAS) which was based on 2 MPa
iv) Advanced Pressure/Volume Controller (ADVDPC).
v) High Pressure Triaxial Automated System (HPTAS) which was based on High
vi) Pressure Controllers (≥ 16MPa).

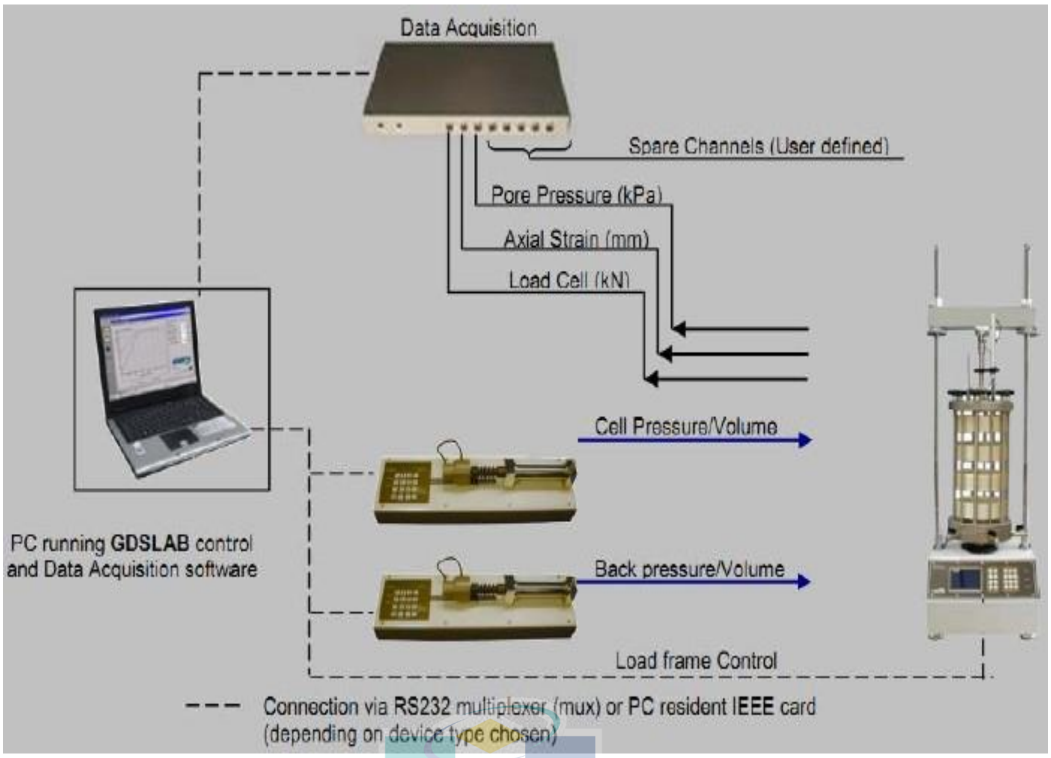

Figure 3.23 Diagram of GDSTAS Hardware elements (www.gdsinstruments.com)

The system that was selected from a variety of hardware that GDS provided was as follows:

a. Load frames

- Velocity controlled devices with serial PC interface were available in two different force capacities: 50 kN and 100 kN.

- The application of velocity, position, and direct load feedback control techniques, incorporating serial or IEEE PC connection, employed force magnitudes of 100 kN, 250 kN, 500 kN, 750 kN, and 1000 kN.

b. Triaxial cells

The triaxial cell used in this study was 1700 kPa capacity, where specimens of up to 50, 100 or 150 mm could be used (load frames > 50 kN for 150 mm cell due to size).

c. Pressure/volume controllers

The pressure controllers utilised in the experiment were the Advanced Pressure/Volume Controller (ADVDPC) as depicted in Figure 3.24. The pressure ranges of the controllers were 2 MPa, 3 MPa, 4 MPa, 8 MPa, 16 MPa, 32 MPa, 64

MPa, and 128 MPa. The apparatus was equipped with a 200 cc volumetric capacity and either an Ethernet or IEEE PC interface. The back pressure controller's function included both applying back pressure and measuring the test specimen's volume change.

Figure 3.24 Cell pressure and back pressure were controlled with an advanced pressure/volume controller

d. Data acquisition devices

A data collecting device called the "serial data pad," or GDS 8 channel, was used in the system configurations. With computer controlled gain ranges, this 16-bit device was specifically made to fit transducers used in triaxial tests, which are:

i) +/-10mV, +/-20mV, +/-30mV (load cells)

ii) +/-100mV, +/-200mV (pressure transducers)

ii) +/- 1V, +/- 5V, +/- 10V (displacement transducers)

e. Connecting devices

The system controller made use of a Microsoft Windows XP-powered personal computer (PC). To ensure that the GDSLAB software was capable of running the hardware, the software was connected to the PC (Figure 3.25).

Figure 3.25 GDSLAB software

3.8.2 Data Analysis using CU Triaxial Test

As mentioned earlier, the specimens in the CU test underwent a sequential process consisting of three distinct phases: saturation, consolidation, and shearing. During the saturation technique, the specimens were saturated until it reached a B-Value (Skempton, 1954) greater than 0.95, which signified a satisfactory level of saturation. This was achieved by applying backpressures of 50kPa, 100kPa, and 200kPa. The specimens were treated to isotropic consolidation at effective confining pressures of 50 kPa, 100 kPa, and 200 kPa during the consolidation stage. Therefore, it was customary to consolidate the specimens before subjecting them to shearing or compression. Section 3.7.2.5 describes the continuous strain rate of 0.15 mm/min for the specimens that were sheared in the undrained condition. The experiments were concluded with the attainment of an axial strain of around 20%. The test strategy devised for the samples in this investigation is depicted in Figure 3.26.

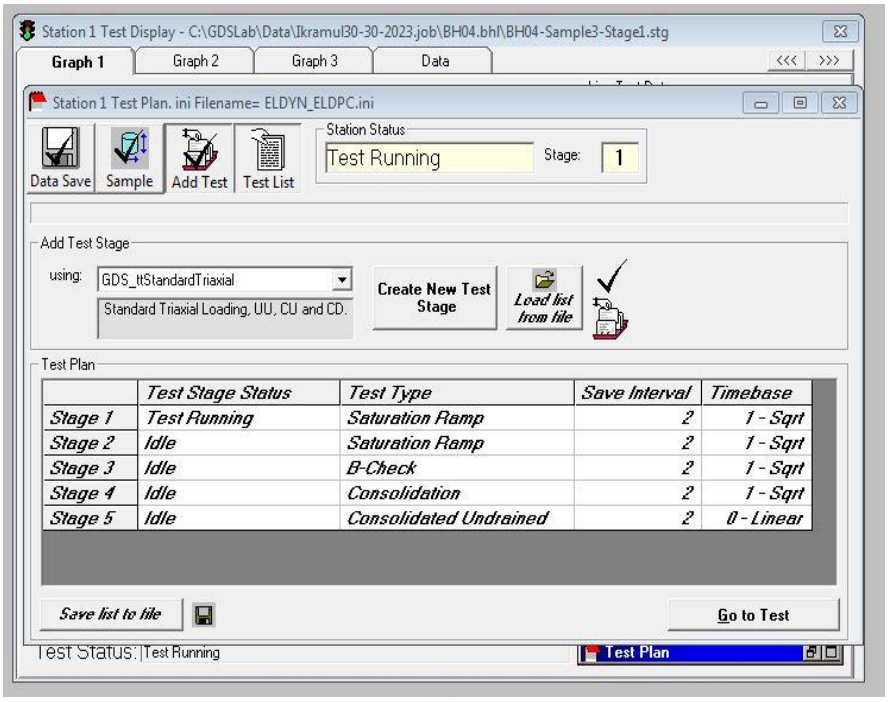

Figure 3.26 GDSLAB test plan for consolidated undrained triaxial test

3.8.2.1 Stage 1 and 2: Saturation Ramp

In this specific phase, the pressure of the target cell was determined, and the back pressure applied was 10 kPa lower than the cell pressure, as recommended by Head (1982). During the saturation stage, cell pressure and back pressure were applied as seen in the screenshot displayed in Figure 3.27. With cell pressures of 100 kPa, 200 kPa, and 400 kPa, respectively, three specimens were chosen for each batch of samples. Once the desired target cell pressure and back pressure were attained, the test seamlessly transitioned to the subsequent stage.

Upon completion of the saturation ramp, the pressure was ordered by the software to be maintained before proceeding to the next stage. The given directive necessitated the maintenance of pressure at the culmination of the stage, as seen in Figure 3.28.

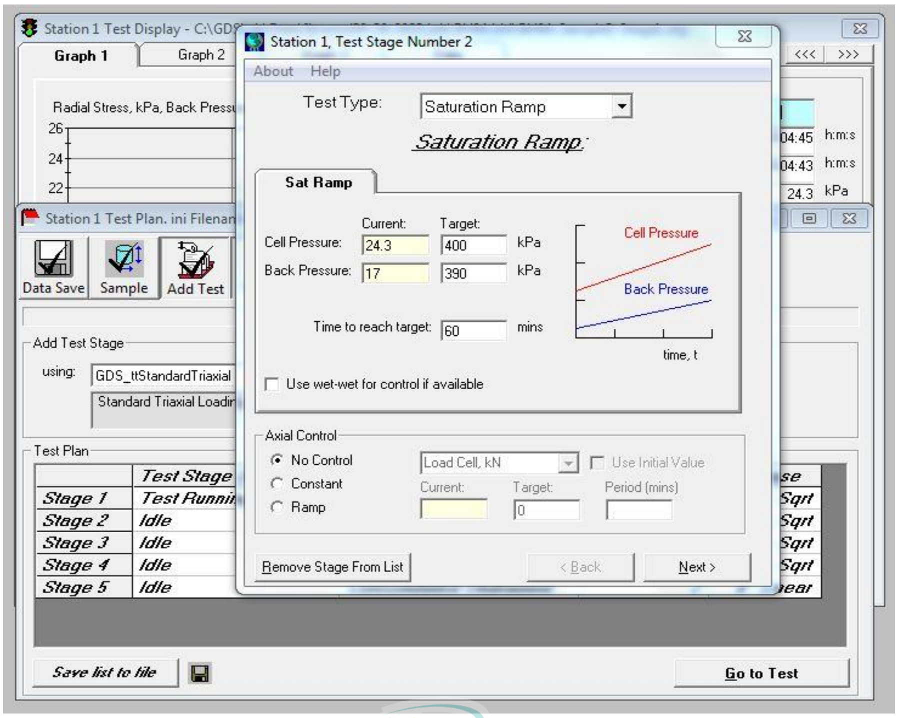

Figure 3.27 Setup for Stage 1

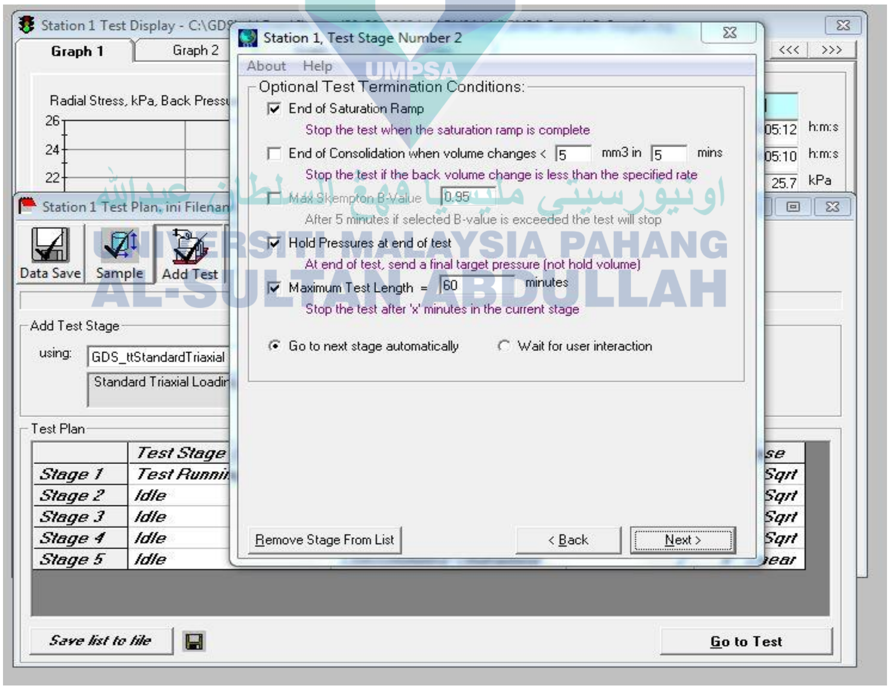

Figure 3.28 Stage 1 offers several optional test termination criteria

3.8.2.2 Stage 3: Saturation Check

The saturation of specimens was checked by determining the coefficient of pore pressure, B-Value (Skempton B-Value). This can be done through the B-Check menu as shown in Figure 3.29. During this phase, it was determined that if the Skempton B-Value surpassed 0.95 for a duration of 5 minutes, the test would proceed to the subsequent level automatically. The condition depicted in Figure 3.30 served as the termination criterion for the saturation stage.

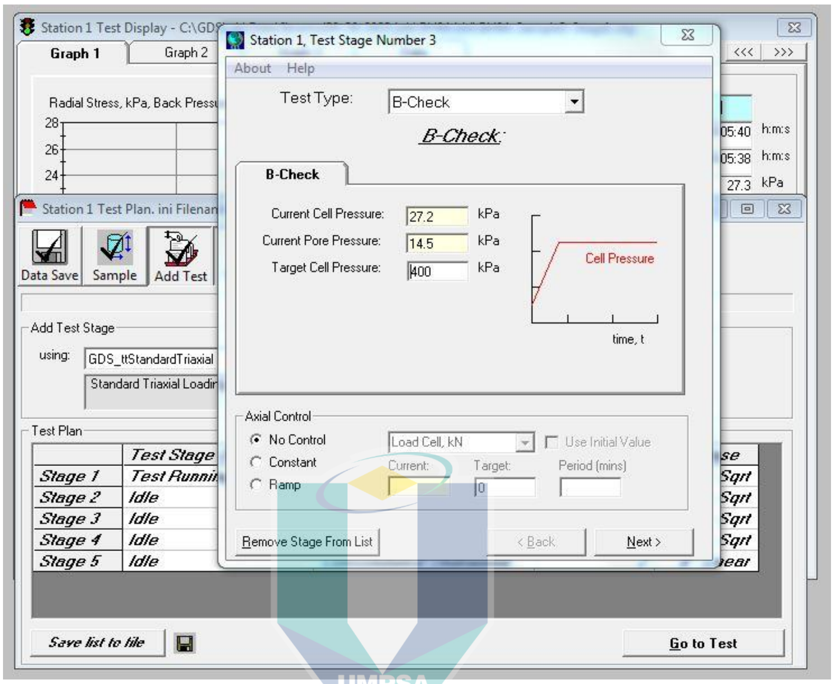

Figure 3.29 Setup for Stage 3

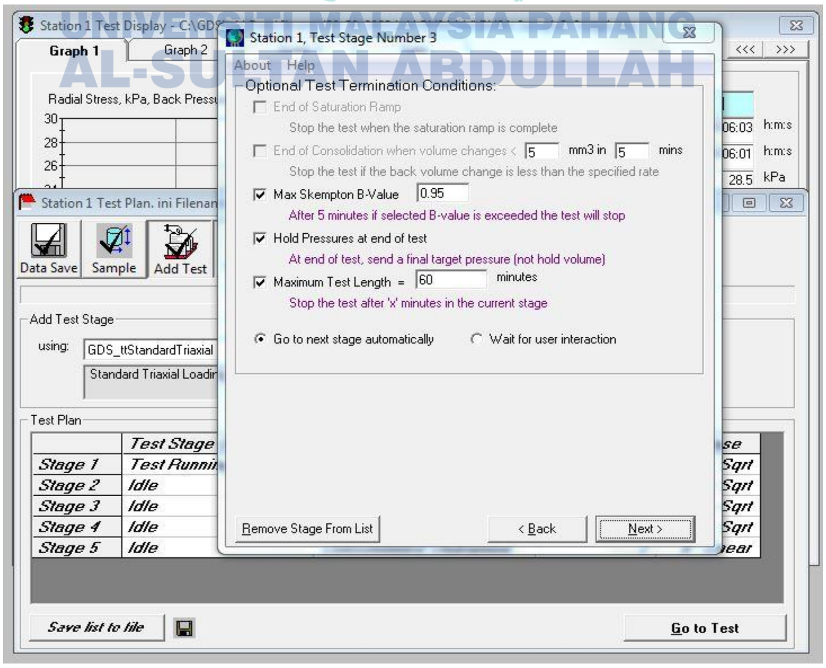

Figure 3.30 Optional test termination condition for Stage 3

3.8.2.3 Stage 4: Isotropic Consolidation

The shearing stage was conducted on specimens that were isotropically normally cemented in this study. According to the data presented in Figure 3.31, the cell pressures selected for three specimens were 100kPa, 200kPa, and 400 kPa, respectively. Additionally, the back pressure was established at 50kPa, 100kPa, and 200kPa. The specimen was consolidated isotropically to obtain a minimum of 90% consolidation. Therefore, a termination condition was established, stipulating that the test might proceed to the following stage (as depicted in Figure 3.32) only if the back volume change remained below 5 mm3 for a duration of at least 5 minutes.

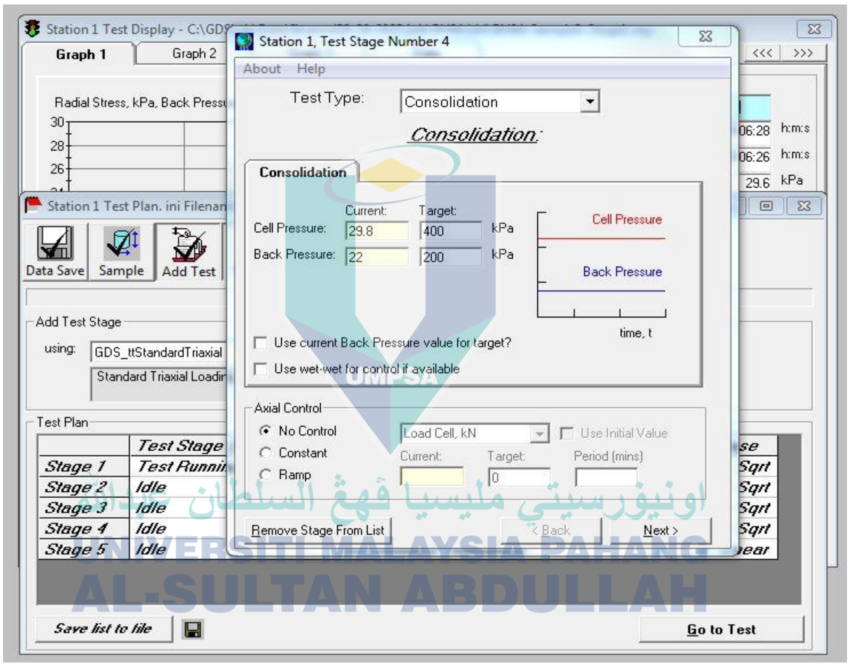

Figure 3.31 Setup for Stage 4

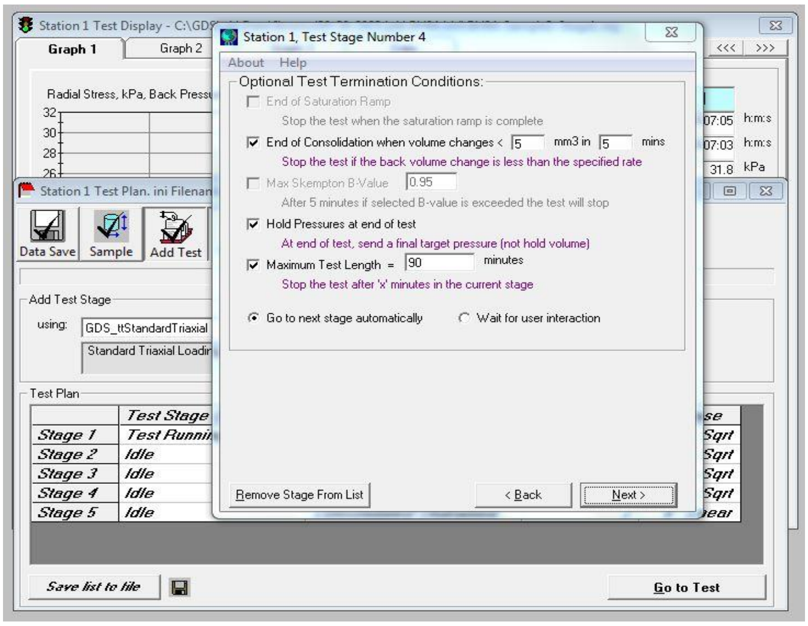

Figure 3.32 Optional test termination condition for Stage 4

3.8.2.4 Stage 5: Shearing

According to Head (1986), the quick occurrence of compression leads to an inaccurate representation of the circumstances inside the centre of a sample when measuring pore water pressure at the sample's base. This study involved conducting tests on samples that were devoid of side drains. Therefore, in the case of a sample lacking side drains, the time to failure (t_f) was computed as:

$$t_f = 1.8 \times t_{100} \text{ minutes} \tag{3.4}$$

The parameter represented by t100 represents the amount of time needed for full consolidation, as ascertained by examining the graph that shows the volume change in proportion to the root-square of time.

The results acquired during the consolidation phase often indicated that the computed t_f values were below 2 hours. According to Head (1986), in cases when the computed t_f value is found to be less than 2 hours, it is recommended to provide a minimum time to failure of 2 hours. Based on the available data, the rate of strain was determined by considering the suggested failure strain.

3.8.2.5 Rate of Strain and Displacement

According to Head (1986), it is advised to cap the highest rate of strain applied during compression at ε_f/t_f % per minute. The investigation utilised samples that were typically consolidated, and a recommended failure strain value of 20% was selected based on the guidance provided by Head (1986) (see Figure 3.34). Hence:

t_f = 2 hrs = 120 minutes, ε_f = 20 % = $\Delta L/L$

L = 100 mm

Maximum rate of axial displacement = $\Delta L/ t_f$

$= \varepsilon_f L/ 100t_f$

= (20 x 100) / (100 x 120)

= 0.167 mm/min

By that, as shown in Figure 3.33, 0.15 mm/min was chosen as the rate of axial displacement in which the value is less than the calculated maximum rate of axial displacement. Figure 3.34 shows the termination condition for shearing with the failure strain set at 20%.

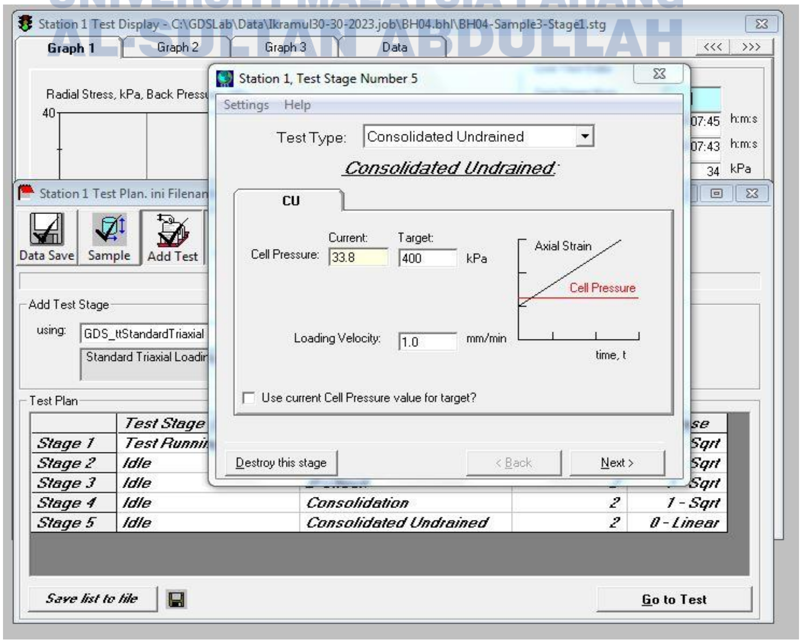

Figure 3.33 Setup for Stage 5

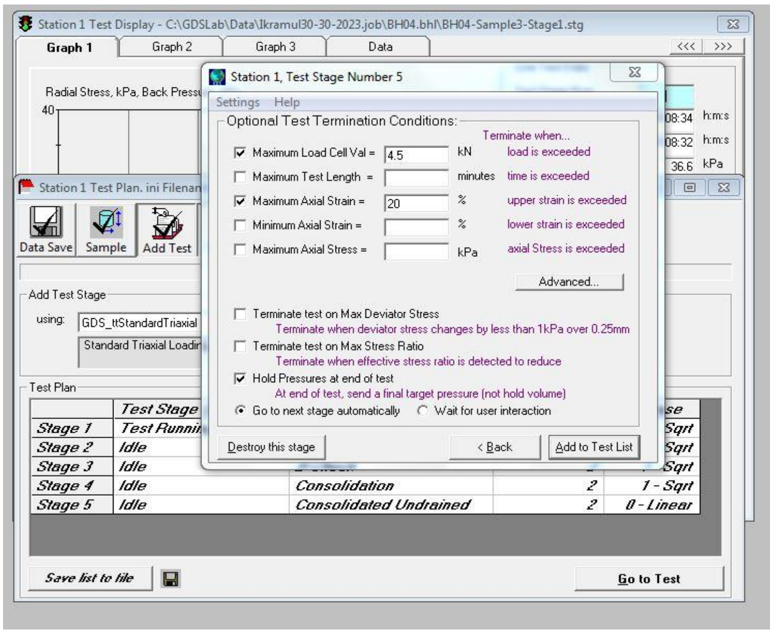

Figure 3.34 Optional test start condition for Stage 5

3.9 Data Analysis and Result Presentation

Using the GDS Report Software, the reports for the samples were generated in Microsoft Excel format once every specimen had successfully completed the CU test (as indicated in APPENDIX L). All the data that was collected throughout each step was converted into an analytical format and displayed graphically in the report.

3.10 Laboratory Tests for the Assessment of Morphological Properties

The primary aim of doing Scanning Electron Microscopy (SEM) examination was to determine the morphological attributes of the materials being studied. Figure 3.35 depicts the apparatus utilised in scanning the electron microscopy. The process of SEM involves the examination of a material through the use of an electron beam. This beam is utilised to scan the specimen and produce a magnified image. SEM analysis and SEM microscopy have demonstrated significant efficacy in the microanalysis of solid inorganic materials and failure analysis. Electron microscopy is a technique that enables the generation of high magnifications, high-resolution pictures, and precise measurements of minute features and objects. The SEM investigation was done to analyse the morphological characteristics of the polypropylene-integrated samples.

Figure 3.35 Scanning Electron Microscope Machine

CHAPTER 4

RESULTS AND ANALYSIS

4.1 Introduction

The primary materials employed in this study were kaolin and polypropylene. This chapter provides coverage of the features of these materials. The engineering characteristics of kaolin were assessed using various laboratory examinations, such as the Atterberg limit test, particle size distribution analysis, compaction test, specific gravity measurement, permeability test, unconfined compression test, and consolidated undrained triaxial test. Several tests were performed on the polypropylene in the laboratory, including the vane shear test, the consolidated undrained triaxial test, the particle size distribution test, the relative density test, the compaction test, the permeability test, the direct shear test, the scanning electron microscope test, and the unconfined compression test.

The results of the consolidated undrained triaxial test and the unconfined compression test are also included in this chapter. The cylindrical specimens, measuring 50 mm in diameter and 100 mm in height, were made of soft kaolin clay and used for experimental research. Both reinforced and unreinforced samples were included in the study. These tests aimed to determine the engineering qualities of the materials investigated in the study. In order to assess the enhancement in shear strength observed at a specific location, an experimental study was conducted by employing polypropylene columns with varying diameters and penetration ratios to reinforce the soft kaolin clay.

4.2 Basic Properties of Polypropylene and Kaolin

The required characteristics of the polypropylene and kaolin were analysed in this laboratory and were summarised in Table 4.2, while the polypropylene used is visually depicted in Figure 4.1. It is evident that polypropylene was a substance with coarse grains, a greyish tint, and rough, gripping surface textures. The results of the tests indicated that polypropylene's engineering qualities are comparable to those of regular sand and fine gravel. This polypropylene material promises numerous opportunities for application in soft soil improvement projects as a replacement for granular columns if it is designed and produced correctly.

Figure 4.1 Polypropylene was acquired from Titan Petchem (M) Sdn. Bhd. (PM201)

The examination of polypropylene's qualities was carried out through a limited number of three trials, while the remaining attributes were obtained from the supplier, Titan Petchem (M) Sdn. Bhd. Table 4.1 illustrates the parameters obtained from the granular polypropylene provider.

Table 4.1 Properties of polypropylene from manufacturer

Paramrter	**Value**
Density	0.9 g/cm^3
Tensile Strength at Yield	330 kg/cm^3
Elongation at Yield	12 %
Flexural Modulus	13000 kg/cm^2
Shrinkage	1.3 - 1.4 %
Water Absorption after 1 day	0.002 %
Melt Flow rate at 230 ºC	20 g/10 min

Table 4.2 Test result found for the properties of polypropylene and kaolin

Material	**Test**	**Parameter**	**No. of Tests**	**Value**
Polypropylene	Soil Classification	AASHTO	03	A-1-a
		USCD (Plasticity Chart)	03	SW
	Relative Density	Min. Density	03	0.57 gm/cm^3
		Max. Density	03	0.74 gm/cm^3
	Constant Head Permeability	Coefficient of Permeability	03	5.73x10^{-3} m/s
	Direct Shear Test	Cohesion	03	8.50 kPa
		Angle of Shear Resistance	03	39.40^0
	Consolidated Undrained Triaxial	Cohesion	03	14.40 kPa
		Angle of Shear Resistance	03	29.60^0
	Morphological Test	Scanning Electron Microscope (SEM)	02	
Kaolin	Soil Classification	AASHTO	03	A-6
		USCD (Plasticity Chart)	03	ML
	Atterberg Limit	Liquid Limit	03	36.6
		Plastic Limit	03	25.1
		Plasticity Index	03	11.5
	Standard Compaction	Maximum Dry Density	03	1.63
		Optimum Moisture Content	03	20%
	Specific Gravity	Specific Gravity	03	2.63
	Falling Head Permeability	Coefficient of Permeability	03	2.27 x 10^{-12} m/s
	Vane Shear	Undrained Shear Strength	03	8.07 kPa
Kaolin Reinforced with Polypropylene	UCT	Undrained Shear Strength	52	11.13 kPa
	Consolidated Undrained Triaxial — Mohr Coloumb Failure Criteria	Cohesion	39	1.37 kPa
		Frictional Angle	39	32.30^0
	Consolidated Undrained Triaxial — Critical State Failure Criteria	Critical Frictional Angle	39	33.50^0
		M	39	1.30
		Γ	39	2.302
		λ	39	0.093

4.2.1 Particle Size Distribution

The present study involved the use of a dry sieve analysis technique to determine the distribution of particle sizes of the kaolin clay used. The importance of soil particle size is in its effect on the characteristics of the soil. The determination of the particle size of kaolin was conducted through the utilisation of hydrometer and wet sieving methodologies. The outcomes derived from the sieve analysis experiments are displayed in Appendix A. Meanwhile, the results obtained from the hydrometer tests are shown in Appendix B. The results are depicted in Figure 4.2. The observed kaolin exhibits a well-graded composition, encompassing a range from clay to fine sand particles. Furthermore, the analysis revealed that a significant proportion of the kaolin particles, specifically 96%, were between the size range of 0.001 to 0.2 mm. Additionally, around 53% of these particles were found to be smaller than 0.063 mm. According to the AASHTO categorisation system, the presence of kaolin in the soil categorises it as Group A-6, which is characterised by its clayey composition.

The particle size distribution of polypropylene was exclusively measured through the utilisation of the dry sieve method as the particles exhibited a coarse character. The results of the examinations are presented in Appendix A and shown in Figure 4.2. As anticipated, the majority of the particles exhibited a size range of 0.100 to 10 mm, which aligns with the characteristics of fine sand and fine gravel. Because polypropylene (PP) is produced under regulated conditions, it has a high degree of uniformity in terms of material size. The polypropylene material that is used generally has a size range of 1.08mm to 3.35mm. The graph also shows that the polypropylene samples that were selected for representation had a similarly graded size distribution and comparable trends. The results showed that the average coefficient of uniformity (Cu) was 10.00, and the average coefficient of curvature (Cc) was 1.11. The obtained results serve to validate this observation.

Polypropylene is classified within the A-1 category of the AASTHO classification system. This particular category includes stone fragments that are mixed with a well-graded binder composed of fine components. Polypropylene is in the categorisation of A-1-a. Polypropylene falls within the classification of well-graded sand (SW) as per the Unified Soil Classification System (USCS). Muhardi et al. (2010) discovered results that were similar to those reported in this study. The polypropylene material examined in their research was categorised in a manner consistent with the present study due to its Cc value of 1.01 and Cu value of 16.56.

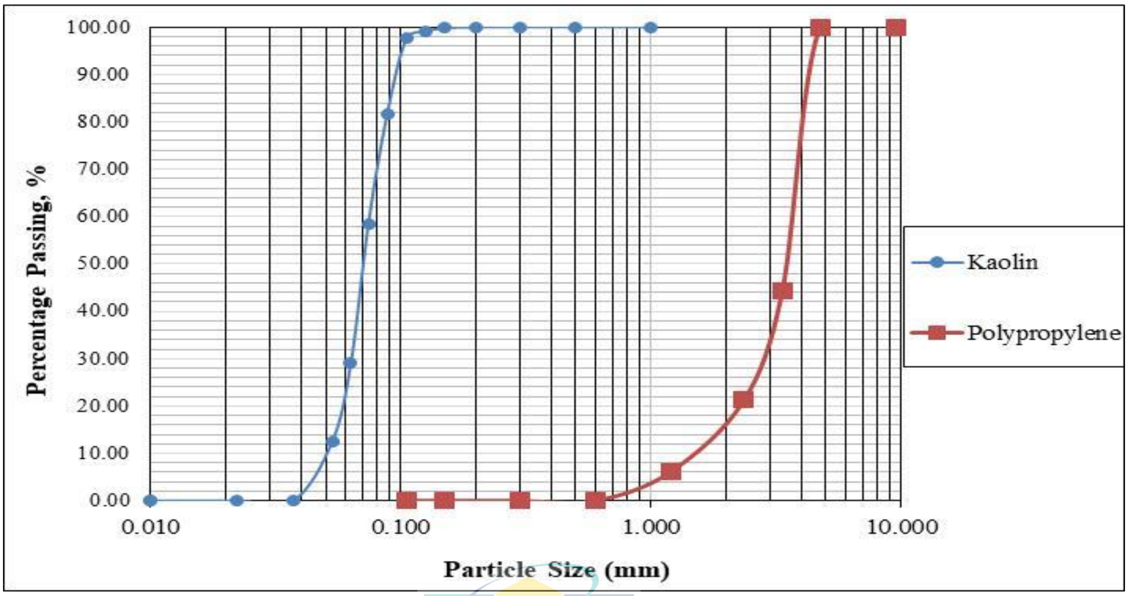

Figure 4.2 Particle size distribution curve of kaolin and polypropylene

4.2.2 Atterberg Limit

The Atterberg limit test was utilised to predict the behaviour of kaolin clay at different levels of moisture content. A soil sample can become more cohesive and exhibit plastic-like properties when water is added. However, the soil may begin to behave more like a liquid if an excessive amount of water is added to the soil sample. Since clayey and silty soils can alter volume in response to changes in moisture content, the Atterberg limit test may be helpful in these situations. The evaluation of the plastic limit, liquid limit, and plastic index is imperative for comprehending the characteristics and attributes of the soil being examined.

The objective of carrying out the Atterberg limit test was to determine the precise quantity of water required to get specific levels of behaviour, namely the liquid limit (w_L), plastic limit (w_P), and shrinkage limit (w_S) of kaolin. The results of this experiment showed that the kaolin clay's liquid limit was 35.50%, and its plastic limit was determined to be 25.10%. It was found that the plasticity index was 10.40%. In the ASTM technique, the shrinkage limit was determined to be 14.30%. The findings of the Atterberg limit test are presented in Appendix C.

The classification of kaolin was established by employing the plasticity chart illustrated in Figure 4.3. This decision was made based on the observation that 53% of the particles had a diameter smaller than that of the 0.063 mm sieve. The kaolin material was categorised as ML (low plasticity silt) due to its moderate plasticity, positioning it below the A-line. Its plasticity index of 10.40% and liquid limit of 35.50% support the aforementioned classification. The shrinkage limit of kaolin was determined to be 14.30%. This number indicates that controlling the moisture level throughout the kaolin drying process is critical to prevent excessive cracking and ensure that it does not exceed the shrinkage limit of 14.30%. Table 4.3 presents a comparative analysis of LL, PL, and PI in relation to earlier researchers.

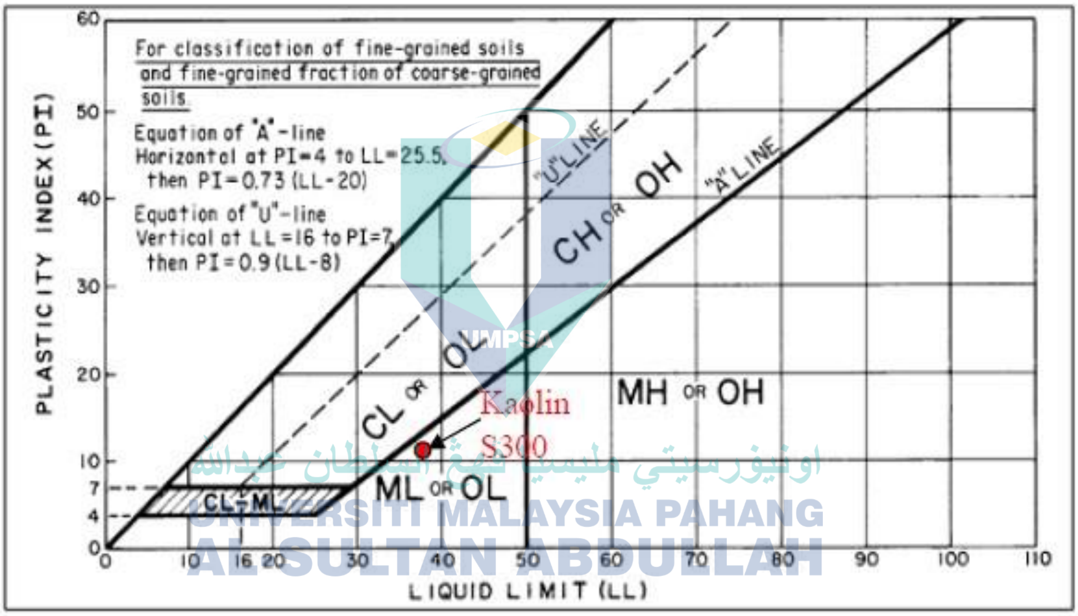

Figure 4.3 Plasticity Chart (ASTM D2487)

Table 4.3 Comparison of LL, PL and PI with previous researchers

Researchers	Liquid Limit (%)	Plastic Limit (%)	Plastic Index
Ali et al. (2021)	54.00	23.00	31.00
Spagnoli et al. (2018)	36.00	28.00	8.00
Hasan et al. (2015)	38.43	20.00	18.43
Current Research (2023)	35.50	25.10	11.40

4.2.3 Relative Density Test

The objective of this study was to investigate the minimum and maximum parameters of density in granular polypropylene. Two primary parameters that may affect the relative density of a particular sample are the volume and mass of the sample. The vibrating table was employed in this experiment to induce particle vibration, facilitate their arrangement into a homogeneous configuration, and minimise the presence of voids inside the sample. As the particles were arranged in a denser state, the porosity of the soil decreased, and thus the maximum density could be reached. Minimum density means that the particles were packed loosely and there were lots of voids between them. The relative density of a sample can affect its overall compressibility, permeability, and California bearing ratio. The result of the relative density test can be found in Appendix D. The maximum density of the polypropylene used in this study was 0.74 g/cm^3, while the minimum density of the polypropylene was 0.57 g/cm^3.

4.2.4 Specific Gravity Test

The specific gravity test is a method that employs the principle of water displacement to ascertain the density of soil particles through the utilisation of a ratio. The specific gravity is a quantitative parameter that measures the ratio between the mass of a soil particle and the volume of distilled water displaced. The specific gravity of the kaolin sample under examination is 2.63, as indicated by the result presented in Appendix E. The reliability of the number is deemed credible as it falls within the range of 2.56 and 2.64, which aligns with the findings of prior researchers. Table 4.4 displays the results obtained from the comparison of specific gravity tests.

Table 4.4 Comparison of specific gravity of kaolin with previous researchers

Researchers	**Specific Gravity**
Ali et al. (2021)	2.64
Spagnoli et al. (2018)	2.56
Hasan et al. (2015)	2.62
Current Research (2023)	2.63

4.3 Mechanical Properties

4.3.1 Standard Compaction

The moisture content and dry density of kaolin, as determined by the compaction test, are graphically illustrated in Figure 4.4. This study's figure illustrates the maximum dry density of kaolin, which was determined to be 1.63 mg/m^3, and the ideal moisture content, which was seen to be 20%. In conclusion, a reduction in air gaps leads to a rise in compaction, which subsequently produces a rise in dry density. The quantity of water that results in maximum dry density is known as the optimum water content. This suggests that kaolin can reach its maximum density when 20% water is added to the soil that has been baked dry. Large void content and low specific gravity often affect the compaction characteristics. The findings of the research are shown in Appendix F.

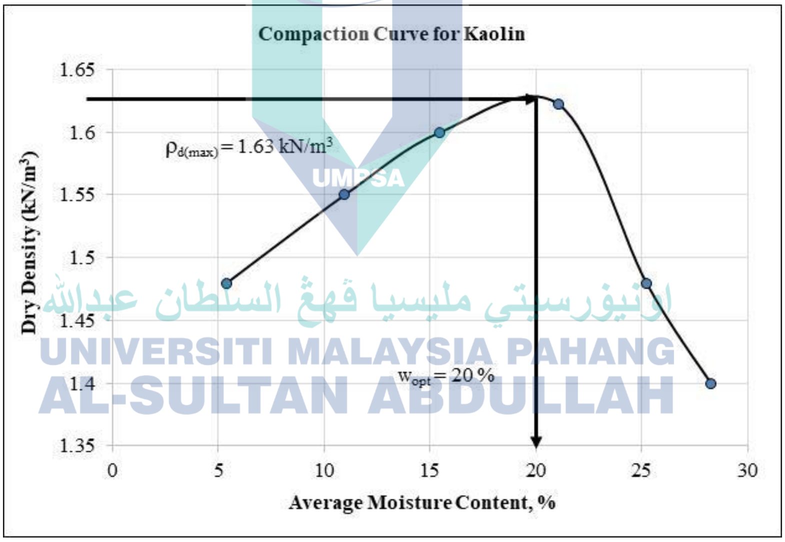

Figure 4.4 Compaction curve for kaolin

The findings derived from this investigation were juxtaposed with those of other scholarly inquiries, and the synthesis of this comparison is presented in Table 4.5. The dry density and optimum moisture content obtained in this investigation were found to be in agreement with findings from other respected studies by Spagnoli et al. (2018) and Hasan et al. (2015).

Table 4.5 Comparison of standard compaction result with previous researchers

Researchers	**Dry Density (Mg/m^3)**	**Optimum Moisture Content (%)**
Spagnoli et al. (2018)	1.64	18
Hasan et al. (2015)	1.53	19.5
Current Research (2023)	1.63	20

4.3.2 Falling Head Permeability

The permeability of the soil can be ascertained using the falling head test, particularly in cases when the soil has tiny grains. Kaolin clay was used as the soft and troublesome soil for this investigation. Fine-grained soil was the classification given to the used kaolin based on the distribution of particle sizes. Thus, in order to determine whether this soft clay is porous, the falling head test must be performed. Water can pass through the soil layer due to the soil's permeability. This soil characteristic is very important since it directly influences the behaviour and strength of the entire soil layer. The findings of this experiment revealed that the permeability of the kaolin utilised in this study was $2.27\text{x}10^{-12}$ m/s. The full testing result is shown in Appendix G, and a tabular summary of the data is provided in Table 4.6.

Table 4.6 Comparison of permeability coefficient of kaolin with previous researchers

Researchers	**Permeability Coefficient (m/s)**
Ali et al. (2021)	$6.77\text{x}10^{-10}$
Spagnoli et al. (2018)	$8.96\text{x}10^{-12}$
Hasan et al. (2015)	$4.806\text{x}10^{-12}$
Current Research (2023)	$2.27\text{x}10^{-12}$

4.3.3 Constant Head Permeability

The polypropylene particles can be classified as coarse aggregate based on the examination of particle size distribution, which indicates that their size ranges from 1.00mm to 3.35mm. The continuous head test was selected as the method of choice to determine the permeability of the granular polypropylene material utilised in this research investigation. During the calculation part, k_{20} represented the permeability of the granular polypropylene at a temperature of 20ºC. The use of k_{20} was because 20ºC is the standard temperature to be used to compare the permeability of a material (Head, 1994). Through this testing, the granular polypropylene in this study had a permeability equal to 5.73 x 10^{-3} m/s. The overall testing result is shown in Appendix H.

The permeability of the kaolin clay soil is quite small in comparison to other materials. One of the primary principles underlying the granular column phenomenon involves the process of reducing the level of the groundwater table by introducing an excessive amount of water into a lower region of the ground. It is possible to reduce clay soil's potential susceptibility, which results from its high capacity for retaining water. In addition, the mitigation of frequent volume fluctuations in soft clay soil can yield significant advantages for the stability of a structure's foundation, as it can effectively minimise uneven settlement beneath the foundation. In summary, the use of polypropylene columns has the potential to enhance soil drainage, leading to a potential decrease in the impact of water on the volumetric behaviour of clay soil and thereby mitigating the occurrence of uneven settlement.

4.3.4 Shear Strength

4.3.4.1 Direct Shear Strength

The raw data from direct shear testing on polypropylene, which had the same density as the polypropylene columns (0.90 Mg/m^3), is shown in Appendix K. Figure 4.5 illustrates the plot of peak shear strength against normal stress, which yielded the internal friction angle (ϕ), cohesion (c), and shear strength parameters. It was found that the internal friction angle was 39.40° and the cohesiveness was 8.50 kPa. Because of this, the cohesiveness and internal friction angle values are now somewhat higher than those found by earlier researchers. For instance, Hasan (2013) stated that the internal friction angle was 38° and the cohesiveness for bottom ash was 6.6 kPa. The disparity could perhaps stem from varying densities of the bottom ash utilised, despite its procurement from an identical source (Tanjung Bin). The fact that the bottom ash is composed of angular, rough-surface particles rather than round, smooth-surface particles may also contribute to the higher score since these particles may provide greater resistance to inter-particle movement. Nevertheless, the research conducted by

Awang et al. (2015) exhibited similar outcomes, with a friction angle of 36° and a cohesiveness of 9.9 kPa.

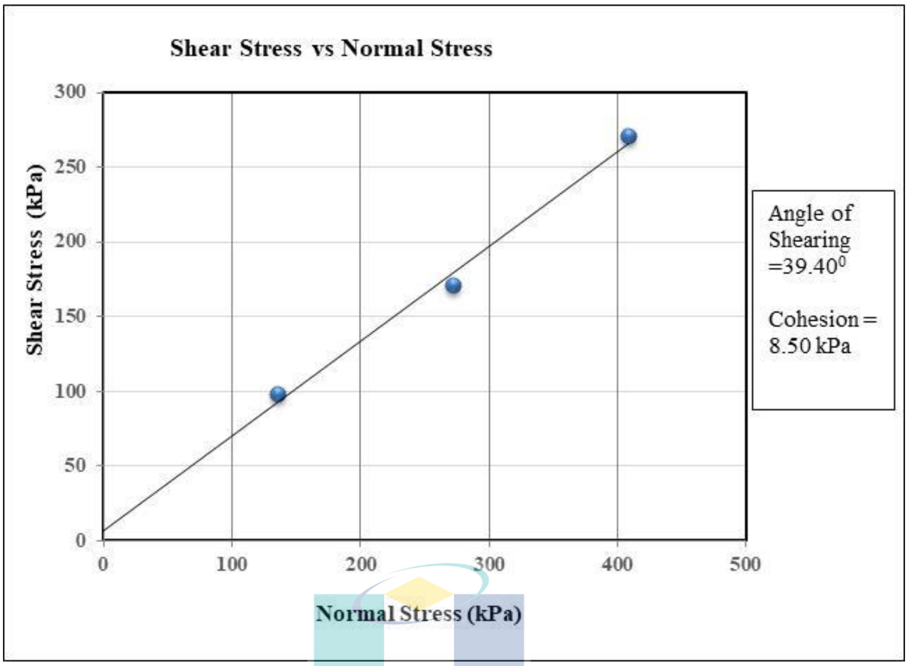

Figure 4.5 Graph showing normal stress vs shear stress

4.3.4.2 Laboratory Vane Shear Test

Table 4.7 displays the results obtained from the vane shear testing. For the purpose of accurately representing the shear strength, statistical analysis was performed. Data outside of the range of the 99% confidence level was eliminated using standard deviation (S_d).

$$S_d = \sqrt{\frac{1}{n-1} \sum_{n=1}^{n} (x_n - \bar{x})}$$

Where:

n: total number of sample

x_n: shear strength of individual sample

$\bar{x}$: Average value of shear strength from all samples

Therefore,

$$S_d = \sqrt{\frac{1}{10-1} \sum_{n=1}^{10} (x_n - 8.01)}$$

$$S_d = \sqrt{\frac{1}{9}\ (6.873)} = 0.873$$

Hence,

$$\overline{x} - S_d = 7.137$$

$$\overline{x} + S_d = 8.883$$

Table 4.7 Statistically analysing shear strength data from vane shear tests

Sample Number	**Shear Strength,** x_n **(kPa)**	**Average Shear Strength,** $\overline{x}$ **(kPa)**	$(x_n - \overline{x})^2$
A1	7.5		0.2601
A2	7.0		1.0201
A3	8.5		0.2401
A4	8.5		0.2401
A5	7.5		0.2601
A6	9.2	8.01	1.4161
A7	8.7		0.4761
A8	7.0		1.0201
A9	7.7		0.9601
A10	9.0		0.9801
			Σ = 12.2375

The results obtained from tests A2, A6, A18, and A10 were excluded from the analysis due to their shear strength values falling outside the range of 7.137 kPa to 8.883 kPa, which corresponds to a confidence level of 99%. Based on the data shown in Table 4.8, the average shear strength result was calculated to be approximately 8.07 kPa, suggesting that the soil can be classified as exhibiting a highly soft characteristic. The undrained shear strength calculated by the vane shear test was found to have a significantly greater magnitude after a comparison analysis of the data acquired from the Unconfined Compression Test, which produced a result of 6.42 kPa.

Table 4.8 Result of undrained shear strength obtained from the vane shear test

Sample Number	Undrained Shear Strength		
	Actual Value (kPa)	Representative Value (kPa)	Average Value (kPa)
A1	7.5	7.5	
A2	7.0	-	
A3	8.5	8.5	
A4	8.5	8.5	
A5	7.5	7.5	
A6	9.2	-	8.07
A7	8.7	8.7	
A8	7.0	-	
A9	7.7	7.7	
A10	9.0	-	

4.3.4.3 Unconfined Compression Test

The Unconfined Compression Test results showed that the four kaolin clay test samples had an average unconfined compressive strength of 12.84 kPa. The data presented indicates that the average undrained shear strength of the clay samples utilised in this experiment was 6.42 kPa. The samples were classified as being composed of highly malleable clay. The results for the four kaolin control samples, in addition to the twelve batches of samples reinforced with polypropylene columns, are consolidated in Table 4.9. The test findings are presented in Appendix J. The detailed results and analysis of this test are discussed in section 4.11.

Table 4.9 Peak deviator stress and axial strain from UCT

Area Replacement Ratio, A_C/A_S	No. of Column	Height Penetration Ratio, H_C/H_S (%)	Unconfined Compressive Strength, q_u (kPa)	Average Axial Strain ε (%)
0	0	0	12.84	2.76
4	1	0.6	19.79	2.43
		0.8	20.37	2.45
		1.0	19.62	2.74
10.24	1	0.6	19.52	2.74
		0.8	23.56	2.54
		1.0	20.64	2.78
12	3	0.6	20.64	2.78
		0.8	23.32	2.86
		1.0	20.32	2.76
30.72	3	0.6	15.94	2.54
		0.8	16.22	2.56
		1.0	15.66	2.48

4.3.4.4 Consolidated Undrained Triaxial Test

(i) Mohr-Coulomb Failure Criteria

The graphs showing the changes in deviator stress and excess pore water pressure with respect to axial strain were generated based on data acquired from consolidated undrained (CU) triaxial tests. In the present study, Figure 4.6 (a) illustrates the observed variations in the reconstructed kaolin sample under three distinct effective confining pressures, namely 50 kPa, 100 kPa, and 200 kPa. The deviator stress and excess pore pressure consistently exhibited an increasing pattern with axial strain, reaching their respective peak values, regardless of the imposed confining pressures. The Mohr-Coulomb failure criteria, namely the peak deviator stress, was employed to analyse the peak stress values and corresponding pore pressures. The examination conducted in this study enabled the development of the Mohr-Coulomb effective strength envelope, shown in Figure 4.7 (a). The analysis reveals that the observed level of effective apparent cohesiveness was deemed statistically negligible, since the recorded value was approximately 1.37 kPa. Nevertheless, the calculated value for the effective friction angle was 32.30°. This indicates that the soil's strength was mostly determined by the internal friction angle when taking into consideration the creation of pore water pressure within the soil.

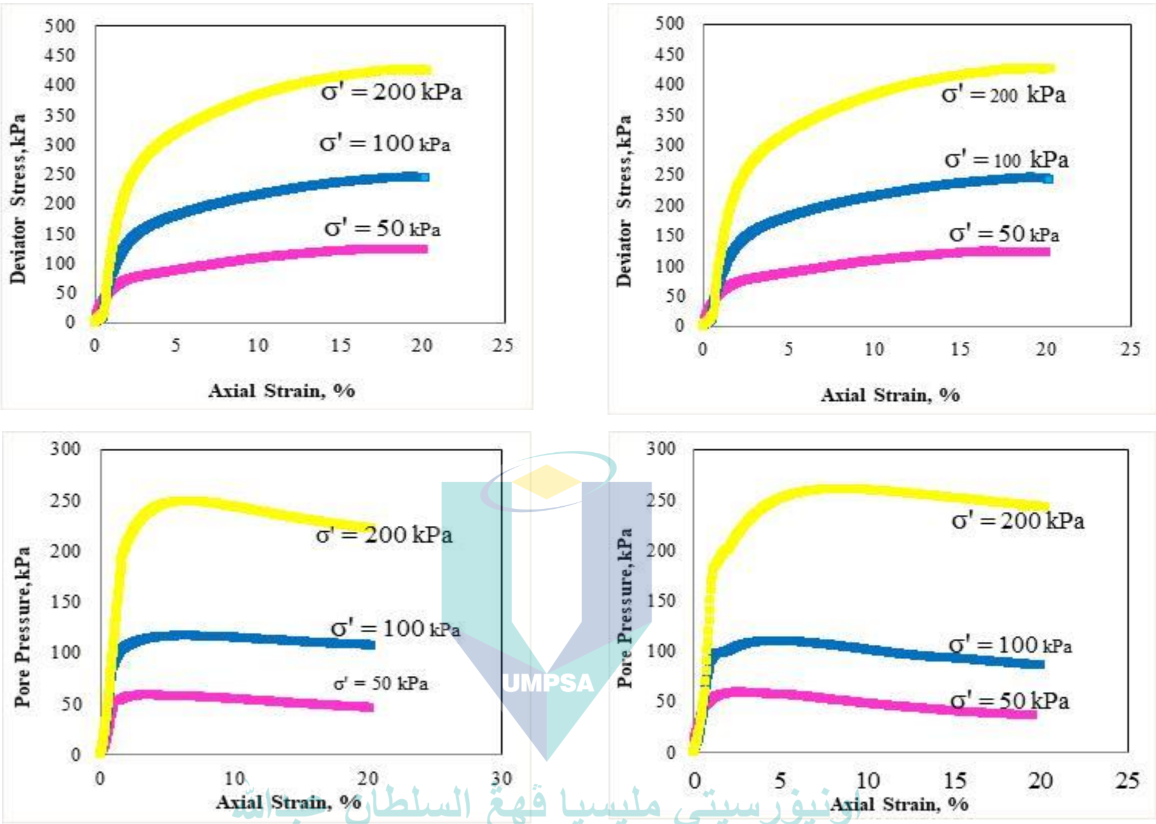

(a) Kaolin (b) Kaolin Reinforced with Polypropylene

Figure 4.6 Deviator stress and excess pore-water pressure versus axial strain for kaolin clay and kaolin reinforced with polypropylene

The determination of the effective shear strength of the polypropylene material was carried out by isotropically consolidated undrained (CU) triaxial experiments. The experimental procedures were conducted using cylindrical specimens of 50 mm in diameter and 100 mm in height. The specimens experienced effective confining pressures of 50 kPa, 100 kPa, and 200 kPa. The methodology applied in this process exhibited parallels to the one employed for kaolin. The specimens of polypropylene were produced with a relative density of 13.31%. A relative density that matched this was demonstrated in the subsequent testing programs by polypropylene columns placed within kaolin samples. In Figure 4.6 (b), excess pore pressures and deviator stresses change as axial strains change, while Figure 4.7 (b) displays the effective shear strength envelope. The empirical findings indicate that the polypropylene material demonstrated an observed friction angle of 29.60° and a perceived cohesiveness of 14.40 kPa. Polypropylene is commonly known for its low cohesion. However, when the sample was prepared with a relative density of 13.31%, there was an important improvement in its apparent cohesion and a small rise in its effective friction angle.

Upon comparing the outcomes of kaolin and polypropylene reinforcement, it became evident that the reinforced polypropylene exhibited significantly more effective cohesiveness in comparison to kaolin. However, the effective friction angles of the two materials were quite similar. The strength of polypropylene was therefore higher than that of the kaolin clay employed in this investigation. Hence, within a theoretical context, the replacement of a certain ratio of kaolin with polypropylene offers the potential to increase the strength characteristics of kaolin. The detailed results and analysis of this test are discussed in section 4.12.

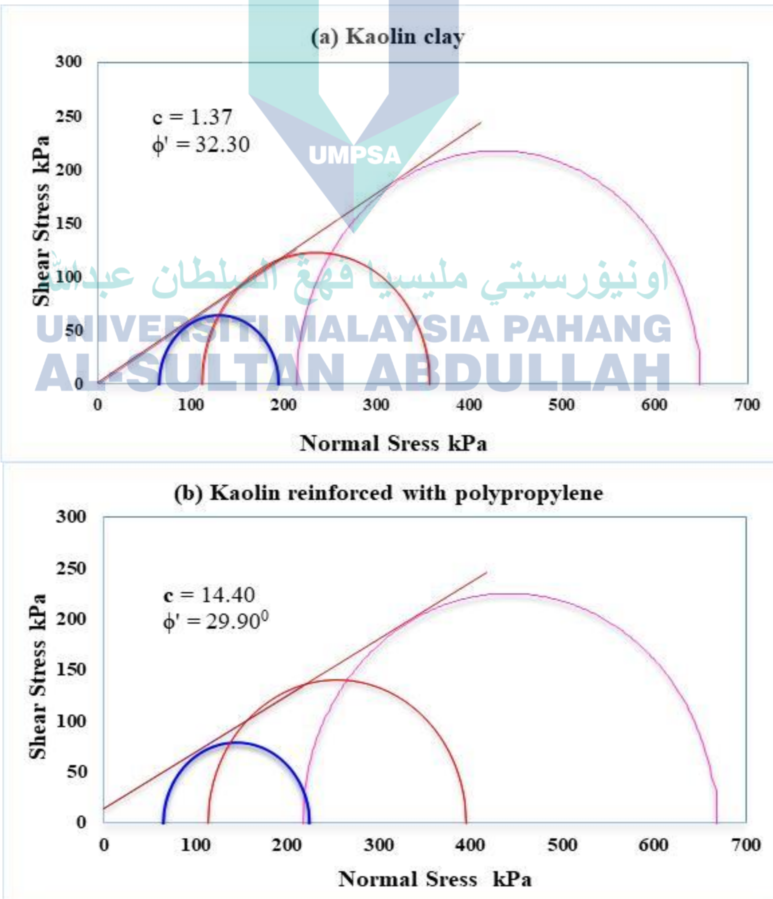

Figure 4.7 Mohr-Coulomb effective stress failure envelopes for (a) Kaolin clay; (b) Kaolin reinforced with polypropylene

4.4 Morphological Properties

The Field Emission Scanning Electron Microscope (FESEM) images demonstrated the texture, roughness, and topology of the polypropylene (Figure 4.8 and Figure 4.9). During the initial investigation, it was seen that the polypropylene particles within the pellets exhibited both cylindrical and spherical shapes, characterized by smooth surface textures. In regions where the pellets had been through the cutting process, it was observed that the texture tended to be comparatively rougher. Referring to Figure 4.8 (A, B, C), three specific areas were marked to show the difference between the cutting areas, and referring to Figure 4.9, three areas were marked areas as D, E and F to differentiate between the process areas. The experimental findings indicated that the cutting area exhibited a higher degree of surface roughness compared to the normal surface area of the polypropylene particle.

The variability of testing findings between polypropylene columns may be attributed to the smoothness and lack of voids observed on the particle surfaces. The column's internal configuration may vary, leading to potential fluctuations in the observed results, characterised by a progressive rise or decline in the average value.

The polypropylene pellets were rigid enough to withstand its shape after compaction. As a result, even under compression, the stacking of polypropylene particles formed more voids inside the column, leading to more space. Subsequently, these spaces aided in speeding up the release of extra pore water pressure from the samples. Thus, by reducing the consolidation time, the process progress accelerated faster.

The interlocking mechanism arises from the arrangement of the PP granules within the polymer matrix. During the processing of the composite material, the PP granules are dispersed and distributed evenly within the polymer matrix. As the polymer matrix solidifies, the granules become embedded within it, forming a network of reinforcing columns. These columns act as barriers against external forces, effectively increasing the material's resistance to deformation and improving its overall strength. Furthermore, the interlocking mechanism also provides additional surface area for interfacial bonding between the PP granules and the polymer matrix. This enhanced bonding strengthens the interface between the two phases, preventing delamination or separation under stress. As a result, the composite material exhibits improved mechanical properties such as higher tensile strength, modulus, and impact resistance.

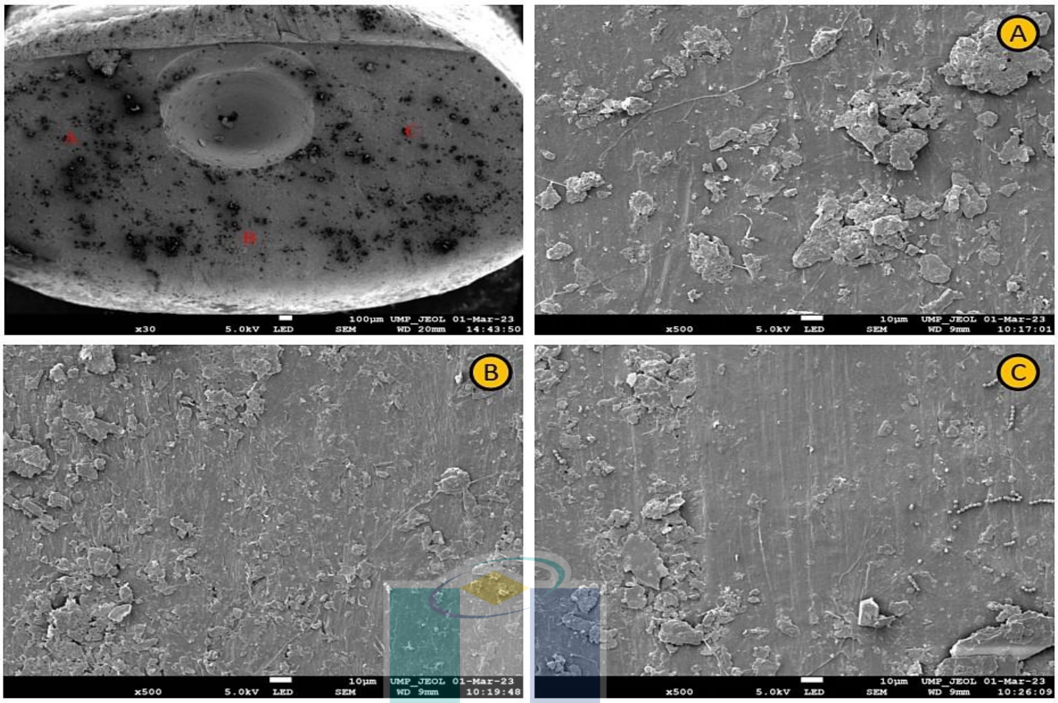

Figure 4.8 Top view of polypropylene particle 30 times zoomed and 500 zoomed areas of selected areas

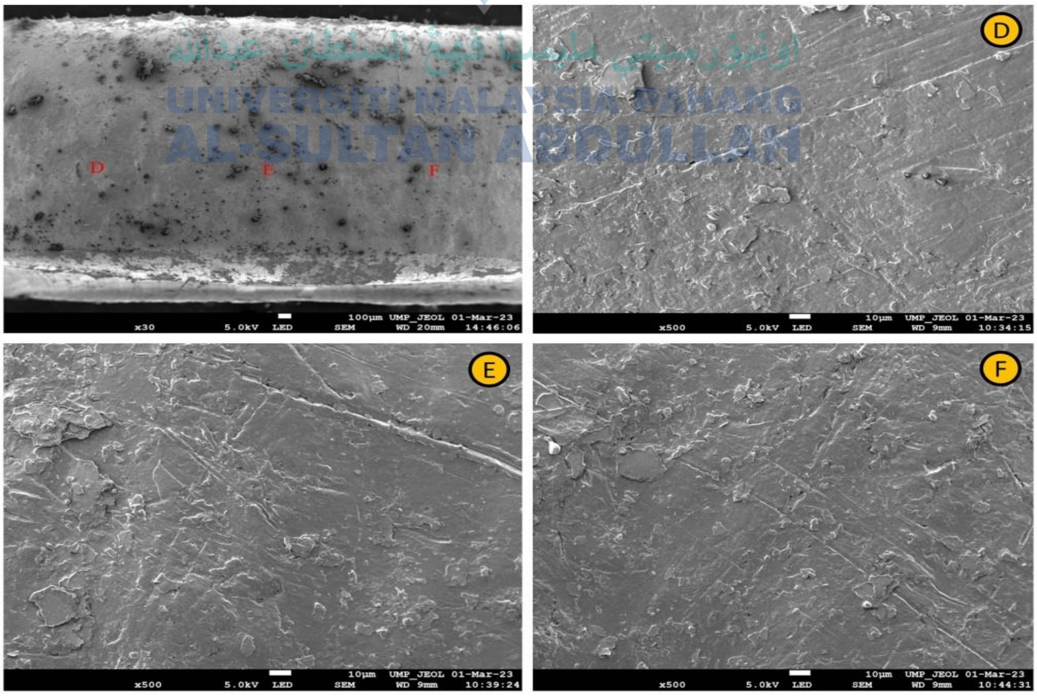

Figure 4.9 Side view of polypropylene particle 30 times zoomed and 500 zoomed areas of selected areas.

4.5 Compressibility

Compressibility study was done for polypropylene columns or any other ground improvement method to find out how the ground would react to applied loads and to ensure that the intended engineering goals were met. The structural design was optimised and the polypropylene column's load bearing capacity was evaluated with the aid of this analysis. Based on the specimens' isotropic consolidation stage results, the analysis of compressibility was examined. The addition of polypropylene in granular columns was anticipated to improve the dissipation of excess pore water pressure in soils, hence facilitating the vertical drainage function of the columns, while also reinforcing the kaolin clay material.

4.6 Consolidation Parameters

At the isotropic consolidation stage, three specimens per sample were assessed at effective confining pressures of 50 kPa, 100 kPa, and 200 kPa. The plot depicting the relationship between changes in volume and pore water pressure served to explain the progression of isotropic consolidation in soil. The consolidation characteristics, comprising the time required to complete consolidation (t_{100}), the coefficient of volume compressibility (m_v), and the coefficient of consolidation (c_v), are presented in Table 4.10. The aforesaid values were computed and are presented in the form of a table.

Table 4.10 Consolidation parameters

Sample	Effective Confining Pressure (kPa)	Consolidated Volume (mm^3)	Volumetric Strain	Coefficient of Volume Compressibility, m_v, (m^2/MN)	Coefficient of Consolidation, c_v (m^2/year)	Completion Time for Consolidation Stage, t_{100} (min)
Control	50	186.67	0.016	0.85	98.38	58.34
	100	180.42	0.027	0.63	88.20	62.15
	200	178.93	0.029	0.38	82.51	76.02
S1060	50	187.73	0.015	0.69	104.81	47.25
	100	160.10	0.023	0.57	86.50	57.12
	200	125.42	0.029	0.41	72.03	68.75

Table 4.10 Continued

Sample	Effective Confining Pressure (kPa)	Consolidated Volume (mm^3)	Volumetric Strain	Coefficient of Volume Compressibility, m_v, (m^2/MN)	Coefficient of Consolidation, c_v (m^2/year)	Completion Time for Consolidation Stage, t_{100} (min)
	50	187.52	0.015	0.70	77.35	64.03
S1080	100	184.79	0.020	0.47	84.92	58.32
	200	181.08	0.026	0.34	121.62	50.72
	50	191.96	0.012	0.73	70.72	70.03
S10100	100	184.92	0.019	0.46	101.07	49.00
	200	184.00	0.021	0.36	104.70	47.30
	50	188.83	0.012	0.72	110.35	44.88
S1660	100	183.97	0.021	0.50	101.37	48.87
	200	150.52	0.027	0.32	105.53	46.93
	50	189.48	0.012	0.66	68.71	72.08
S1680	100	183.46	0.021	0.51	82.46	60.06
	200	182.05	0.024	0.34	61.89	74.02
	50	187.16	0.015	0.77	109.56	45.20
S16100	100	183.91	0.021	0.50	60.78	60.02
	200	180.81	0.026	0.33	64.33	68.98
	50	186.91	0.016	0.86	115.57	42.85
G1060	100	183.12	0.022	0.53	107.78	45.95
	200	179.43	0.029	0.38	102.17	48.47
	50	156.84	0.021	0.67	97.82	50.63
G1080	100	125.69	0.034	0.53	104.40	47.70
	200	104.49	0.061	0.39	92.69	53.43
	50	187.18	0.016	0.69	117.72	42.07
G10100	100	183.57	0.022	0.49	100.15	49.45
	200	181.23	0.026	0.32	82.51	60.02

Table 4.10 Continued

Sample	Effective Confining Pressure (kPa)	Consolidated Volume (mm^3)	Volumetric Strain	Coefficient of Volume Compressibility, m_v, (m^2/MN)	Coefficient of Consolidation, c_v ($m^2/year$)	Completion Time for Consolidation Stage, t_{100} (min)
	50	189.48	0.012	0.87	84.19	58.82
G1660	100	183.46	0.022	0.71	100.35	49.35
	200	182.05	0.025	0.57	107.08	46.25
	50	185.92	0.018	0.83	70.72	70.03
G1680	100	152.60	0.031	0.65	116.33	42.57
	200	110.12	0.050	0.53	103.28	47.95
	50	156.84	0.021	0.89	81.15	61.03
G16100	100	125.69	0.034	0.75	120.94	40.95
	200	104.49	0.061	0.59	111.72	44.33

4.7 Controlled Sample

Figure 4.10 illustrates the relationship between the change in volume throughout the consolidation phase of the controlled sample and the square root of time. The consolidated volumes of specimens with effective confining pressures of 50 kPa (Specimen 1), 100 kPa (Specimen 2), and 200 kPa (Specimen 3) were determined to be 186.67 cm^3, 180.42 cm^3, and 178.93 cm^3, respectively. Based on the findings, it can be observed that there was a drop in consolidated volumes as the confining pressures increased.

The present research included the determination of the coefficient of volume compressibility for specimens that were exposed to effective confining pressures of 50 kPa, 100 kPa, and 200 kPa. The obtained values were 0.85, 0.63, and 0.38 m^2/MN, respectively. The data demonstrates a positive correlation between the values and the corresponding confining pressures. The values of the coefficients of consolidation at effective confining pressures of 50 kPa, 100 kPa, and 200 kPa were obtained as 98.38, 88.20, and 82.51 m^2/year, respectively, through analysing the observed value of t_{100} from the corresponding figure.

The data presented in Figure 4.11 illustrates the consolidation stage of the cumulative percentage of pore pressure dissipation as a function of logarithmic time for the controlled sample. The total excess pore pressure values were measured at effective confining pressures of 50 kPa, 100 kPa, and 200 kPa, obtaining results of 1.81 kPa, 3.94 kPa, and 2.53 kPa, respectively. However, at an effective confining pressure of 100 kPa, the highest excess pore pressure was observed. The phenomenon was particularly significant because it was expected to reach its maximum value at an effective confining pressure of 200 kPa.

The highest excess pore pressure was observed at an effective confining pressure of 100 kPa, indicating a possible non-linear response, which could be due to sample heterogeneity or specific experimental conditions. The dissipation curves indicate that the rate of consolidation slows down as the effective confining pressure increases, which is typical due to reduced permeability and higher soil stiffness at higher pressures.

The comparison between the controlled sample and the reinforced sample indicates that the column installation significantly enhances the consolidation process by increasing soil rigidity and reducing compressibility. The practical implications of these findings suggest that column installation can optimize foundation designs by shortening consolidation times and reducing settlement.

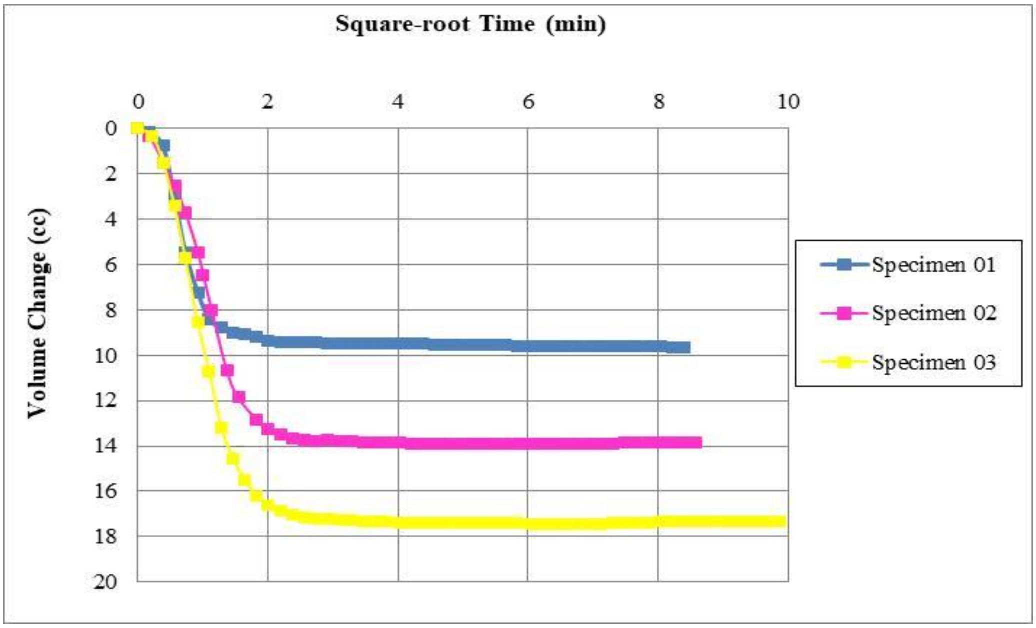

Figure 4.10 Volume change against square root time for consolidation stage of controlled sample

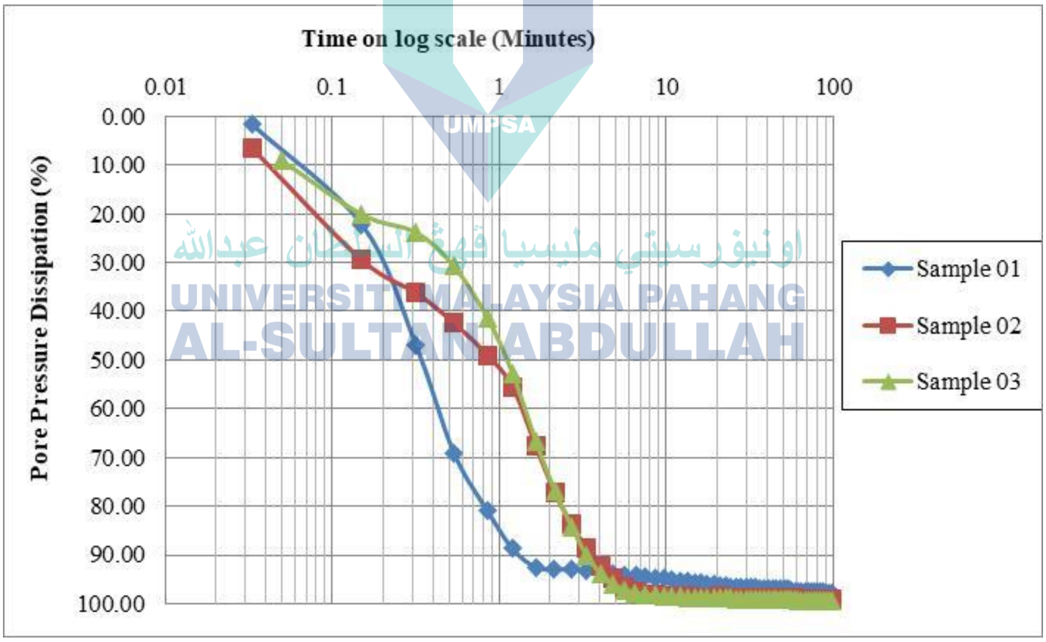

Figure 4.11 Pore pressure dissipation against log time for consolidation stage of controlled sample

4.8 Samples Reinforced with a Single Polypropylene Column

4.8.1 Height Penetrating Ratio, $H_c/H_s = 0.6$

Figure 4.12 illustrates the volume increases over square root time during the consolidation stage of the sample, wherein reinforcement was provided by a single column with a diameter of 10 mm and a penetration ratio of 60% of its height. The consolidated volumes for specimens with a 10 mm diameter column and effective confining pressures of 50 kPa, 100 kPa, and 200 kPa were 187.73 cm^3, 160.10 cm^3, and 125.42 cm^3, respectively. The specimens exhibited volume compressibility coefficients of 0.69, 0.57, and 0.41 m^2/MN under effective confining pressures of 50 kPa, 100 kPa, and 200 kPa, respectively. The coefficients of consolidation at effective confining pressures of 50 kPa, 100 kPa, and 200 kPa were determined to be 104.81, 86.50, and 72.03 m^2/year, respectively, by the determination of the value of t_{100}.

The graph presented in Figure 4.13 shows the dissipation of pore pressure during logarithmic time during the consolidation phase of the specimen. This particular specimen was reinforced with a single column of 10 mm in diameter, with a penetration ratio equivalent to 60% of its height. The additional pore pressures of 2.95 kPa, 4.51 kPa, and 5.13 kPa were measured at effective confining pressures of 50 kPa, 100 kPa, and 200 kPa, correspondingly. The results suggest that there exists a direct relationship between an increase in effective confining pressure and the resulting increase in excess pore pressures.

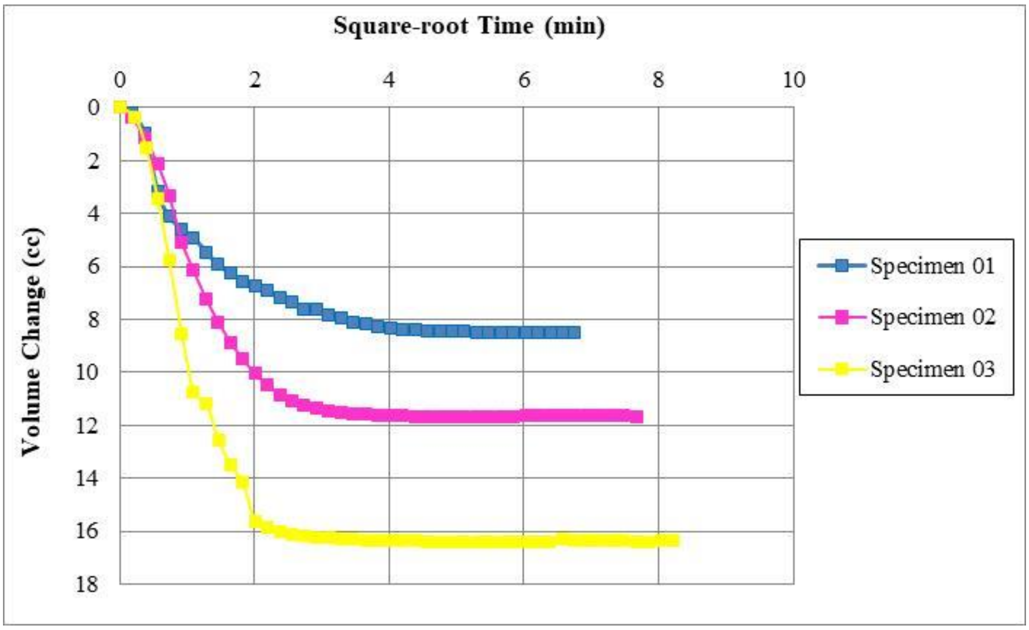

Figure 4.12 Volume change vs square root time for the sample's consolidation stage when it was reinforced by a single column with a diameter of 10 mm and a height penetration ratio of 60%

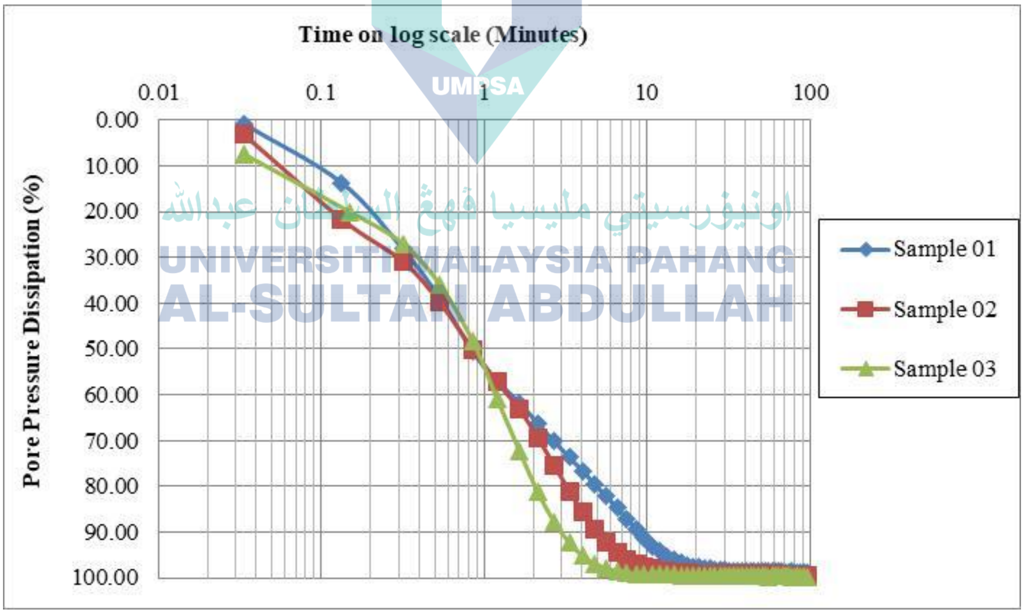

Figure 4.13 Pore pressure dissipation vs logarithmic time during consolidation stage of sample reinforced by a single column 10 mm in diameter and 60% in height.

The graph in Figure 4.14 illustrates the volume change throughout the consolidation stage of the sample, which was subjected to reinforcement by a single column with a diameter of 16 mm that penetrated 60% of the sample's height. The results showed that the specimens reinforced with single 16 mm diameter columns generated consolidated volumes of 188.83, 183.97, and 150.52 cm^3 under effective confining pressures of 50 kPa, 100 kPa, and 200 kPa, respectively. Comparatively, for specimens with effective confining pressures of 50 kPa, 100 kPa, and 200 kPa, the coefficients of volume compressibility were 0.72, 0.50, and 0.32 m^2/MN. Following the computation of t_{100} from the figure, the coefficients of consolidation were 110.35, 101.37, and 105.53 m^2/year for effective confining pressures of 50 kPa, 100 kPa, and 200 kPa, respectively.

The graphical representation in Figure 4.15 illustrates the dissipation of pore pressure over logarithmic time during the consolidation phase of the sample that had been reinforced with a single column measuring 16 mm in diameter, with a penetration ratio of 60% of its height. The applied confining pressures were 50 kPa, 100 kPa, and 200 kPa, whereas the corresponding excess pore pressures were measured as 1.24 kPa, 2.10 kPa, and 3.92 kPa, respectively. This observation illustrates a positive correlation between excess pore pressures and effective confining pressures.

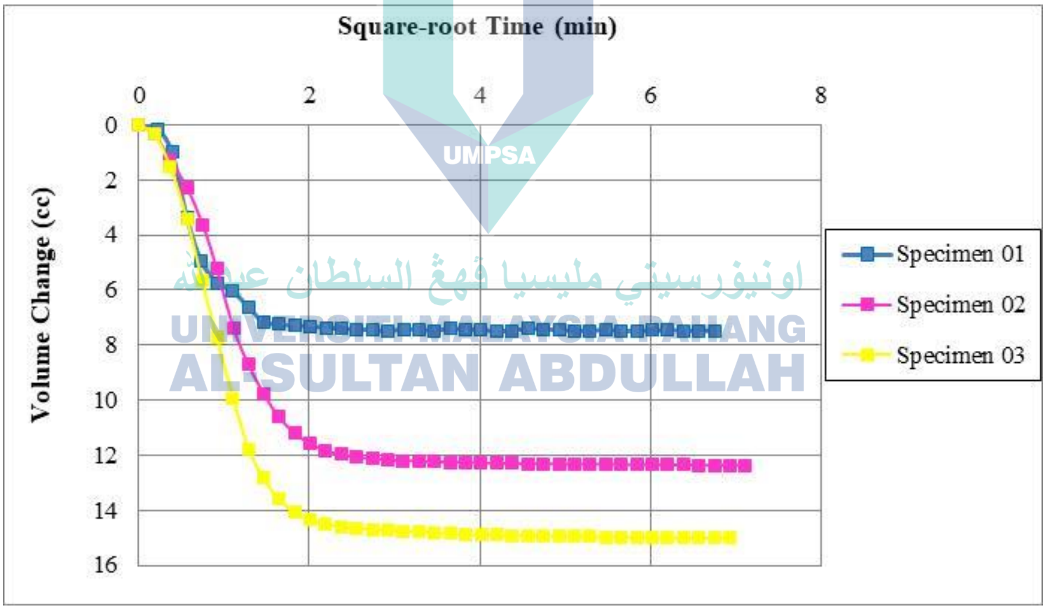

Figure 4.14 Volume change vs square root time for the sample's consolidation stage when it was reinforced by a single column with a diameter of 16 mm and a height penetration ratio of 60%.

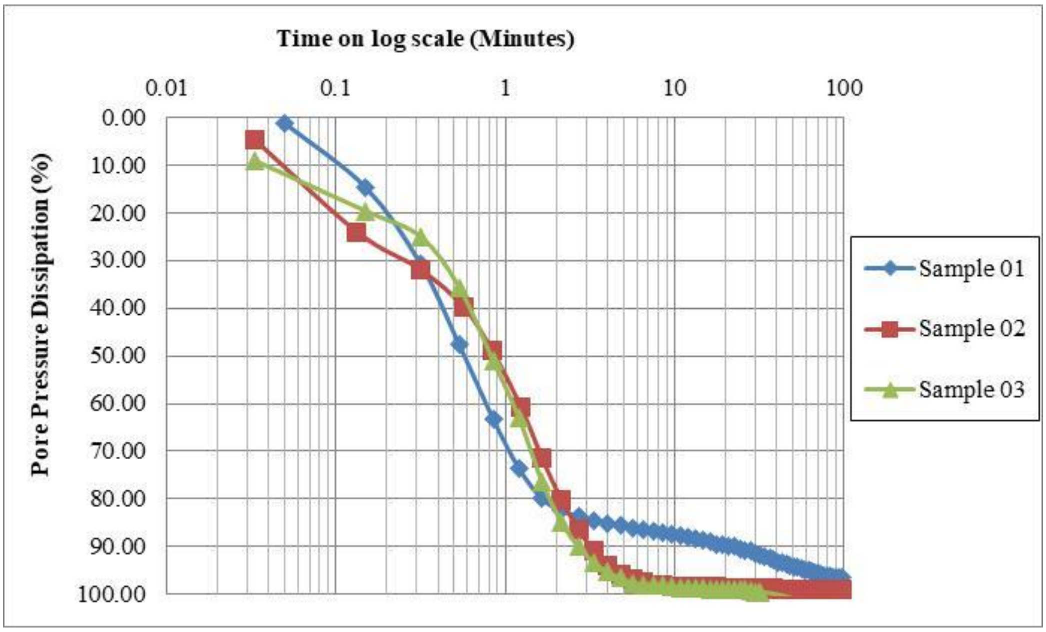

Figure 4.15 Pore pressure dissipation vs logarithmic time during consolidation stage of sample reinforced by a single column 16 mm in diameter and 60% in height.

4.8.2 Height Penetrating Ratio, H_c/H_s = 0.8

The graph illustrated in Figure 4.16 demonstrates the correlation between the change in volume and the square root of time during the consolidation stage of the specimen. The consolidation stage was complemented by a cylindrical column measuring 10 mm in diameter and showed a penetration ratio of 80% relative to its height. The consolidated volumes of specimens reinforced with a 10 mm diameter column at effective confining pressures of 50 kPa, 100 kPa, and 200 kPa were measured to be 187.52 cm^3, 184.79 cm^3, and 181.08 cm^3, respectively. The coefficients of volume compressibility for specimens subjected to confining pressures of 50 kPa, 100 kPa, and 200 kPa were determined to be 0.70, 0.47, and 0.34 m^2/MN, respectively. The coefficients of consolidation at confining pressures of 50, 100, and 200 kPa were determined as 77.35, 84.92, and 121.62 m^2/year, respectively, utilising the t_{100} value.

The data depicted in Figure 4.17 shows the dissipation of pore pressure throughout a logarithmic duration during the consolidation phase of the specimen. The specimen had been reinforced with a single column of 10 mm in diameter, with a penetration ratio equivalent to 80% of its height. The excess pore pressures recorded were 1.48 kPa, 1.60 kPa, and 3.04 kPa, respectively. These measurements were taken at effective confining pressures of 50 kPa, 100 kPa, and 200 kPa, respectively.

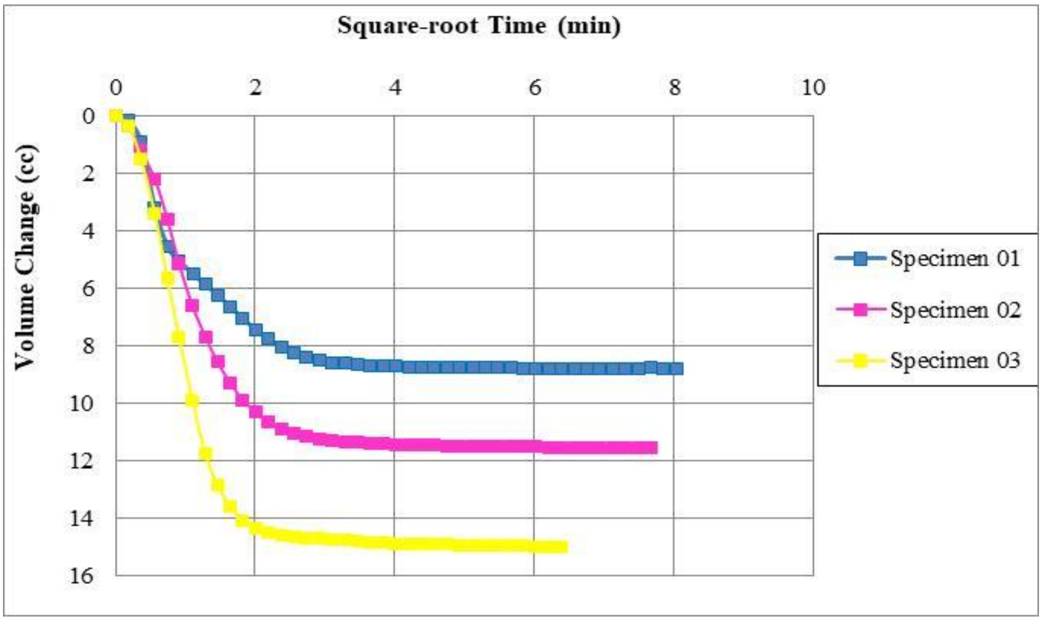

Figure 4.16 Volume change vs square root time for the sample's consolidation stage when it was reinforced by a single column with a diameter of 10 mm and a height penetration ratio of 80%

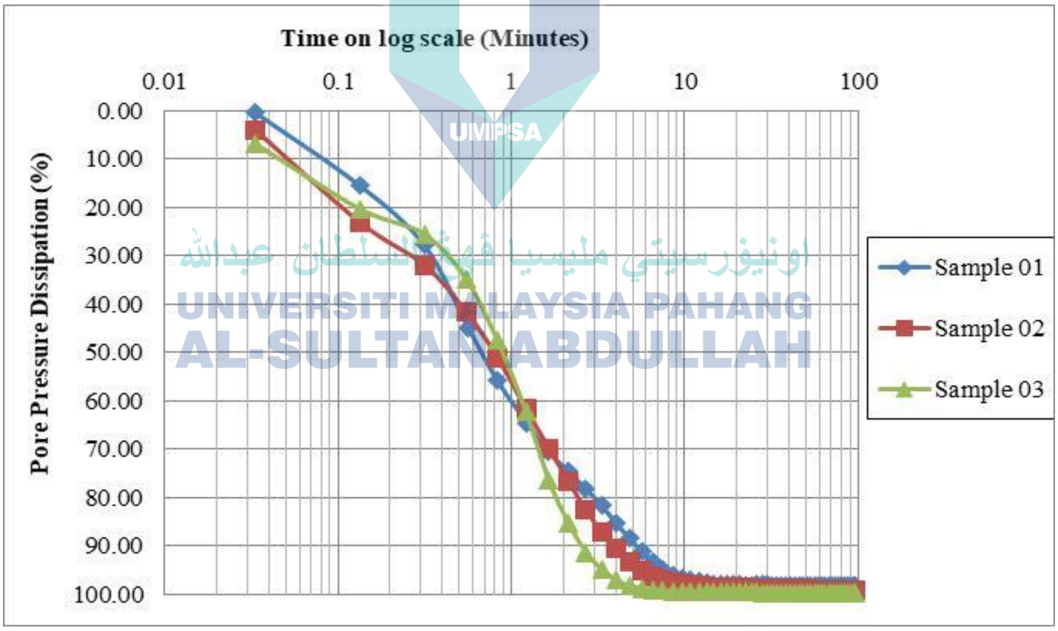

Figure 4.17 Pore pressure dissipation vs logarithmic time during consolidation stage of sample reinforced by a single column 10 mm in diameter and 80% in height.

The graph illustrated in Figure 4.18 shows the correlation between the change in volume and the square root of time during the consolidation phase of the specimen. The subsequent phase ensued subsequent to the reinforcement of the sample through the insertion of a single column having a diameter of 16 mm, which had successfully penetrated the sample to an extent equivalent to 80% of its height. The consolidated volumes of specimens reinforced with 16 mm diameter columns at effective confining pressures of 50 kPa, 100 kPa, and 200 kPa were measured to be 189.48 cm^3, 183.46 cm^3, and 182.05 cm^3, respectively. The coefficients of volume compressibility for specimens subjected to confining pressures of 50 kPa, 100 kPa, and 200 kPa were determined to be 0.66, 0.51, and 0.34 m^2/MN, respectively. The coefficient of consolidation for confining pressures of 50 kPa, 100 kPa, and 200 kPa was determined to be 68.71, 82.46, and 61.89 m^2/year, respectively, based on the value of t_{100}.

The graph displayed in Figure 4.19 shows the gradual dissipation of pore pressure over a logarithmic time scale in the consolidation stage of the specimen. This particular specimen had been reinforced with a single column of 10 mm in diameter, and exhibited a penetration ratio equivalent to 80% of its height. The extra pore pressures recorded for confining pressures of 50 kPa, 100 kPa, and 200 kPa were 3.26 kPa, 2.49 kPa, and 1.71 kPa, respectively.

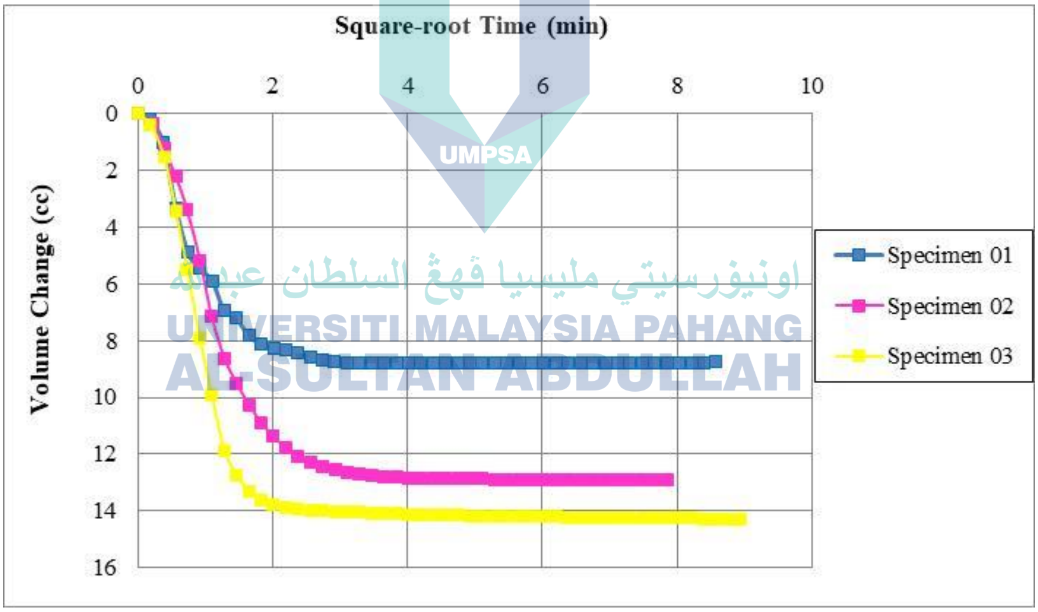

Figure 4.18 Volume change vs square root time for the sample's consolidation stage when it was reinforced by a single column with a diameter of 16 mm and a height penetration ratio of 80%.

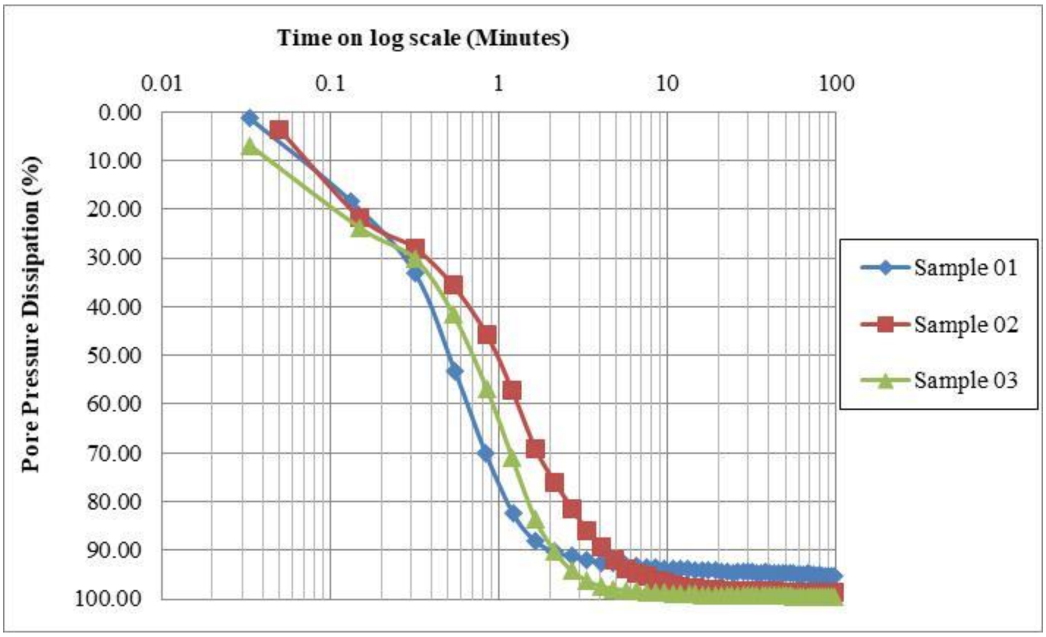

Figure 4.19 Pore pressure dissipation vs logarithmic time during consolidation stage of sample reinforced by a single column 16 mm in diameter and 80% in height

4.8.3 Height Penetrating Ratio, H_c/H_s = 1.0

Figure 4.20 illustrates the relationship between the volume change during the consolidation stage and the square root of time for a sample that is reinforced by a single column with a diameter of 10 mm and a penetration ratio of 100%. The consolidated volumes of specimens reinforced with a column of 10 mm diameter and subjected to effective confining pressures of 50 kPa, 100 kPa, and 200 kPa were measured as 191.96 cm^3, 184.92 cm^3, and 184.00 cm^3, respectively. The specimens with effective confining pressures of 50 kPa, 100 kPa, and 200 kPa exhibited coefficients of volume compressibility of 0.73, 0.46, and 0.36 m^2/MN, respectively. The values of the coefficients of consolidation were obtained as 70.12, 101.07, and 104.70 m^2/year at effective confining pressures of 50 kPa, 100 kPa, and 200 kPa, respectively, through the identification of the t_{100} value.

Figure 4.21 illustrates the dissipation of pore pressure over logarithmic time during the consolidation stage of the sample, which was reinforced by a single column of 10 mm diameter, penetrating up to 100% of the sample's height. The applied confining pressures were 50 kPa, 100 kPa, and 200 kPa, whereas the corresponding excess pore pressures were measured to be 5.40 kPa, 1.17 kPa, and 1.90 kPa, respectively.

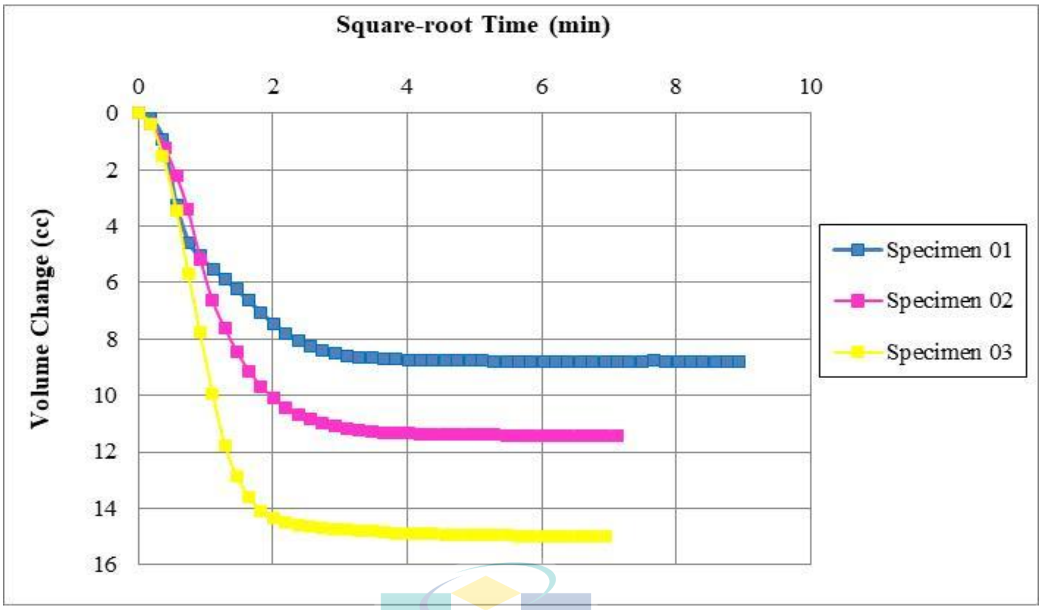

Figure 4.20 Volume change vs square root time for the sample's consolidation stage when it was reinforced by a single column with a diameter of 10 mm and a height penetration ratio of 100%.

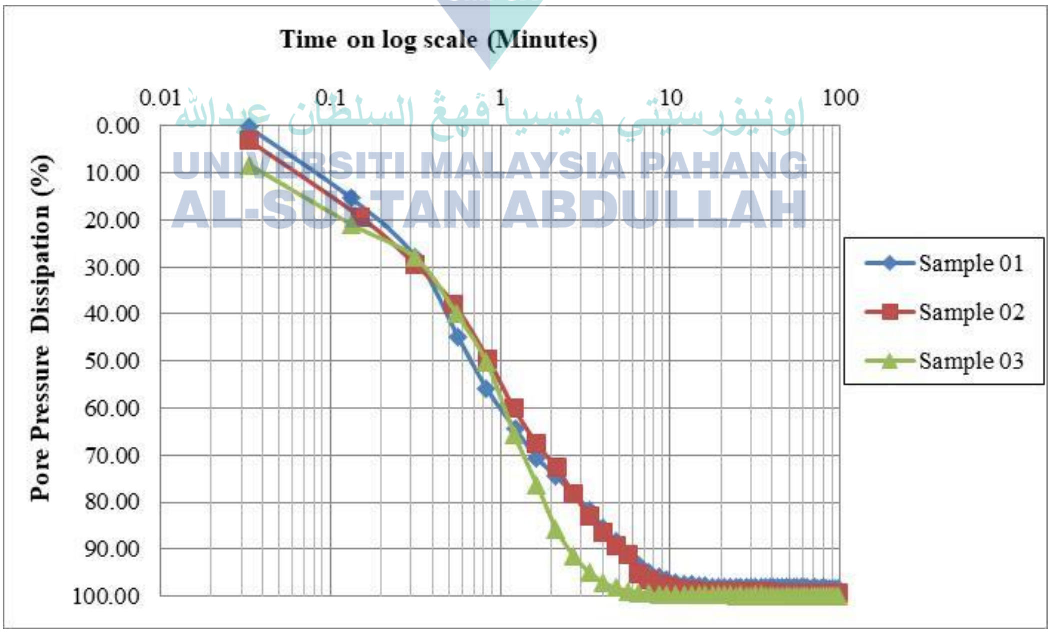

Figure 4.21 Pore pressure dissipation vs logarithmic time during consolidation stage of sample reinforced by a single column 10 mm in diameter and 100% in height.

Figure 4.22 illustrates the relationship between volume change and the square root of time during the consolidation phase of a sample that is reinforced with a single column measuring 16 mm in diameter, with a penetration ratio of 100% of the sample's height. At confining pressures of 50 kPa, 100 kPa, and 200 kPa, the consolidated volumes of specimens containing a column with a diameter of 16 mm were measured to be

187.16 cm^3, 183.91 cm^3, and 180.81 cm^3, respectively. The specimens at effective confining pressures of 50 kPa, 100 kPa, and 200 kPa exhibited volume compressibility coefficients of 0.77, 0.50, and 0.33 m^2/MN, respectively. The coefficient of consolidation was determined to be 109.56, 60.78, and 64.33 m^2/year at effective confining pressures of 50 kPa, 100 kPa, and 200 kPa, respectively, through the calculation of the t_{100} value.

The graph depicted in Figure 4.23 illustrates the dissipation of pore pressure over logarithmic time during the consolidation phase of the sample, which had been reinforced with a single column measuring 16 mm in diameter and achieving a 100% height penetration ratio. The excess pore pressures were measured at effective confining pressures of 50 kPa, 100 kPa, and 200 kPa, yielding values of 3.39 kPa, 3.31 kPa, and 1.65 kPa, respectively.

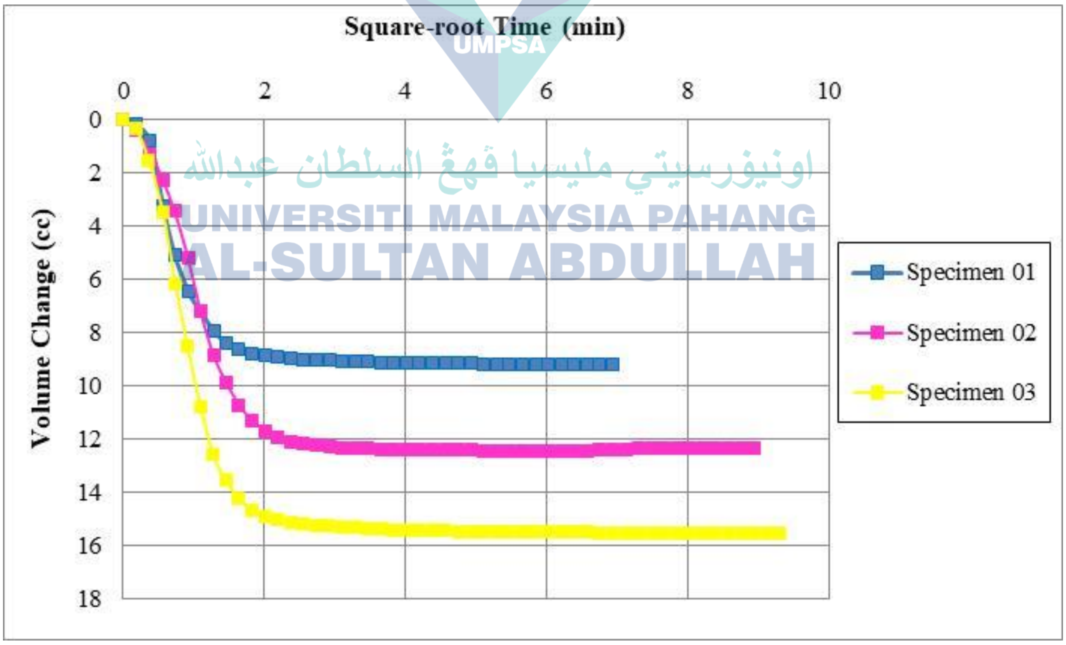

Figure 4.22 Volume change vs square root time for the sample's consolidation stage when it was reinforced by a single column with a diameter of 16 mm and a height penetration ratio of 100%

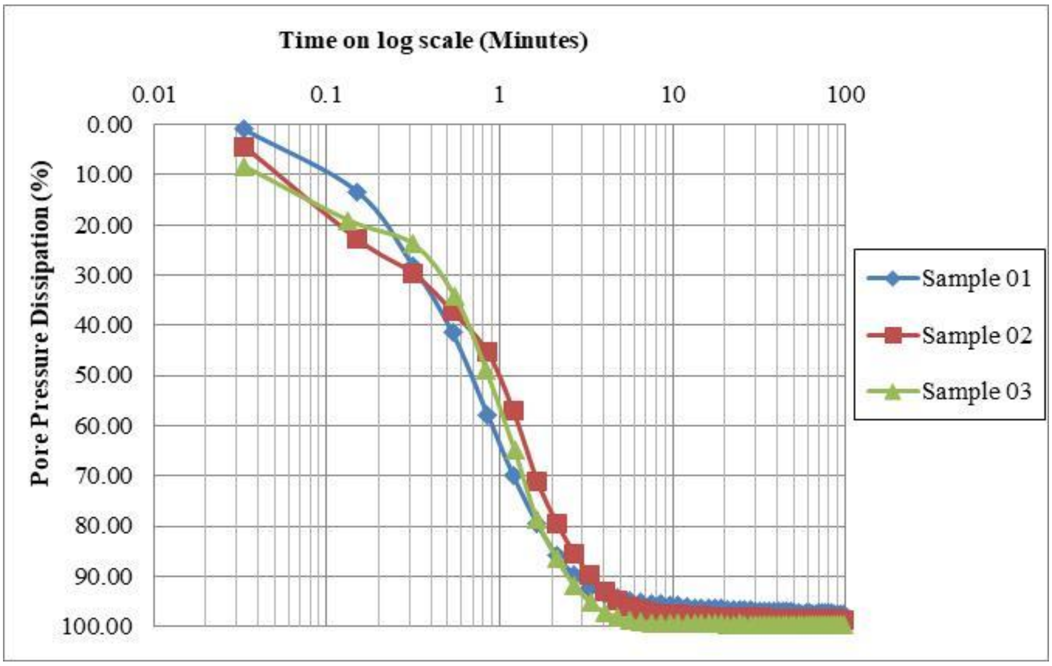

Figure 4.23 Pore pressure dissipation vs logarithmic time during consolidation stage of sample reinforced by a single column 16 mm in diameter and 100% in height

4.9 Samples Reinforced with a Group of Polypropylene Columns

4.9.1 Height Penetrating Ratio, H_c/H_s = 0.6

The graph illustrated in Figure 4.24 displays the correlation between changes in volume and the square root of time, with a particular emphasis on the consolidation stage of the sample. The given specimen was reinforced by a cylindrical column measuring

10 mm in diameter, showing a penetration ratio of 60% relative to its height. The measured volumes of the specimens, which were exposed to confining pressures of 50 kPa, 100 kPa, and 200 kPa, were found to be 186.91 cm^3, 183.12 cm^3, and 179.43 cm^3, respectively. The specimens exhibited volume compressibility coefficients of 0.86, 0.53, and 0.38 m^2/MN under effective confining pressures of 50 kPa, 100 kPa, and 200 kPa, respectively. The values of the coefficients of consolidation, specifically 115.57, 107.78, and 102.17 m^2/year, were obtained through the determination of the value of t_{100} at effective confining pressures of 50 kPa, 100 kPa, and 200 kPa, respectively.

The graph depicted in Figure 4.25 demonstrates the decrease of pore pressure over a logarithmic time scale throughout the consolidation stage of the specimen, which had been increased using a group column of 10 mm in diameter and having a penetration ratio equivalent to 60% of its height. The extra pore pressures recorded were 2.50kPa, 4.51 kPa, and 3.23 kPa, corresponding to effective confining pressures of 50kPa, 100 kPa, and 200 kPa, respectively.

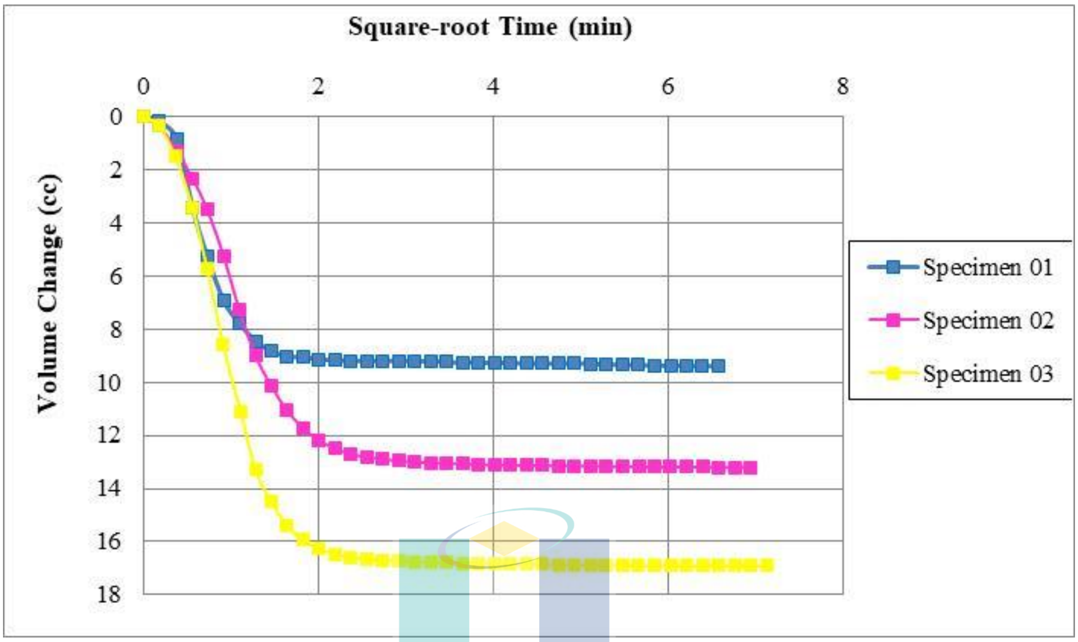

Figure 4.24 Volume change vs square root time for the sample's consolidation stage when it was reinforced by a group column with a diameter of 10 mm and a height penetration ratio of 60%

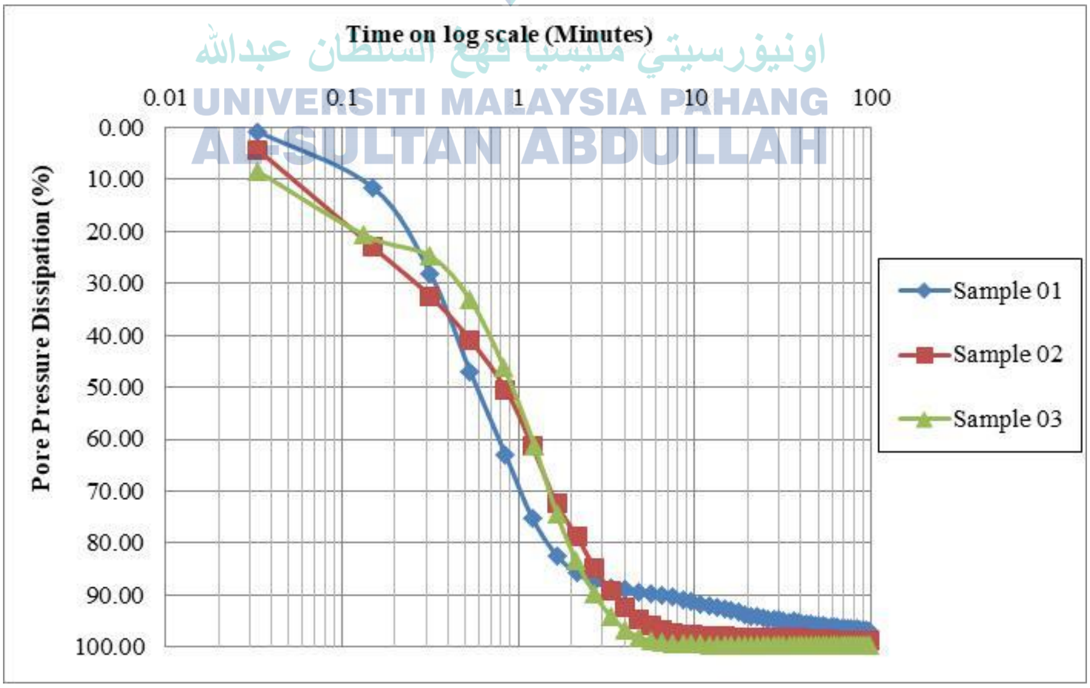

Figure 4.25 Pore pressure dissipation vs logarithmic time during consolidation stage of sample reinforced by a group column 10 mm in diameter and 60% in height

Figure 4.26 shows the correlation between the change in volume and the square root of time during the consolidation phase of the sample, which had been reinforced by a group column measuring 16 mm in diameter. The penetration ratio of the column was 60% of its height. The measured consolidated volumes of the specimens, which were exposed to confining pressures of 50 kPa, 100 kPa, and 200 kPa, were found to be 189.48 cm^3, 183.46 cm^3, and 172.05 cm^3, respectively. The coefficients of volume compressibility for specimens subjected to confining pressures of 50 kPa, 100 kPa, and 200 kPa were determined to be 0.87, 0.71, and 0.57 m^2/MN, respectively. The values of the coefficients of consolidation at effective confining pressures of 50 kPa, 100 kPa, and 200 kPa were determined to be 84.19, 100.35, and 107.08 m^2/year, respectively, through the calculation of the t_{100} value.

Figure 4.27 illustrates the relationship between pore pressure dissipation and logarithmic time during the consolidation stage for the specimen reinforced with a group column of 16 mm diameter and a height penetration ratio of 60%. The extra pore pressures of 2.82 kPa, 3.38 kPa, and 1.33 kPa were observed at effective confining pressures of 50 kPa, 100 kPa, and 200 kPa, respectively.

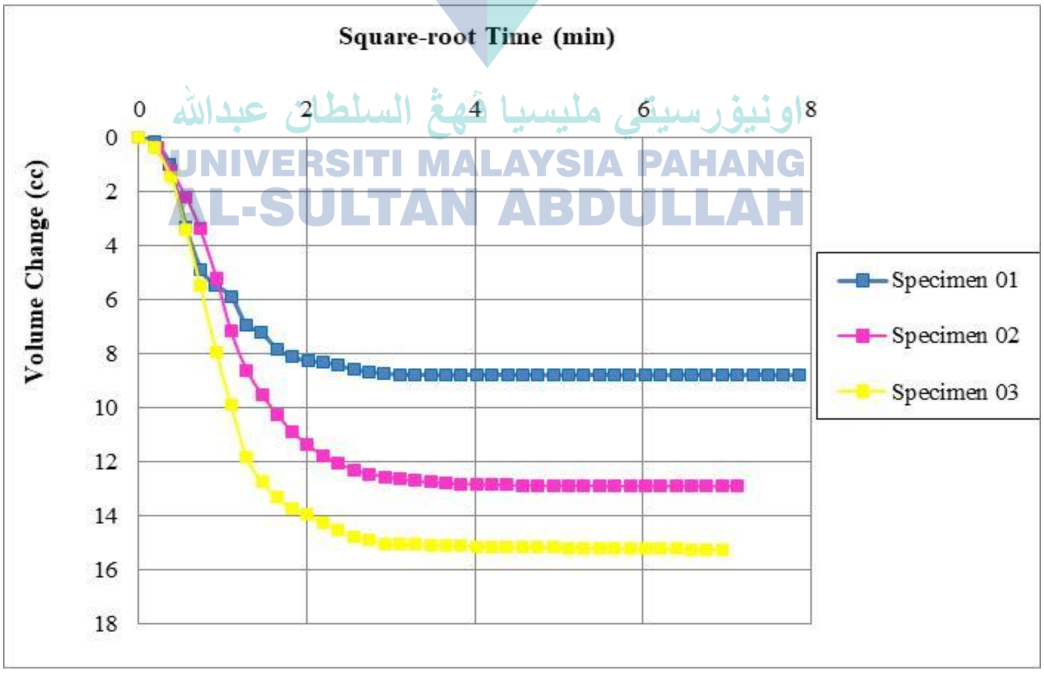

Figure 4.26 Volume change vs square root time for the sample's consolidation stage when it was reinforced by a group column with a diameter of 16 mm and a height penetration ratio of 60%

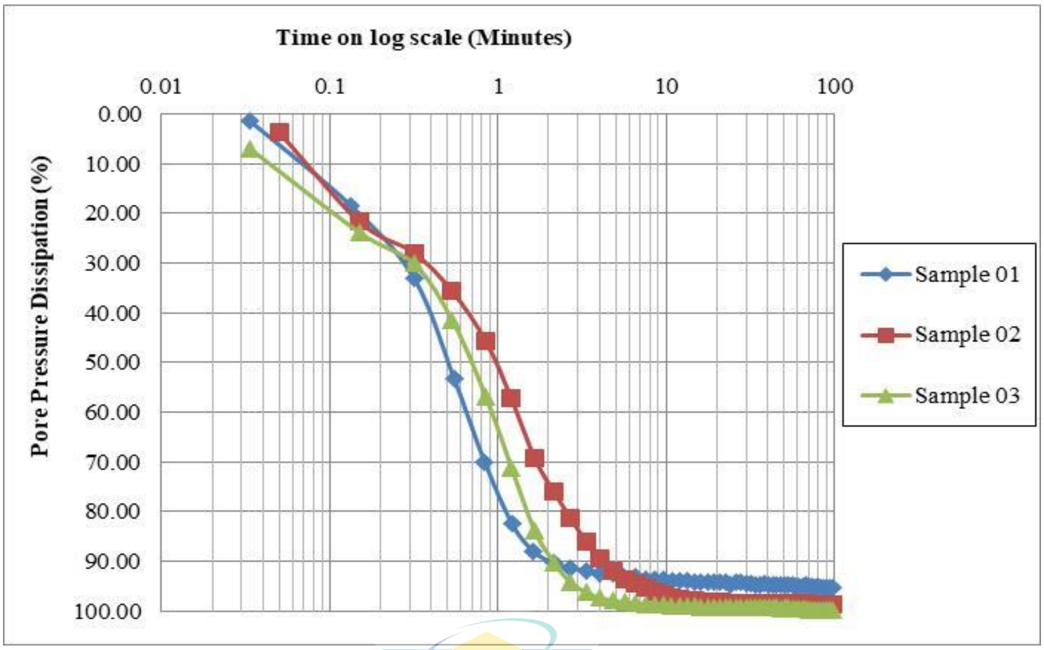

Figure 4.27 Pore pressure dissipation vs logarithmic time during consolidation stage of sample reinforced by a group column 10 mm in diameter and 60% in height

4.9.2 Height Penetrating Ratio, Hc/Hs = 0.8

The graph depicted in Figure 4.28 illustrates the relationship between the change in volume and the square root of time during the consolidation phase of the specimen, which had been reinforced with a group column of 10 mm diameter and an 80% height penetration ratio. The consolidated volumes of specimens reinforced with a column of 10 mm diameter and effective confining pressures of 50 kPa, 100 kPa, and 200 kPa, respectively, were measured to be 156.84 cm^3, 125.69 cm^3, and 104.49 cm^3. The specimens, subjected to confining pressures of 50 kPa, 100 kPa, and 200 kPa, respectively, exhibited coefficients of volume compressibility measuring 0.67, 0.53, and 0.39 m^2/MN. The values of the coefficients of consolidation at effective confining pressures of 50 kPa, 100 kPa, and 200 kPa were calculated to be 97.82, 104.40, and 92.69 m^2/year, respectively. These values were obtained by calculating the value of t_{100}.

The consolidation stage of the sample is shown in Figure 4.29, in which a reinforced group column with a diameter of 16 mm and a penetration ratio of 80% was employed. This phenomenon was apparent based on the observed decrease in pore pressure over logarithmic time. The extra pore pressures measured at effective confining pressures of 50 kPa, 100 kPa, and 200 kPa were determined to be 1.18 kPa, 3.49 kPa, and 2.47 kPa, respectively.

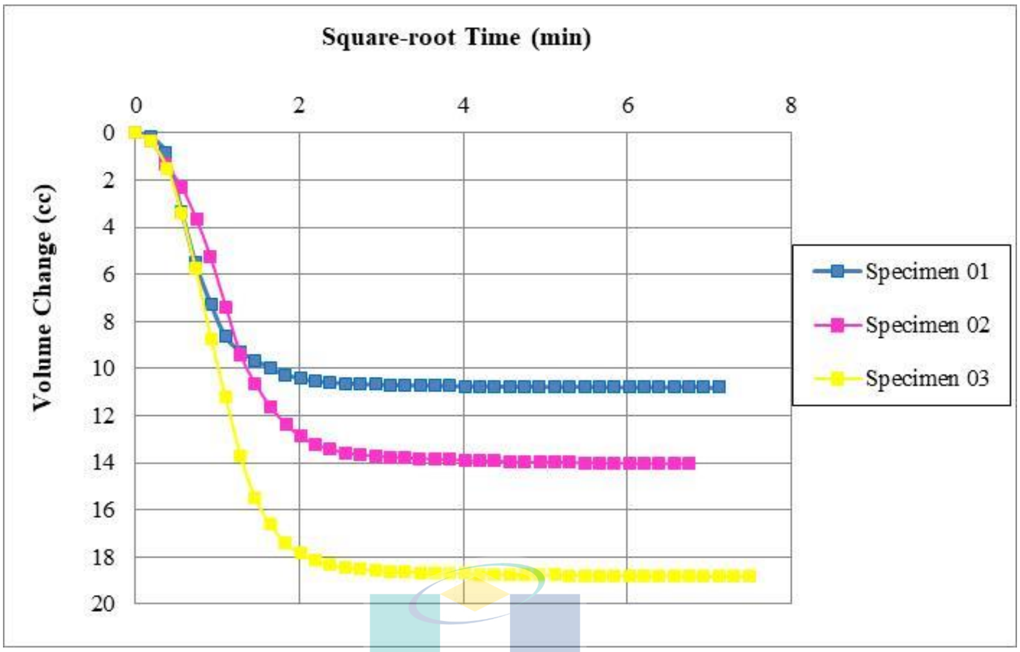

Figure 4.28 Volume change vs square root time for the sample's consolidation stage when it was reinforced by a group column with a diameter of 10 mm and a height penetration ratio of 80%

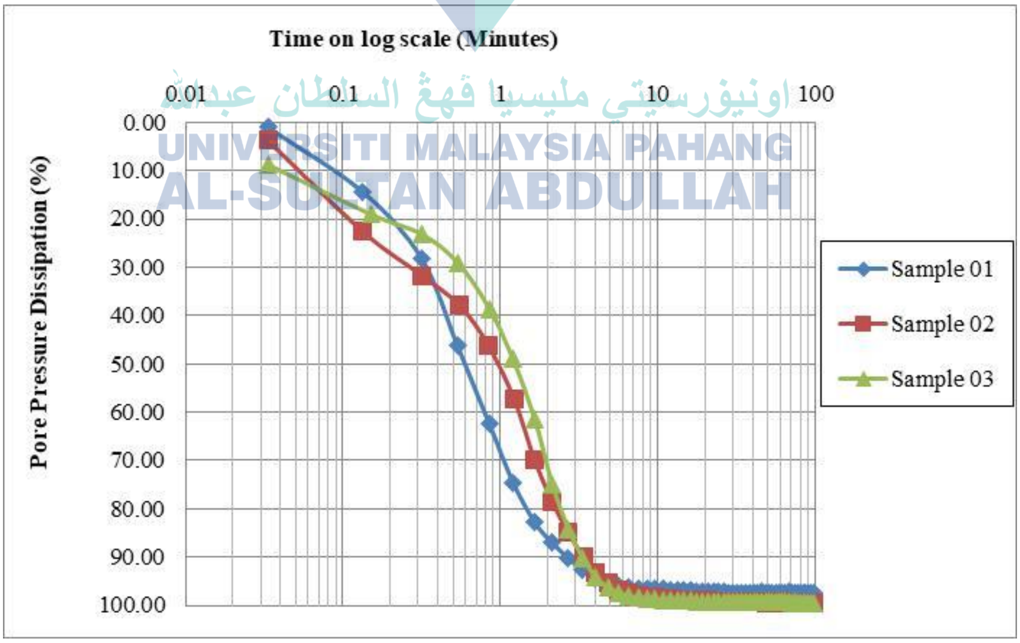

Figure 4.29 Pore pressure dissipation vs logarithmic time during consolidation stage of sample reinforced by a group column 10 mm in diameter and 80% in height

The graph presented in Figure 4.30 displays the correlation between the change in volume and the square root of time in the consolidation stage of the specimen. The specimen had been reinforced with a group column of 16 mm diameter, and the penetration ratio was 80% of its height. The consolidated volumes of specimens reinforced with a 16 mm diameter group column at effective confining pressures of 50 kPa, 100 kPa, and 200 kPa were measured to be 185.92 cm^3, 152.60 cm^3, and 110.12 cm^3, respectively. The specimens exhibited volume compressibility coefficients of 0.83, 0.65, and 0.53 m^2/MN under effective confining pressures of 50 kPa, 100 kPa, and 200 kPa, respectively. The values of the coefficients of consolidation at effective confining pressures of 50, 100, and 200 kPa were determined to be 70.72, 116.33, and 103.28 m^2/year, respectively, through the calculation of the t_{100} value.

The graph shown in Figure 4.31 illustrates the dissipation of pore pressure through a logarithmic time scale during the consolidation phase of the sample. The sample had been reinforced with a group column of 16 mm diameter, with a penetration ratio equivalent to 80% of its height. The extra pore pressures measured at effective confining pressures of 50 kPa, 100 kPa, and 200 kPa were determined to be 14.06 kPa, 1.86 kPa, and 3.81 kPa, respectively.

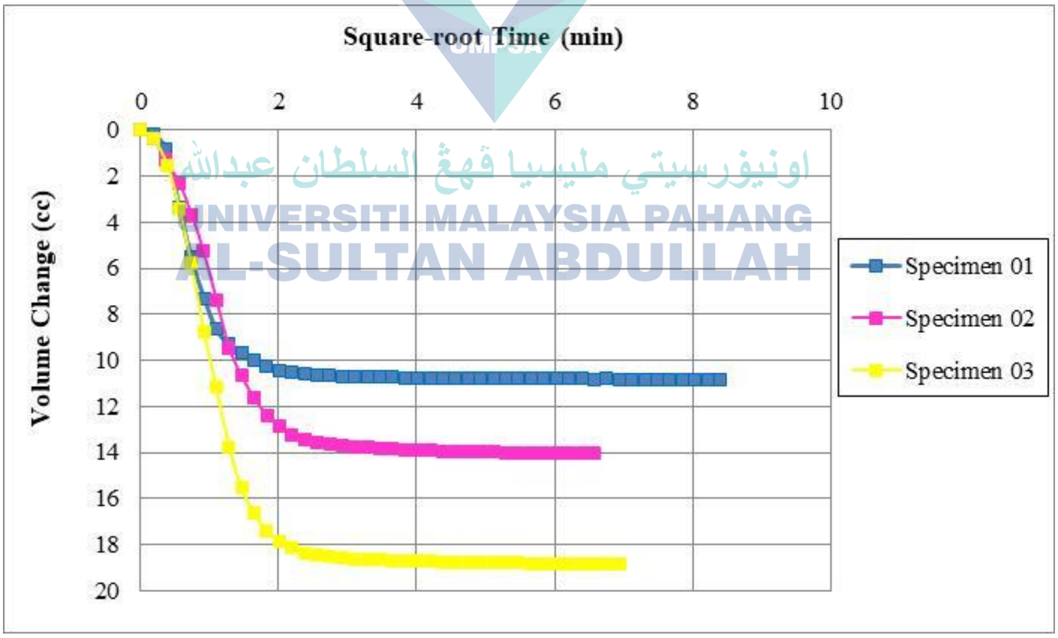

Figure 4.30 Volume change vs square root time for the sample's consolidation stage when it was reinforced by a group column with a diameter of 16 mm and a height penetration ratio of 80%

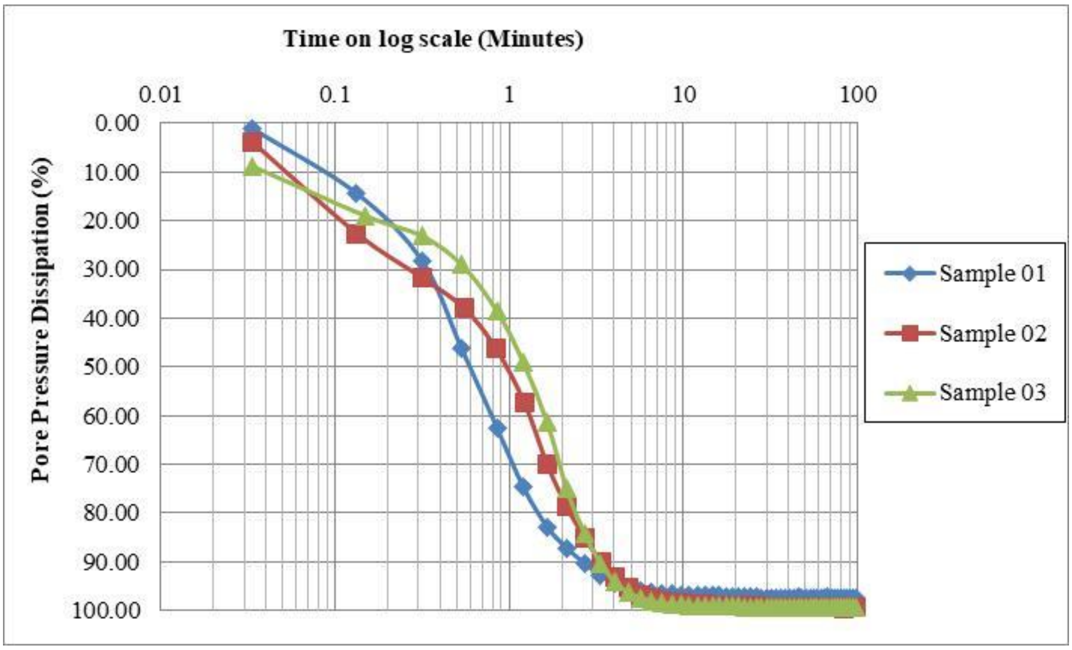

Figure 4.31 Pore pressure dissipation vs logarithmic time during consolidation stage of sample reinforced by a group column 16 mm in diameter and 80% in height

4.9.3 Height Penetrating Ratio, H_c/H_s = 1.0

The graph presented in Figure 4.32 shows the correlation between the alteration in volume and the square root of time in the consolidation stage of the specimen. This specimen has been reinforced with a group column of 10 mm in diameter and a penetration ratio equal to 100% of its height. The measured volumes of consolidated specimens, which were reinforced with a column of 10 mm diameter and exposed to effective confining pressures of 50 kPa, 100 kPa, and 200 kPa, were measured as 187.18 cm^3, 183.57 cm^3, and 181.23 cm^3, respectively. The specimens, subjected to confining pressures of 50 kPa, 100 kPa, and 200 kPa, respectively, exhibited coefficients of volume compressibility measuring 0.69, 0.49, and 0.32 m^2/MN. The values of the coefficients of consolidation at effective confining pressures of 50 kPa, 100 kPa, and 200 kPa were determined to be 117.72, 100.15, and 82.51 m^2/year, respectively, through the calculation of the t_{100} value. Figure 4.33 illustrates the dissipation of pore pressure over logarithmic time during the consolidation stage of the sample reinforced with a group column of 10 mm diameter, with a penetration ratio of 100% in terms of height. The extra pore pressures seen under effective confining pressures of 50 kPa, 100 kPa, and 200 kPa were measured to be 4.41 kPa, 4.80 kPa, and 0.77 kPa, respectively.

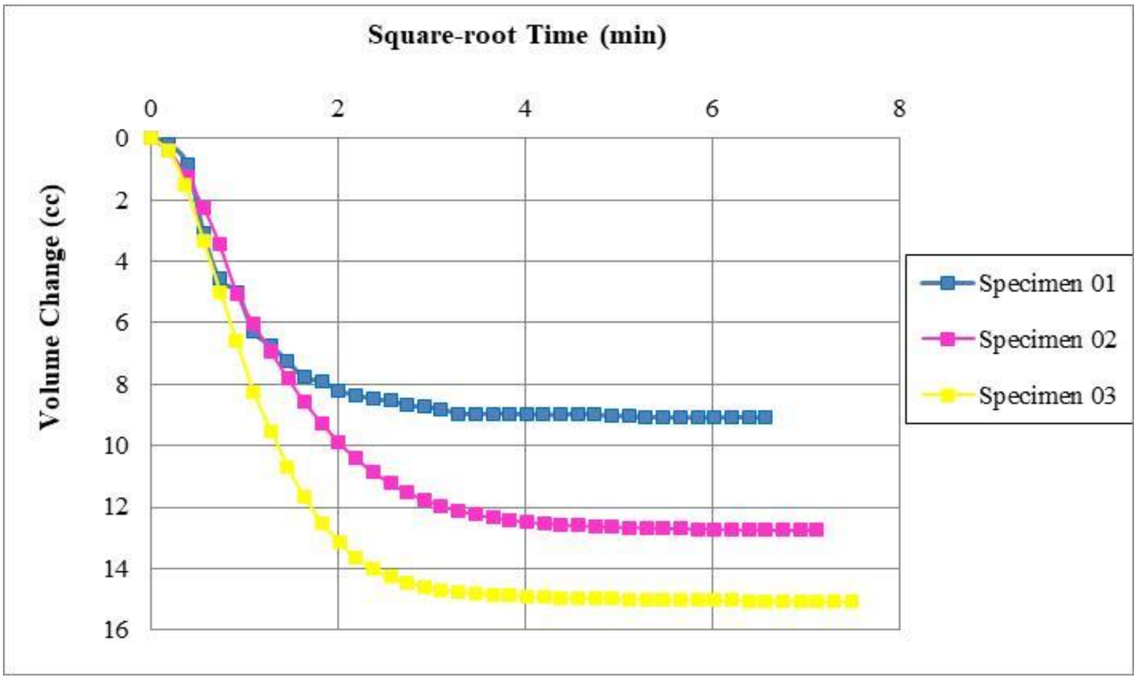

Figure 4.32 Volume change vs square root time for the sample's consolidation stage when it was reinforced by a group column with a diameter of 10 mm and a height penetration ratio of 100%

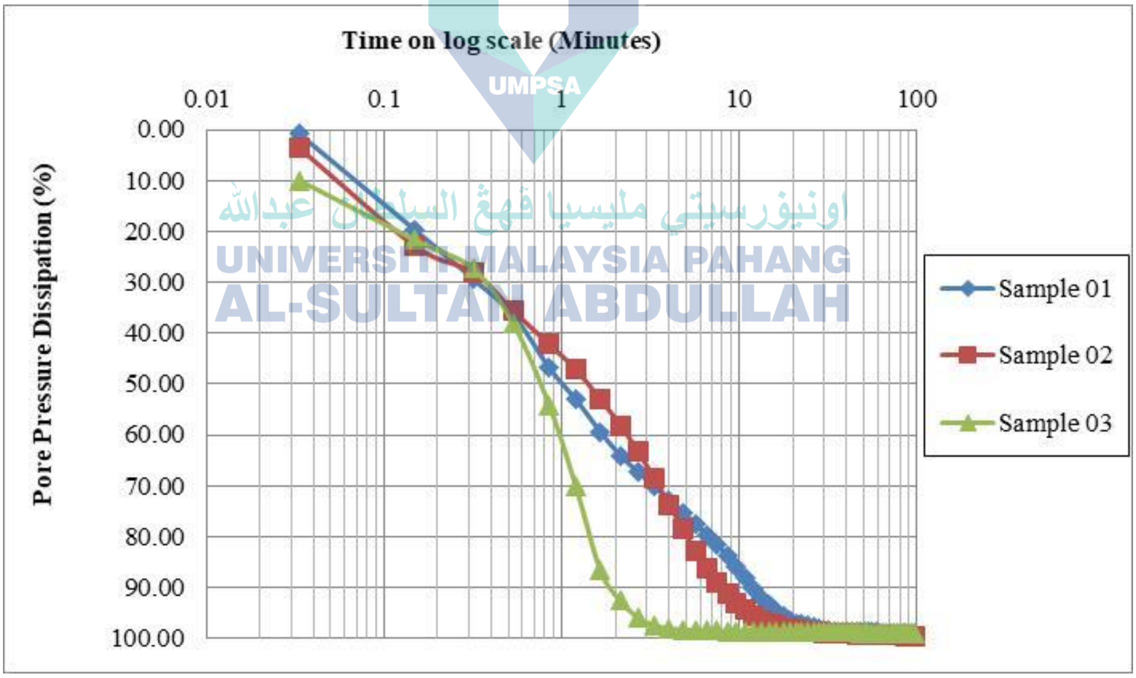

Figure 4.33 Pore pressure dissipation vs logarithmic time during consolidation stage of sample reinforced by a group column 10 mm in diameter and 100% in height

The data shown in Figure 4.34 demonstrates the correlation between the alteration in volume and the square root of time in the consolidation stage of the specimen that was reinforced with a group column of 16 mm in diameter, with a penetration ratio equivalent to 100% of its height. The measured volumes of consolidated specimens, which were strengthened with a 16 mm diameter column under effective confining pressuresof 50 kPa, 100 kPa, and 200 kPa, were found to be 156.84 cm^3, 125.69cm^3, and 104.49 cm^3, respectively. The specimens, subjected to confining pressures of 50 kPa, 100 kPa, and 200 kPa, respectively, exhibited coefficients of volume compressibility measuring 0.89, 0.75, and 0.59 m^2/MN. The coefficients of consolidation for confining pressures of 50 kPa, 100 kPa, and 200 kPa were determined to be 81.15, 120.94, and 111.72 m^2/year, respectively, utilising the value of t_{100}.

Figure 4.35 shows the consolidation stage of a sample, where a group column with a diameter of 16 mm and a penetration ratio of 100% is utilised. The provided figure illustrates the correlation between the dissipation of pore pressure and the logarithmic progression of time. The extra pore pressures seen at effective confining pressures of 50 kPa, 100 kPa, and 200 kPa were recorded as 2.50 kPa, 2.44 kPa, and 0.01 kPa, correspondingly.

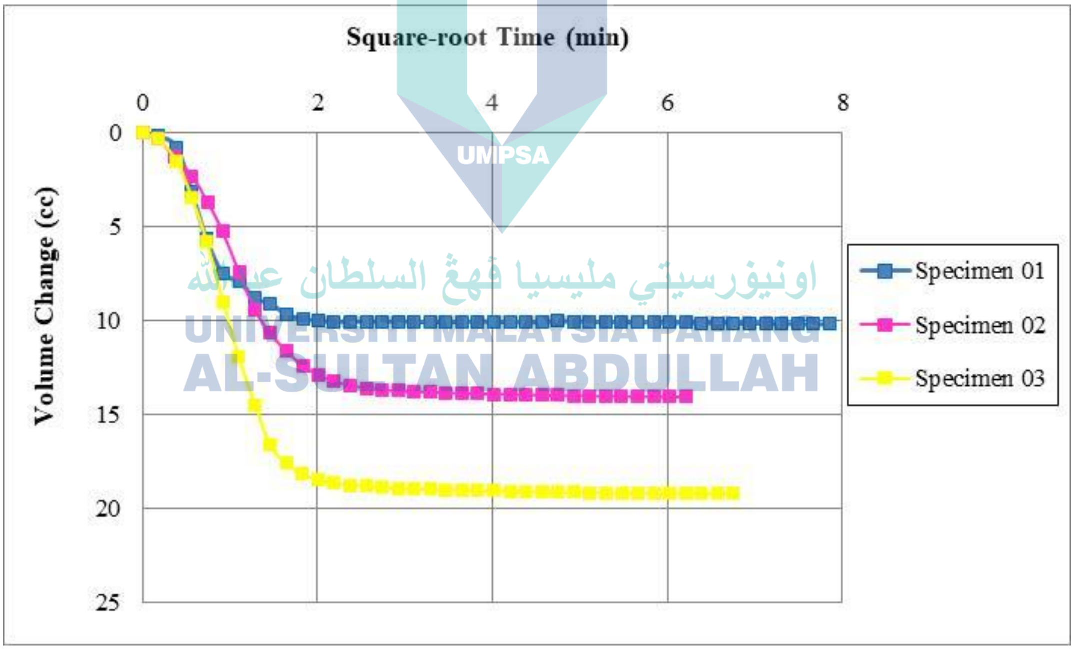

Figure 4.34 Volume change vs square root time for the sample's consolidation stage when it was reinforced by a group column with a diameter of 16 mm and a height penetration ratio of 100%

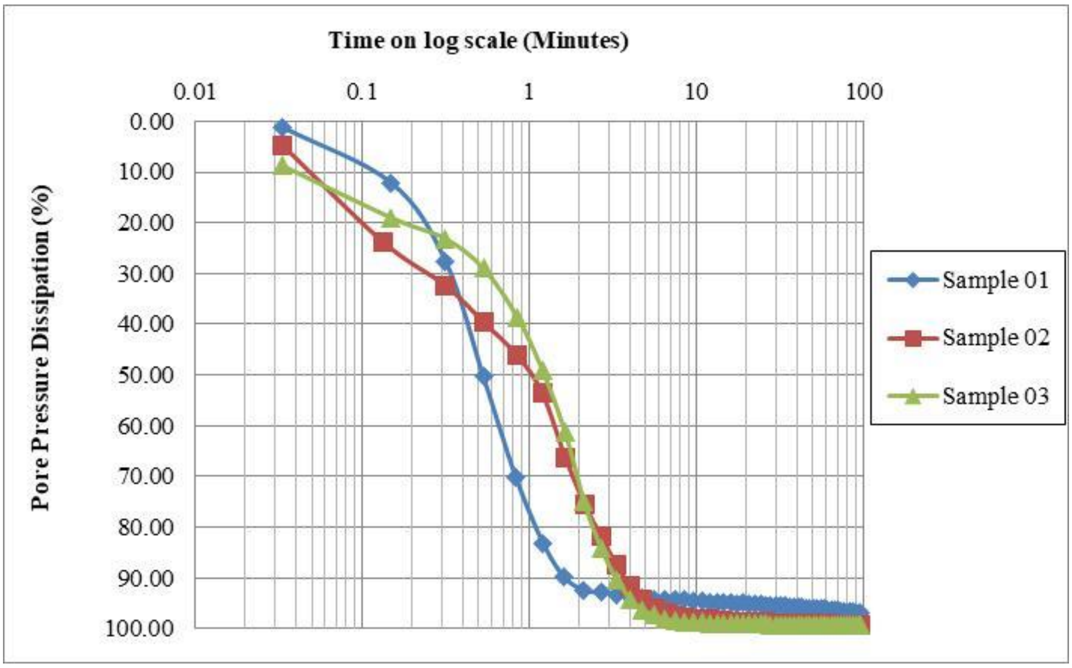

Figure 4.35 Pore pressure dissipation vs logarithmic time during consolidation stage of sample reinforced by a group column 16 mm in diameter and 100% in height

4.10 Summary of Compressibility Analysis

In the triaxial test, the time it took for each specimen to completely consolidate was recorded during the consolidation phase. Figures 4.36(a) and (b) show plots of the time required to achieve full consolidation versus effective confining pressure for single and group columns, respectively. By comparing the consolidation times of samples reinforced with polypropylene columns to those of the controlled sample, one can analyse the function of columns as vertical drains. The accelerated consolidation process is often facilitated by the installation of polypropylene columns under a confining pressure of 100 kPa. The scanning electron microscopy (SEM) analysis shows that the surface textures of polypropylene had a spherical morphology with rough and gritty characteristics. These surface features were found to possess a significant quantity of pores, which enabled the quick dissipation of excess pore water pressure from the samples. The characteristics of the polypropylene particles are intricately connected to this improvement. Based on the findings of the permeability test conducted on polypropylene and kaolin, it is apparent that polypropylene shows a significantly higher coefficient of permeability in comparison to kaolin clay. This shows the effectiveness of inserting polypropylene columns within kaolin clay to accelerate the dissipation of pore water pressure.

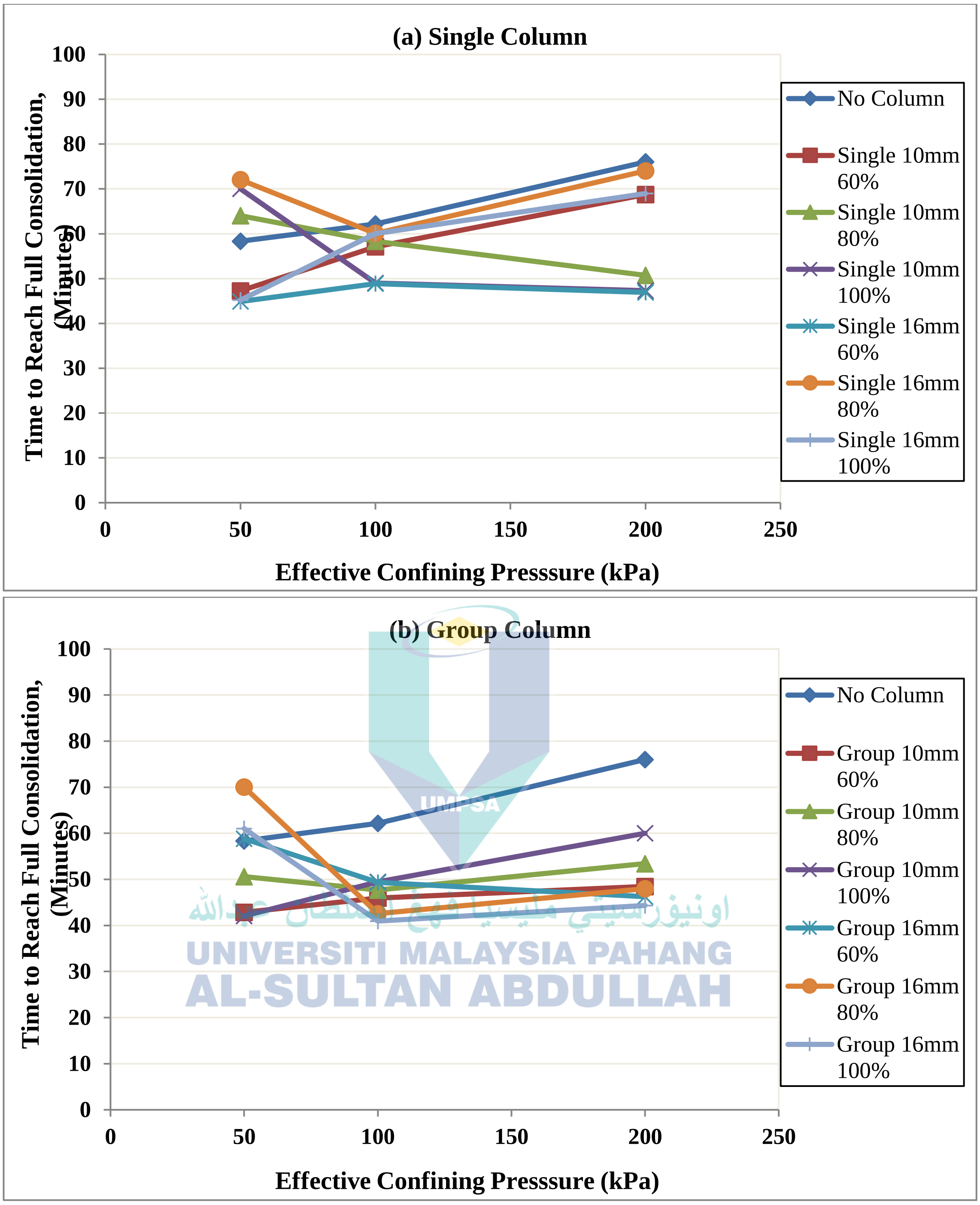

Figure 4.36 For (a) single and (b) group polypropylene columns, the time to obtain full consolidation vs effective confining pressure

However, only half of the reinforced samples showed an improvement in the time it took to reach full consolidation, suggesting that the results for the specimens treated to an effective confining pressure of 100 kPa were varied. The specimens subjected to the highest effective confining pressure of 200 kPa showed improvement in consolidation time when installed with a group of polypropylene columns, in particular; all specimens reached full consolidation at intervals shorter than the control specimen.

The consolidation time of the reinforced sample for effective confining pressures of 100 kPa and 200 kPa is less than the consolidation time of the control sample. Besides, the consolidation time for an effective confining pressure of 100 kPa was less than the consolidation time for an effective confining pressure of 200 kPa when compared to the control sample.

In Figure 4.37, the state during isotropic consolidation was schematically illustrated. Consolidation rate increased with decreasing effective confining pressure. Compared to the control sample, the time taken to reach full consolidation either increased or stayed constant as the effective confining pressure increased. With an effective confining pressure of only 50 kPa, the specimens were able to withstand external pressure, and the water inside the clay specimens swiftly drained via the polypropylene columns. On the other hand, greater surrounding pressure resulted in higher effective confining pressures when applied to polypropylene columns.

The failure of the polypropylene column's vertical drain function under high confining pressure may have been largely attributed to the material's brittleness. The particles were "squeezed", which resulted in finer crushing because polypropylene is brittle and could not sustain the external pressure. These small pieces of crushed polypropylene were then used to fill the gaps. Furthermore, the high confining pressure caused the smearing condition to form between the clay and polypropylene. Fine particles, such soil and broken polypropylene, were carried into the column by the radial water flow and eventually clogged it (Holtz et al., 1991; Muir Wood et al., 2000). This lowered the number of pores in the polypropylene and caused the polypropylene column to enter a "clogging" state. This meant that the polypropylene column could not help the clay specimens' extra pore water to drain. In other words, the effective diameter of the drainage column decreased from when it was initially installed. The grouping of the polypropylene columns made the issue worse because it is possible that during installation, the degree of smearing on the columns was higher than on a single polypropylene column. Because of the installation process, a smear zone was also likely to develop surrounding the drain. This results in a disturbance of the soil structure close to the vertical drain, which reduced horizontal permeability and decreased drainage efficiency relative to ideal conditions (Onoue et al., 1991).

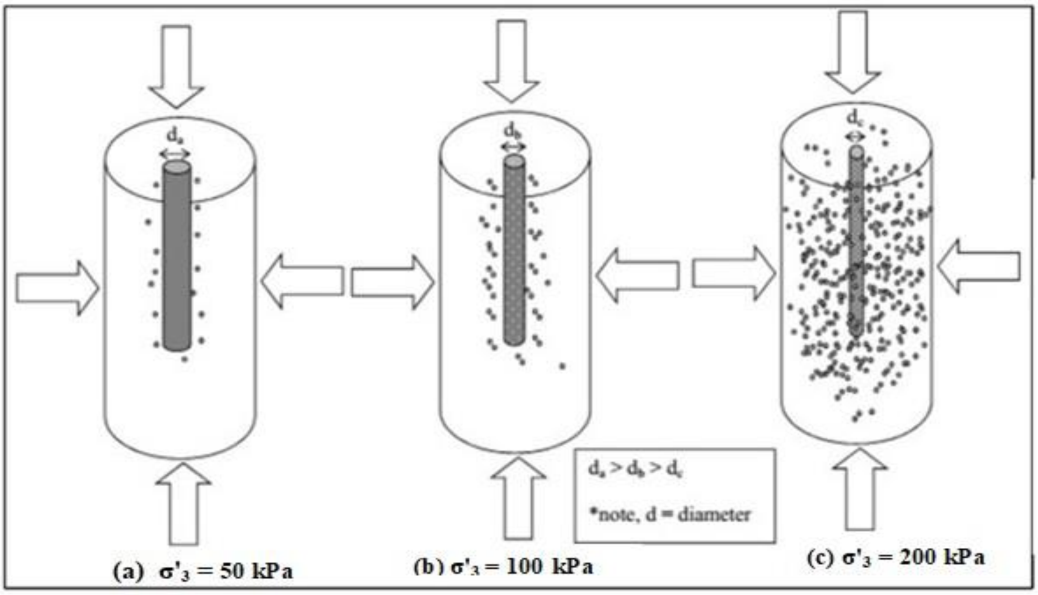

Figure 4.37 Diagram illustrating the impact of different effective confining pressures on smearing and crushing kaolin specimens reinforced with polypropylene columns

Stone columns are mostly used for ground improvement in fine-grained soils, according to Weber et al. (2010). This is done to accelerate the clay's consolidation processes, enhance ground drainage, and lower the danger of bearing failure and settlement. However, compared to what is theoretically conceivable, the installation of polypropylene columns produced smearing and distracting effects that decreased consolidation performance. Weber et al. (2010) asserted that the installation of stone columns induces smearing and disruption, resulting in the division of the impacted region into three distinct categories:

i) Penetration Zone: This is the region where sand particles are pushed through the clay during column installation. This zone experiences direct penetration, leading to localized compression and disturbance of the soil.

ii) Smear Zone: In this zone, the soil particles undergo significant reorientation due to the installation process. The smearing effect leads to a reduction in soil permeability as the natural drainage paths are disrupted, hindering the effectiveness of the stone columns in facilitating drainage and accelerating consolidation.

iii) Densification Zone: This is the area where the clay undergoes measurable compaction. Although the soil density increases in this zone, the overall soil structure may remain largely unchanged. However, the densification contributes to the overall disturbance and can affect the soil's response to loading and consolidation.

The smearing effect primarily reduces permeability in the smear zone, while the disruption effect causes a broader disturbance, impacting soil density and structure in all three zones. Understanding these effects is crucial for optimizing the design and installation of stone columns to enhance consolidation performance effectively.

4.11 Unconfined Compression Test

4.11.1 Undrained Shear Strength

Unconfined compression tests were performed on samples of soft clay reinforced with polypropylene columns to determine their shear strength. The findings of the research are presented in Table 4.11. In order to calculate the average values of shear strength, a total of four sets of tests were conducted for each penetration ratio. Additionally, there was no polypropylene column reinforcement used in the control sample. Finally, 52 samples were produced and analysed (Appendix I).

Table 4.11 Summary of analysis on unconfined compression test

Samples	No. of Columns	Column Diameter (mm)	Area Replacement Ratio Ac/As (%)	Column Height (mm)	Column Height Penetration Ratio, Hc/Hs	Average Max. Shear Strength (kPa)	Improvement of Shear strength (%)
Controlled Sample							
C	0	0	0	0	0	12.75	
Single Columns							
S10-60	1	10	4	60	0.6	18.48	44.95%
S10-80	1	10	4	80	0.8	19.22	51.94%
S10-100	1	10	4	100	1.0	17.97	40.90%
S16-60	1	16	10.24	60	0.6	19.35	51.75%
S16-80	1	16	10.24	80	0.8	22.25	74.50%
S16-100	1	16	10.24	100	1.0	19.02	49.20%

Table 4.11 Continued

Samples	No. of Columns	Column Diameter (mm)	Area Replacement Ratio Ac/As (%)	Column Height (mm)	Column Height Penetration Ratio, Hc/Hs	Average Max. Shear Strength (kPa)	Improvement of Shear strength (%)
				Group Columns			
G10-60	3	10	12	60	0.6	18.94	48.50%
G10-80	3	10	12	80	0.8	21.49	68.50%
G10-100	3	10	12	100	1.0	18.29	43.50%
G16-60	3	16	30.72	60	0.6	15.05	18.00%
G16-80	3	16	30.72	80	0.8	15.58	22.20%
G16-100	3	16	30.72	100	1.0	14.91	17.00%

4.11.2 The Effect of Area Replacement Ratio

The results shown in Figure 4.38 demonstrate that increasing the width of a polypropylene column can result in greater shear strengths. The mentioned relationship shows that the shear strength demonstrates improvement with an increase in the area replacement ratio (Ac/As). The research showed that the polypropylene columns, which had a height of 80 mm, demonstrated a much greater shear strength of 10.24% for the area replacement ratio compared to the lower value of 4.00%. This observation shows the possibility of improving shear strength by increasing the area replacement ratio. At a column height of 80 mm, it was observed that the shear strength of the polypropylene column was comparatively lower for the area replacement ratio of 4.00% as compared to the column with an area replacement ratio of 10.24%. This is a result of the high particle size and gaps in polypropylene, which makes the material less resistant to compression. The 10.24% area replacement ratio exhibited superior performance compared to the 4.00% area replacement ratio for an 80 mm column height, owing to its higher compactness and reduced inter-particle spacing. Moreover, the compressive strength experienced a significant increase due to the large surface area of the polypropylene pellets that made contact with the upper conical plate.

Figure 4.38 shows the relationship between the increase in shear strength and the area replacement ratio (Ac/As). This indicates that an increase in the diameter of the polypropylene column may result in a corresponding enhancement in its shear strength. For the polypropylene columns, the shear strength for the area of 12.00% was greater than the shear strength for the area replacement ratio of 30.72% at a column height of only 80 mm, which may increase the shear strength as well. This finding indicates the potential of improving the shear strength. This is a result of the high particle size and gaps in polypropylene, which makes the material less resistant to compression. The improvement in the area replacement ratio of 12.00% was more significant compared to the 30.72% area replacement ratio for an 80 mm column height due to denser packing of particles and reduced intermediate spaces. In addition, the large contact area between the polypropylene pellets and the upper conical plate resulted in a significant increase in the compression strength.

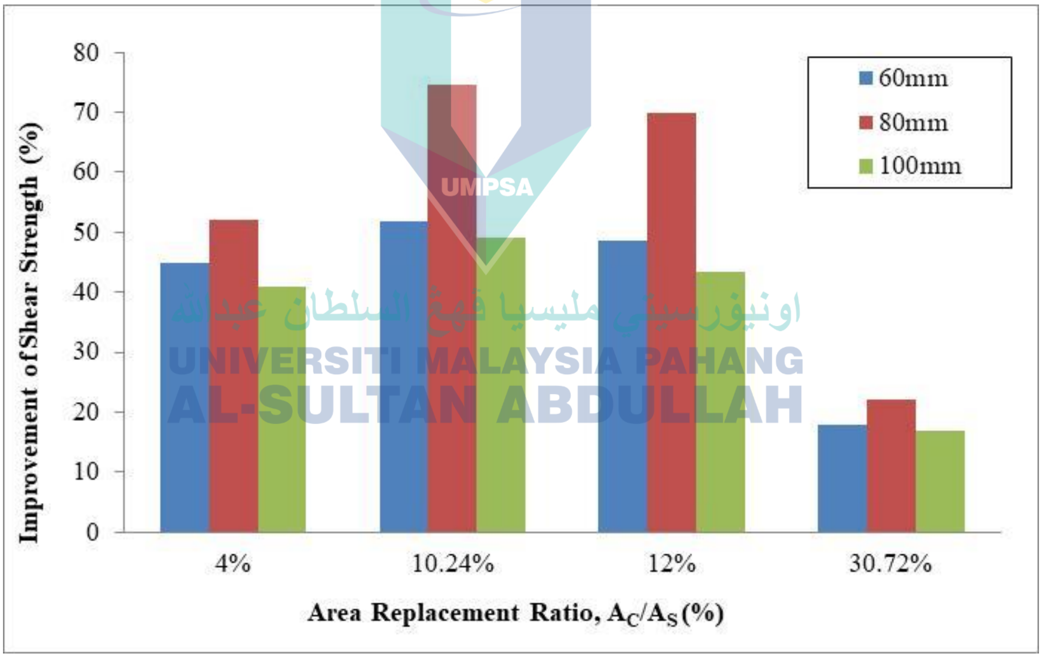

Figure 4.38 Improvement of shear strength vs area replacement ratio Ac/As (%)

The relationship between the area replacement ratio and the ratio of column height to column diameter was investigated in research done by Najjar et al. (2010) and Black et al. (2015) using sand columns. This research examined how much soft clay has improved. The shear strength of the soft clay was expected to improve significantly with an increase in the area replacement ratio. Table 4.12 illustrates the findings pertaining to the impact of the completely penetrating area replacement ratio on the columns, as shown by the earlier research. However, it was evident that the shear strength of single-column penetration showed improvement, corresponding with the observations and theories put out in earlier research. On the other hand, the shear strength of group column penetration did not experience any improvement, likely due to the bigger size of the polypropylene particles. Establishing a full penetration sample for this experiment was challenging due to the potential harm inflicted on the inner wall of the column by the 16 mm diameter drill. Consequently, height penetration ratios of 0.8 and 1.0 were chosen for the group of columns with complete penetration.

Table 4.12 Effect of area replacement ratio for fully penetrating polypropylene columns on improvement shear strength of kaolin clay

Researcher	**Area Replacement Ratio, Ac/As (%)**	**Improvement of Shear Strength (%)**
Black et al. (2014)	10	33
	12	55
Najjar et al. (2010)	7.9	19.5
	17.8	75
Hasan (2013)	4	64.11
	10.24	61.20
	12	61.96
	32.72	14.42
Current Study (2023)	4	46.75
	10.24	74.50
	12	58.90
	32.72	22.20

However, the result was consistent with previous research by Tandel et al. (2012) and Najjar et al. (2010), which discovered that the reduced performance was caused by the smaller polypropylene column mobilisation of larger confining forces. Hence, the more restricting pressures a column contains, the smaller its diameter and the stiffer it becomes.

The findings of the study suggest that the shear strength had been substantially improved in the single column with a diameter of 16 mm and an area replacement ratio of 10.24% as compared to the single column with a diameter of 10 mm and an area replacement ratio of 4.00%. The insufficient area replacement ratio of the column was the underlying factor contributing to this issue. The construction developed a bulge when the vertical stress was dispersed within the column due to the excessively thick soil sample surrounding it. It was sufficient for the soil sample's circular perimeter area to allow the column to improve the shearing strength. This is the reason why the shear strength improved despite the soil sample having a high area replacement ratio.

The results of the study also revealed that the group column with a diameter of 16 mm and an area replacement ratio of 30.72% showed a comparatively slower rate of shear strength increase compared to the group column with a diameter of 10 mm and an area replacement ratio of 12.00%. The cause for this was the excessively high area replacement ratio of the column. There was a bulge in the column when the vertical weight was dispersed inside the soil sample because there was insufficient width remaining to support the column. The soil sample's circular peripheral area was not as large as the column required to boost the shearing strength. Because of this, the shear strength decreased even if the area replacement ratio of the soil sample was high. The shear strength of the soil sample remained unchanged despite its high area replacement ratio as the circular peripheral area of the soil sample is insufficient when compared to the column necessary to increase the shearing strength.

The results also showed that if a significant portion of the soil had been drilled out of the samples previously to the installation of the polypropylene columns, this would have an impact on the natural condition of the soil while also lowering the initial shear strength of the soil itself. This showed that it significantly affected the soil's shear strength, given the constraints imposed by the samples' smaller dimensions.

4.11.3 The Effect of Column Penetration Ratio

Figure 4.39 was used to investigate the potential impact of the ratio between the height and diameter of the column on undrained shear strength. This was accomplished by graphically representing the relationship between these two variables. A variety of results from the study conducted by Maakaroun et al. (2015) are illustrated on one graph for easier comparison. According to previous research, the dark grey area in the image is known as "the critical column length" and it is four to eight times the column's diameter (Dc).

The findings are consistent with the hypothesis that there is a critical column length over which there is very little increase in undrained shear strength. Based on all the area ratios, the grey area showed the most gain. Higher increases were often observed in single columns instead of in group columns. When it reached 8Dc, the undrained shear strength increased the most with area replacement ratios of 4% and 12%. The area replacement ratios at 5Dc, which were 10.24% and 30.76%, showed the greatest improvement.

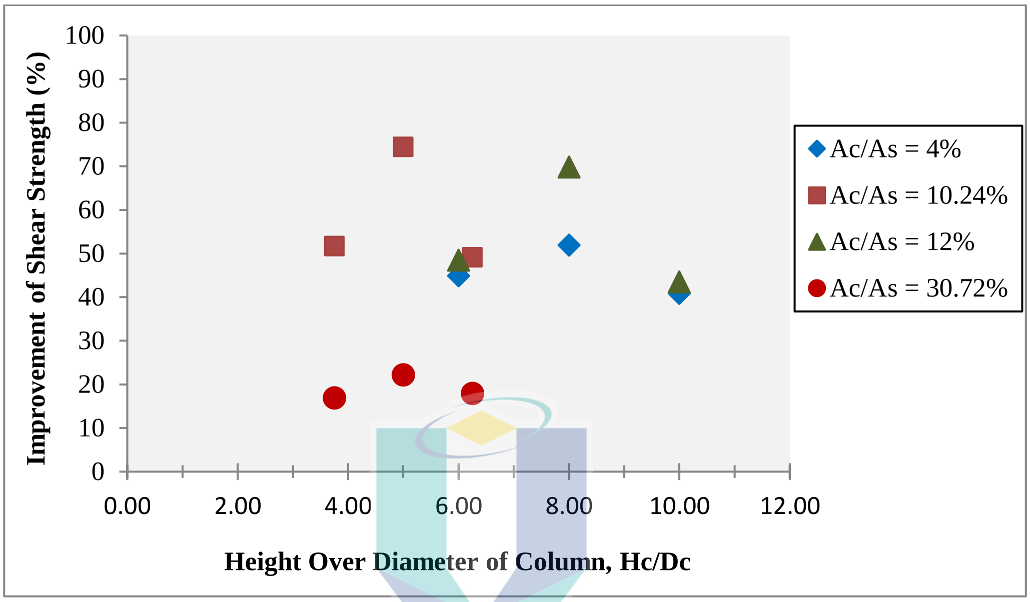

Figure 4.39 Undrained shear strength is affected by the column height to diameter ratio

In order to improve the ratio of shear strength to height penetration for both single and grouped polypropylene columns, an unconfined compression test was employed, as shown in Figure 4.40. The height penetrating ratio (Hc/Hs) indicated consistency, with the most significant enhancement seen at Hc/Hs = 0.8 across all samples. The findings of the investigation suggest that the height penetration ratio had a greater influence on the improvement of undrained shear strength in clay soil, in comparison to the height-to-diameter ratio of the column.

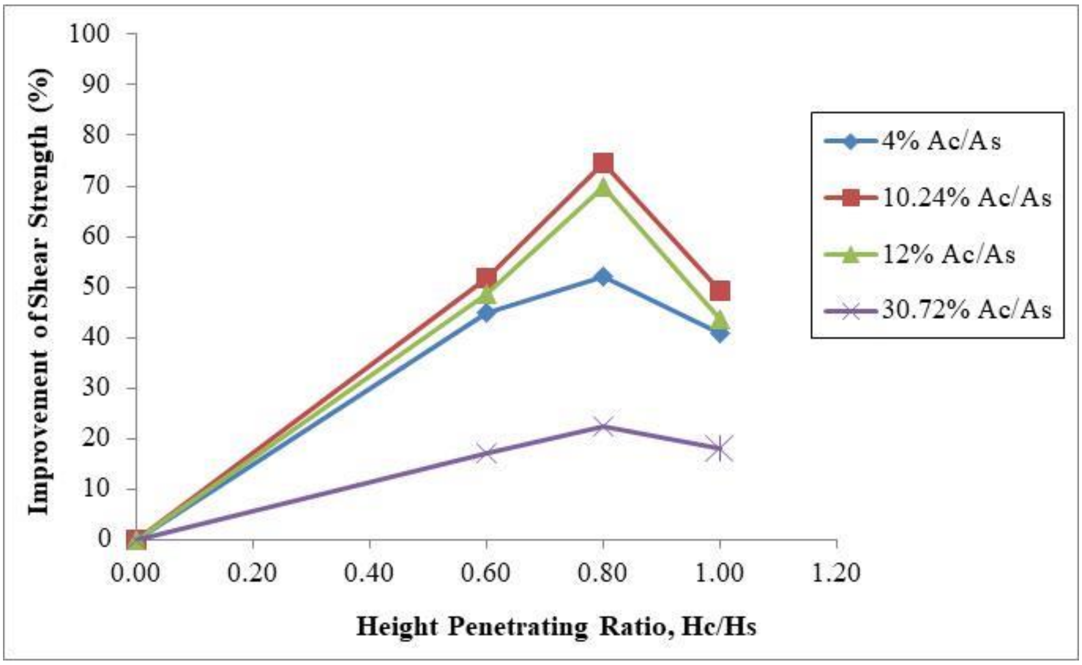

Figure 4.40 Improvement of undrained shear strength for both single and group polypropylene columns through the height penetrating ratio

Muir Wood et al. (2000) suggested that the interactions between the individual stone columns, the filled area, and the surrounding soil may be explained by piles with non-linear, sand-like axial stiffness properties. If a column is short enough to support a significant weight at its base, it will eventually break through the clay underneath it. The plunge lowers as columns go longer because fewer weights are supported at their bases. This model exhibits behaviour that is extremely similar to a sand pile.

Fleming et al. (1985) showed that, similar to compressible piles, shaft friction results in the loss of any additional weight applied to the base of the pile or stone column. The real models also showed that to be the case. The mobilisation of shear strength throughout the pile or column was significantly affected by radial constraints from the surrounding soil, compared to a conventional pile example. Figure 4.41 illustrates the circumstances.

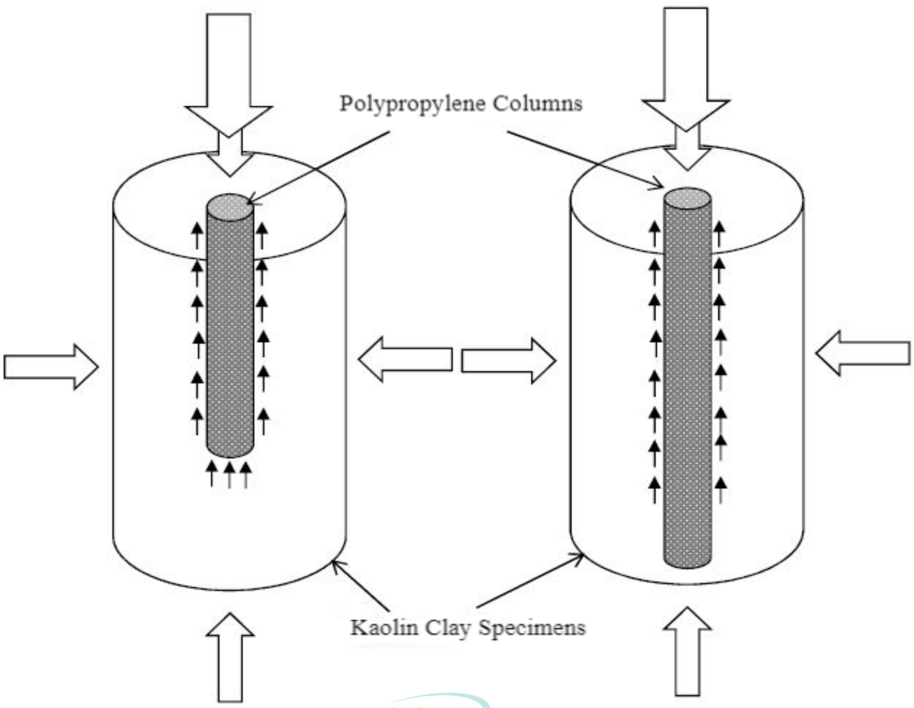

Figure 4.41 Schematic illustrations of soft kaolin clay that are reinforced with partially and fully penetrated granular columns and confined by the surrounding soil pressure

4.11.4 The Effect of Volume Replacement Ratio

The results illustrated in Table 4.13 demonstrate an increased undrained shear strength in a relationship with the volume ratio (Vc/Vs). The table presents data that demonstrates an increase in the undrained shear strength of the kaolin sample following the installation of the polypropylene column. The undrained shear strength indicated substantial improvements of 44.95%, 51.94%, and 40.90% for specimens with a single column diameter of 10 mm and heights of 60 mm, 80 mm, and 100 mm, respectively. Similarly, samples with a single column diameter of 16 mm had comparable percentage increases of 51.75%, 74.50%, and 49.20%. However, the advancement became more apparent as the volume replacement ratio increased.

The results presented in Table 4.13 indicate that the presence of the polypropylene column leads to a significant enhancement in the undrained shear strength of the kaolin specimen. The undrained shear strength of the samples increased by 48.50%, 68.50%, and 43.50% for samples with group column diameters of 10 mm and heights of 60 mm, 80 mm, and 100 mm, respectively. Conversely, samples with group column diameters of 16 mm had comparatively lower improvements of 18.00%, 22.20%, and 17.00%. However, as the volume replacement ratio was raised, there was a corresponding increase in the level of improvement observed.

The decrease in improvement was caused by the fact that a sizable piece of the soil was drilled out of the samples, changing the soil's original state. The samples' shear strength decreased as a result. There was also a greater likelihood of the soil collapsing because no restricting pressure was applied to the samples throughout the test (Hasan, 2013).

Table 4.13 Volume replacement ratio with improvement shear strength

Sample UCT Test	**No. of Column**	**Column Diameter (mm)**	**Volume of Sample Vs (mm^3)**	**Volume of Column Vc (mm^3)**	**Volume Replacement Ratio Vc/Vs**	**Improvement Shear Strength (%)**
CS	0		1.96×10^5	0	0	
S10-60				4710	0.024	44.95%
S10-80	1	10	1.96×10^5	6280	0.032	51.94%
S10-100				7850	0.040	40.90%
S16-60				12058	0.062	51.75%
S16-80	1	16	1.96×10^5	16077	0.082	74.50%
S16-100				20096	0.103	49.20%
G10-60				14130	0.072	48.50%
G10-80	3	10	1.96×10^5	18840	0.096	68.50%
G10-100				23550	0.120	43.50%
G16-60				36174	0.185	18.00%
G16-80	3	16	1.96×10^5	48231	0.246	22.20%
G16-100				60288	0.307	17.00%

Figure 4.42 shows a graph of the volume penetration ratio vs the rise in shear strength. The column with a diameter of 16 mm showed the highest improvement percentage, reaching 74.50%. In comparison, the group of columns with a diameter of 10 mm had a slightly lower improvement percentage of 68.50%.

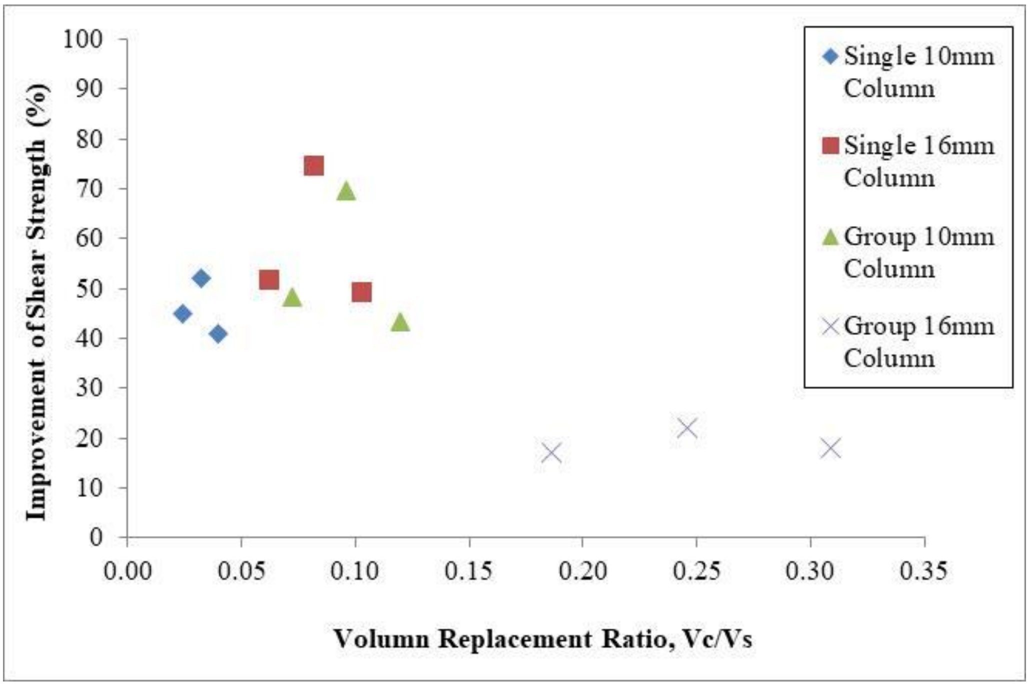

Figure 4.42 Improved undrained shear strength with an increased volume replacement ratio

4.12 Consolidated Undrained Triaxial Test

The results obtained from consolidated undrained triaxial tests conducted on normally consolidated kaolin clay samples unreinforced and reinforced with single and group polypropylene columns are discussed in this part. Test results were analysed and presented in tabulated and graphic forms. The summary results from the consolidated undrained triaxial test are shown in Table 4.14 (Appendix-J).

Table 4.14 Summary of results from consolidated undrained triaxial test

Formation	Cell Pressure	Back Pressure	Effective Confining Pressure	Effective Shear Stress Failure Parameters		Excess Pore Water Pressure (kPa)	Reduction in Excess Pore Pressure (kPa)	Maximum Deviator Stress	
				Apparent Cohesion, c' (kPa	Effective Friction Angle, ϕ'			Axial Strain (%)	Maximum Deviator Stress (kPa)
C	100	50	50	1.37	32.30	51.30	-	19.92	122.86
	200	100	100			99.10	-	19.13	245.70
	400	20	200			195.80	-	18.09	391.10
S1060	100	50	50	4.96	31.17	47.90	3.40	18.96	148.69
	200	100	100			93.30	5.80	19.27	271.31
	400	200	200			179.40	16.40	19.28	429.24
S1080	100	50	50	7.32	30.24	50.90	0.40	17.35	164.08
	200	100	100			95.90	3.20	16.95	266.67
	400	200	200			187.30	8.10	20.12	435.25
S10100	100	50	50	5.72	31.00	49.00	2.30	19.80	158.98
	200	100	100			98.60	0.50	19.33	244.62
	400	200	200			192.60	3.20	19.51	417.53
S1660	100	50	50	9.86	29.98	46.70	4.40	20.05	142.90
	200	100	100			98.60	0.50	19.78	276.75
	400	200	200			194.70	1.10	17.08	437.72
S1680	100	50	50	14.40	29.60	52.60	-1.30	19.96	159.49
	200	100	100			97.60	1.50	16.01	281.36
	400	200	200			176.60	19.20	17.56	451.89

Table 4.14 Continued

Formation	Cell Pressure	Back Pressure	Effective Confining Pressure	Effective Shear Stress Failure Parameters		Excess Pore Water Pressure (kPa)	Reduction in Excess Pore Pressure (kPa)	Maximum Deviator Stress	
				Apparent Cohesion, c' (kPa	Effective Friction Angle, ϕ'			Axial Strain (%)	Maximum Deviator Stress (kPa)
	100	50	50			51.80	0.50	19.01	142.75
G1060	200	100	100	6.10	30.60	97.90	1.20	19.09	241.62
	400	200	200			186.40	9.40	19.60	435.80
	100	50	50			51.60	-2.30	19.42	154.42
G1080	200	100	100	13.85	30.80	98.60	0.50	17.32	288.68
	400	200	200			199.20	-3.40	19.86	454.55
	100	50	50			49.60	1.30	19.78	143.80
G10100	200	100	100	7.66	29.70	98.20	0.10	19.44	231.18
	400	200	200			196.60	-0.80	19.95	367.00
	100	50	50			52.60	-1.30	19.37	145.60
G1660	200	100	100	4.10	30.90	97.60	1.50	18.56	269.35
	400	200	200			176.90	18.90	18.09	437.50
	100	50	50			51.60	-0.30	18.28	143.64
G1680	200	100	100	5.90	31.90	98.60	0.50	16.32	264.90
	400	200	200			198.20	1.60	20.06	477.54
	100	50	50			54.00	-2.70	15.77	107.56
G16100	200	100	100	2.82	32.00	98.80	0.70	18.72	232.20
	400	200	200			198.90	-3.10	17.75	452.25

4.12.1 Stress Strain Behaviour

4.12.1.1 Single Columns

Figures 4.43, 4.44, and 4.45 present graphs illustrating the changes in excess pore-water pressure and deviatoric stress as a result of axial strain for controlled specimens and clay specimens reinforced with polypropylene columns. These figures correspond to effective confining pressures of 50 kPa, 100 kPa, and 200 kPa, respectively.

The maximum deviatoric stresses for specimens reinforced with single polypropylene columns are higher than those for controlled specimens at an effective confining pressure of 50 kPa. In comparison to specimens with smaller column diameters, those reinforced with larger column diameters show higher maximum deviatoric stresses. The curves also showed that the highest maximum deviatoric stress and axial strain, at 164.08 kPa and 17.35%, respectively, were found in specimens reinforced with a 10 mm diameter and an 80% penetration ratio.

The findings also show that following the peak deviatoric stress, the pore-water pressure continued to decrease. The reduced extra pore-water pressure during shear in the tests for this study was probably due to the increased stiffness and dilatational tendency of the polypropylene columns. As area replacement ratios and column penetration ratios improve, these effects became more apparent.

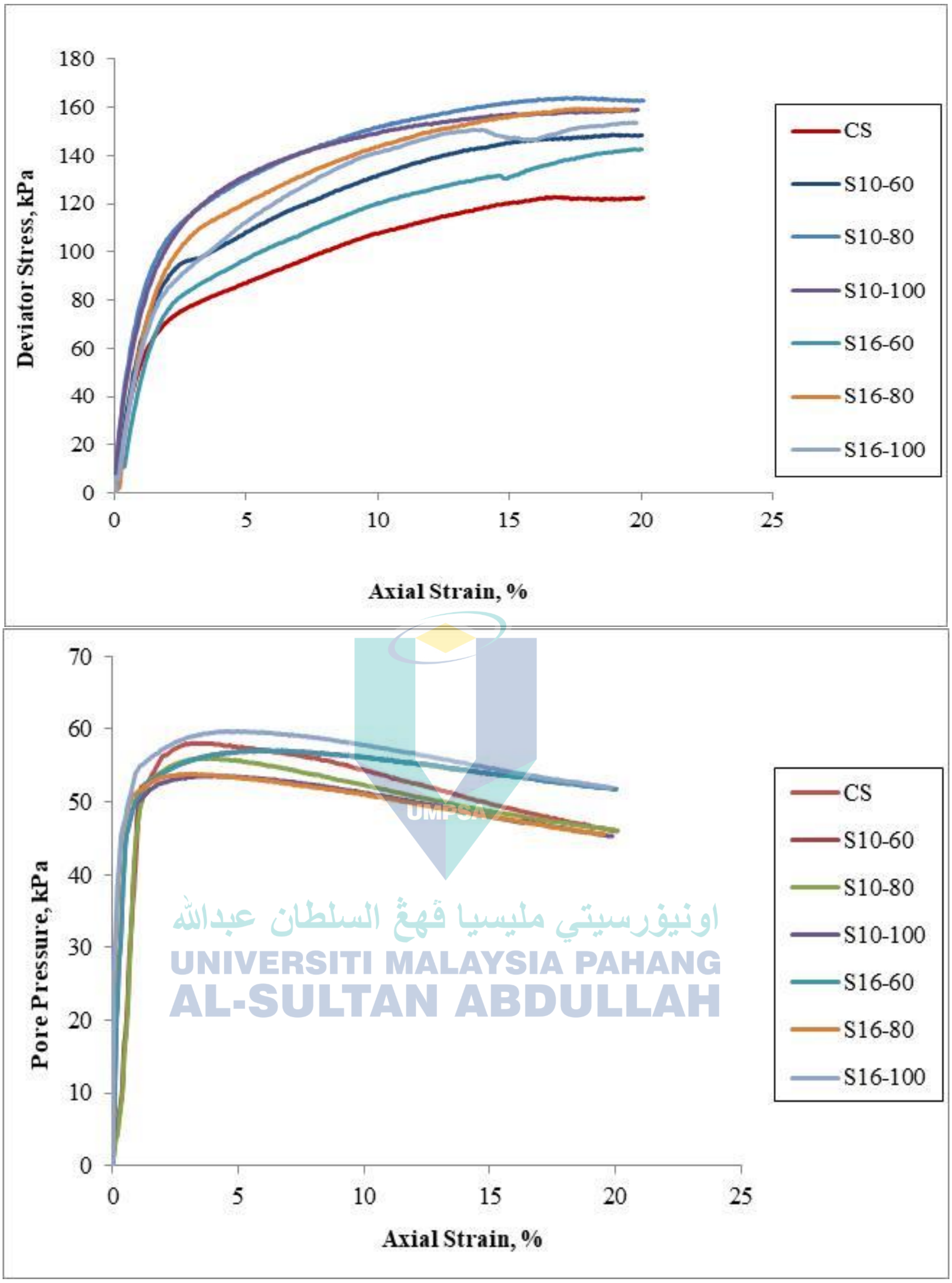

Figure 4.43 Deviator stress versus axial strain and pore pressure versus axial strain for kaolin specimens reinforced at an effective confining pressure of 50 kPa using a single polypropylene column

The maximum deviatoric stresses for specimens reinforced with single polypropylene columns were higher than those for controlled specimens with an effective confining pressure of 100 kPa, with the exception of specimens reinforced with a 10 mm diameter and a height penetration ratio of 60% and 100%. The maximum deviatoric stresses of specimens reinforced with greater column diameters were higher than those of specimens with smaller column diameters, with the exception of specimens reinforced with a 10 mm diameter and an 80% height penetration ratio. A possible explanation for some of the reinforced specimens failing at lower maximum deviator stress than the controlled sample is that the specimen was unable to maintain the effective confining pressure at that point. Additionally, the curves showed that the specimens with the highest maximum deviatoric stress and axial strain 281.36 kPa and 16.01%, respectively were reinforced with a 16 mm diameter and an 80% penetration ratio.

Maximal deviatoric stress is found under conditions of constant pore-water pressure, which is comparable with the results obtained from specimens exposed to an effective confining pressure of 100 kPa. As previously stated, the reduction in excess pore-water pressure observed during shear in the experiments conducted in this research can be attributed to the increased stiffness and tendency for enlargement of the polypropylene columns. These effects are anticipated to become more pronounced as the area replacement ratios and column penetration ratios increase.

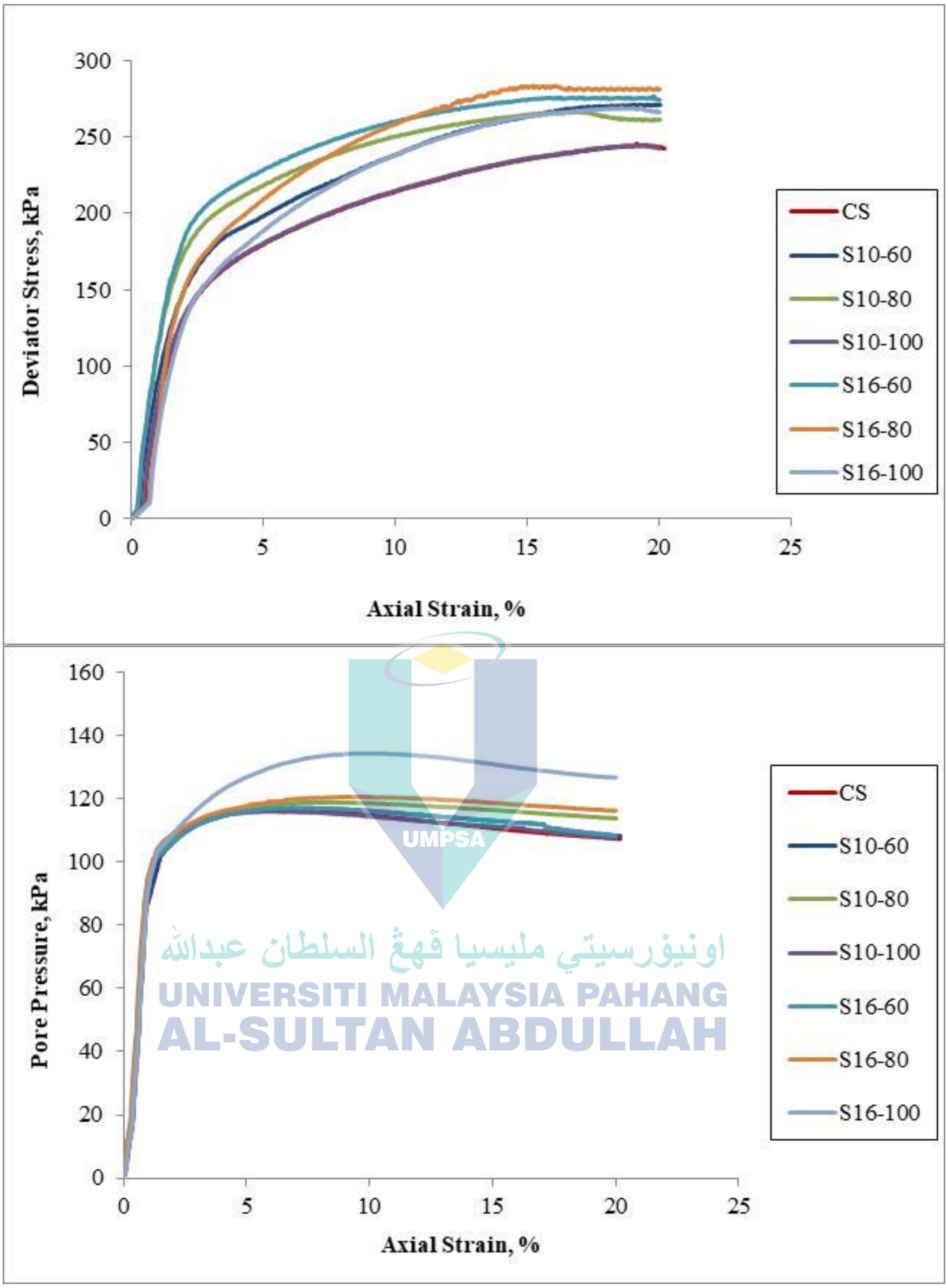

Figure 4.44 Deviator stress versus axial strain and pore pressure versus axial strain for kaolin specimens reinforced at an effective confining pressure of 100 kPa using a single polypropylene column

At an effective confining pressure of 200 kPa, specimens reinforced with single polypropylene columns exhibited greater maximal deviatoric stresses compared to controlled specimens. In comparison to specimens with a smaller column diameter, specimens reinforced with a larger column diameter exhibited higher maximum deviatoric stresses. There is a possibility that the specimen could not sustain the effective confining pressure at that point, which resulted in some of the reinforced specimens failing at lower maximum deviator stress compared to the controlled sample. The curves also showed that the maximum deviatoric stress and axial strain, at 451.89 kPa and 17.56%, respectively, were found in specimens reinforced with a 16 mm diameter and an 80% penetration ratio.

The results show that the deviatoric stress achieved its maximum value at constant pore-water pressure circumstances, showing a similar pattern to samples exposed to an effective confining pressure of 200 kPa. The results also show that, with the exception of the sample reinforced with a single 16 mm reinforcement with an 80% height penetration ratio, the pore-water pressure slowly decreased until the maximum value of the deviatory stress was reached.

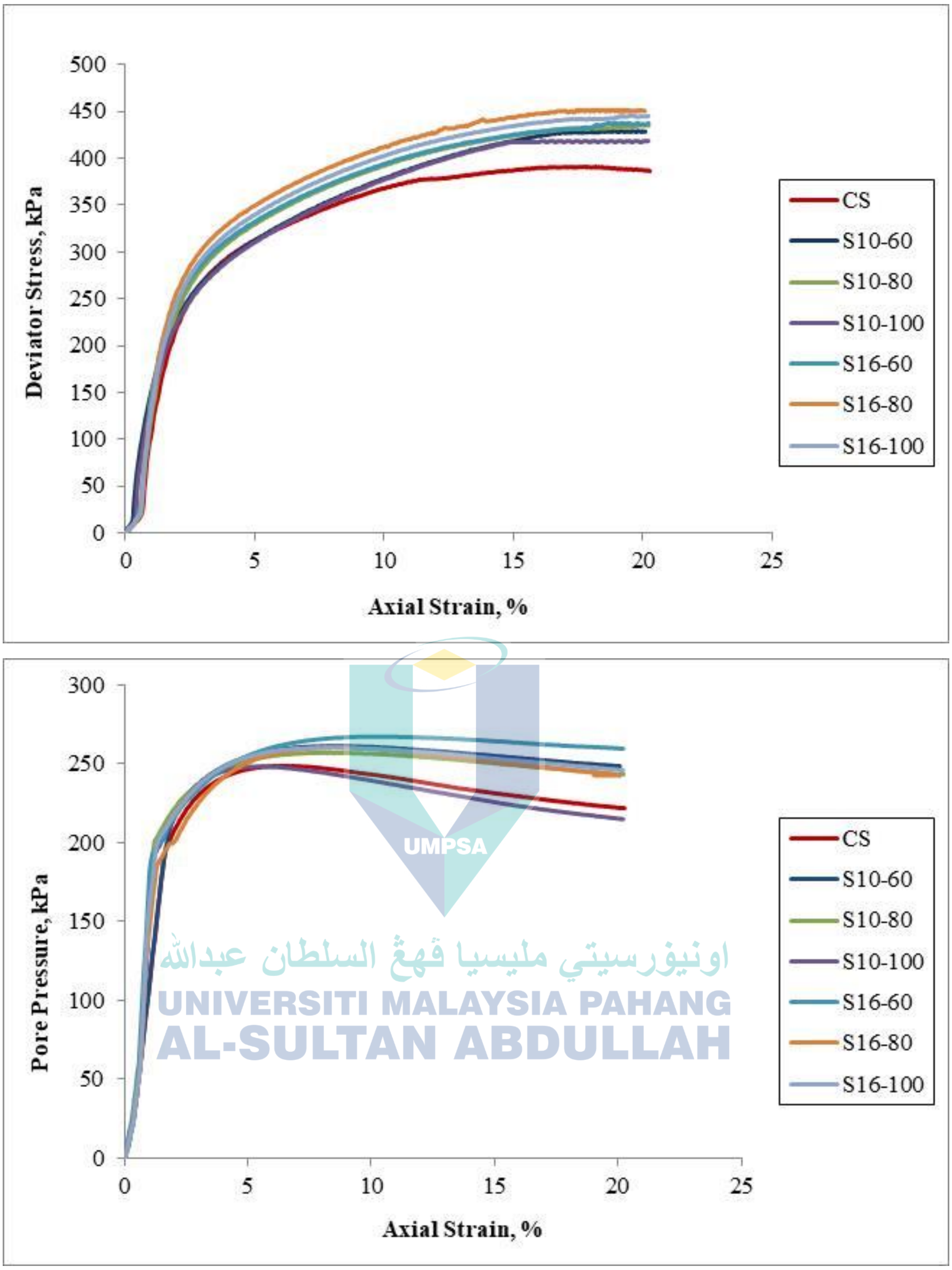

Figure 4.45 Deviator stress versus axial strain and pore pressure versus axial strain for kaolin specimens reinforced at an effective confining pressure of 200 kPa using a single polypropylene column

4.12.1.2 Group Columns

Based on Figure 4.46, it can be observed that the deviatoric stresses reached their highest values for specimens reinforced with polypropylene columns, surpassing those of the controlled specimens, except for specimens reinforced with group 16 mm diameter columns that exhibited a 100% height penetration ratio. An effective confining pressure of 50 kPa was used to observe this behaviour. This behaviour is seen at 50 kPa of effective confining pressure. At 154.42 kPa, the maximum deviatoric stresses of the specimens reinforced with polypropylene columns with an 80% height penetration ratio were greater than those of the other specimens. The curves also showed that the highest maximum deviatoric stress and axial strain, at 154.42 kPa and 19.42% respectively, were found in specimens reinforced with a 10 mm diameter and an 80% penetration ratio.

The results show that when the deviatoric stress gets closer to its maximum value, specimens that are exposed to an effective confining pressure of 50 kPa show a minor decrease in pore-water pressure. The greater area replacement ratio, which allowed the specimens to support more loads even under extreme strain, was primarily responsible for the phenomena that was observed. This might have possibly led to a greater tendency for the sand column to dilate during shear.

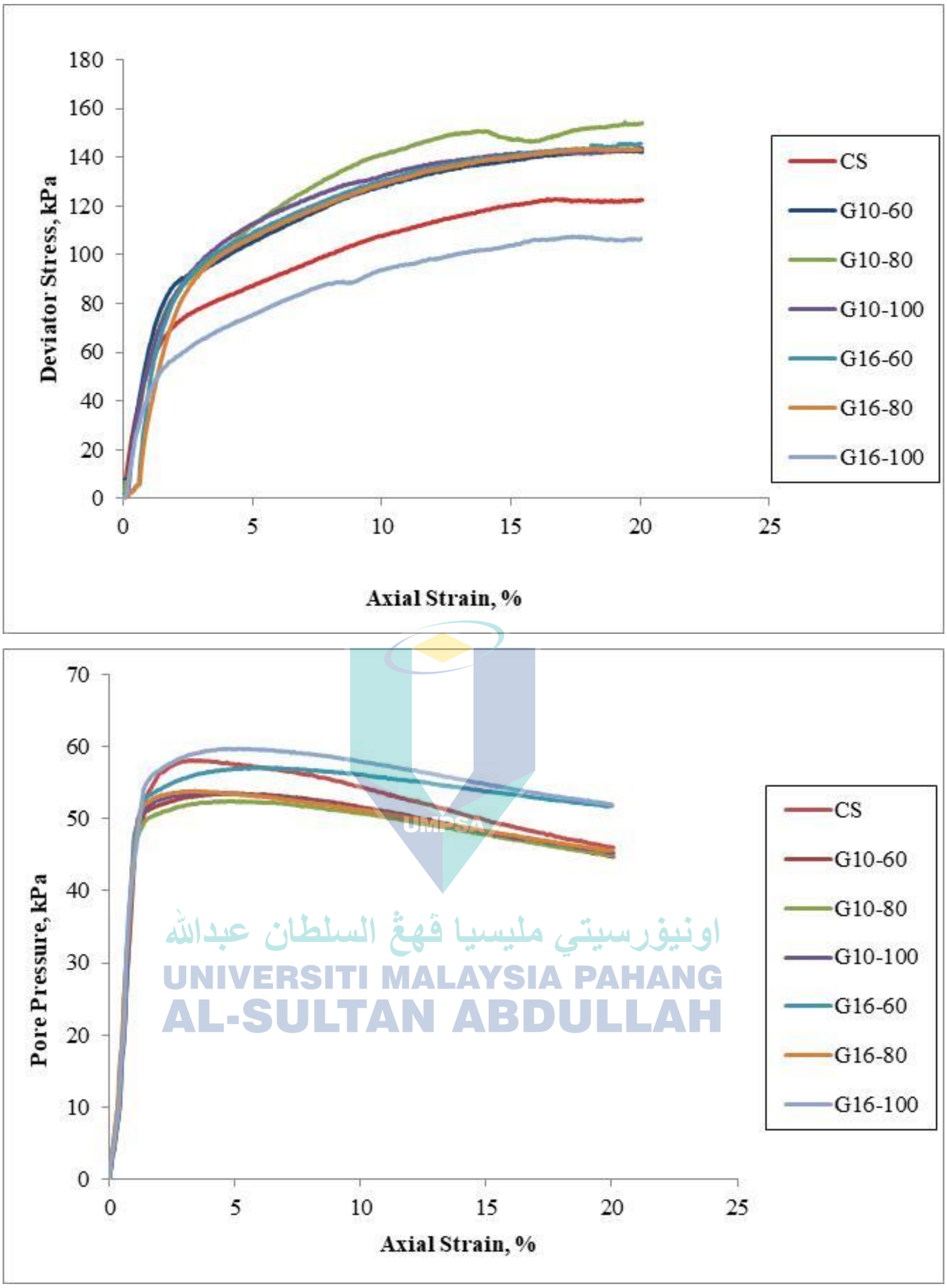

Figure 4.46 Deviator stress versus axial strain and pore pressure versus axial strain for kaolin specimens reinforced at an effective confining pressure of 50 kPa using a group polypropylene column

Figure 4.47 shows that with the exception of specimens reinforced with columns measuring 16 mm in diameter and 100% height penetration, the deviatoric stresses reached their maximum values for specimens reinforced with group polypropylene columns. These maximum deviatoric stresses were found to be higher compared to the controlled specimen, given an effective confining pressure of 100 kPa. Based on the curves, the specimens reinforced with a 10 mm diameter and 80% penetration ratio had the highest maximum deviatoric stress, which was 288.68 kPa. Values from 15% to 18% were the maximum axial strains.

The results showed a similar trend to samples that were exposed to a confining pressure of 100 kPa, where the deviatoric stress reached its maximum value and the pore-water pressure slightly decreased. The pattern shown here is similar to that of specimens reinforced with group polypropylene columns and exposed to an effective confining pressure of 100 kPa.

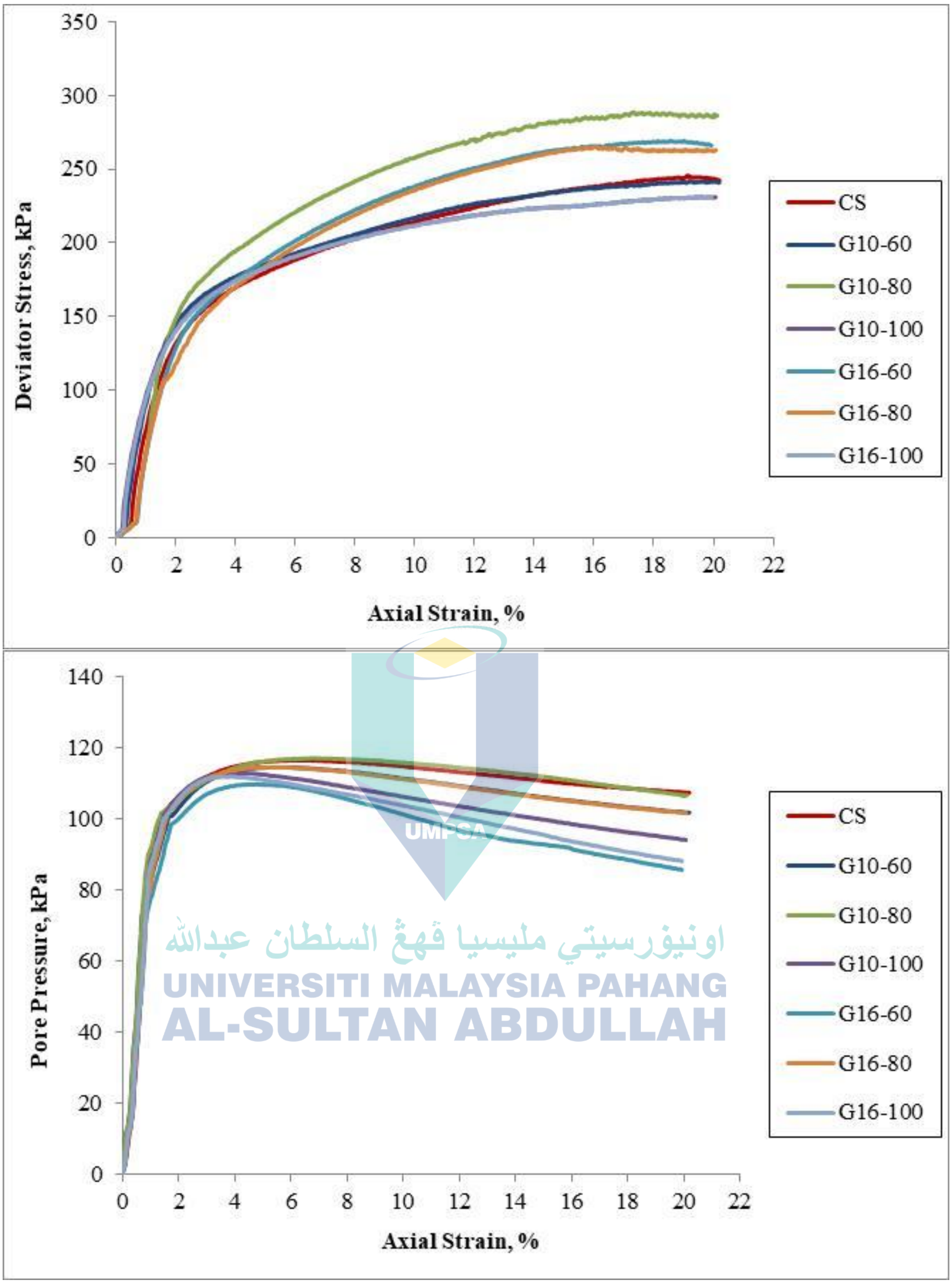

Figure 4.47 Deviator stress versus axial strain and pore pressure versus axial strain for kaolin specimens reinforced at an effective confining pressure of 100 kPa using a group polypropylene column

Based on the findings presented in Figure 4.48, it can be observed that when subjected to an effective confining pressure of 200 kPa, the maximum deviatoric stresses demonstrated by specimens reinforced with group polypropylene columns exceeded those of the controlled specimens. Nevertheless, it is essential to acknowledge that this advancement does not persist in specimens that are reinforced with a 10 mm diameter and a height penetrating ratio of 100%. The maximum deviatoric stresses of specimens reinforced with larger column diameters were higher than those of specimens with lower diameters, with the exception of specimens reinforced with 16 mm diameters and a height penetration ratio of 60%. Additionally, the curves showed that specimens with the highest maximum deviatoric stress and axial strain of 477.54 kPa and 20.06%, respectively, were reinforced with a 16 mm diameter and an 80% penetration ratio.

As a result, when specimens reinforced with a single polypropylene column were exposed to an effective confining pressure of 200 kPa, the maximum deviatoric stresses revealed a decrease compared to the controlled specimen. It was possible for the specimens to reach failure before the shearing process began as they were unable to withstand effective pressure at that time. The brittleness of the polypropylene, which could only function at specific effective pressure points, may have had an impact on this situation. If these pressures were exceeded, the polypropylene would crash into each other and rupture the specimens. This is why the maximum deviatoric stresses for samples reinforced with polypropylene columns showed a lower value than the controlled sample.

The results were in accordance with specimens with an effective confining pressure of 200 kPa because deviatoric stress increased with decreasing pore-water pressure. The pattern in this setting was comparable to samples reinforced at an effective confining pressure of 100 kPa using a group of polypropylene columns.

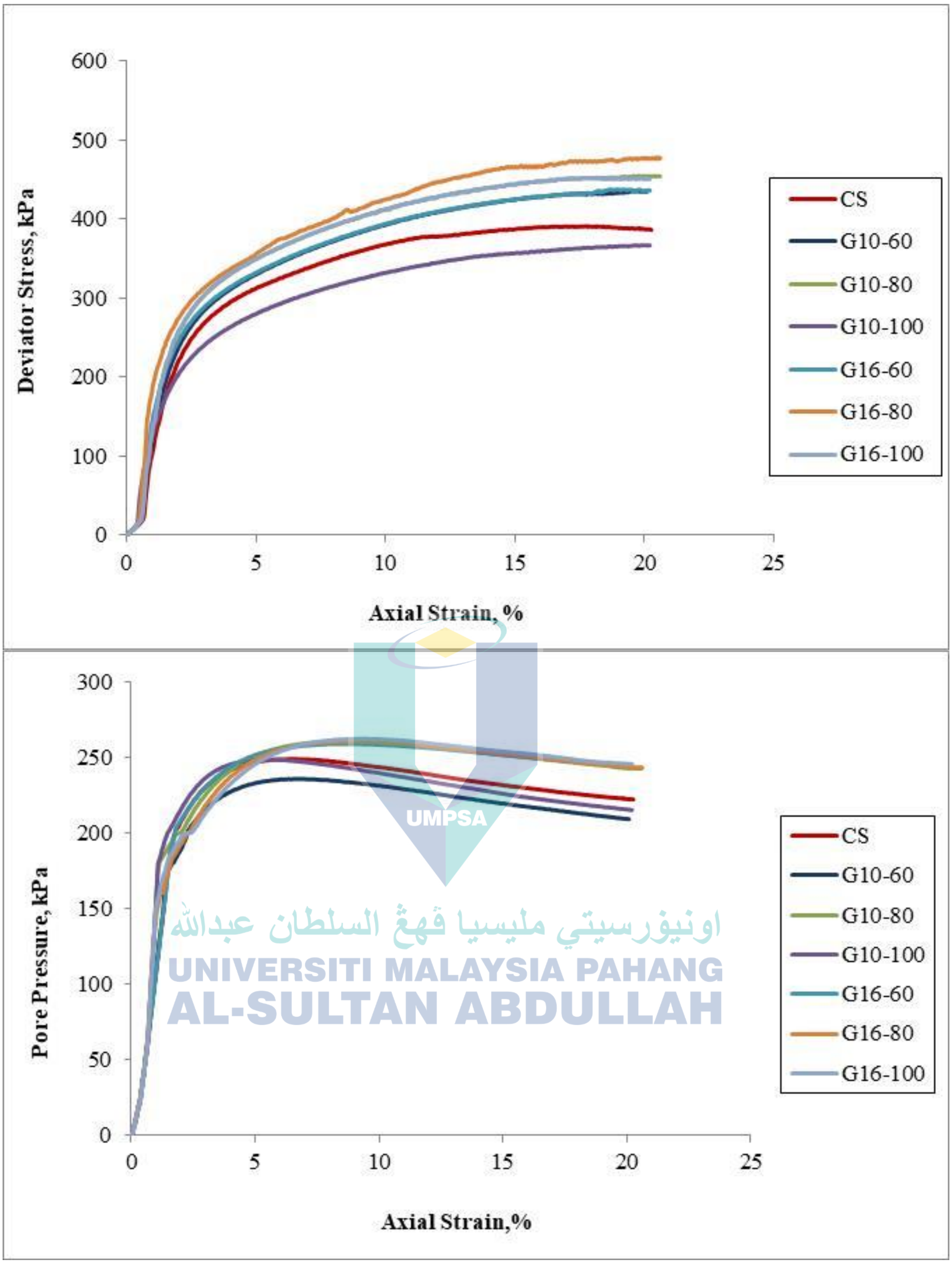

Figure 4.48 Deviator stress versus axial strain and pore pressure versus axial strain for kaolin specimens reinforced at an effective confining pressure of 200 kPa using a group polypropylene column

4.12.2 Excess Pore Pressure

Based on the data analysis, samples reinforced with single polypropylene columns at various effective confining pressures of 50 kPa had an average decrease in excess pore-water pressure of 3.96% and 3.51%, respectively, for area replacement ratios of 4.0% and 10.24%. The greater stiffness and dilatational tendency of the polypropylene columns likely resulted in less extra pore-water pressure being produced during undrained stress. The average reductions in excess pore-water pressure for single columns at various effective confining pressures of 100 kPa were found to be around 3.19% and 0.63%, with area replacement ratios of 4.0% and 10.24%, respectively.

The samples, which were reinforced with single polypropylene columns, had area replacement ratios of 4.0% and 10.24% respectively. These samples were subjected to a different effective confining pressure of 200 kPa, resulting in an average decrease in excess pore-water pressure of 11.39% and 3.44% respectively. Consequently, the addition of polypropylene columns under undrained loading led to a decrease in the generation of excess pore-water pressure. As their height and area replacement ratio increased, single columns with an effective confining pressure of 200 kPa became an exception that was excellent at reducing water pressure. This can be attributed to the brittle nature of polypropylene and the samples' inability to maintain high confining pressure, which crushed the material and caused the "clogging" state. The process of consolidation and pore pressure dissipation in the clay may be delayed by smearing the results from installing polypropylene columns between the column and the surrounding clay.

It is expected that the sheared polypropylene columns would function as drains. However, none of the triaxial tests conducted for this inquiry allowed for any global drainage through the polypropylene columns. This was due to the extreme field conditions caused by the minimal amount of drainage permitted between the columns and the surrounding clay sample. The differences in drainage conditions could be attributed to two main outcomes.

The first conclusion was that the polypropylene columns used in the laboratory testing technique may exhibit the development of unfavourable pore-water pressure, as previously found and demonstrated in this research. This state is quite improbable in the majority of applications that employ polypropylene columns unless there are extremely rapid loading circumstances. The second result of this study was that the clay used in the laboratory testing program does not exhibit infinite drainage across the polypropylene columns, indicating that pore pressure was not easily transmitted across the polypropylene columns. Moreover, it should be noted that this behaviour is not relevant in practical field settings since the dissipation of partial pore pressure in clay is expected under typical construction loads. The anticipated increases in the undrained shear strength of the composite clay-polypropylene column are expected to be influenced in distinct ways by the two implications that were previously highlighted.

This chapter presents a review of appropriate stress pathways for experiments with fully penetrated non-encased sand columns, considering the three effective confining pressures employed in this study. This will facilitate a better understanding of how polypropylene columns affect the amount of undrained shear strength improvement and the potential relationship between that improvement and the creation of pore pressures during shear.

4.12.3 Shear Strength Parameters

The overall findings of the test data are shown in Table 4.15. All samples reinforced with polypropylene columns exhibited a decrease in the effective friction angle and an increase in the apparent cohesion as compared to the control sample. This was due to the fact that compared to controlled samples, polypropylene columns have a higher apparent cohesiveness and a lower effective friction angle. Additionally, the findings demonstrated that the height penetration ratio decreased to 0.8 and the apparent cohesiveness increased.

Table 4.15 Summary of results from consolidated undrained triaxial test for shear stress at failure and effective normal stress

Formation	Cell Pressure	Back Pressure	Effective Confining Pressure	Apparent Cohesion, c' (kPa)	Effective Friction Angle, ϕ'	Shear Stress at Failure	Effective Normal Stress at Failure
C	100	50	50	1.37	32.30	61.43	109.43
	200	100	100			122.85	234.25
	400	200	200			195.55	372.95
S1060	100	50	50	4.96	31.17	74.35	136.45
	200	100	100			135.66	252.15
	400	200	200			214.62	407.22
S1080	100	50	50	7.32	30.24	82.04	151.14
	200	100	100			133.34	250.94
	400	200	200			217.62	420.02
S10100	100	50	50	5.72	31.00	79.49	145.04
	200	100	100			122.31	228.81
	400	200	200			208.77	395.50
S1660	100	50	50	9.86	29.98	71.45	130.45
	200	100	100			138.38	251.48
	400	200	200			218.86	423.98
S1680	100	50	50	14.40	29.60	79.75	144.95
	200	100	100			140.68	254.68
	400	200	200			225.95	440.15
S16100	100	50	50	6.73	31.20	76.20	140.10
	200	100	100			136.20	244.90
	400	200	200			222.88	421.33
G1060	100	50	50	6.10	30.60	71.38	130.48
	200	100	100			120.81	226.31
	400	200	200			217.90	417.84
G1080	100	50	50	13.85	30.80	77.21	129.82
	200	100	100			144.34	240.25
	400	200	200			227.28	419.90

Table 4.15 Continued

Formation	Cell Pressure	Back Pressure	Effective Confining Pressure	Apparent Cohesion, c' (kPa)	Effective Friction Angle, ϕ'	Shear Stress at Failure	Effective Normal Stress at Failure
	100	50	50			76.90	138.70
G10100	200	100	100	7.66	29.70	115.59	222.19
	400	200	200			183.50	369.90
	100	50	50			72.80	132.10
G1660	200	100	100	4.10	30.90	134.68	248.68
	400	200	200			218.50	422.75
	100	50	50			71.82	125.32
G1680	200	100	100	5.90	31.90	134.45	246.45
	400	200	200			238.77	441.30
	100	50	50			53.78	100.67
G16100	200	100	100	2.82	32.00	116.10	210.00
	400	200	200			226.13	423.51

This study investigated the efficacy of Mohr-Coulomb failure envelopes in relation to kaolin samples that had been reinforced with both single and grouped polypropylene columns. The findings indicated that the validity of these envelopes remained for all combinations of area replacement ratio and column penetration ratio that were examined. There were significant similarities observed in the failure envelopes of the clay specimens that had been reinforced with polypropylene columns and the control specimens. Therefore, the incorporation of polypropylene columns exhibiting a friction angle of 32.30° and an apparent cohesion of 1.37 kPa within clay layers possessing comparable characteristics to those examined in this investigation may not yield favourable outcomes in terms of enhancing the effective shear strength parameters of the reinforced clay in relation to bearing capacity concerns under long-term circumstances.

The data presented in Figure 4.49 show the shear stress failure versus effective normal stress failure envelopes for single and group column-reinforced kaolin specimens. The nearly identical plots raised concerns regarding the potential insensitivity of the test setup or the actual behavior of the columns

The testing equipment was carefully calibrated and verified to ensure precision and accuracy. Calibration involved adjusting the equipment using known reference materials, while verification included consistency checks with multiple tests under identical conditions. Control tests without columnar inclusions also showed distinct behaviors, confirming the sensitivity of the test setup.

The similar failure envelopes for single and group columns suggest that the reinforcement provided by the columns is effective and consistent across different scenarios. The homogeneity of the kaolin specimens and the consistent installation techniques likely contributed to the similar shear stress versus effective normal stress behavior. These findings indicate that both single and group columnar inclusions effectively enhance the shear strength of the soil, reflecting a true improvement rather than an insensitivity of the test setup.

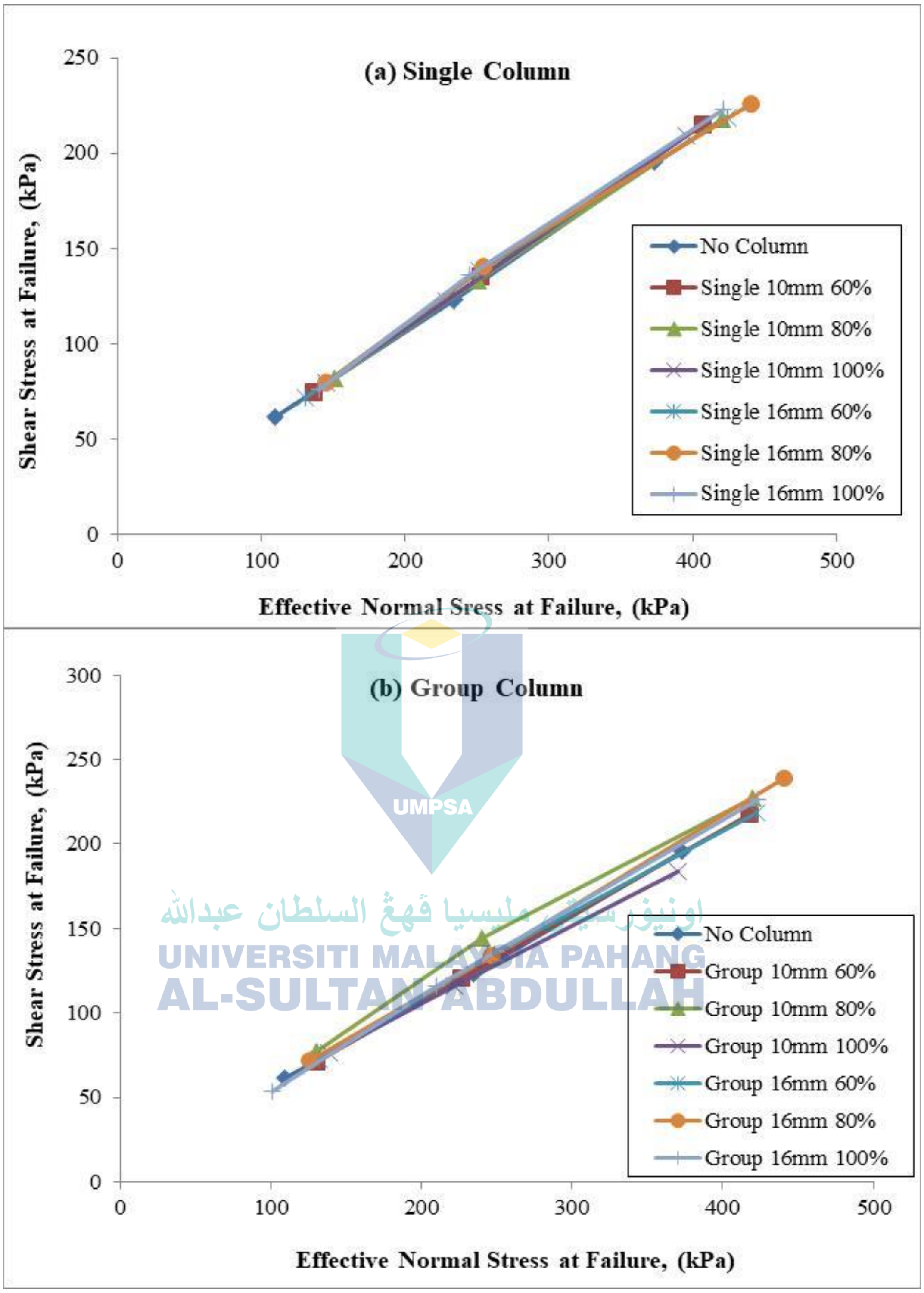

Figure 4.49 Shear stress failure vs. effective normal stress failure envelopes for single and group column-reinforced kaolin specimens

The results showed that installing polypropylene columns in soft clay specimens did not significantly alter the effective friction angle (Figure 4.50). The effective friction angles had somewhat decreased, except for one sample. The apparent cohesiveness of the reinforced sample increased with decreasing friction angle at a height penetration ratio of 0.8, but then dropped. The data shown in Figure 4.51 demonstrates that samples reinforced with fully penetrated columns had a comparatively smaller increase in apparent cohesiveness compared to samples reinforced with partially penetrating columns. This observation became particularly apparent when the height penetration ratio was 0.8 for both single and group columns.

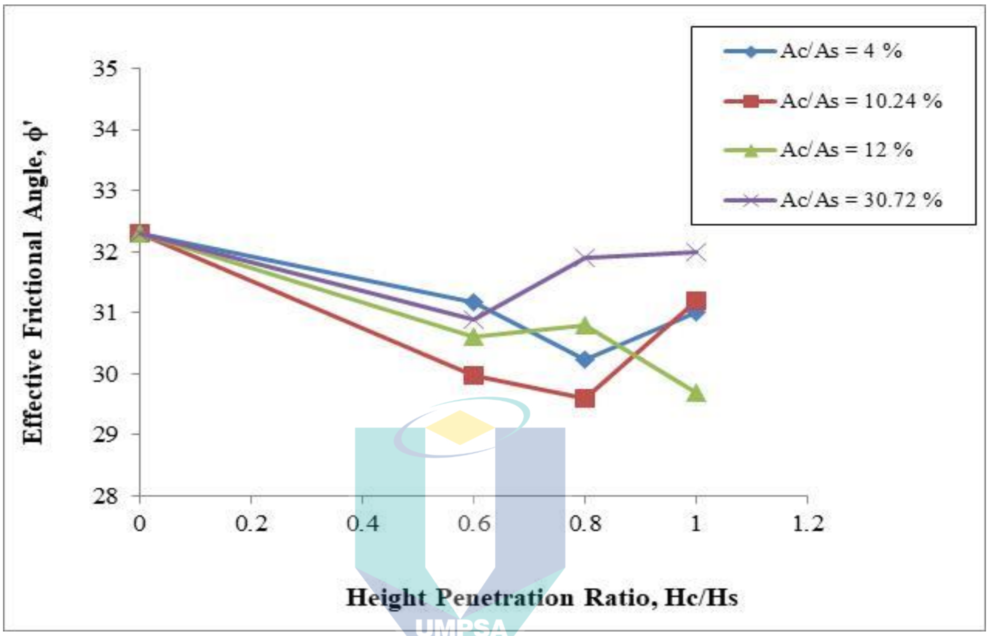

Figure 4.50 Height penetration ratio in relation to effective frictional angle

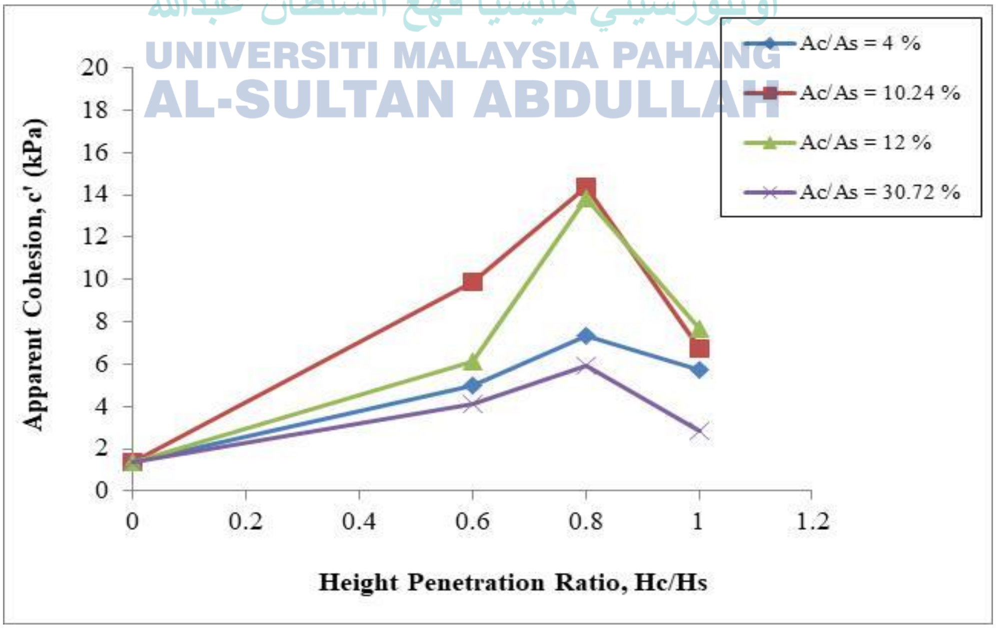

Figure 4.51 Height penetration ratio in relation to apparent cohesion

For single columns, the completely penetrated column exhibited an apparent cohesion value of 5.72 kPa. Conversely, samples including partially penetrated columns with a diameter of 10 mm had apparent cohesion values of 4.96 kPa and 7.32 kPa for height penetration ratios of 0.6 and 0.8, respectively. On the other hand, for completely penetrated columns with a diameter of 16 mm, the apparent cohesion was 6.73 kPa, and for partially penetrated columns, they were 14.40 kPa and 9.86 kPa with ratios of 0.8 and 0.6 for height penetration ratio, respectively. In the case of samples reinforced with group polypropylene columns, the measured cohesion values were 6.10 kPa and 13.85 kPa for partially penetrated columns with a diameter of 10 mm and height penetration ratios of 0.6 and 0.8, respectively. On the other hand, the cohesion value for completely penetrated columns was determined to be 7.66 kPa. The observed cohesion values for different types of columns were as follows: a partially penetrating column with a height penetration ratio of 0.6 had a cohesion of 4.10 kPa, a partially penetrated column with a height penetration ratio of 0.8 had a cohesion of 5.90 kPa, and a completely penetrating column with a diameter of 16 mm had a cohesion of 2.82 kPa.

In single columns, the partially penetrating columns with a 10 mm diameter had frictional angles of 31.17 and 30.24 for height penetration ratios of 0.6 and 0.8, respectively, while the completely penetrated column had a frictional angle of 31.00. In the event that individual 16 mm diameter columns were completely penetrated, the frictional angle was 31.20 kPa; for partially penetrated columns with 0.6 and 0.8 height penetration ratios, respectively, they were 29.98 and 29.60. In samples reinforced with group columns, the frictional angle for completely penetrated columns was equal to 29.70 kPa, while for partially penetrated columns with a diameter of 10 mm, they were equivalent to 30.60 and 30.80 for height penetration ratios of 0.6 and 0.8, respectively. The frictional angle for the 16-mm diameter column with a partially penetrated height penetration ratio of 0.6, 0.8, and 31.90 kPa, respectively, was 30.90 kPa; for a completely penetrated column, it was 32.00.

In the case of single columns, it was shown that samples reinforced with larger diameter columns exhibited a greater rise in c' values compared to samples reinforced with smaller diameter columns. This shows that the greater strength of the specimens was mostly influenced by the area ratio. Columns with a diameter of 10 mm had a greater c' than single columns with the same diameter because group columns have greater surface ratio. This is because the specimens' capacity to tolerate stress was significantly improved by the group column's area and volume of polypropylene columns, which replaced the soil, being three times larger than those of the single column. Furthermore, when pore pressure is released into polypropylene columns, the water content of clay specimens might decrease, increasing the specimens' shear strength.

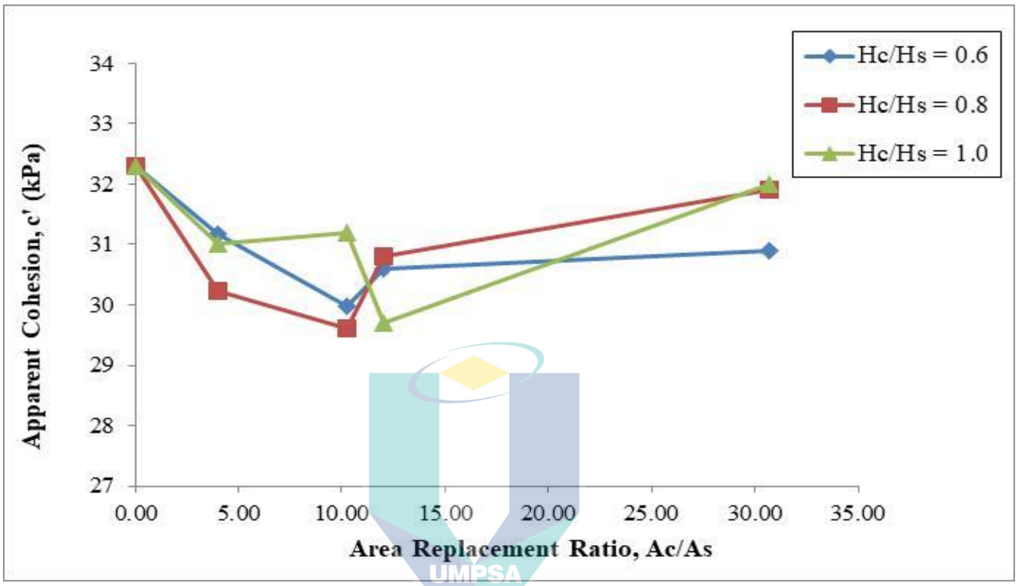

Figure 4.52 Area replacement ratio relatio to apparent cohesion

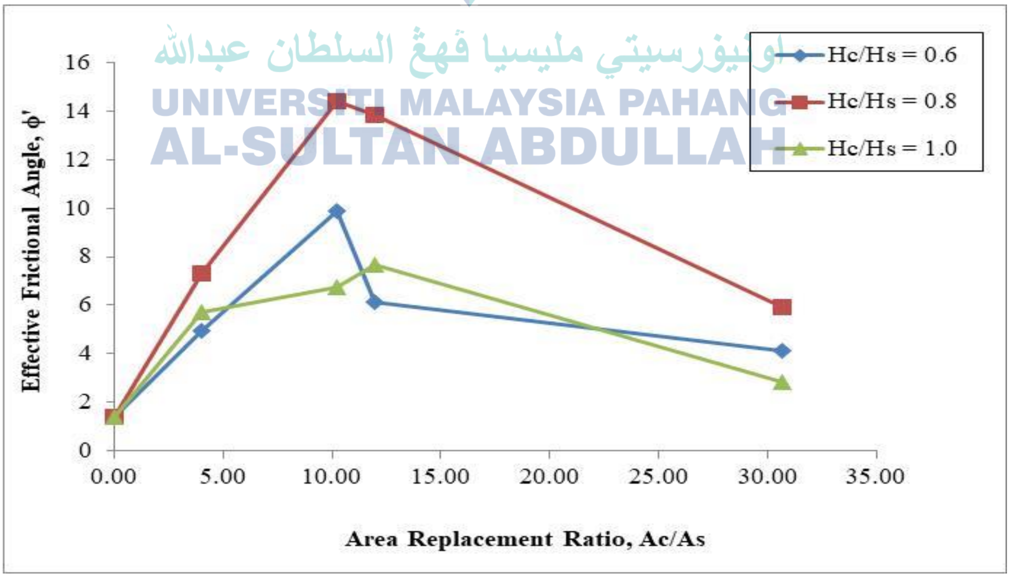

Figure 4.53 Area replacement ratio relation to effective frictional angle

As Figure 4.52 illustrates, the completely penetrating columns with the highest area replacement ratio of 30.72 (16 mm diameter group column) did not exhibit the greatest improvement among all the samples. The samples reinforced with a column that had a height penetration ratio of 0.8 had the highest apparent cohesion value. This might be because a significant number of the clay specimens' fully penetrating columns had been drilled out. This caused the specimens' structural integrity to be disturbed, despite the fact that the clay specimens were extremely delicate and prone to failure even before the polypropylene columns were placed. Consequently, the apparent cohesion for an area replacement ratio of 30.72 was significantly lower than what one might expect for a higher ratio. With the exception of the completely penetrating columns at the maximum area ratio, the effective friction angle typically decreased as the area ratio increased (Figure 4.53).

The findings of the study suggest that the enhancement observed in completely penetrating columns appeared to be more significant when compared to partially penetrating columns, regardless of whether they are arranged singly or in groups. This observation holds true when considering a height penetration ratio of 0.8. Compared to completely penetrated columns, which have both ends of the polypropylene column exposed to the load, this results in only one end of the column being instantly exposed to the load due to the other end being partially covered by clay. The interaction of the column's polypropylene and clay may be the cause of its superior enhancement. This may be the result of the polypropylene column's tendency to punch inside the remaining dirt rather than crushing it and failing, which is the opposite of what would be predicted for a fully penetrating column. Because the column was longer, there was a significantly greater chance that it may have failed earlier.

Sivakumar et al. (2011) stated that increasing the column length over the "critical column length" has no effect on the composite ground's capacity to carry loads. This also suggests that the ability of the columns to carry loads may not be as significant for settlement design criteria as the length of the columns beyond the optimal value. As with axially compressible piles, Baziar et al. (2015) stated that physical simulations have shown that once a certain length is achieved, any further load is dispersed through shaft friction and cannot reach the base of the pile or stone column. The comparison between a fundamental pile comparison and the mobilisation of shear strength inside the pile/column differs due to the predominant impact of the radial constraint exerted by the surrounding soil.

CHAPTER 5

CRITICAL STATE ANALYSIS

5.1 Introduction

This chapter presents a foundational framework utilising the Cambridge stress field for the purpose of analysing the mechanical strength of reinforced kaolin clay. The framework can be described as a theoretical model that draws inspiration from the critical state model of soil mechanics, as proposed by Schofield and Wroth in 1968. The corresponding graphs were produced using the results of isotropically typically consolidated undrained triaxial testing. Additionally, a stress path analysis of the corresponding specimens was done. At the University of Cambridge, Roscoe et al. (1958) established the Cambridge stress routes that were used in this investigation (Head, 1985). Plotting of the stress routes was done in terms of the invariants q (deviator stress) and p' (mean normal effective stress), where q and p' were defined using the Cambridge stress field previously provided in Equations 2.5 and 2.6. The formation of pore pressure during shear from the initial condition (after consolidation) was represented by the mean normal effective stress, p', while the undrained shear strength, Su, in which Su = q/2, was represented by the magnitude of the deviator stress at a critical state. Rather than using a mathematical formulation, the critical state model (CSM) offers a more general understanding of reinforced soil behaviour. Each and every soil in q: p': v space will eventually fail on a unique failure surface, according to the basic principle of CSM. As a result, the CSM takes into account changes in volume, in contrast to the Mohr-Coulomb failure criterion, which alone defines failure as the attainment of maximum stress obliquity. Failure cannot be guaranteed by the failure stress condition alone, according to CSM; there must also be enough loose soil structure. Thus, the critical void ratio is taken into account by CSM.

5.2 Stresses and Void Ratio at Critical State

The deviator stress and excess pore water pressure plotted against axial strain were used to determine the stress at the critical condition for each batch. Specifically, the point at which the pore water pressure developed and displayed a constant value was determined to be the deviator stress at a critical condition. As previously mentioned in Chapter 2, the void ratio at the critical condition was determined. For this reason, Table 5.1 displays the stresses and void ratio at the critical state. In the same table, all sample particular volumes, v = 1+e, are also displayed.

Table 5.1 Deviator stress, mean normal effective stress, void ratio and specific volume at critical state

Sample	**Effective Confining Pressure σ'3 (kPa)**	**Deviator Stress, q (kPa)**	**Mean Normal Effective Stress, p' (kPa)**	**Void ratio e**	**Specific Volume, v = 1+e**
C	50	122.86	109.43	0.85	1.85
	100	245.70	234.25	0.80	1.80
	200	391.10	372.95	0.73	1.73
S1060	50	148.69	136.45	0.73	1.73
	100	271.31	252.15	0.70	1.70
	200	429.24	407.22	0.67	1.67
S1080	50	164.08	151.14	0.75	1.75
	100	266.67	250.94	0.72	1.72
	200	435.25	420.02	0.70	1.70
S10100	50	158.98	145.04	0.73	1.73
	100	244.62	228.81	0.69	1.69
	200	417.53	395.50	0.66	1.66
S1660	50	142.90	130.45	0.77	1.77
	100	276.75	251.48	0.74	1.74
	200	437.72	423.98	0.71	1.71
S1680	50	159.49	144.95	0.74	1.74
	100	281.36	254.68	0.72	1.72
	200	451.89	440.15	0.69	1.69
S16100	50	152.40	140.10	0.73	1.73
	100	272.40	244.90	0.72	1.72
	200	445.76	421.33	0.70	1.70
G1060	50	142.75	130.48	0.79	1.79
	100	241.62	226.31	0.75	1.75
	200	435.80	417.84	0.72	1.72

Table 5.1 Continued

Sample	Effective Confining Pressure σ'3 (kPa)	Deviator Stress, q (kPa)	Mean Normal Effective Stress, p' (kPa)	Void ratio e	Specific Volume, v = 1+e
G1080	50	154.42	129.82	0.76	1.76
	100	288.68	240.25	0.73	1.73
	200	454.55	419.90	0.71	1.71
G10100	50	143.80	138.70	0.73	1.73
	100	231.18	222.19	0.70	1.70
	200	367.00	369.90	0.69	1.69
G1660	50	145.60	132.10	0.74	1.74
	100	269.35	248.68	0.71	1.71
	200	437.50	422.75	0.69	1.69
G1680	50	143.64	125.32	0.70	1.70
	100	264.90	246.45	0.67	1.67
	200	477.54	441.30	0.65	1.65
G16100	50	107.56	100.67	0.69	1.69
	100	232.20	210.00	0.67	1.67
	200	452.25	423.51	0.66	1.66

To provide a more comprehensive understanding of the effects of polypropylene columns on the enhancement of undrained shear strength and its potential correlation with pore pressure generation during shear, stress paths were examined for tests conducted on all samples reinforced with polypropylene columns using three effective confining pressures (equivalent to the initial mean normal effective stress, p'_o). The effective stress pathways (ESP) for controlled samples and samples reinforced with single and group polypropylene columns are plotted in q: p' space, as depicted in Figure 5.1.

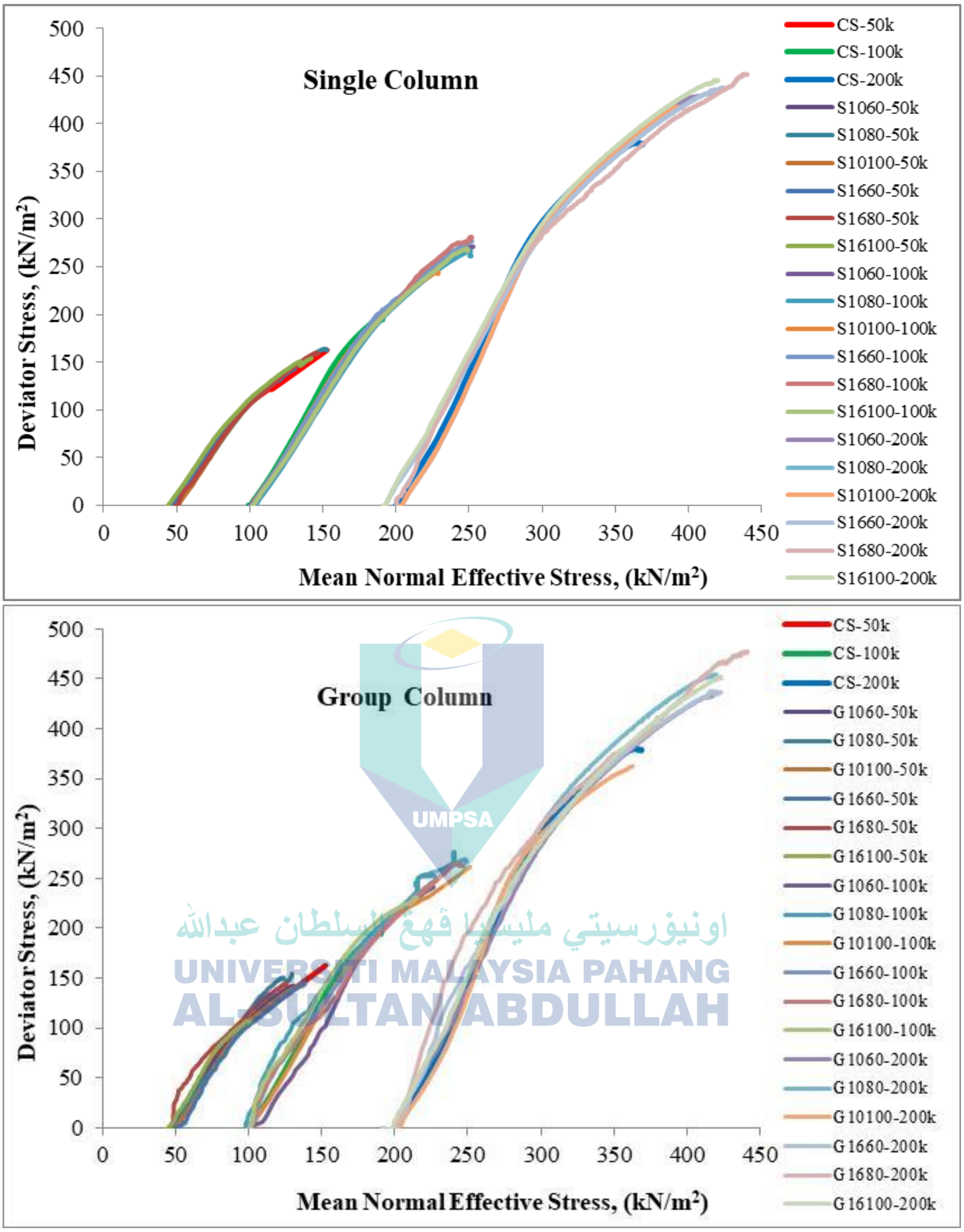

Figure 5.1 Effective stress paths for kaolin clay sample reinforced with single and group polypropylene columns

The figures in Figure 5.1 demonstrate the substantial correlation between the excess pore pressure in a critical condition (failure) and the undrained shear strength of the clay polypropylene column composite. An example of this may be seen in the stress paths shifting to the right, which indicates that for a given initial stress state, the pore pressure at the critical state decreases and becomes larger than the undrained shear strength value.

5.3 Controlled Sample

Figure 5.2 (a) displays the stress pathways for the controlled samples. Plotted graphs for specimens that were isotropically normally consolidated to effective confining pressures of 50 kPa, 100 kPa, and 200 kPa illustrate the Total Stress Paths (TSP) and Effective Stress Paths (ESP). For samples reinforced with polypropylene columns, the ESP curves serve as a baseline so that any changes resulting from the installation of the columns can be identified.

The critical state line (CSL) in the q – p' plane was determined by analysing the results of experiments conducted on isotropically consolidated samples at three different confining pressures. The best fitting line, based on Equation 2.1, was determined to be q = 1.30p'. The value of the critical state parameter, denoted as M, was determined to be 1.30. Therefore, by utilising Equation 2.2, the friction angle at the critical state, denoted as ϕ_c, was determined to be around 32.30° for a specimen consisting only of kaolin clay. The obtained M value was higher than the result found by other researchers on kaolin clay, as reported by Marto (1996). The difference might have been due to the different stress histories of the samples, resulting in different initial void ratios. The critical state parameter M or ϕ'_c therefore varied between those samples.

Figure 5.2 (b) shows the CSL of controlled sample in e : p' space. In this plot, the graph forms a curve. By replotting in v – ln p' plane, the curve became a straight line with the slope -λ and the line intersected the v axis at Γ, as shown in Figure 5.3. From the figure, the equation of the CSL was obtained as:

$$v = 2.302 - 0.093 \ln p' \quad (5.1)$$

With the coefficient of determination, R^2 = 0.9993. Although there were only three points, the fitting was excellent as the R^2 was close to 1.0.

Based on Equations 2.3 and 5.1, the critical state parameters, λ was obtained as 0.093 and Γ as 2.302. Compared to the results for kaolin clay shown in Table 2.4, the results obtained from this research were slightly smaller for both λ and Γ. The stress path, as depicted in Figure 5.2(a), is characterised by a straight line with a slope of 1H: 3V, starting at p'_o and ascending to the right. When extra pore water pressure increased, the ESP curved toward the critical state line after starting at p_o and moved up vertically or slightly to the right. The ESP eventually stopped at the critical state line, to the left of TSP. This shows that positive excess pore water pressure was developed during shearing and when critical state occurred. The behaviour of these stress pathways is comparable to that of normally consolidated soil, according to reports from Marto (1996), Whitlow (2001), and Budhu (2007).

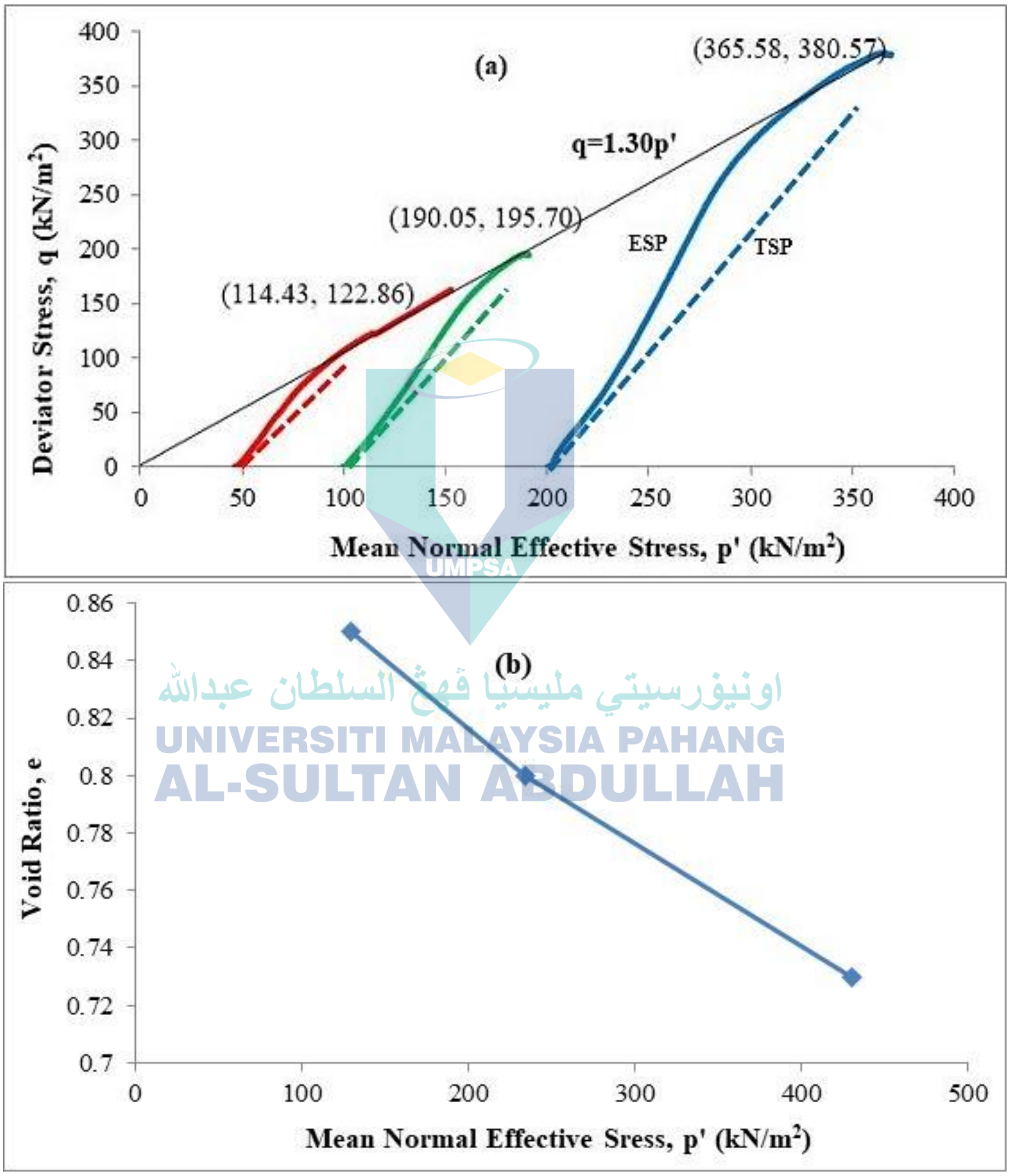

Figure 5.2 (a) Stress paths and CSL in q : p' space and (b) CSL in e : p' space for controlled sample

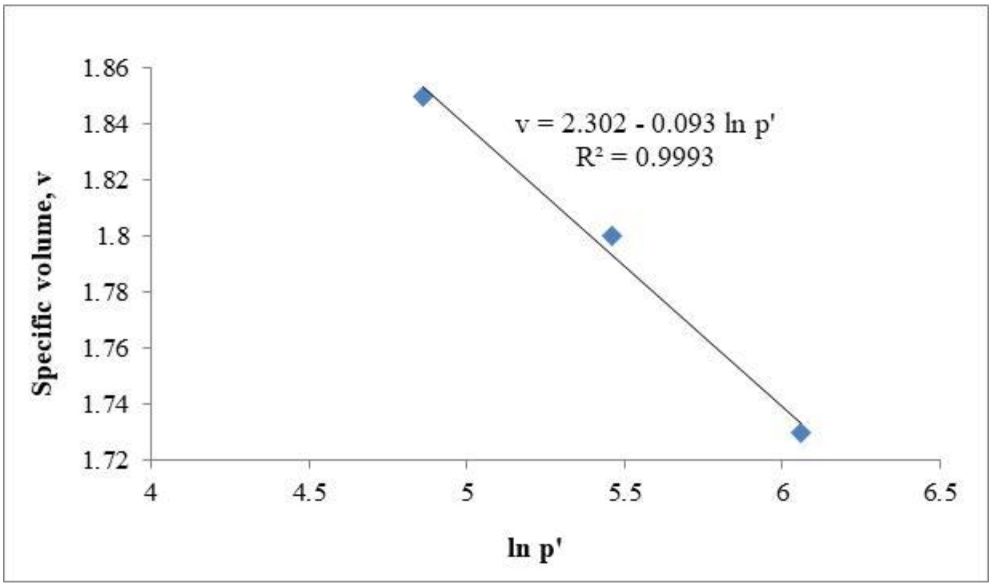

Figure 5.3 Critical state line in v : ln p' space for controlled sample

5.4 Samples Reinforced with Polypropylene Column

5.4.1 Single Column

Figure 5.4 shows the stress pathways for samples reinforced with single columns, which show that effective confining pressures, or initially mean normal effective stress, p'_o, have a significant impact on the degree to which the undrained shear strength is improved at the critical state. For samples with p'_o of 50 kPa and 100 kPa, the stress paths for samples reinforced with polypropylene columns shifted to the right of the stress paths of the respective controlled samples. This finding suggests that the undrained shear strength of the sample reinforced with polypropylene columns was greater. However, the scenario is different for samples with p'_o of 200 kPa, where the stress paths for samples reinforced with polypropylene columns tended to shift slightly to the left of the stress path of the controlled samples. This indicates that the undrained shear strength value achieved in the critical state for the reinforced samples was slightly lower compared to the control samples.

This situation occurred possibly due to the combination of the softness of kaolin specimens and the brittleness of polypropylene columns. There is a possibility that clogging occurred since the specimens could not sustain the high confining pressure, which resulted in the specimens being pressurised and the polypropylene being crushed since it could not sustain the high-pressure condition. The crushed polypropylene turned into fine particles, and this did not help the pore water pressure to dissipate effectively from the specimens during consolidation, thus, it could not be helped to improve the undrained shear strength of the samples.

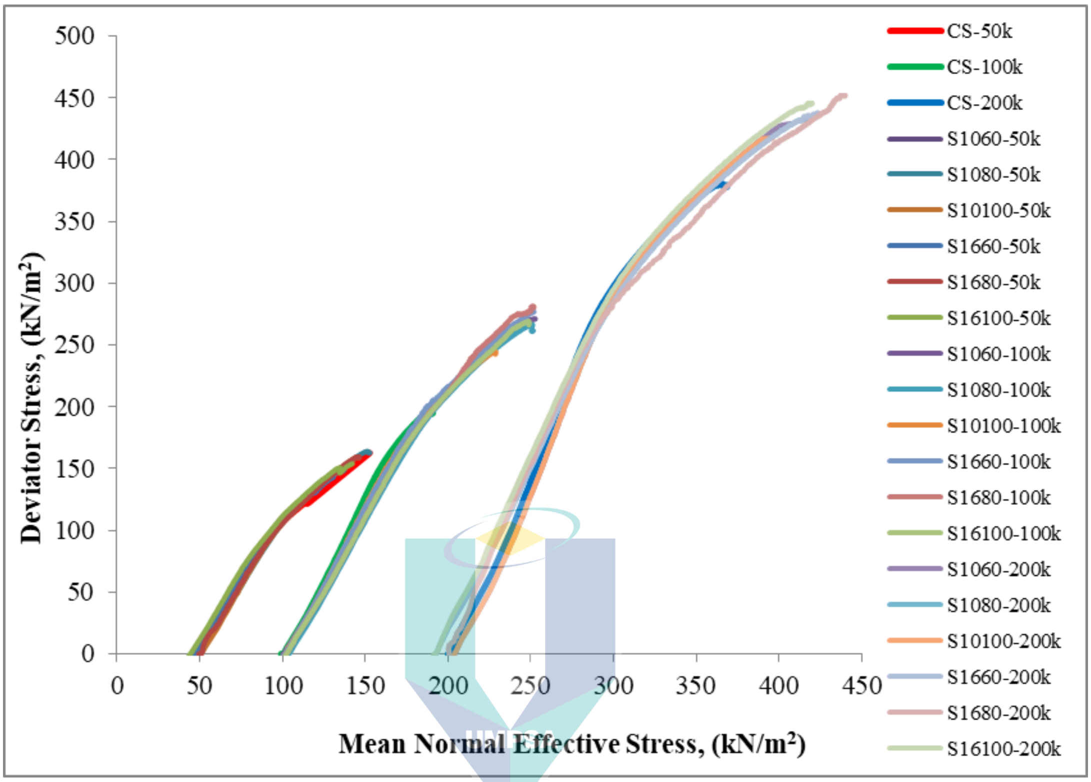

Figure 5.4 Effective stress paths for clay samples reinforced with single polypropylene columns

5.4.1.1 Height Penetrating Ratio, Hc/Hs = 0.6

Figure 5.5 (a) illustrates the TSP and ESP for the sample that was 60% penetrating in height and reinforced with a single 10 mm diameter polypropylene column. From the CSL, the M value obtained from the figure was 1.25, hence the ϕ_c was 31.17°. Meanwhile, Figure 5.5 (b) shows CSL for the same sample in e: p' space. The projection of the critical state line (CSL) was subsequently replotted on a v – ln p' plane, as depicted in picture 5.6. By analysing the picture, the equation representing the critical state line was determined:

$$v = 2.001 - 0.055 \ln p' \qquad 5.2$$

With the coefficient of determination, $R^2 = 0.9953$. The critical state parameters, λ (slope of the line) was obtained as 0.055 and Γ as 2.001.

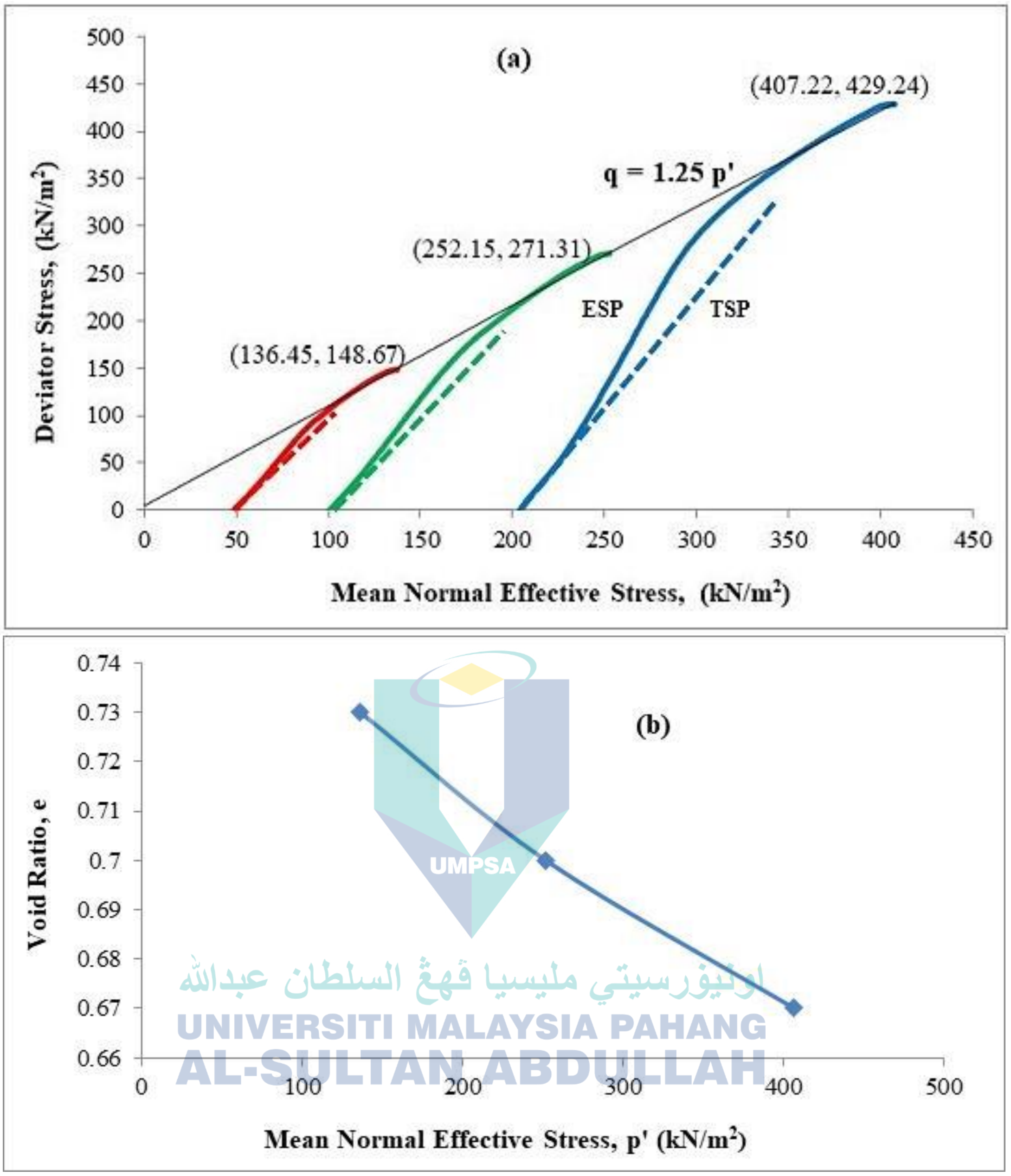

Figure 5.5 (a) Critical state line and stress pathways in q: p' space; (b) Critical state line in e: p' space for a clay sample reinforced at 60% penetration using a 10 mm-diameter single polypropylene column

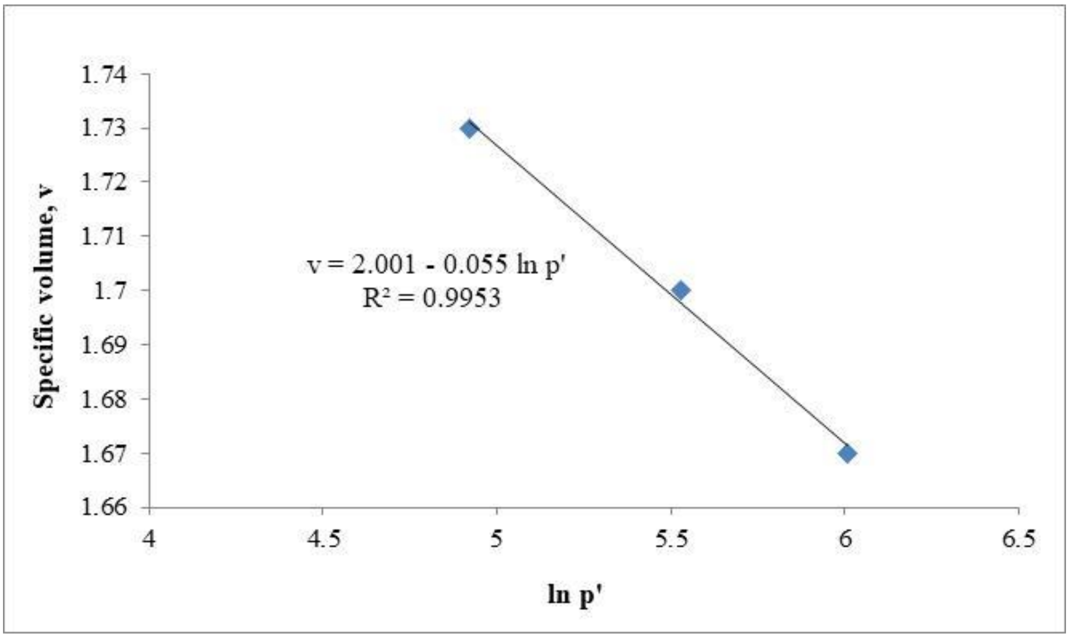

Figure 5.6 Critical state line in v: ln p' space for kaolin clay reinforced with a single polypropylene column with a diameter of 10 mm and 60% penetration

Figure 5.7 (a) illustrates the stress pathways and the critical state line (CSL) for the specimen that had been reinforced with a single polypropylene column of 16 mm diameter, with a height penetration ratio of 60%, in the q: p' space. The M value obtained from the figure was 1.20, and therefore, the ϕ_c was 29.98°. Figure 5.7 (b) displays the CSL of the same sample in e: p' space, while Figure 5.8 displays the projection of the CSL replotted on a v - ln p' plane. From the figure, the equation of the CSL was found to be:

$$v = 2.018 - 0.051 \ln p' \tag{5.3}$$

With the coefficient of determination, $R^2 = 0.9954$. The critical state parameters, λ (slope of the line) was obtained as 0.051 and Γ as 2.018.

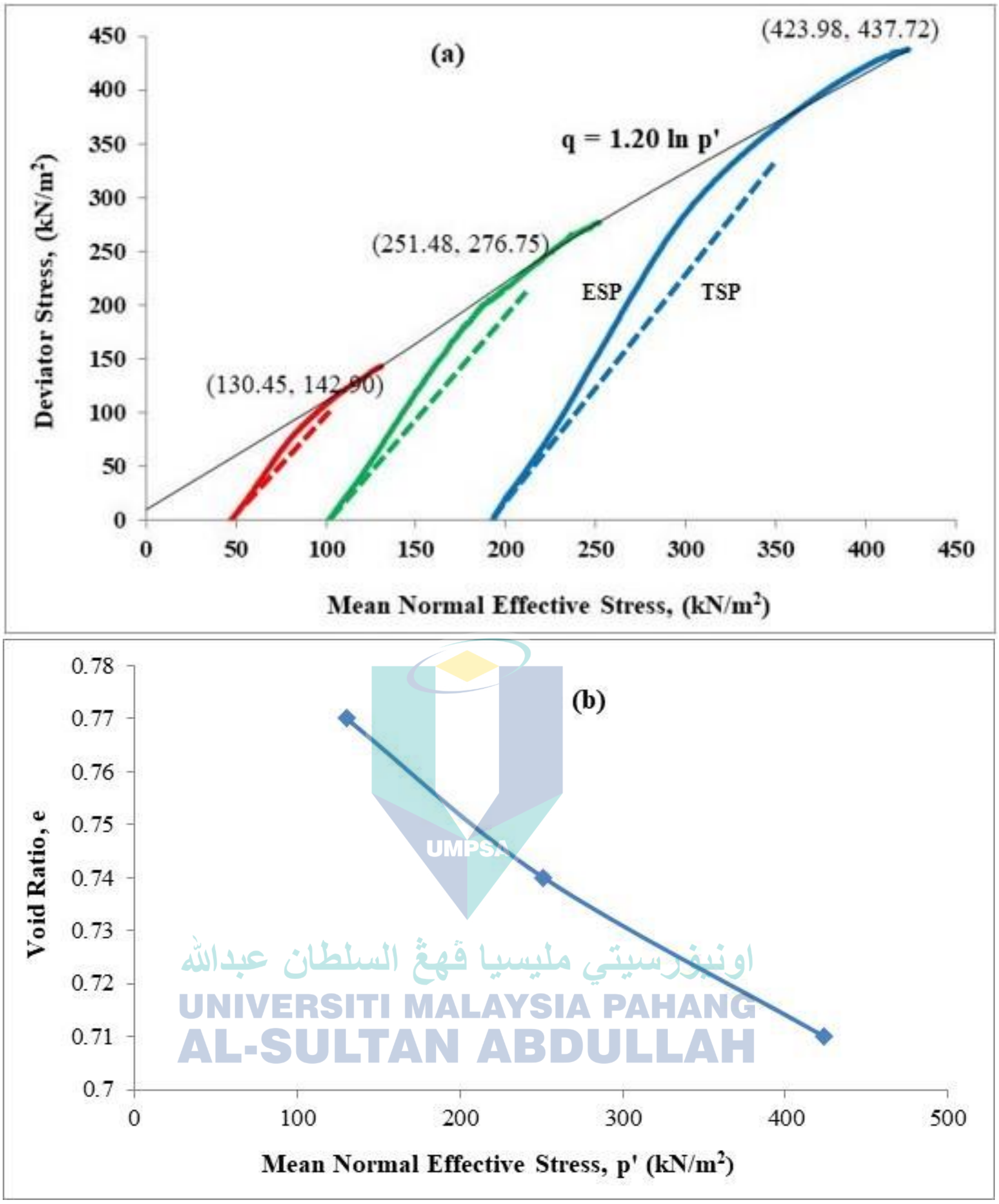

Figure 5.7 (a) Critical state line and stress pathways in q: p' space; (b) Critical state line in e: p' space for a clay sample reinforced at 60% penetration using a 16 mm-diameter single polypropylene column

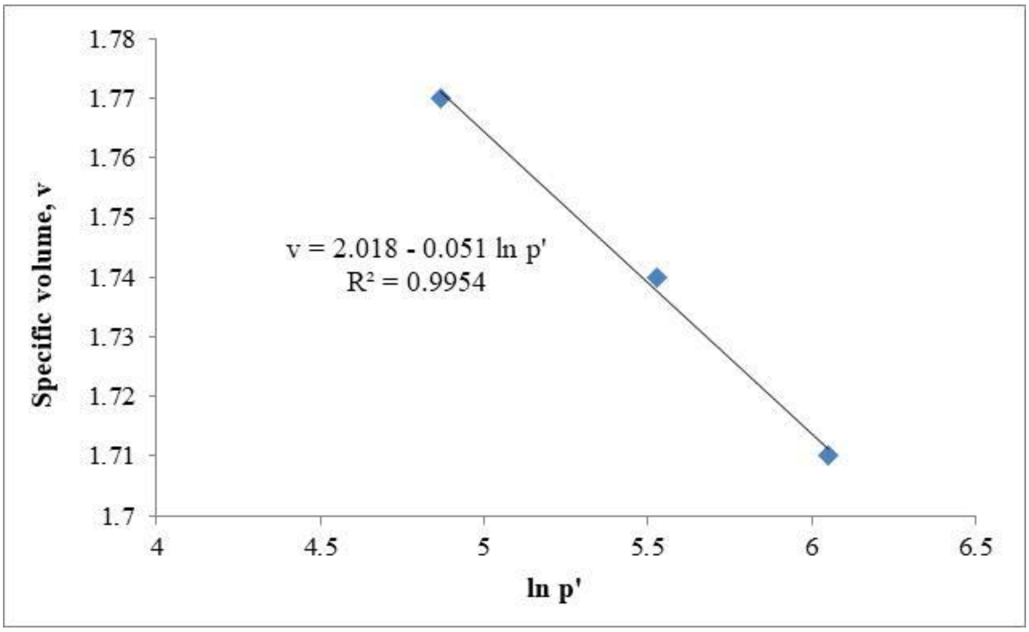

Figure 5.8 Critical state line in v: ln p' space for kaolin clay reinforced with a single polypropylene column with a diameter of 16 mm and 60% penetration

5.4.1.2 Height Penetrating Ratio, Hc/Hs = 0.8

Figure 5.9 (a) illustrates the TSP and ESP of the specimen that had been reinforced with a single polypropylene column of 10 mm in diameter. The column was installed to a height penetration ratio of 80%. From the CSL, the M value obtained from the figure was 1.21, and hence the ϕ_c was 30.24°. Meanwhile, Figure 5.9 (b) shows the CSL for the same sample in e: p' space. The projection of CSL was then replotted on a *v* – ln p' plane (Figure 5.10), and from the figure, the equation of the critical state line was found to be:

$$v = 1.994 - 0.049 \ln p' \qquad 5.4$$

With the coefficient of determination, $R^2 = 0.9868$. The critical state parameters, λ (slope of the line) was obtained as 0.049 and Γ as 1.994.

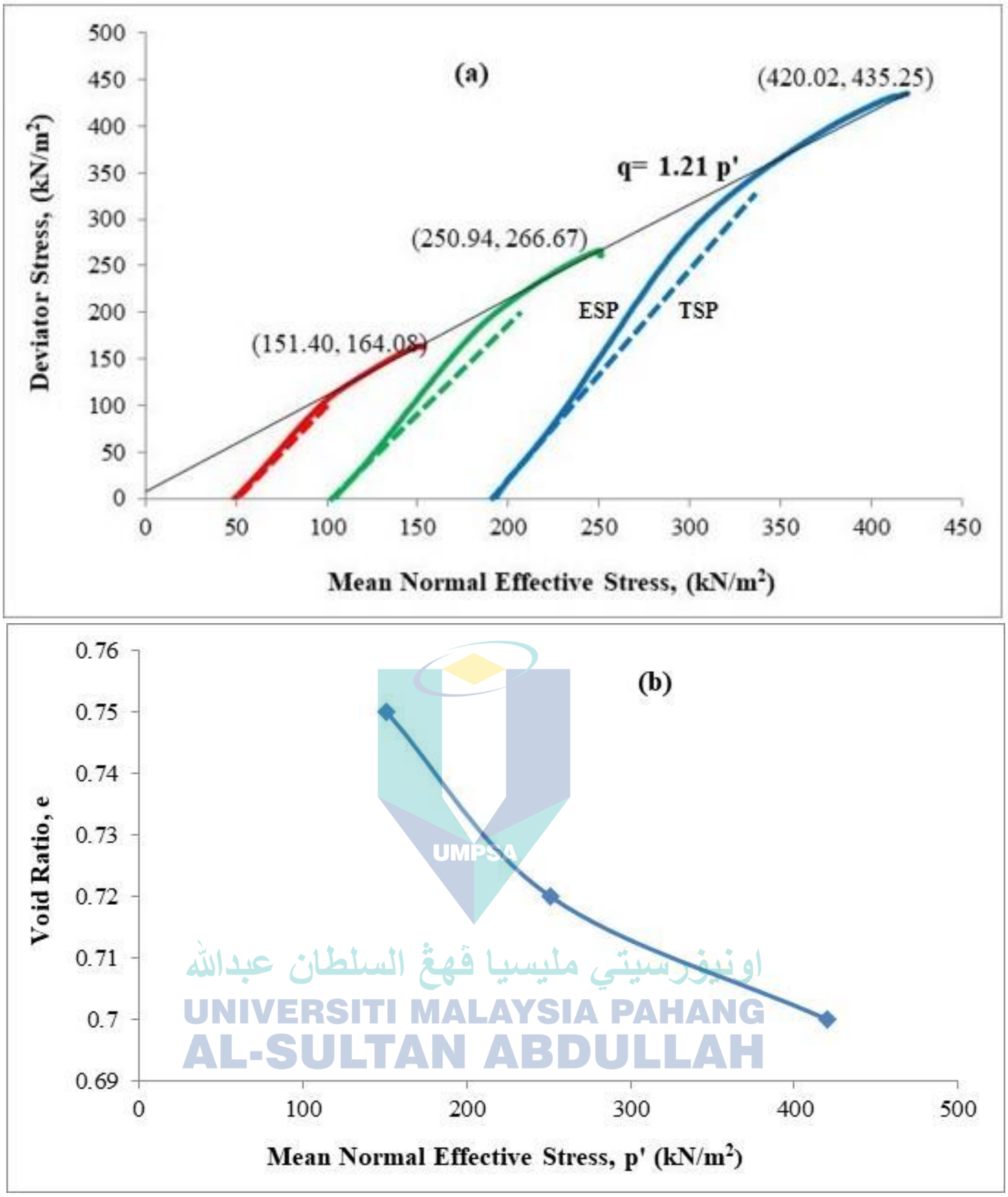

Figure 5.9 (a) Critical state line and stress pathways in q: p' space; (b) Critical state line in e: p' space for a clay sample reinforced at 80% penetration using a 10 mm-diameter single polypropylene column

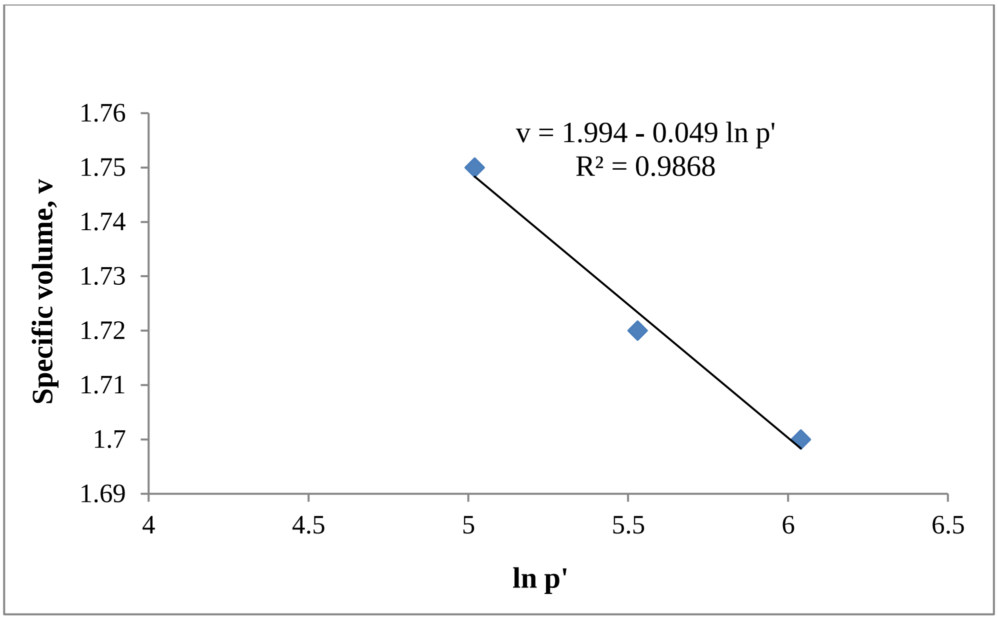

Figure 5.10 Critical state line in v: ln p' space for kaolin clay reinforced with a single polypropylene column with a diameter of 10 mm and 80% penetration

Figure 5.11 (a) illustrates the CSL and stress pathways for the sample reinforced with a single 16 mm diameter polypropylene column at a height penetration ratio of 80% in q: p' space. The M value obtained from the figure was 1.18, and therefore the ϕ_c was 29.60°. Figure 5.11 (b) shows the CSL of the same sample in e : p' space, and the projection of the CSL is illustrated on a v – ln p' plane in Figure 5.12. Based on the provided figure, the equation representing the CSL can be determined as:

$$v = 1.994 - 0.049 \ln p' \quad (5.5)$$

With the coefficient of determination, $R^2 = 0.9868$. The critical state parameters, λ (slope of the line) was obtained as 0.049 and Γ as 1.994.

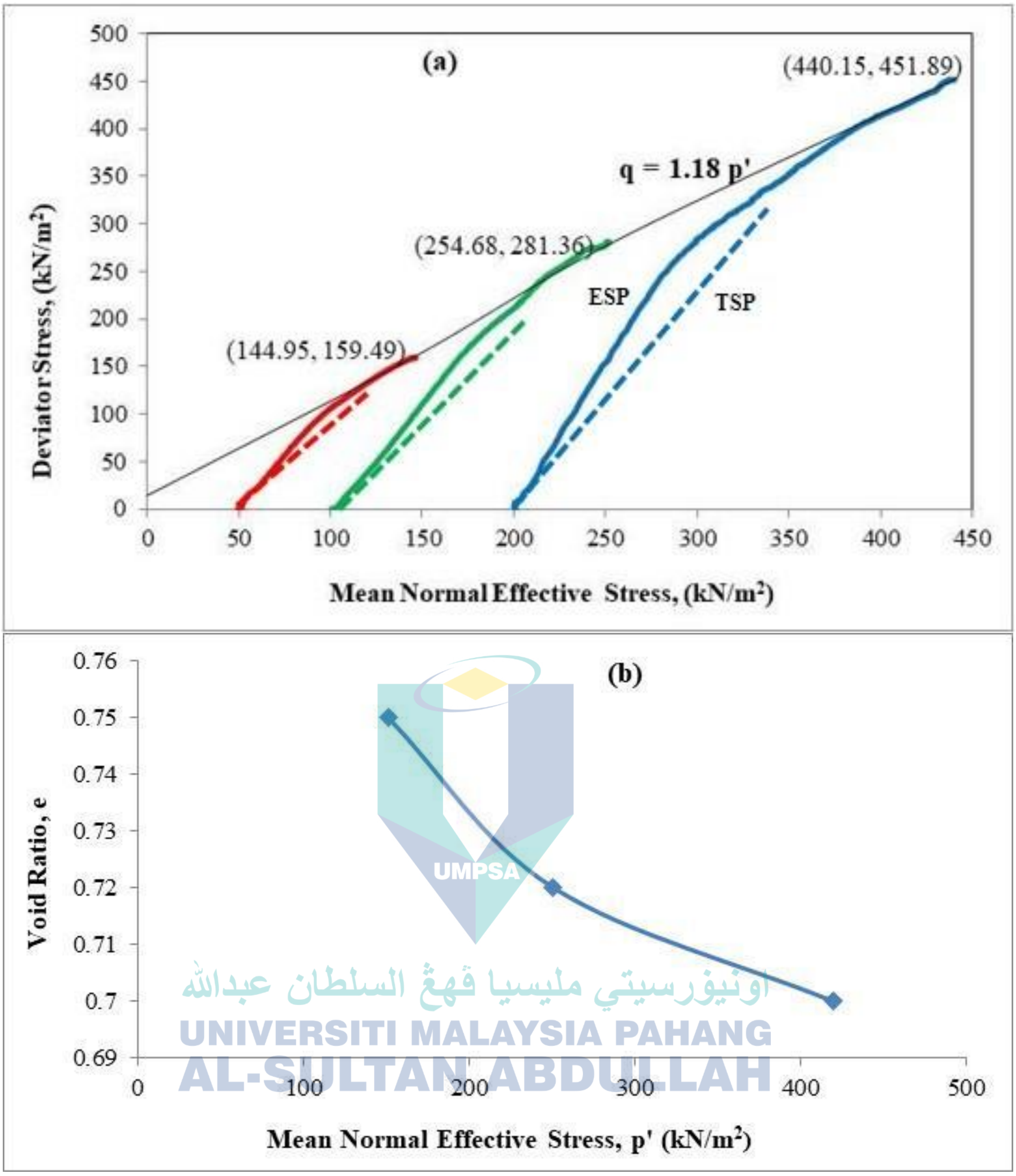

Figure 5.11 (a) Critical state line and stress paths in q : p' space; (b) Critical stale line in e : p' space for a clay sample reinforced at 80% penetration with a single polypropylene column of 16 mm in diameter

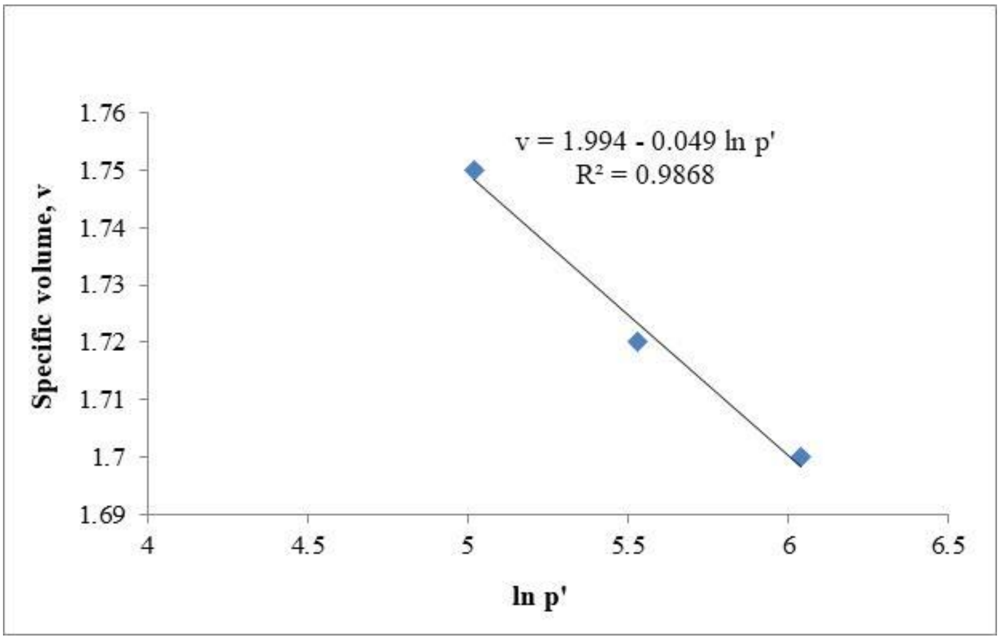

Figure 5.12 Critical state line in v: ln p' space for kaolin clay reinforced with a single polypropylene column with a diameter of 16 mm and 80% penetration

5.4.1.3 Height Penetrating Ratio, Hc/Hs = 1.0

In Figure 5.13 (a), the TSP and ESP are depicted for a specimen that had been reinforced with a single polypropylene column measuring 10 mm in diameter. The column was installed to a height penetration ratio of 100%. From the CSL, the M value obtained from the figure was 1.24, and hence the ϕ_c was 31.0°. Meanwhile, Figure 5.13 (b) shows CSL for the same sample in e: p' space. Following that, the CSL projection was replotted on a v-ln p' plane (Figure 5.14), from which the CSL equation can be obtained as:

$$v = 2.073 - 0.069 \ln p' \quad 5.6$$

With the coefficient of determination, $R^2 = 0.9805$. The critical state parameters, λ (slope of the line) was obtained as 0.069 and Γ as 2.073.

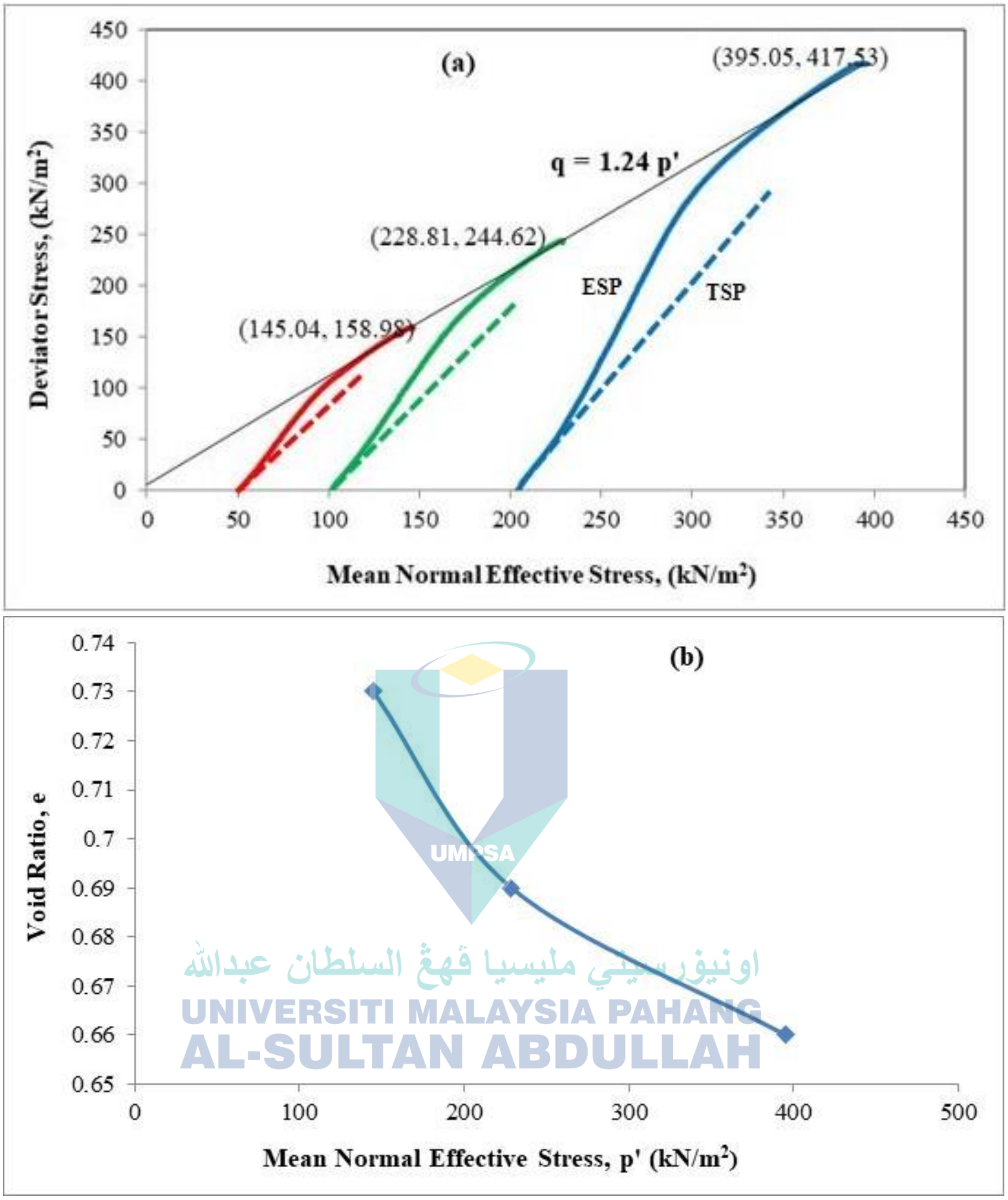

Figure 5.13 (a) Critical state line and stress pathways in q: p' space; (b) Critical state line in e: p' space for a clay sample reinforced at 100% penetration using a 10 mm-diameter single polypropylene column

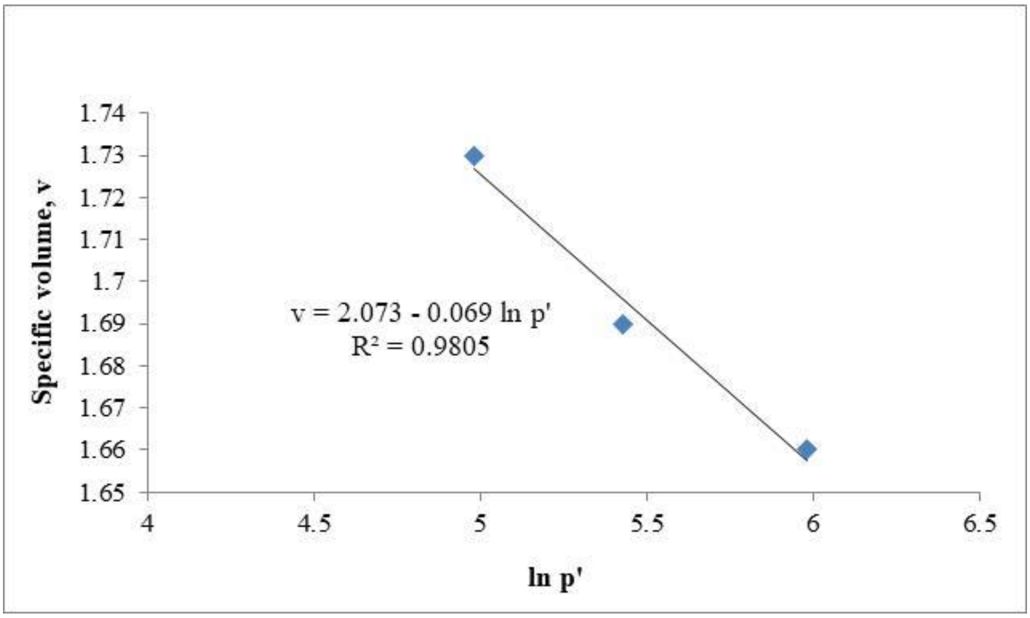

Figure 5.14 Critical state line in v: ln p' space for kaolin clay reinforced with a single polypropylene column with a diameter of 10 mm and 100% penetration

Figure 5.15 (a) illustrates the stress pathways and the CSL for the specimen that had been reinforced with a single polypropylene column of 16 mm diameter, with a height penetration ratio of 100%, in the q: p' space. The M value obtained from the figure was 1.25, and therefore the ϕ_c was 31.20°. Figure 5.15 (b) shows the CSL of the same sample in e : p' space, and Figure 5.16 shows the projection of the CSL replotted on a v – ln p' plane. From the figure, the equation of the CSL was found to be:

$$v = 1.918 - 0.037 \ln p' \tag{5.7}$$

With the coefficient of determination, R^2 = 9999. Although there were only three points, the fitting was excellent, as the R^2 was close to 1.0. The critical state parameters, λ (slope of the line) were obtained as 0.037 and Γ as 1.918.

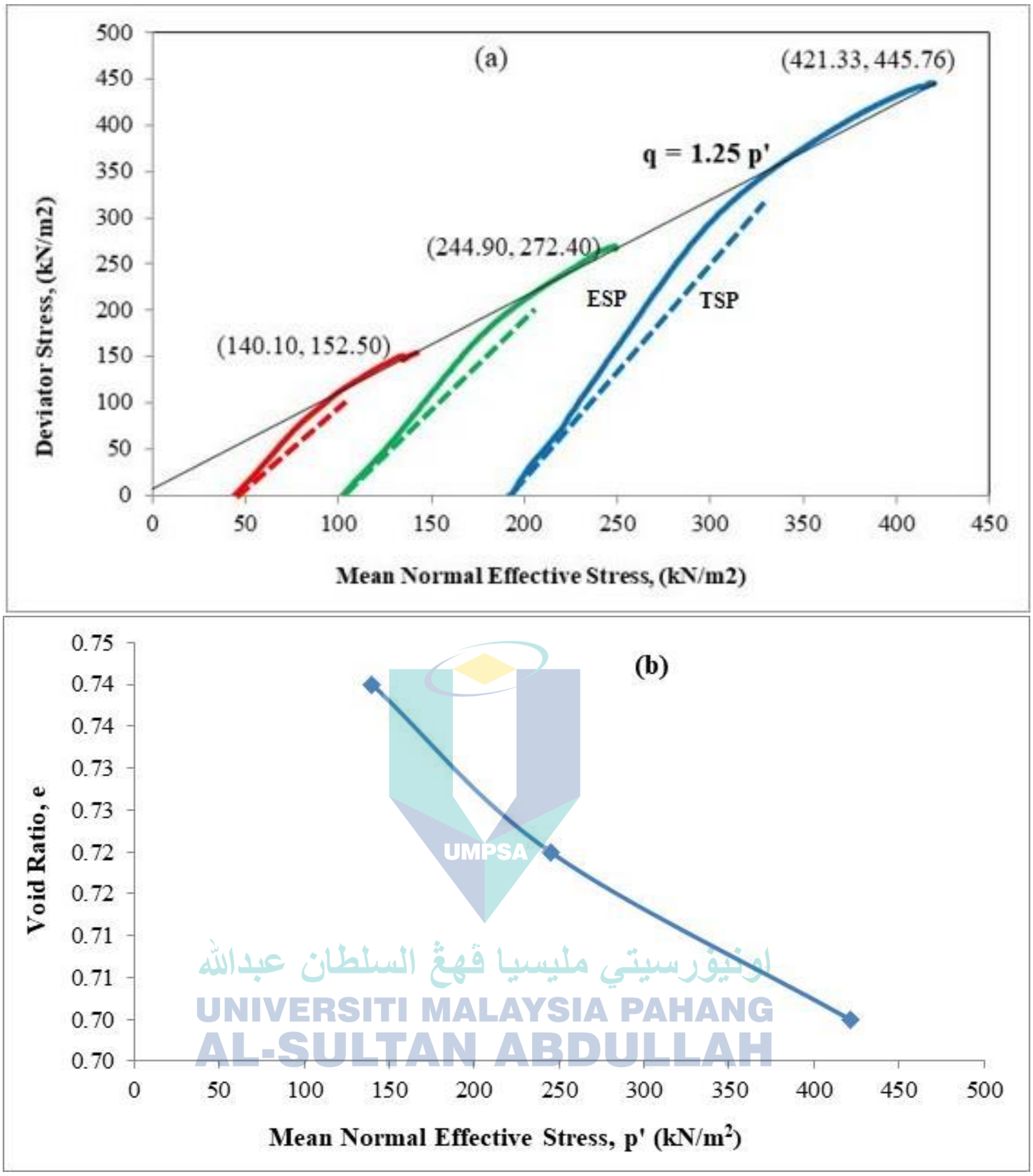

Figure 5.15 (a) Critical state line and stress pathways in q: p' space; (b) Critical state line in e: p' space for a clay sample reinforced at 100% penetration using a 16 mm-diameter single polypropylene column

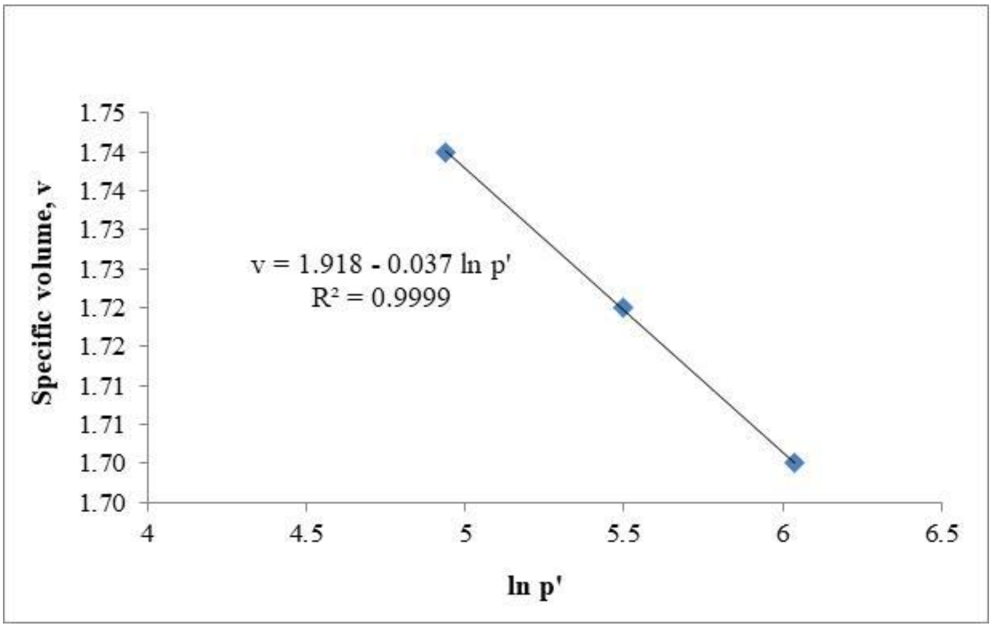

Figure 5.16 Critical state line in v: ln p' space for kaolin clay reinforced with a single polypropylene column with a diameter of 16 mm and 100% penetration

5.4.2 Group Columns

Figure 5.17 illustrates the stress pathways for samples reinforced with group columns. The degree of improvement in undrained shear strength was significantly influenced by effective confining pressures, σ'_3 (also known as the consolidation pressure or the initial mean normal effective stress, p'_o). The stress paths of samples reinforced with polypropylene columns, subject to effective confining pressures of 50 kPa, exhibited a rightward shift (excluding 10 mm and 16 mm columns with 100% height penetrating ratio) in comparison to the stress paths of controlled samples. This shift suggests a higher value of the undrained shear strength. In contrast, it was observed that samples reinforced with polypropylene columns exhibited a rightward shift in stress paths when compared to the stress paths of control samples, specifically for samples subjected to effective confining pressures of 100 kPa and 200 kPa.

Generally, most of the stress paths for samples reinforced with group polypropylene columns indicated undrained shear strength improvement compared to single columns, especially during higher effective confining pressure. This circumstance demonstrated that the area ratio may be significant in enhancing the undrained shear strength of samples reinforced with polypropylene columns. This is because the group column possessed three times higher area ratio compared to a single column.

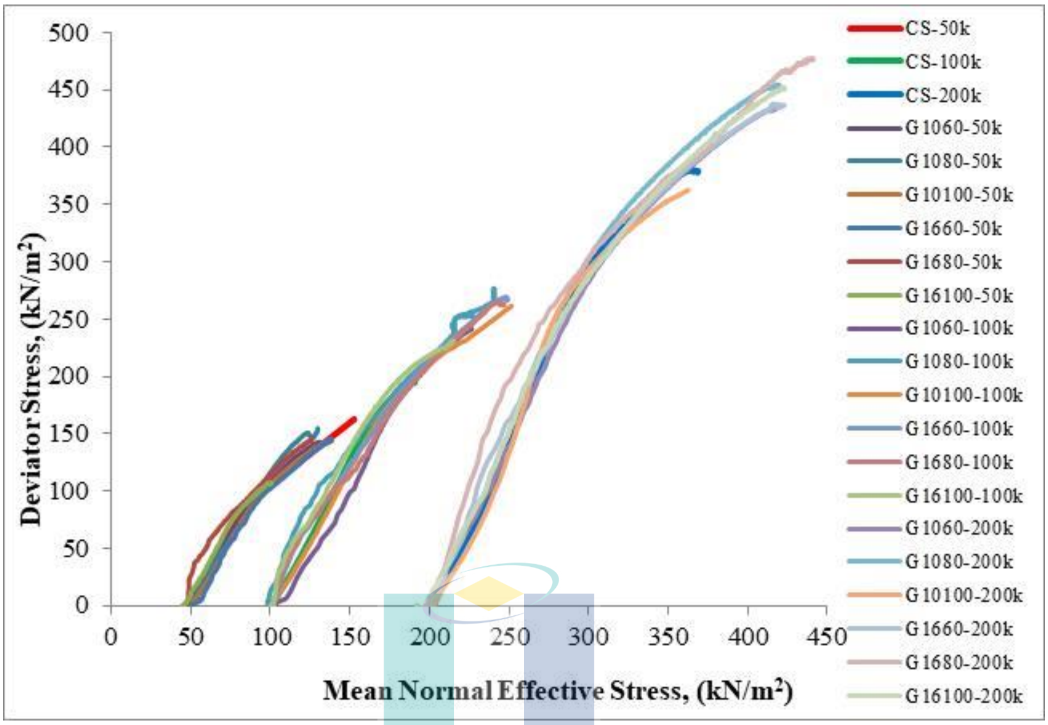

Figure 5.17 Effective stress pathways for clay sample reinforced with group polypropylene columns

5.4.2.1 Height Penetrating Ratio, Hc/Hs = 0.60

Figure 5.18 (a) displays the stress pathways for the sample reinforced with a group 10 mm diameter column with a 60% height penetration ratio. The figures presented illustrate the TSP and ESP for specimens that completed isotropic consolidation at effective confining pressures of 50 kPa, 100 kPa, and 200 kPa. For samples reinforced with polypropylene columns, the ESP curves of control samples were utilised as a baseline to identify any alterations resulting from the installation of the columns.

The CSL in the q- p' plane was determined by analysing the results of experiments conducted on isotropically consolidated samples at three different confining pressures. The best fitting line calculated from these data provided the equation q = 1.23p', as described in Equation 2.1. The value of the critical state parameter, denoted as M, was determined to be 1.23. Therefore, the friction angle at the critical condition, ϕ_c, was found to be around 30.60° using Equation 2.2. Meanwhile,

Figure 5.18 (b) shows the CSL of the same sample, and the projection of CSL was then replotted on the v – ln p' plane, as shown in Figure 5.19. From the figure, the equation of the CSL was obtained as follows:

$$v = 2.077 - 0.060 \ln p' \quad (5.8)$$

With the coefficient of determination, $R^2 = 0.9864$. The critical state parameters, λ was obtained as 0.060 and Γ as 2.077.

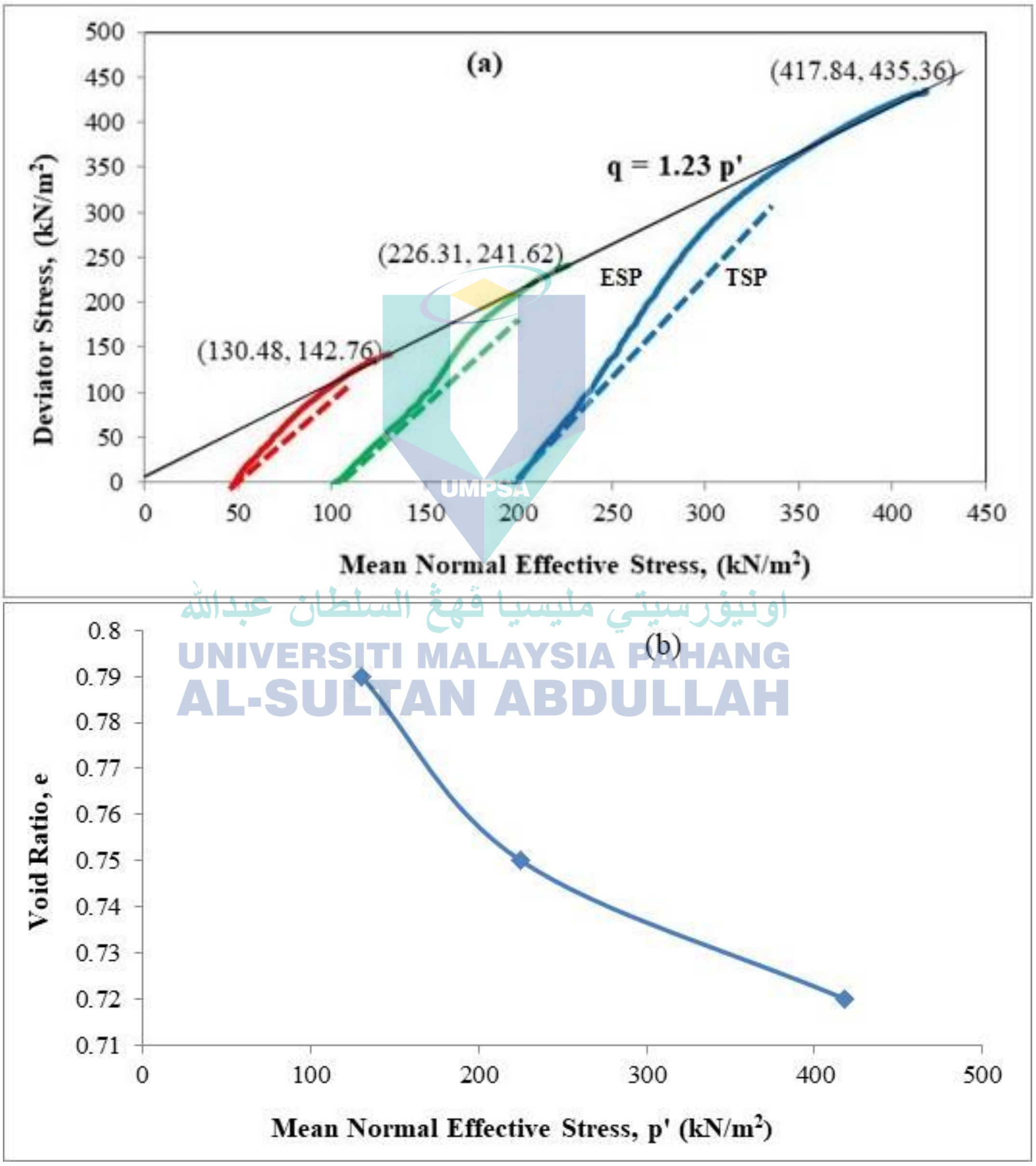

Figure 5.18 (a) Critical state line and stress pathways in q: p' space; (b) Critical state line in e: p' space for a clay sample reinforced at 60% penetration using a 10 mm-diameter group polypropylene column

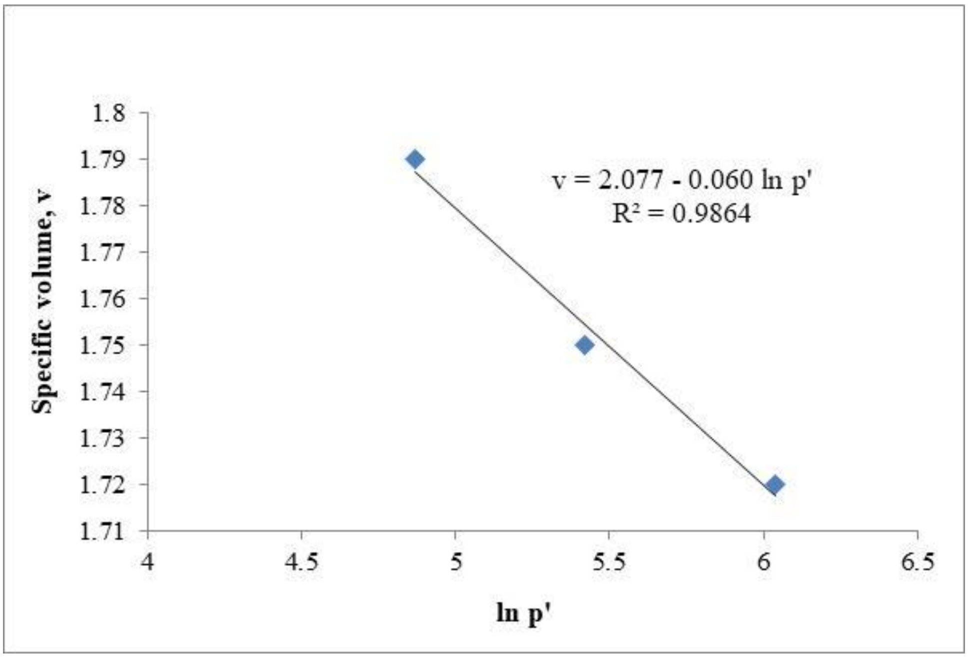

Figure 5.19 Critical state line in v: ln p' space for kaolin clay reinforced with a group polypropylene column with a diameter of 10 mm and 60% penetration

Figure 5.20 (a) illustrates the stress pathways in the q - p' plane for samples reinforced with a set of 16 mm diameter columns at a 60% height penetration ratio. The M value obtained from the figure was 1.24, therefore, the ϕ_c was 30.90°. Meanwhile, Figure 5.20 (b) shows CSL of the same sample, and the projection of CSL was then replotted on the v – ln p' plane, as shown in Figure 5.21. From the figure, the equation of the CSL was obtained as follows:

$$v = 1.948 - 0.043 \ln p' \qquad 5.9$$

With the coefficient of determination, $R^2 = 0.9963$. The critical state parameters, λ (slope of the line), was obtained as 0.043 and the point in which CSL crosses v axis, Γ was 1.948.

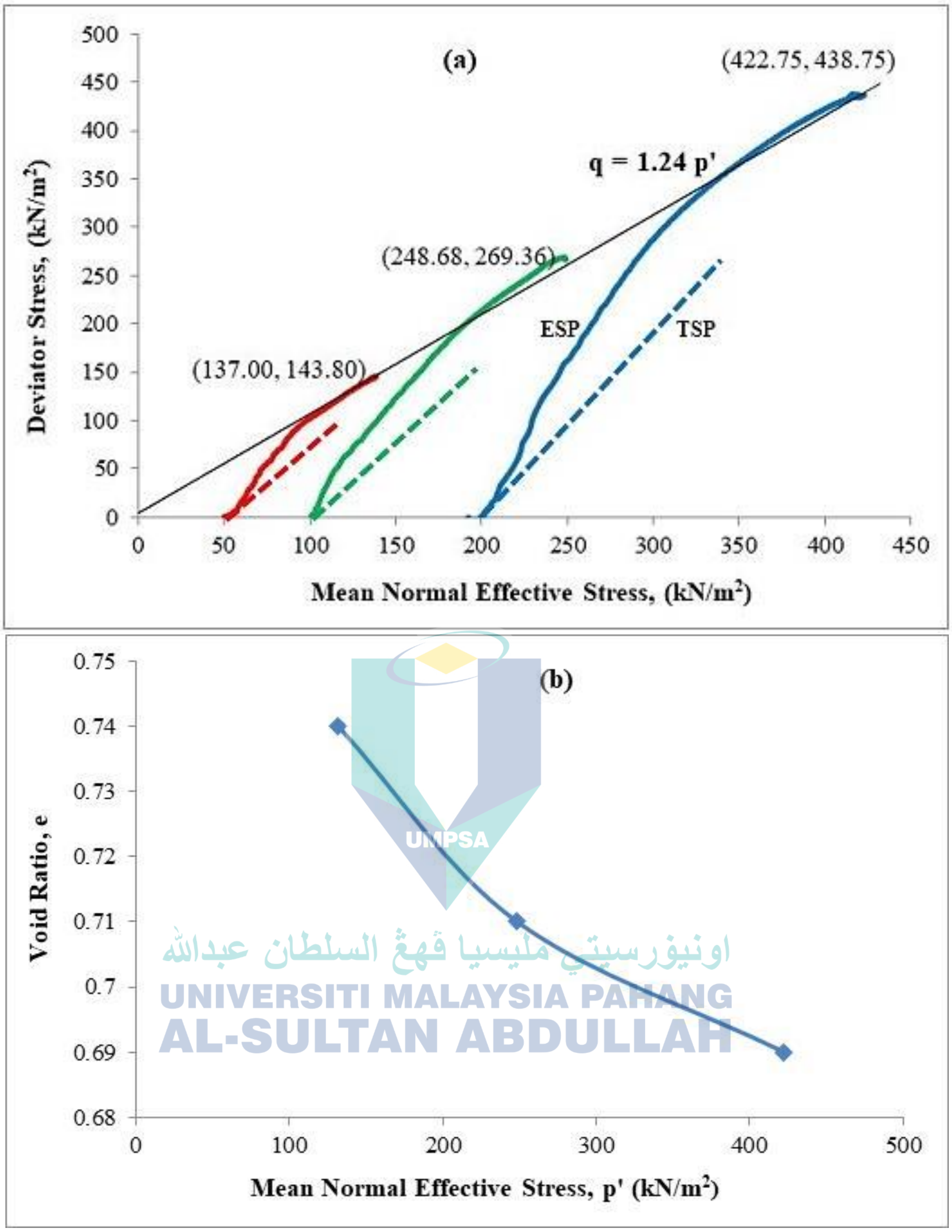

Figure 5.20 (a) Critical state line and stress pathways in q: p' space; (b) Critical state line in e: p' space for a clay sample reinforced at 60% penetration using a 16 mm-diameter group polypropylene column

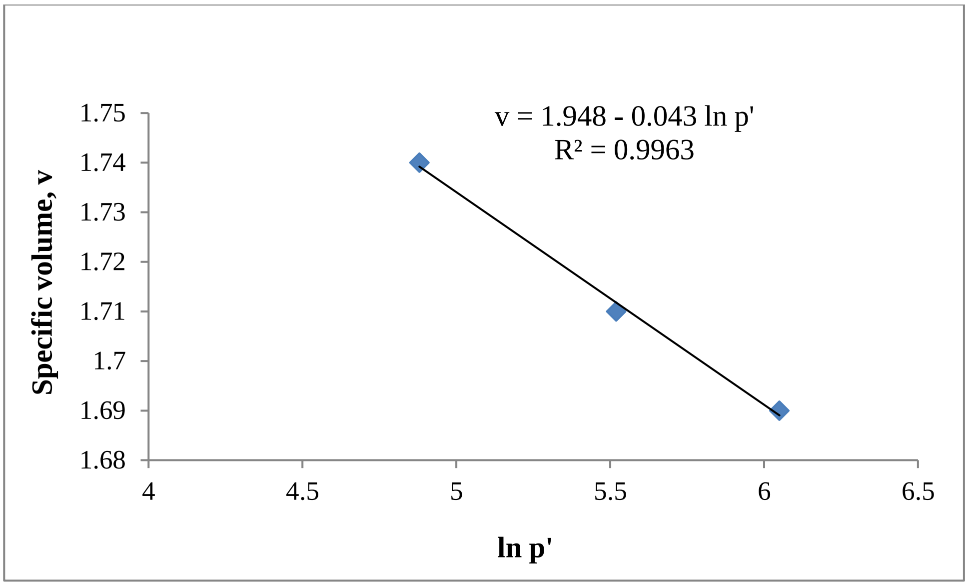

Figure 5.21 Critical state line in v: ln p' space for kaolin clay reinforced with a group polypropylene column with a diameter of 16 mm and 60% penetration

5.4.2.2 Height Penetrating Ratio, Hc/Hs = 0.80

Figure 5.22 (a) illustrates the stress pathways in the q - p' plane for samples reinforced with a set of 10 mm diameter columns at a 80% height penetration ratio. The M value obtained from the figure was 1.24, therefore, the ϕ_c was 30.80°. Meanwhile, Figure 5.22 (b) shows CSL of the same sample, and the projection of CSL was then replotted on the v – ln p' plane, as shown in Figure 5.23. From the figure, the equation of the CSL was obtained as follows:

$$v = 1.967 - 0.043 \ln p' \qquad 5.10$$

With the coefficient of determination, $R^2 = 0.9919$. The critical state parameters, λ was obtained as 0.043 and Γ as 1.967.

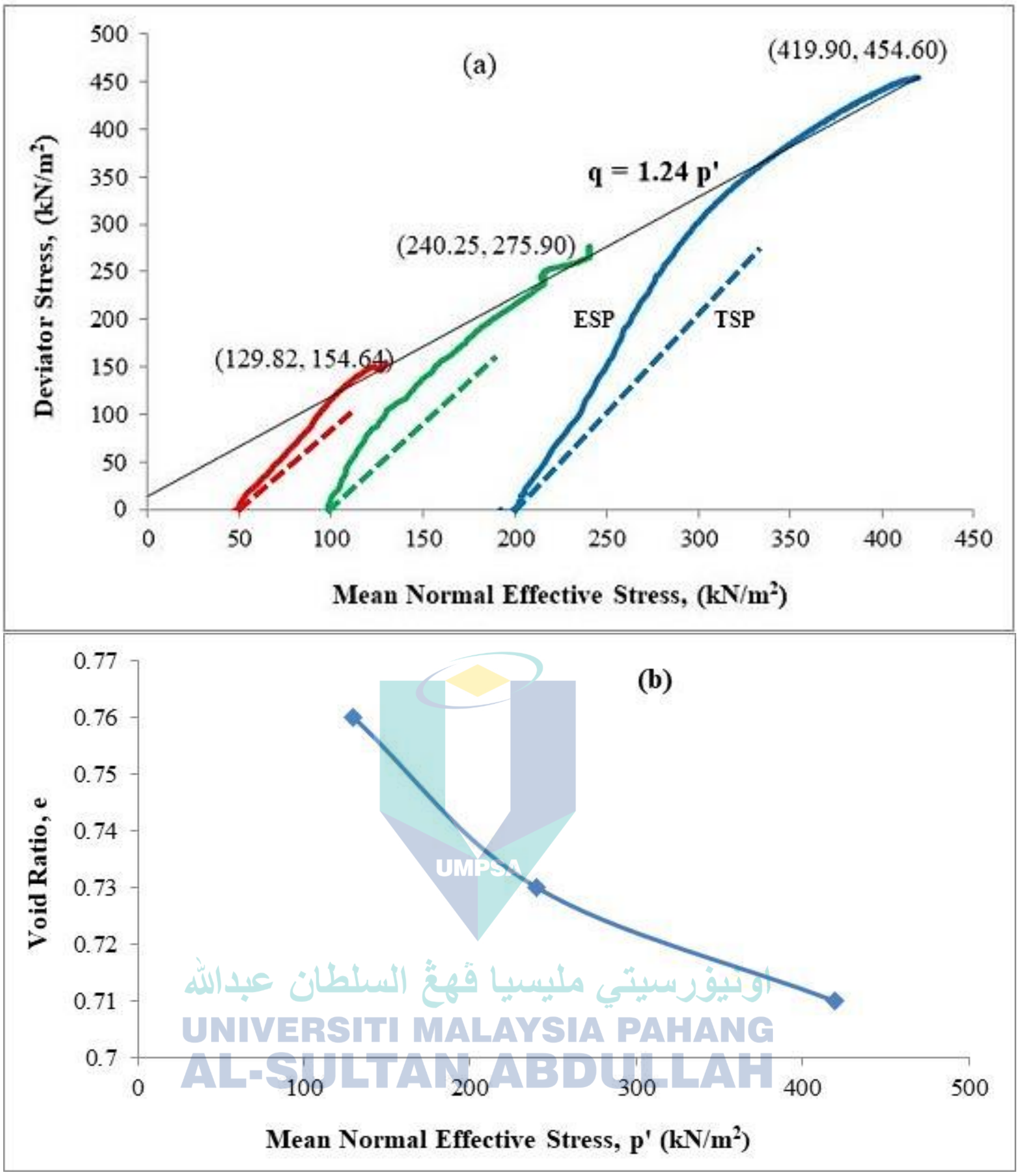

Figure 5.22 (a) Critical state line and stress pathways in q: p' space; (b) Critical state line in e: p' space for a clay sample reinforced at 80% penetration using a 10 mm-diameter group polypropylene column

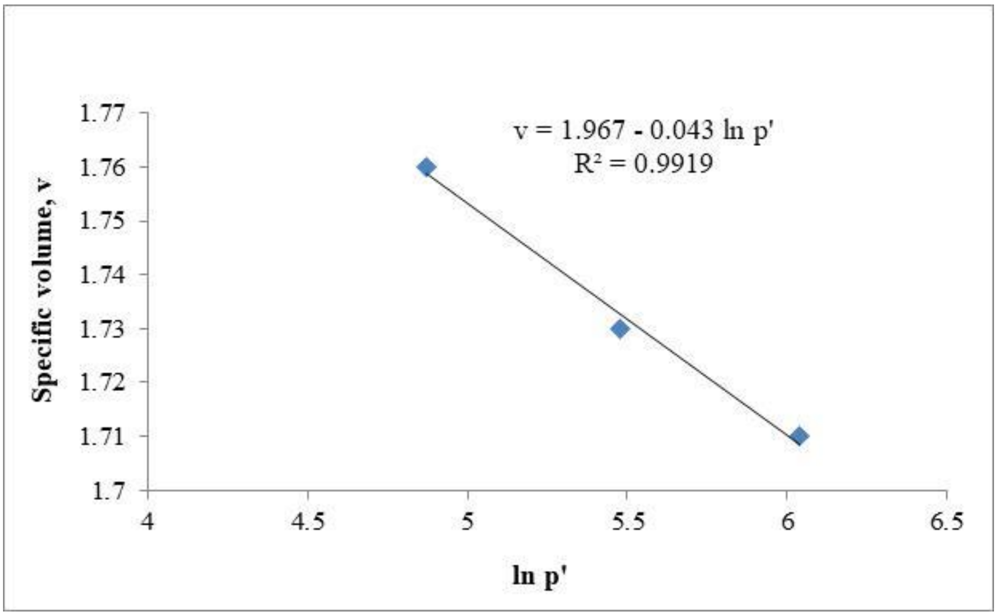

Figure 5.23 Critical state line in v: ln p' space for kaolin clay reinforced with a group polypropylene column with a diameter of 10 mm and 80% penetration

Figure 5.24 (a) illustrates the stress pathways relevant to a specimen that had been reinforced with a column of 16 mm diameter, with a height penetration ratio of 80%. The plotted graphs include the TSP and ESP for specimens at p'_o of 50, 100, and 200 kPa. The M value obtained from the figure was 1.28, therefore, ϕ_c was 31.90°. Meanwhile,

Figure 5.24 (b) shows the CSL of the same sample which indicated the same pattern as the controlled sample. The projection of CSL on the v – ln p' plane gave a straight line, as shown in Figure 5.25. From the figure, the equation of the CSL was obtained as follows:

$$v = 1.892 - 0.040 \ln p' \qquad 5.11$$

With the coefficient of determination, $R^2 = 0.9952$. The critical state parameters, λ was obtained as 0.040 and Γ as 1.892.

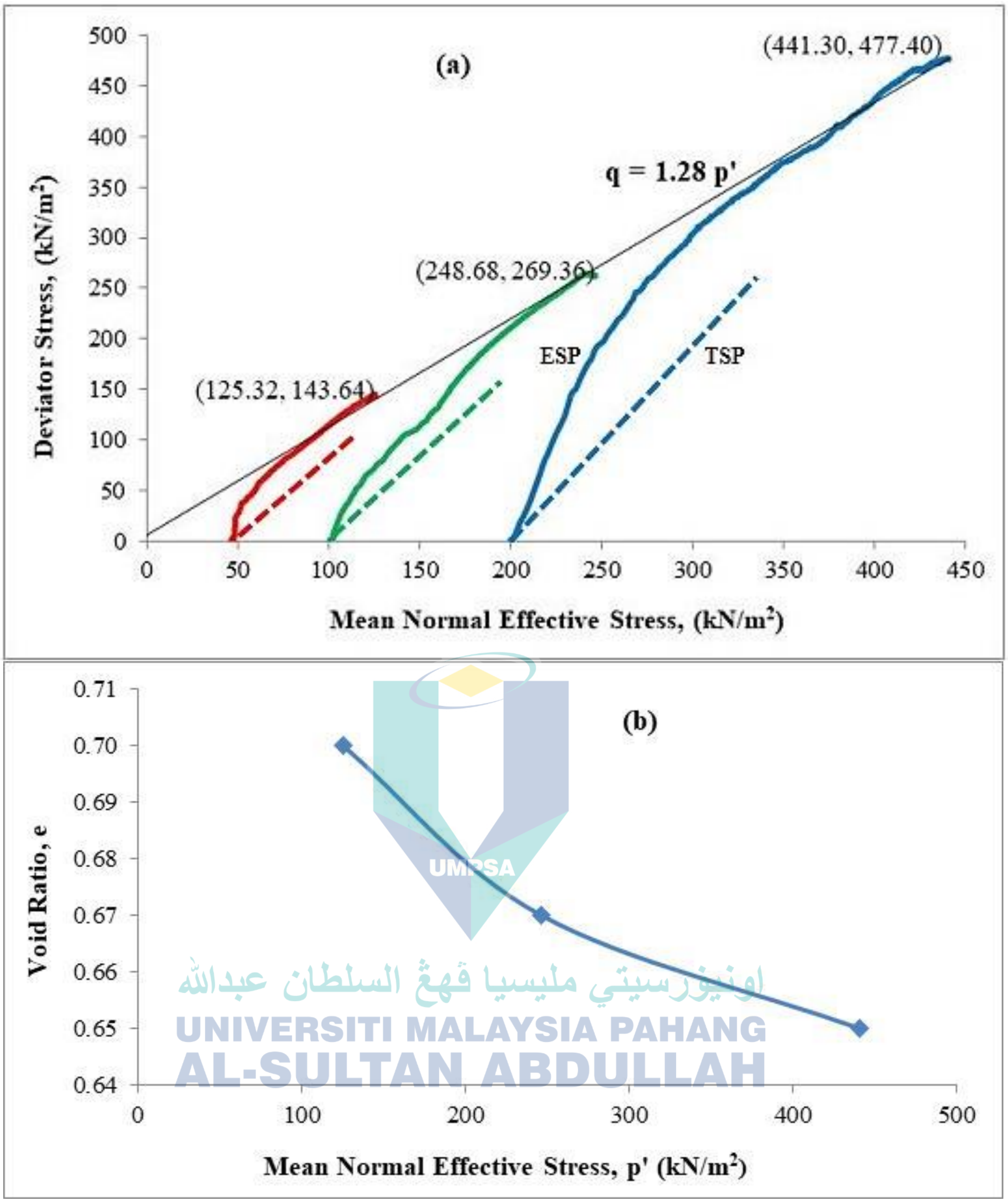

Figure 5.24 (a) Critical state line and stress pathways in q: p' space; (b) Critical state line in e: p' space for a clay sample reinforced at 80% penetration using a 16 mm-diameter group polypropylene column

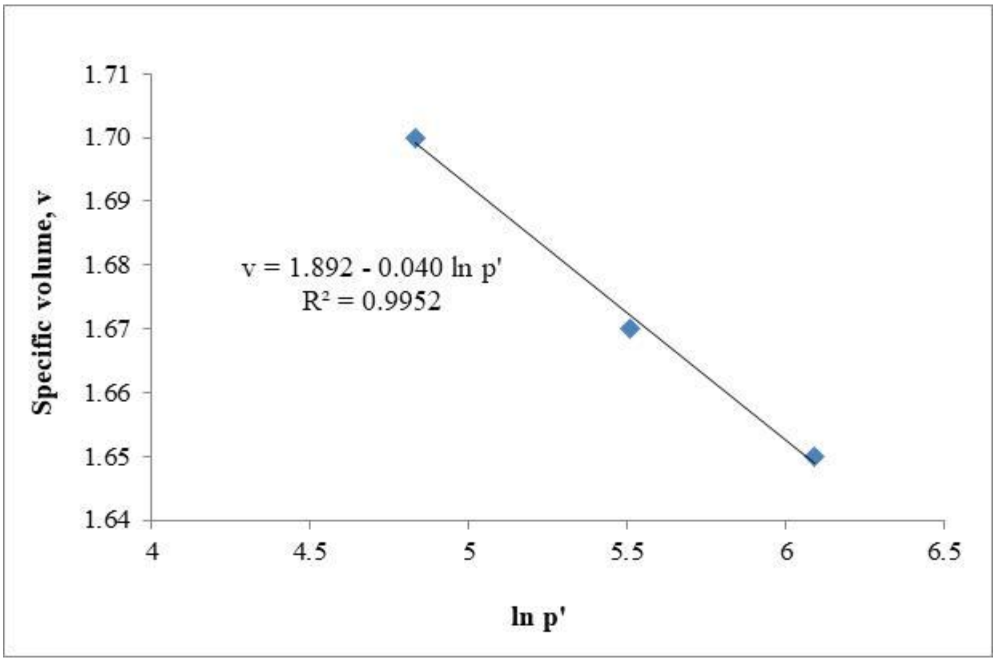

Figure 5.25 Critical state line in v: ln p' space for kaolin clay reinforced with a group polypropylene column with a diameter of 16 mm and 80% penetration

5.4.2.3 Height Penetrating Ratio, Hc/Hs = 1.00

Figure 5.26 (a) illustrates the stress pathways in the q: p' plane of kaolin clay specimens that had been reinforced with a collection of polypropylene columns of 10 mm in diameter, with a height penetration ratio of 100%. The M value obtained from the figure was 1.19, and the ϕ_c was 29.70°. Conversely, Figure 5.26 (b) depicts the CSL of the identical sample. The projection of CSL, replotted on the *v* – ln p' plane as in Figure 5.27, gives a straight line with λ as the slope and Γ as the point of intersection between the CSL and *v* axis. From the figure, the equation of the CSL was obtained as follows:

$$v = 1.873 - 0.031 \ln p' \tag{5.12}$$

With the coefficient of determination, $R^2 = 0.8918$. The critical state parameters, λ was obtained as 0.031 and Γ as 1.873.

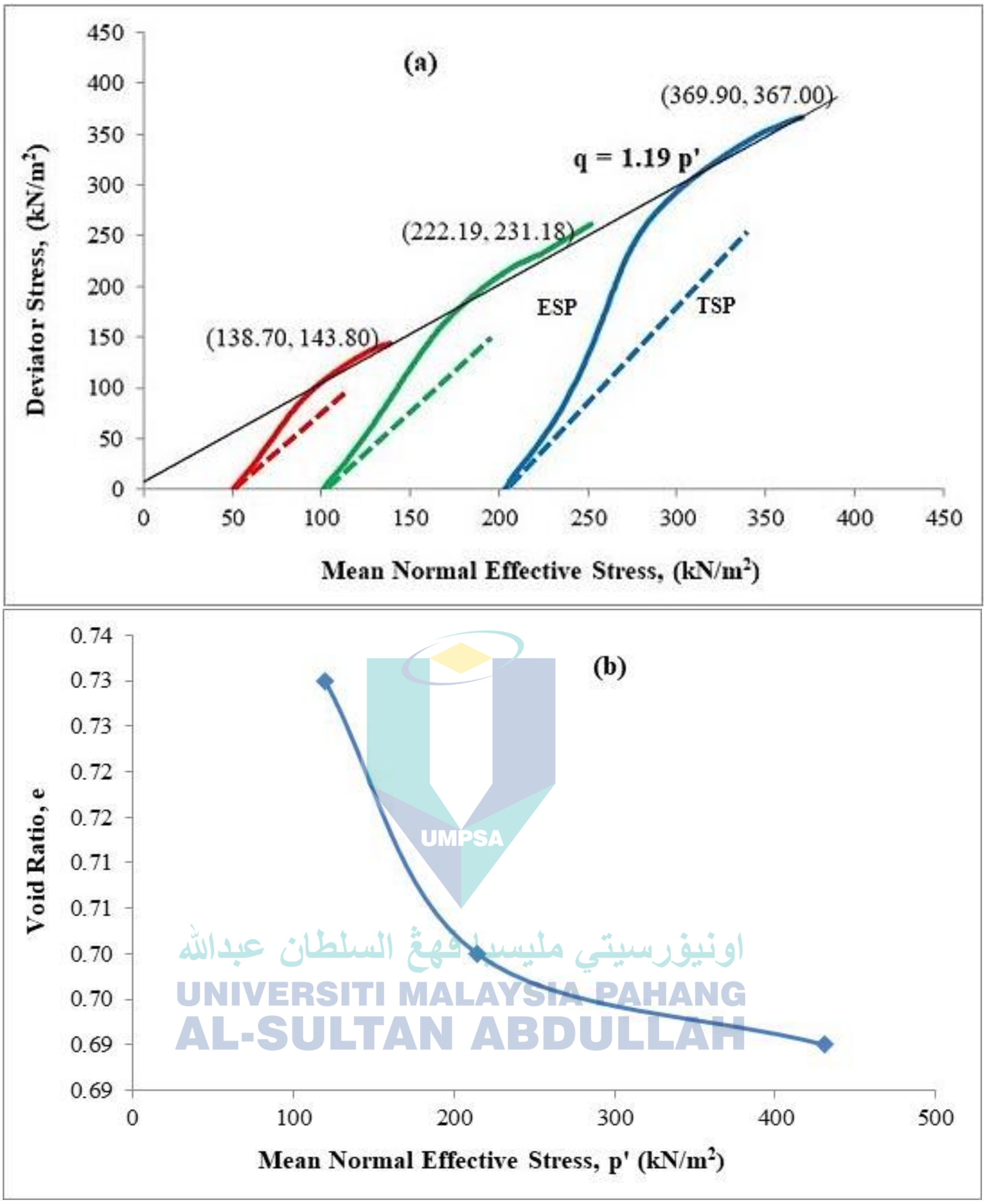

Figure 5.26 (a) Critical state line and stress pathways in q: p' space; (b) Critical state line in e: p' space for a clay sample reinforced at 100% penetration using a 10 mm-diameter group polypropylene column

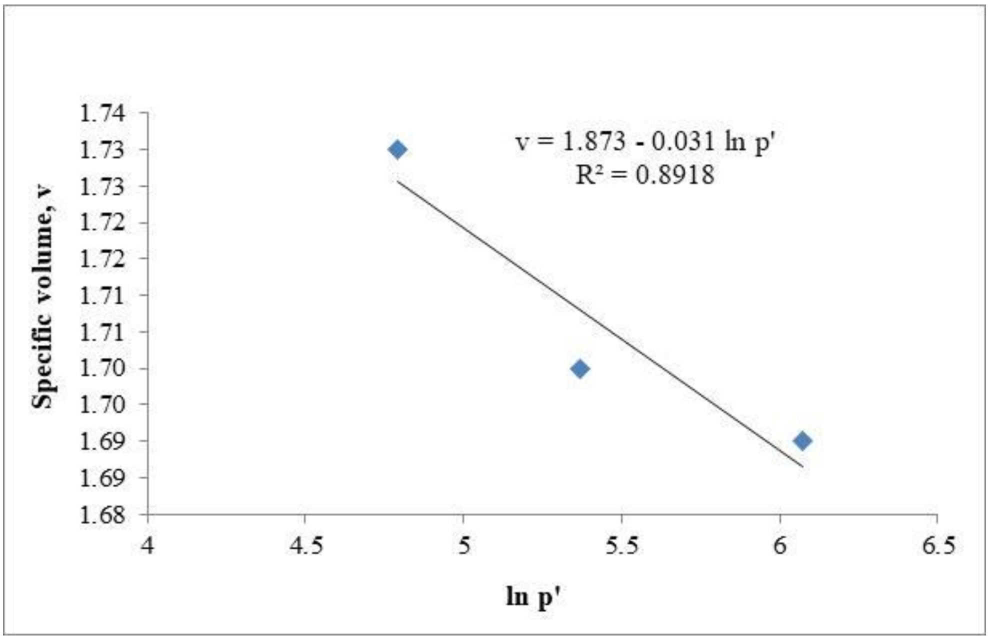

Figure 5.27 Critical state line in v: ln p' space for kaolin clay reinforced with a group polypropylene column with a diameter of 10 mm and 100% penetration

Figure 5.28 (a) illustrates the stress pathways relevant to a specimen that had been reinforced with a column of 16 mm diameter, with a height penetration ratio of 80% (full penetration). The plotted graphs include the TSP and ESP for specimens at p'_o of 50, 100, and 200 kPa. The M value obtained from the figure was 1.29, therefore ϕ_c was 32.00°. Meanwhile, Figure 5.28 (b) shows the CSL of the same sample which indicated the same pattern as the same sample plotted in e: p' space. The projection of CSL on the v – ln p' plane gave a straight line, as shown in Figure 5.29. From the figure, the equation of the critical state line was obtained as:

$$v = 1.873 - 0.031 \ln p' \qquad 5.13$$

With the coefficient of determination, $R^2 = 0.8918$. The critical state parameters, λ (slope of the line), was obtained as 0.031 and Γ as 1.873.

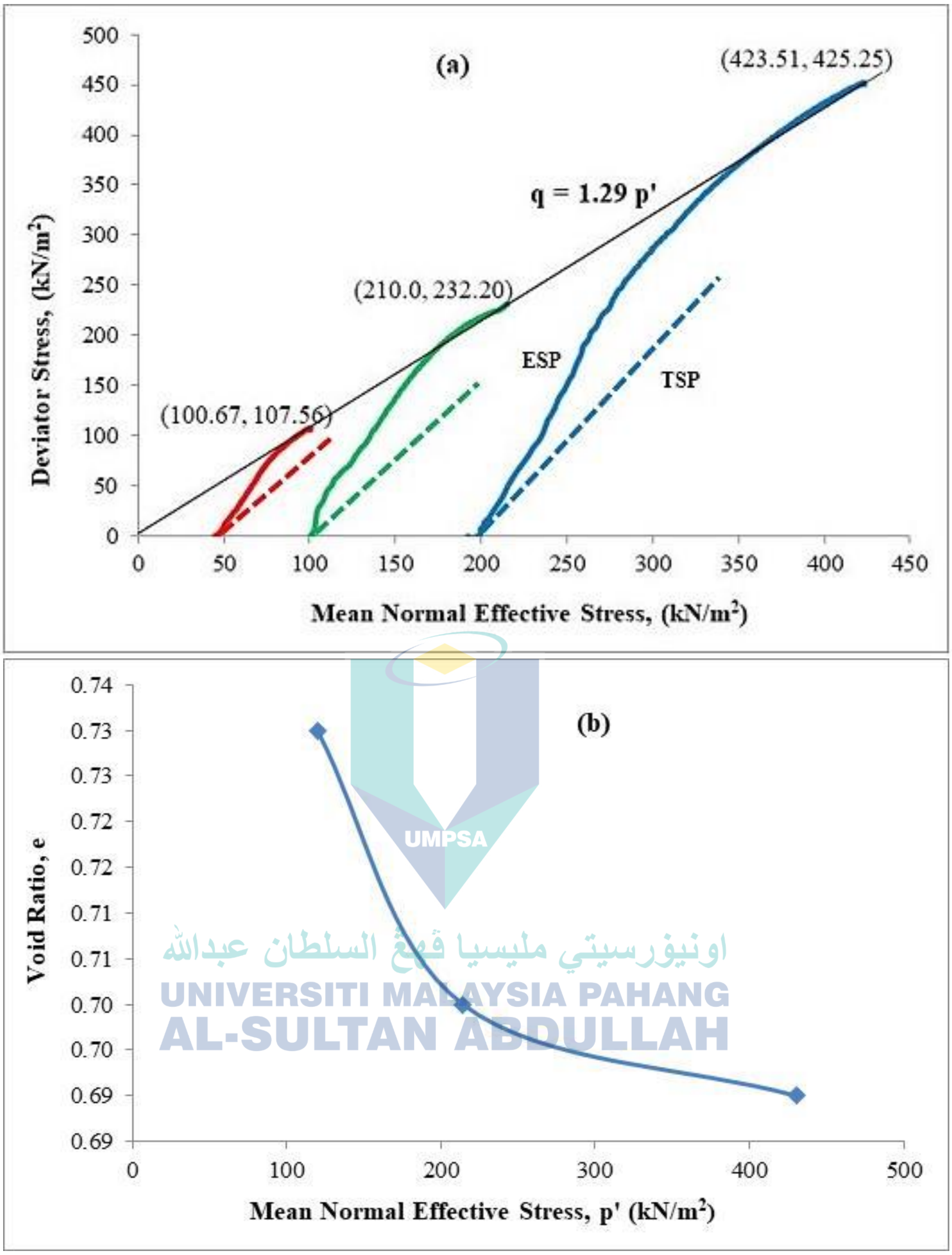

Figure 5.28 (a) Critical state line and stress pathways in q: p' space; (b) Critical state line in e: p' space for a clay sample reinforced at 100% penetration using a 16 mm-diameter group polypropylene column

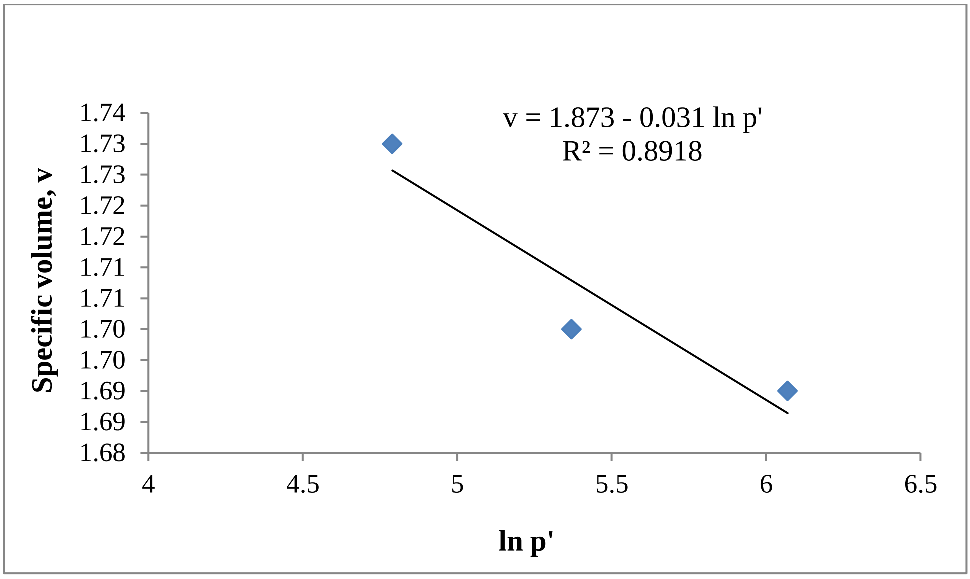

Figure 5.29 Critical state line in v: ln p' space for kaolin clay reinforced with a group polypropylene column with a diameter of 16 mm and 100% penetration

5.5 Critical State Line Equations and Critical State Parameters

The CSL equations, the parameters for each sample reinforced with polypropylene columns, and the controlled sample parameters are presented in Table 7.2. The M value for polypropylene column-reinforced samples is usually either slightly lower or equal to that of a control or unreinforced sample. From this, it is evident that merely examining the M value (or c) alone was insufficient to ascertain whether adding polypropylene columns as a reinforcing strategy had a significant effect on the system when doing a critical state analysis. In critical states, the critical void ratio or specific volume change is critical, and the effect of volume change has to be considered. Because of this, additional important state attributes dictate the consequences.

The comparison between the friction angle in the critical state and the peak friction angle derived from the peak stress Mohr-Coulomb failure criteria is presented in Table 5.2. In general, it may be seen that the friction angles in critical states tended to be smaller than the peak friction angles. This phenomenon can be attributed to Coulomb's model, as discussed by Budhu (2007), which stated that the maximum friction angle for soil undergoing dilation is:

$$\phi'_p = \phi'_c + \alpha_p \qquad 5.14$$

The peak dilatancy angle, denoted as α_p, typically falls between the range of 0 to 15°. Therefore, ϕ'_c should be less than ϕ'_p as obtained in this research. Another characteristic of ϕ'_p is that it depends on the value of normal effective stress, On the other hand, regardless of the initial state of the soil or the size of the mean normal effective stress, the value of ϕ'_c remains constant. This shows that evaluating the strength of the soil through a critical state framework is theoretically more reliable than the Mohr-Coulomb failure criteria.

Table 5.2 Critical state line equations and critical state parameters from CU tests for kaolin reinforced with polypropylene columns

Sample	V_c/V_s (%)	CSL Equations	λ	Γ	M	ϕ'_c	ϕ'_p
C	0	$q = 1.30p'$ $v = 2.302 - 0.093 \ln p'$	0.093	2.302	1.30	32.30	33.50
S1060	2.40	$q = 1.25p'$ $v = 2.001 - 0.055 \ln p'$	0.055	2.001	1.25	31.17	32.75
S1080	3.20	$q = 1.21p'$ $v = 1.994 - 0.049 \ln p'$	0.049	1.994	1.21	30.24	33.50
S10100	4.00	$q = 1.24p'$ $v = 2.073 - 0.069 \ln p'$	0.069	2.073	1.24	31.00	34.50
S1660	6.15	$q = 1.20p'$ $v = 2.018 – 0.051 \ln p'$	0.051	2.018	1.20	29.98	30.75
S1680	8.19	$q = 1.18p'$ $v = 1.966 – 0.045 \ln p'$	0.045	1.966	1.18	29.60	31.70
S16100	10.24	$q = 1.25p'$ $v = 1.920 – 0.036 \ln p'$	0.036	1.920	1.25	31.20	33.50
G1060	7.20	$q = 1.23p'$ $v = 2.078 – 0.060 \ln p'$	0.060	2.078	1.23	30.60	32.30
G1080	9.60	$q = 1.24p'$ $v = 1.967 – 0.043 \ln p'$	0.043	1.967	1.24	30.80	31.30
G10100	12.00	$q = 1.19p'$ $v = 1.873 – 0.031 \ln p'$	0.031	1.873	1.19	29.70	30.20
G1660	18.45	$q = 1.24p'$ $v = 1.948 - 0.043 \ln p'$	0.043	1.948	1.24	30.90	30.50
G1680	24.57	$q = 1.28p'$ $v = 1.891 - 0.040 \ln p'$	0.040	1.891	1.28	31.90	30.40
G16100	30.72	$q = 1.29p'$ $v = 1.785 - 0.021 \ln p'$	0.021	1.785	1.29	32.00	30.00

Note: CSL – Critical State Line, CS – Critical State

5.6 Variation of M, λ and Γ with Volume Replacement Ratio

Since analyses were carried out for critical state conditions in which volume change is considered, the variations of critical state parameters were plotted against the percentage of soil volume replaced by polypropylene columns. Using the results in Table 5.2, the relationship between the volume replacement ratio and the variations in M, λ, and Γ. V_c/V_s for all samples was plotted, and the results are shown in Figure 5.30.

The plot of M against column volume replacement ratio, depicted in Figure 5.30(a), is highly dispersed, indicating that there was no identifiable pattern or relationship between them. The range of values for the friction angle in the critical state was between 30° and 35°, with the majority falling between 1.18 and 1.30. Comparing this with the value obtained for other soils reported by Budhu (2007), the range of ϕ'_c gained for the soil-polypropylene composite fell under the "mixtures of gravel and sand with fine-grained soils" and "gravel" categories.

Figure 5.30 (b) and (c) illustrate the variations of λ and Γ with column volume replacement ratio, respectively, which shows that there seemed to be a general trend. The λ and Γ were observed to decrease with the increase in volume replacement ratio, except for the volume replacement ratio of 7.20%. However, there was no suitable correlation that could fit the plots as the coefficient of determinations, R^2 for the intended correlation was smaller than 0.25, showing poor correlation (Marto, 1996).

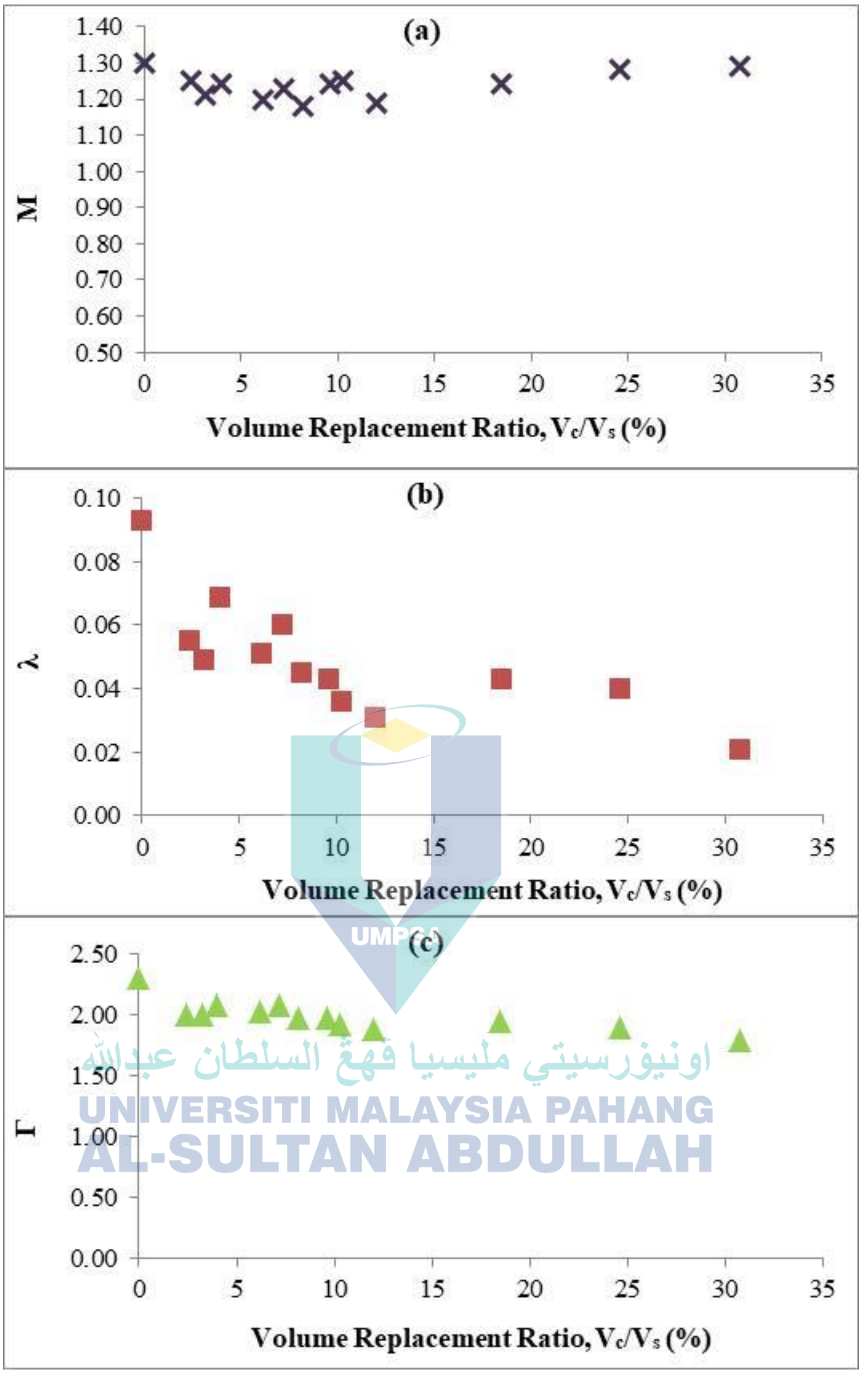

Figure 5.30 Variation of (a) M, (b) λ, and (c) Γ with volume replacement ratio for kaolin clay reinforced with polypropylene columns

5.7 Undrained Shear Strength at Critical State

The undrained shear strengths of the soil at a critical state could be taken as half of the deviator stress achieved at a critical state (Whitlow, 2001 and Budhu, 2007. Table 5.3 illustrates the undrained shear strengths for all samples derived from this study. For every single and group of polypropylene column-reinforced samples, the increase in undrained shear strength was also computed using the value of S_u of the unreinforced sample at the corresponding initial mean normal effective stress, p'_o. The findings are also summarised in Table 5.3.

Table 5.3 Undrained shear strength and increased in the strength at critical state

Sample	**Volume Replacement Ratio, Vc/Vs (%)**	**Effective Confining Pressure, σ'_3 (kPa)**	**Deviator Stress, q (kPa)**	**Undrained Shear Strength, S_u (kPa)**	**Increased in Undrained Shear Strength, ΔS_u (%)**
C	0	50	122.86	61.43	-
		100	245.70	122.85	
		200	391.10	195.55	
S1060	2.40	50	148.69	74.35	21.03
		100	271.31	135.66	10.43
		200	429.24	214.62	9.75
S1080	3.20	50	164.08	82.04	33.55
		100	266.67	133.34	8.54
		200	435.25	217.62	11.29
S10100	4.00	50	158.98	79.49	29.40
		100	244.62	122.31	-0.44
		200	417.53	208.77	6.76
S1660	6.15	50	142.90	71.45	16.31
		100	276.75	138.38	12.64
		200	437.72	218.86	11.92
S1680	8.19	50	159.49	79.75	29.82
		100	281.36	140.68	14.51
		200	451.89	225.95	15.55
S16100	10.24	50	152.40	76.20	24.04
		100	272.40	136.20	10.87
		200	445.76	222.88	13.98
G1060	7.20	50	142.75	71.38	16.20
		100	241.62	120.81	-1.66
		200	435.80	217.90	11.43
G1080	9.60	50	154.42	77.21	25.69
		100	288.68	144.34	17.49
		200	454.55	227.28	16.22

Table 5.3 Continued

Sample	Volume Replacement Ratio, Vc/Vs (%)	Effective Confining Pressure, σ'_3 (kPa)	Deviator Stress, q (kPa)	Undrained Shear Strength, S_u (kPa)	Increased in Undrained Shear Strength, ΔS_u (%)
		50	143.80	76.90	25.18
G10100	12.00	100	231.18	115.59	-5.90
		200	367.00	183.50	-6.16
		50	145.60	72.80	18.51
G1660	18.45	100	269.35	134.68	9.63
		200	437.50	218.50	11.74
		50	143.64	71.82	16.88
G1680	24.57	100	264.90	134.45	9.44
		200	477.54	238.77	22.10
		50	107.56	53.78	-12.45
G16100	30.72	100	232.20	116.10	-5.50
		200	452.25	226.13	15.64

Note: -ve values means decreased in strength

5.7.1 Theoretical Correlation between Undrained Shear Strength and Specific Volume at Critical States

Equations 2.1 and 2.3 provide the two critical state line equations that, in theory, can be combined to connect the critical specific volume to the undrained shear strength at the critical state. q = Mp' from Equation 2.1 and v = Γ-λln p' from Equation 2.3. Therefore, by replacing p' from Equation 2.3 into Equation 2.1, the deviator stress at critical state has been expressed as shown in Equation 2.10 below:

$$q = M \exp[\frac{\Gamma - v}{\lambda}]$$

Meanwhile, the undrained shear strength can be obtained from Equation 2.11 as below:

$$S_u = \frac{M}{2} \exp[\frac{\Gamma - v}{\lambda}]$$

Since the critical state parameters M, Γ, and λ of the corresponding kaolin clay-polypropylene column composites had been obtained from the respective CSL equations, the undrained shear strength of kaolin reinforced with single and group polypropylene columns may be computed using Equation 2.11. Together with the undrained shear strength determined by the laboratory experiments, the outcomes are displayed in Table 5.4. The predicted and laboratory-obtained S_u was plotted against the volume replacement ratio given in Figures 5.31 to 5.33, respectively, for p'_o equal to 50 kPa, 100 kPa, and 200 kPa, to investigate the fluctuation of Su with a volume of replaced weak soils.

Table 5.4 Calculated and laboratory values of undrained shear strengths, and specific volumes of samples at critical states

Sample	**Volume Replacement Ratio, Vc/Vs (%)**	**Initial Mean Normal Effective Stress, p'_o (kPa)**	**Specific Volume at critical state, v**	**Calculated Undrained Shear strength, $S_u = \frac{M}{2}\exp[\frac{\Gamma - v}{\lambda}]$ (kPa)**	**Undrained Shear Strength obtained from Test, (kPa)**
		50	1.85	83.87	61.43
C	0	100	1.80	143.91	122.85
		200	1.73	295.66	195.55
		50	1.73	85.63	74.35
S1060	2.40	100	1.70	148.41	135.66
		200	1.67	257.24	214.62
		50	1.75	88.01	82.04
S1080	3.20	100	1.72	161.98	133.34
		200	1.70	244.07	217.63
		50	1.73	89.30	79.49
S10100	4.00	100	1.69	159.49	122.31
		200	1.66	245.17	208.77
		50	1.77	77.65	71.45
S1660	6.15	100	1.74	139.65	138.38
		200	1.71	251.94	218.86
		50	1.74	89.33	79.75
S1680	8.19	100	1.72	139.54	140.68
		200	1.69	271.07	225.95

Table 5.4 Continued

Sample	**Volume Replacement Ratio, Vc/Vs (%)**	**Initial Mean Normal Effective Stress, p'$_o$ (kPa)**	**Specific Volume at critical state, v**	**Calculated Undrained Shear strength, $S_u = \frac{M}{2}\exp[\frac{\Gamma - v}{\lambda}]$ (kPa)**	**Undrained Shear Strength obtained from Test, (kPa)**
		50	1.73	122.73	76.20
S16100	10.24	100	1.72	160.77	136.20
		200	1.70	281.46	222.88
		50	1.79	74.73	71.38
G1060	7.20	100	1.75	145.46	120.81
		200	1.72	240.78	217.90
		50	1.76	76.09	77.21
G1080	9.60	100	1.73	153.54	144.34
		200	1.71	245.17	227.28
		50	1.73	60.39	76.90
G10100	12.00	100	1.70	157.72	115.59
		200	1.69	219.38	183.50
		50	1.74	78.41	72.80
G1660	18.45	100	1.71	156.33	134.68
		200	1.69	250.13	218.50
		50	1.70	76.22	71.82
G1680	24.57	100	1.67	160.57	134.45
		200	1.65	266.06	238.77
		50	1.69	59.41	53.78
G16100	30.72	100	1.67	154.70	116.10
		200	1.66	248.02	226.13

From Figures 5.31 to 5.33, it is observed that the plots of calculated S_u with V_c/V_s were more scattered than the plots of actual values. This may be due to the simplification of the CSL parameters, which enhanced the errors. Therefore, the Su values obtained from the laboratory were utilised in the development of the design charts presented in a subsequent section of this chapter.

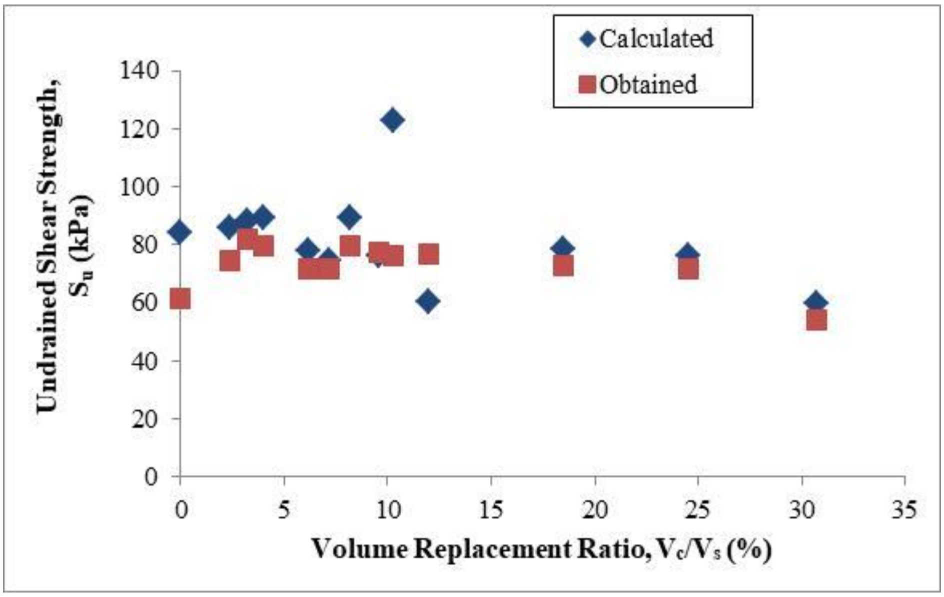

Figure 5.31 Variation of undrained shear strengths with volume replacement ratio for all samples at p'_o = 50 kPa

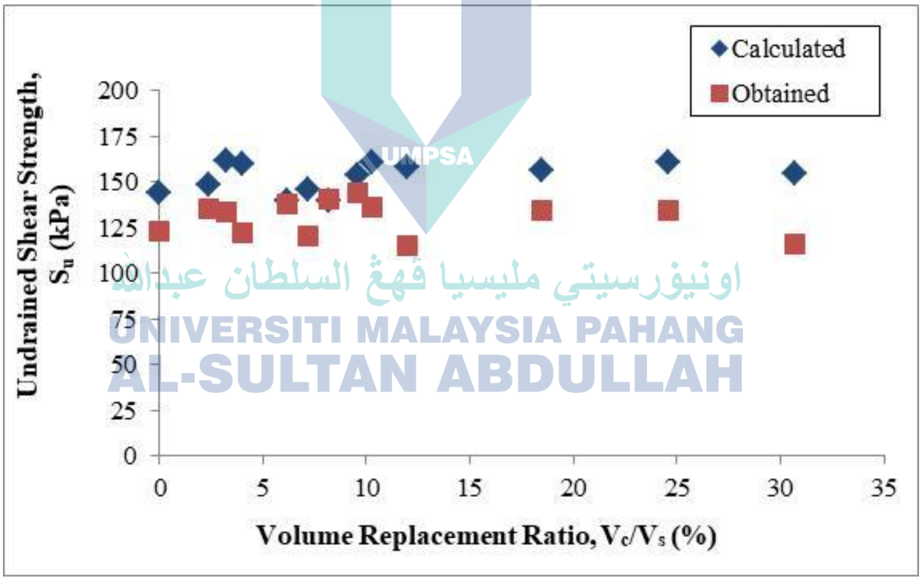

Figure 5.32 Variation of undrained shear strengths with volume replacement ratio for all samples at p'_o = 100 kPa

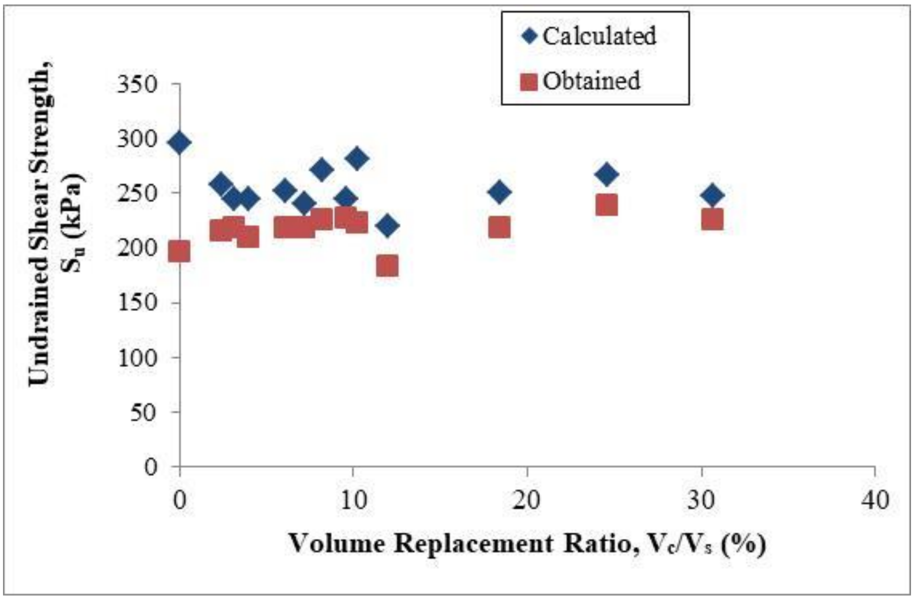

Figure 5.33 Variation of undrained shear strengths with volume replacement ratio for all samples at p'_o = 200 kPa

5.7.2 Variation of Undrained Shear Strength with Specific Volume

Table 5.5 presents an overview of the undrained shear strength and the variations in undrained shear strength for each sample. These variations correlate to the critical specific volume, which was equivalent to the initial specific volume. Figures 5.34 (a) to (c) illustrate the variation graphs between undrained shear strength and specific volume for samples with p'_o (effective confining pressure) of 50 kPa, 100 kPa, and 200 kPa.

Table 5.5 Undrained shear strength at critical state and the corresponding initial specific volume

Sample	Volume Replacement Ratio, Vc/Vs (%)	Effective Confining Pressure, σ'_3 or p'_o (kPa)	Undrained Shear Strength, S_u (kPa)	Specific Volume at Critical State, v
C	0	50	61.43	1.85
		100	122.85	1.80
		200	195.55	1.73
S1060	2.40	50	74.35	1.73
		100	135.66	1.70
		200	214.62	1.67

Table 5.5 Continued

Sample	**Volume Replacement Ratio, Vc/Vs (%)**	**Effective Confining Pressure, σ'_3 or p'_o (kPa)**	**Undrained Shear Strength, S_u (kPa)**	**Specific Volume at Critical State, v**
		50	82.04	1.75
S1080	3.20	100	133.34	1.72
		200	217.63	1.70
		50	79.49	1.73
S10100	4.00	100	122.31	1.69
		200	208.77	1.66
		50	71.45	1.77
S1660	6.15	100	138.38	1.74
		200	218.86	1.71
		50	79.75	1.74
S1680	8.19	100	140.68	1.72
		200	225.95	1.69
		50	76.20	1.73
S16100	10.24	100	136.20	1.72
		200	222.88	1.70
		50	71.38	1.79
G1060	7.20	100	120.81	1.75
		200	217.90	1.72
		50	77.21	1.76
G1080	9.60	100	144.34	1.73
		200	227.28	1.71
		50	76.90	1.73
G10100	12.00	100	115.59	1.70
		200	183.50	1.69
		50	72.80	1.74
G1660	18.45	100	134.68	1.71
		200	218.50	1.69
		50	71.82	1.70
G1680	24.57	100	134.45	1.67
		200	238.77	1.65
		50	53.78	1.69
G16100	30.72	100	116.10	1.67
		200	226.13	1.66

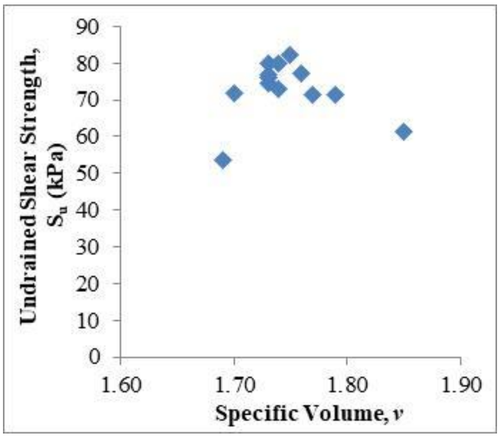

(a) p'_o = 50 kPa

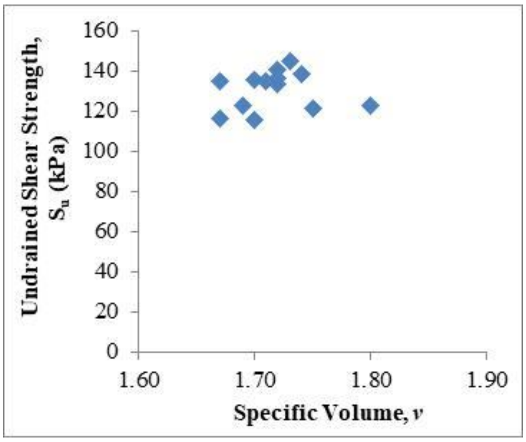

(b) p'_o = 100 kPa

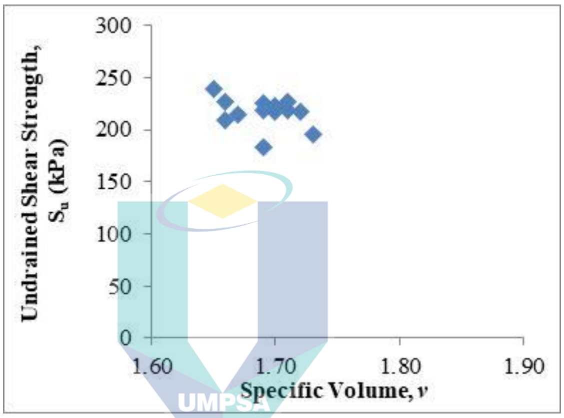

(c) p'_o = 200 kPa

Figure 5.34 Variation of undrained shear strength with specific volume

As shown in Figure 5.34, there is no obvious correlation between the change in undrained shear strength and the initial or critical specific volume, and there was none to be found in the scattered graph. Theoretically, as the initial specific volume increases, the undrained shear strength of pure fine-grained soil should decrease. The purpose of this was to find out if the soil had been consolidated with a low mean normal effective stress, p'_o, which is indicated by a high starting specific volume and a high soil moisture content. In contrast, the polypropylene columns used in this study to support the kaolin clay created a composite material with complex behaviour. As a result of the points' scatter, it was unable to establish a correlation between S_u and the initial specified volume.

Nevertheless, it was found that the volume of kaolin clay that had been replaced by polypropylene columns was generally correlated with the initial specific volume of the composite samples made of kaolin and polypropylene columns that were formed following the isotropic consolidation. As the volume replacement ratio increased, the initial specific volume decreased, as shown by the plots of the volume replacement ratio against the specific volume in Figure 5.35. This was to be expected, as during the consolidation step, voids may be shifted in proportion to the volume of polypropylene that replaces the kaolin clay. As a result, the initial specific volume before the shearing would be less (as opposed to the specific volume after the shearing as it was an undrained compression test).

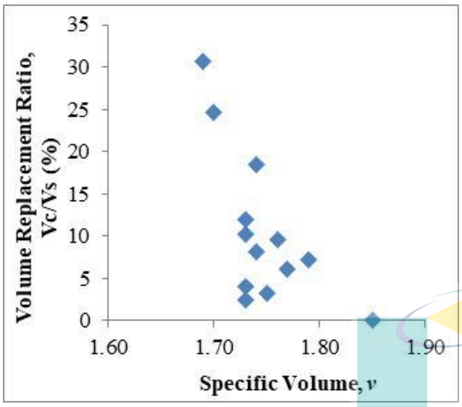

(a) p'_o = 50 kPa

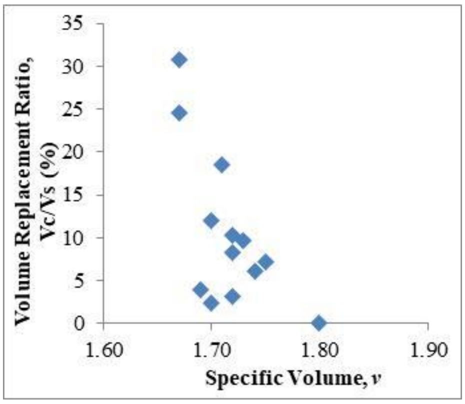

(b) p'_o = 100 kPa

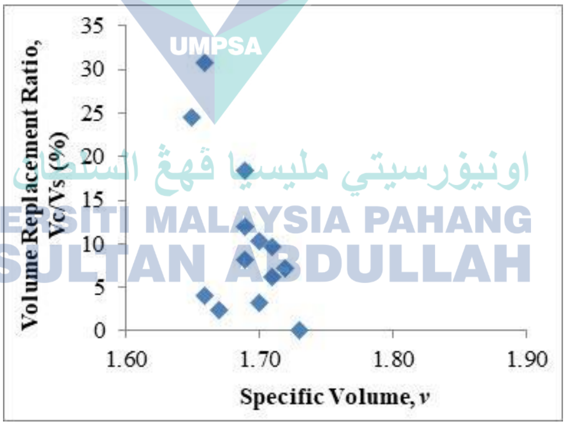

(c) p'_o = 200 kPa

Figure 5.35 Variation of volume replacement ratio with specific volume

5.7.3 Effect of Volume Replacement Ratio

The effect of the polypropylene reinforcement was determined by analysing the undrained shear strength of reinforced kaolin clay with a polypropylene volume replacement ratio and initial mean normal effective stresses p'_o of 50 kPa, 100 kPa, and 200 kPa. The graphs are shown in Figure 5.36. Generally, the graphs show that there is a correlation between S_u and the volume replacement ratio. However, while it indicates an increase in S_u with Vc/Vs for that range, the correlation seemed to be more noticeable for replacement up to 9.60%. Su afterwards decreased as Vc/Vs increased, but afterwards, within 18.45% of volume replacement, S_u gradually increased yet again. All the graphs also showed their peak at a volume replacement ratio of about 8.19%. After examining the samples illustrated in Figure 5.37 for increased undrained shear strength, it was also clear that the increased strength increased up to 10.24 % of the volume replacement ratio, which then decreased thereafter. This situation was more pronounced for p'_o of 50 kPa and 100 kPa, while for large p'_o of 200 kPa, most of the points showed a slight decrease in undrained shear strength (less than 10%). This might be due to the brittle nature of polypropylene, which at high confining pressure squeezes and crushes particles. Budhu (2007) observed that particle crushing affects the shearing resistance at high confining pressure, however, this makes it difficult to measure the exact contribution of crushing.

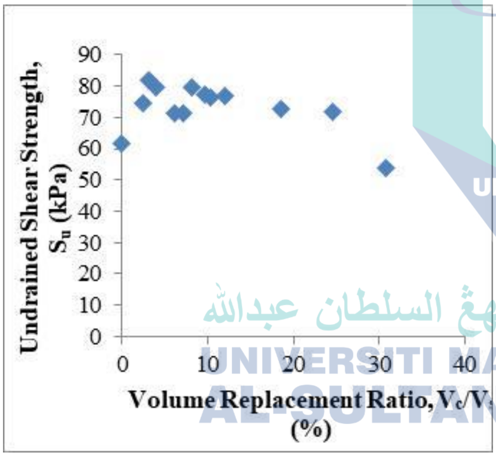

(a) p'_o = 50 kPa

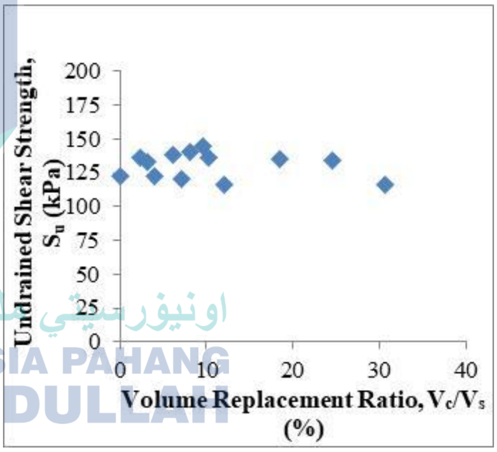

(b) p'_o = 100 kPa

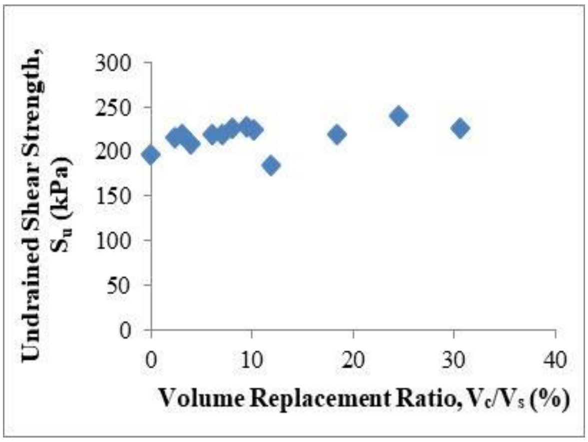

(c) p'_o = 200 kPa

Figure 5.36 Variation of undrained shear strength with volume replacement ratio

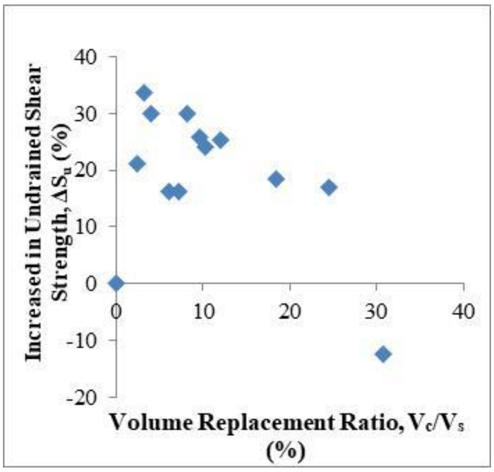

(a) p'_o = 50 kPa

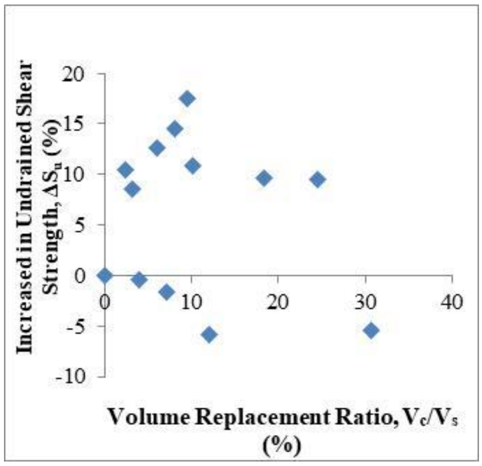

(b) p'_o = 100 kPa

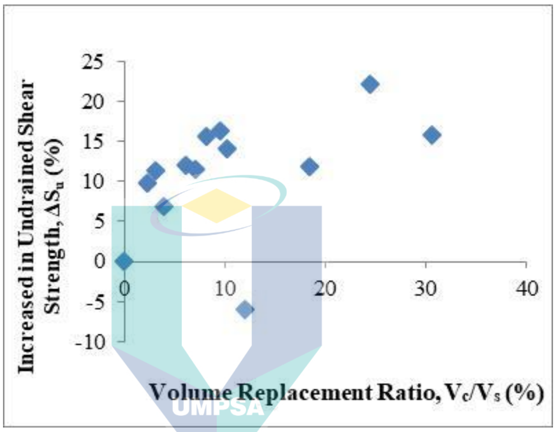

(c) p'_o = 200 kPa

Figure 5.37 Variation of the volume replacement ratio-induced increase in undrained shear strength

In the context of soil improvement work, such as replacing weak soils, it was determined that a volume replacement of 10% was both sufficient and economically acceptable. Therefore, a correlation was found within the range of 0 to 10% for establishing mean normal effective stresses of 50 kPa, 100 kPa, and 200 kPa. The findings are illustrated in Figure 5.38. The exponential equation that represents the correlation between the undrained shear strength, Su, and the volume replacement ratio,

$$S_u = A\, e^{B\left(\frac{Vc}{Vs}\right)} \qquad 5.15$$

Vc/Vs, has been calculated as follows:

In which A and B are constants that vary with p'_o. The plots of A versus p'_o and B versus p'_o shown in Figures 5.39 and 5.40, respectively resulted in linear graphs with the following equations:

$$A = 0.68p'_o \qquad 5.16$$

$$B = 0.035 - 8x10^{-05}p'_o \qquad 5.17$$

By substituting Equations 5.16 and 5.17 into Equation 5.15, the correlation between undrained shear strength and volume replacement ratio can be written as:

$$S_u = 0.68p'_o \exp[(0.035 - 8x10^{-05}p'_o)(\frac{Vc}{Vs})] \qquad 5.18$$

A design chart was then produced using Equation 5.18, as shown in Figure 5.41. Based on the presented chart, it is possible to determine the predicted undrained shear strength of the soil reinforced with polypropylene if the percentage of volume replacement has been selected and the initial mean normal effective stress is known.

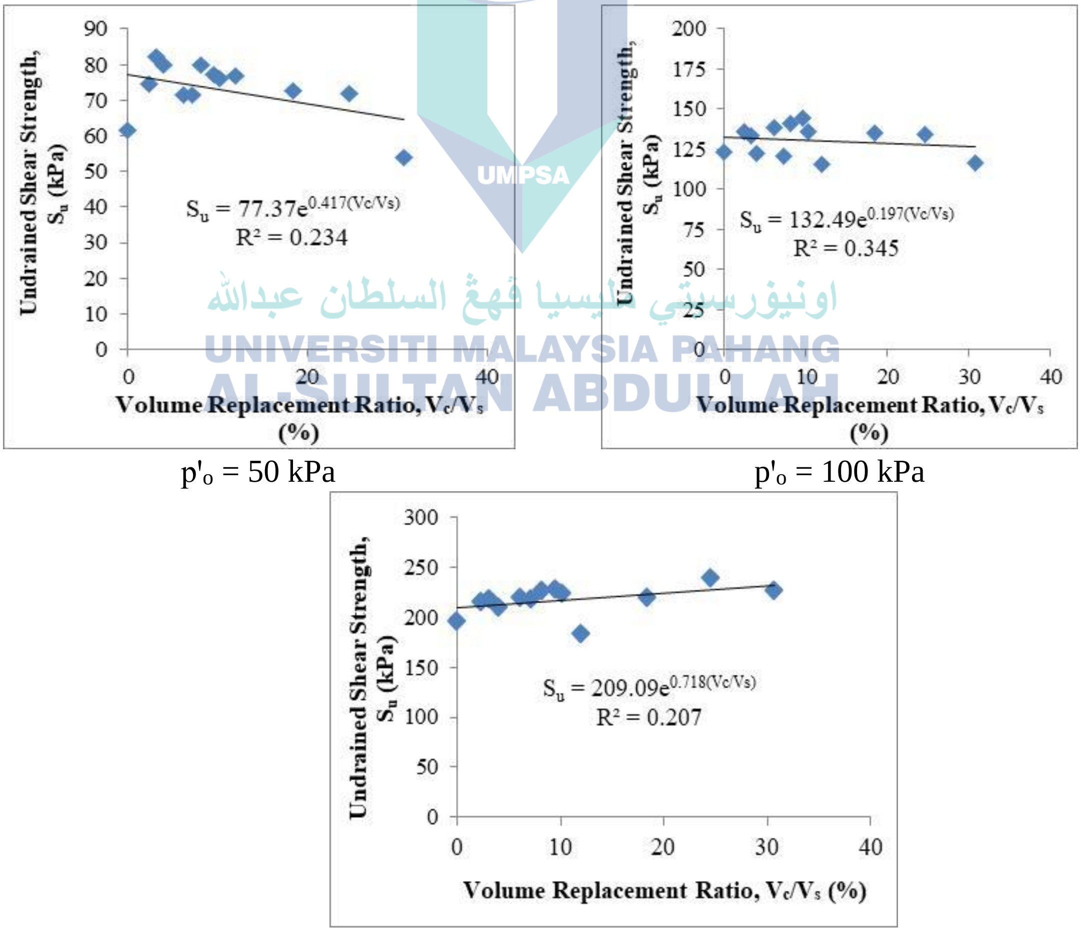

p'_o = 50 kPa

p'_o = 100 kPa

p'_o = 200kPa

Figure 5.38 Variation of undrained shear strength with volume replacement ratio

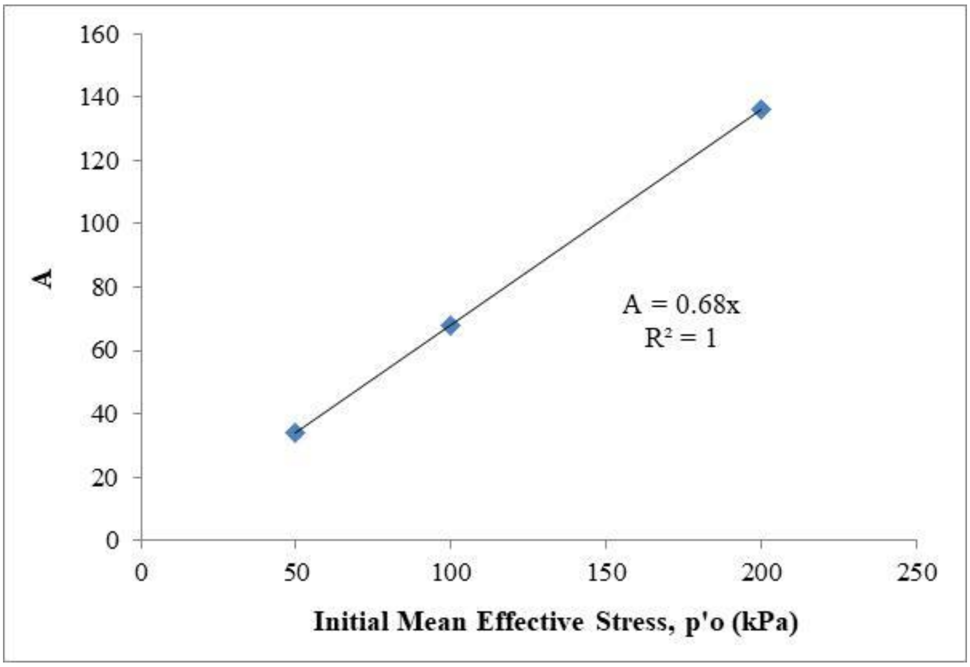

Figure 5.39 Correlation between a constant A and p'_o

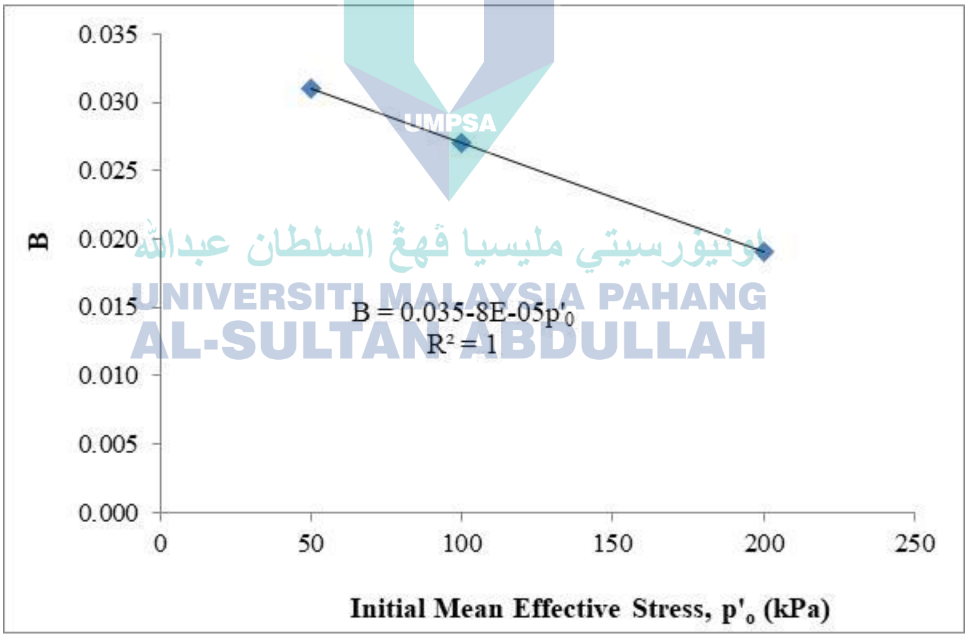

Figure 5.40 Correlation between a constant B and p'_o

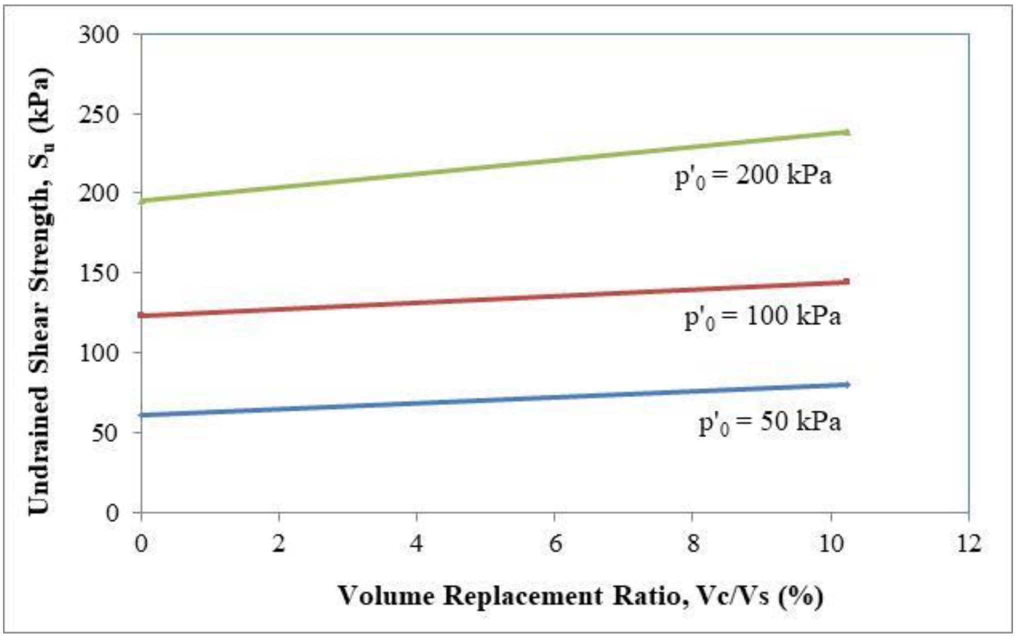

Figure 5.41 Design chart shows the undrained shear strength of kaolin clay reinforced with polypropylene at different volume replacement ratios

5.8 Summary of Critical State Analysis

The analysis of the CU triaxial test outcomes for kaolin reinforced with polypropylene columns within the critical state framework includes the incorporation of volume change in the failure criterion. The critical state parameters M, Γ, and λ were determined through analysis for all samples of isotropically normally consolidated kaolin clay, both unreinforced and reinforced with single and group polypropylene columns. The undrained shear strength can be calculated by evaluating the volume change indicated by the specific volume of the sample, based on the specific critical state parameters. During shearing, the ESP of the samples showed a typical normally consolidated soil behaviour in which all ESP curved towards the CSL to the left of TSP, which eventually achieved the critical state when ESP touched the CSL. A correlation and a design chart relating the undrained shear strength with the initial mean normal effective stress and volume replacement ratio was then established. This chart can be used to determine the undrained shear strength of soft, normally consolidated clay to be reinforced with polypropylene columns of a selected volume replacement ratio and a known initial mean normal effective stress.

CHAPTER 6

CONCLUSION AND RECOMMENDATION

6.1 Introduction

The research has been effectively conducted and achieved the predetermined objectives established at the outset of the study. The study aimed to examine the effectiveness of reinforcing soft clay by employing single and group polypropylene columns with different diameters and height penetrating ratios. The columns were arranged in a triangular configuration for the group. This chapter presents a detailed summary of the study findings and contributions of the research while also offering recommendations for future investigations.

6.2 Conclusion

The primary objective of this study was to examine the impact of polypropylene columns on the shear strength and compressibility properties of soft, normally consolidated clays. A laboratory testing programme was conducted to achieve the required objectives by using consolidated undrained triaxial tests. The design of foundation systems supported by soft, often consolidated clay is primarily impacted by short-term stability conditions. The fundamental principle of the polypropylene column revolves around the replacement of poor or unstable soils with stronger materials, hence improving the shear strength and compressibility of the soft soil for use in construction projects. The main purpose of the polypropylene granular column is to serve as a material for reinforcement. The existence of interstitial gaps between the polypropylene particles has the potential to speed up the dissipation of pore water pressure. Nevertheless, the primary determinant in the selection of polypropylene should be its strength, with drainage capability being a secondary criterion to be taken into consideration. Polypropylene, which is renowned for its high strength and stiffness, has been used to replace a portion of the soft soil samples in order to increase the shear strength. When comparing the reinforced soft kaolin clay samples to the control sample, which was not reinforced and without polypropylene columns, the findings demonstrate a significant enhancement in both shear strength and compressibility. The incorporation of polypropylene, a material exhibiting higher stiffness in comparison to the soft soil, led to a significant alteration in the strength properties of the soft soil. The conclusions of the study are presented in the sections that follow.

i. Determination of the physical and mechanical characteristics of kaolin clay and polypropylene

The plasticity chart indicates that kaolin has an LL of 36.60% and PI of 11.50%, which may be classed as low plasticity silt, organic silt of medium compressibility, or organic silt (ML). Furthermore, based on the AASHTO table, kaolin was classified under Group A-6. With a specific gravity of 2.63, kaolin was found to be within the range of inorganic silt. Additionally, the standard compaction test produced maximum dry density and optimum moisture content values of 1.63 g/cm^3 and 20%, respectively.

The plasticity chart classifies polypropylene into three groups: well-graded gravels (SW), little or no fines, and gravel-sand mixtures. Furthermore, according to the AASHTO chart, polypropylene was classified under Group A-1-a. Furthermore, utilising a vibratory table, the maximum density of polypropylene at 100% and 0% compaction was found to be 0.74 g/cm^3 and 0.57 g/cm^3, respectively.

ii. Evaluation of parameters effect on strength of the soft soil

The shear strength of both single and group polypropylene columns was improved by implementing an unconfined compression test, resulting in an improvement in shear strength by area replacement ratio. The polypropylene column with maximum shear strength at an 80 mm column height and an area replacement ratio (Ac/As) of 10.24% could also improve the shear strength. The observed increases in strength for single columns were found to be larger compared to those for group columns. The undrained shear strength exhibited the highest increments at an area replacement ratio of 10.24% when it reached a value of 5Dc.

For both single and group polypropylene columns, the shear strength improvements by height penetration ratio were determined using an unconfined compression test. Consistency was observed in the height penetrating ratio; the largest improvement was observed with a 16 mm penetrating single column with Hc/Hs = 0.8.

The results could suggest that, compared to the column's height over diameter ratio, the height penetrating ratio may be of greater significance to the clay soil's undrained shear strength.

Regarding the volume replacement ratio (Vc/Vs), the undrained shear strength showed improvement. The kaolin specimen's undrained shear strength improved as a result of the installation of the polypropylene column. Samples with an 80 mm height and a 16 mm single column diameter showed an increased shear strength of 74.50%, accordingly. However, shear strength increased when the volume replacement ratio approached 0.082.

iii. Analysing the effect of polypropylene columns using Mohr-Coulomb failure criteria and critical state failure criteria

The effective confining pressure significantly influenced soft clay's compressibility and shear strength reinforced with polypropylene columns. Under high confining pressure, clay reinforced with polypropylene columns could not function well. High surrounding pressures at high effective confining pressures squeezed polypropylene columns. Because polypropylene is brittle, it was squeezed because it could not withstand the pressure of the environment. This caused the polypropylene particles to be crushed and the spaces between them to be filled with crushed particles. Additionally, smearing conditions developed between clay and polypropylene. As a result, the polypropylene column developed a "clogging" state, making it difficult to adequately disperse the extra pore water from the clay specimens and speed up the water's dissipation.

Specific critical state parameters for every sample, M, Γ, and λ, were found by analysis using the critical state soil mechanics framework. "Mixtures of sand and gravel with fine-grained soils" was the group that the majority of M values associated with the soil polypropylene composites fell into since they vary between 1.18 and 1.30, which gives a variance on the angle of friction at a critical state between 30° and 35°.

iv. Establishing a correlation between volume replacement ratio and mean normal effective stress

In order to determine the effect of polypropylene reinforcement, the undrained shear strength for kaolin clay reinforced with various percentages of polypropylene replacement of volume had to be analysed. This analysis was carried out with different initial mean normal effective stresses, particularly at 50 kPa, 100 kPa, and 200 kPa. The observed relationship between undrained shear strength and volume replacement ratio appeared to be significantly greater through the range of up to 10.24% replacement. Subsequently, undrained shear strength decreased as the volume replacement ratio increased but it gradually rebounded after approximately 18.45% of volume replacement. Additionally, the outcome demonstrated that the undrained shear strength peaked at a volume replacement ratio of approximately 8.19%. The increased undrained shear strength increased to 10.24% of the volume replacement ratio, which decreased afterwards.

v. Formulation of a design chart using the critical state soil mechanics framework

Based on current literature, no such research studied the performance of clay-polypropylene composite materials using the critical state soil mechanics framework. It gives a promising perspective on how volume changes after failure. The requisite shear strength of the improved clay soil is comparable to the required shear strength of the vertical column. A design chart has been also developed to help engineers calculate the quantity of polypropylene required for the construction of the columns.

This research can tackle the limitations of conventional construction methods by harmonizing Polypropylene reinforced Kaolin Clay Columns. This research also heralds a paradigm shift in construction practices, redefining the boundaries of soil improvement, particularly for construction in soft clay areas. The method also suggested that this process will be economically scaled down to reduce costs in foundation and embankment building, particularly when employing by-product materials like polypropylene. To properly comprehend the nature of the improvement, however, extensive field experiments are needed.

6.3 Recommendations for Future Research

There is great promise for this field of research in the future. Based on the lab experiment results, soft clay soil's compressibility and shear strength can be significantly increased by adding polypropylene columns. The following are some suggestions and recommendations for potential future studies:

i) A greater array of effective confining pressure ratios should be used in the same investigation to discover the maximum pressure that a soft clay sample can withstand without failing.

ii) To compare the results of this investigation with the fieldwork, a full-scale test needs to be carried out. The reason for this is mostly attributed to the influential role played by the lateral support offered by the adjacent clay, which greatly affects the overall performance of the polypropylene material. On the ground, this is more accurate to reality.

iii) The passive resistance provided by the surrounding soil as a result of the polypropylene column's lateral expansion under axial stress is the primary source of the shear strength of clay reinforced with polypropylene columns. It is recommended for geosynthetic encasement be added inside the pre-drilled holes to improve the sample's capacity to support greater weight. More research can compare the improvement of soil shear strength using a sand column with and without the geosynthetic encasing.

iv) It is necessary to perform a numerical analysis to validate the results of this study.

v) More research should be done to determine the ideal diameter for installing a number of polypropylene columns into the soft clay. The space between the polypropylene columns must also be measured to prevent the influence zone from overlapping and reduce the sample's ability to support its weight.

REFERENCES

Abdelhamid, M., Ali, N., & Abdelaziz, T. (2023). A Literature Review of Factors Affecting the Behavior of Encased Stone Columns, *Geotechnical and Geological Engineering, Springer*, 1–36.

Adeniyi, A. G., Iwuozor, K. O., & Emenike, E. C. (2023). Material Development Potential of Nigeria's Kaolin. *Chemistry Africa*, Springer, 6(1), 9–25.

Adriyati, M. *et al.* (2023). Numerical analysis of combined surcharge preloading using prefabricated vertical drain and stone column on runway construction, *AIP Conference Proceddings*, 030001. https://doi.org/10.1063/5.0147483

Al-Khalili, A. M., Ali, A. S., & Al-Taie, A. J. (2021). Effect of metakaolin and silica fume on the engineering properties of expansive soil, *Journal of Physics: Conference Series*, 1895(1), 12017. https://doi.org/10.1088/1742-6596/1895/1/012017

Al-Obaidy, N., Jefferson, I., & Ghataora, G. (2016). Treatment of Iraqi collapsible soil using encased stone columns, *Japanese Geotechnical Society Special Publication*, The Japanese Geotechnical Society, 2(14), 564–569. https://doi.org/10.3208/jgssp.IRQ-01

Alaba, P. A., Sani, Y. M., & Daud, W. M. A. W. (2015). Kaolinite properties and advances for solid acid and basic catalyst synthesis, *RSC advances*, 122(5), 101127–101147. https://doi.org/10.1002/chin.201609232

Alrubaye, A. J., Hasan, M., & Fattah, M. Y. (2017). Stabilization of soft kaolin clay with silica fume and lime, *International Journal of Geotechnical Engineering*, 11(1), 90–96. https://doi.org/10.1080/19386362.2016.1187884

Alrubaye, A. J., Hasan, M., and Fattah, M. Y. (2018). Effects of using silica fume and lime in the treatment of kaolin soft clay, *Geomechanics and Engineering*, 14(3), 247–255. https://doi.org/10.12989/gae.2018.14.3.247

Annammala, K. V. *et al.* (2018). Environmental forensics: a multi-catchment approach to detect origin of sediment featuring two pilot projects in Malaysia, *Improving Flood Management, Prediction and Monitoring*. Emerald Publishing Limited, 49–61.

Ashour, S., Ghataora, G., & Jefferson, I. (2022). Behaviour of model stone column subjected to cyclic loading, *Transportation Geotechnics*, (35), 100777.

Aslani, M., Nazariafshar, J., & Ganjian, N. (2019). Experimental Study on Shear Strength of Cohesive Soils Reinforced with Stone Columns, *Geotechnical and Geological Engineering*, 37(3), 2165–2188. https://doi.org/10.1007/s10706-018-0752-z

Balaam, N. P., & Booker, J. R. (1981). Analysis of rigid rafts supported by granular piles, *International Journal for Numerical and Analytical Methods in Geomechanics*, 5(4), 379–403. https://doi.org/10.1002/nag.1610050405

Basack, S. *et al.* (2017). Modeling the stone column behavior in soft ground with special emphasis on lateral deformation, *Journal of Geotechnical and Geoenvironmental Engineering*, 143(6), 4017016. https://doi.org/10.1061/(ASCE)GT.1943-5606.0001652

Baziar, M. H., Saeedi Azizkandi, A., & Kashkooli, A. (2015). Prediction of pile settlement based on cone penetration test results: an ANN approach, *KSCE Journal of Civil Engineering. Springer*, (19), 98–106.

Beyene, A., Merka, H., & Tsige, D. (2023). Suitability analysis of vertically installed scoria gravel drains for enhancing consolidation performance of clayey ground, Results in Engineering. Elsevier, (17), 100975.

Black, J. A., Sivakumar, V., & Bell, A. (2011). The settlement performance of stone column foundations, *Géotechnique*, 61(11), 909–922.

Black, J. A., Sivakumar, V., & Bell, A. (2015). The settlement performance of stone column foundations. *Géotechnique*, 61(11), 909–922. https://doi.org/10.1680/geot.9.P.014.

Budsaereechai, S., Hunt, A. J., & Ngernyen, Y. (2019). Catalytic pyrolysis of plastic waste for the production of liquid fuels for engines, *RSC advances*, 9(10), 5844–5857. https://doi.org/10.1039/C8RA10058F

Casagrande, A. (1938). The shearing resistance of soils and its relation to the stability of earth dams, Proc. Soils Found. Conf.

Castro Gonzalez, J., & others (2017). Groups of encased stone columns: Influence of column length and arrangement, *Geotextiles and Geomembrane*, 45(2), 68-80. https://doi.org/10.1016/j.geotexmem.2016.12.001

Castro, J. (2016). An analytical solution for the settlement of stone columns beneath rigid footings, *Acta Geotechnica*, 11, 309–324. https://doi.org/10.1007/s11440-014-0358-4

Chambers, L. G. et al. (2016). Developing the scientific framework for urban geochemistry, *Applied Geochemistry*, 67, 1–20. https://doi.org/10.1016/j.apgeochem.2016.01.005

Chen, G. N. et al. (2020). Comparison of Adsorption Behaviors of Kaolin from Column and Batch Tests: Concept of Dual Porosity, Journal of Environmental Engineering, 146(9), 1–10. https://doi.org/10.1061/(asce)ee.1943-7870.0001792

Chen, J. F. et al. (2022). Effect of basal reinforcement on performance of floating geosynthetic encased stone column-supported embankment, *Geotextiles and Geomembranes*, 50(4), 566–580. https://doi.org/10.1016/j.geotexmem.2022.01.006

Cheng, G. et al. (2020). Experimental investigation of consolidation properties of nano-bentonite mixed clayey soil. Sustainability, 12(2), 459. https://doi.org/10.3390/su12020459

Chigondo, F., Nyamunda, B.C., & Bhebhe, V. (2015). Extraction of water treatment coagulant from locally abundant kaolin clays', *Journal of Chemistry*, 2, 1-7. https://doi.org/10.1155/2015/705837

Choudhury, D., Reang, R., & Paul, S. (2023). An Experimental Study to Determine the Best Aggregate Mix for Stone Columns. *Springer Nature*, 125–134. https://doi.org/0.1007/978-981-19-6727-6_12.

Correia, A. A. S., Venda Oliveira, P. J., & Custódio, D. G. (2015). Effect of polypropylene fibres on the compressive and tensile strength of a soft soil, artificially stabilised with binders', *Geotextiles and Geomembranes*, 43(2), 97–106. https://doi.org/10.1016/j.geotexmem.2014.11.008.

Damoerin, D., Prakoso, W. A., & Utami, Y. (2015). Improving shear strength of clay by using cement column reinforcement under consolidated undrained test, I*nternational Journal of Technology*, 6(4), 709–717.

Das, A. & Soni, D. K. (2015). Variation in the properties of kaolinite by varying the percentage of ground granulated blast furnace slag (GGBS) and lime added in kaolinite, *International Journal of Electronics, Electrical and Computational System*, 4(8), 260–266.

Das, B. M., & Sivakugan, N. (2018). *Principles of foundation engineerin*g. Cengage learning inc. , PP 233-239.

Deshpande, T. D. et al. (2021). Analysis of railway embankment supported with geosynthetic-encased stone columns in soft clays: a case study, *International Journal of Geosynthetics and Ground Engineering*, 07(2), 43.

Dill, H. G. (2020). A geological and mineralogical review of clay mineral deposits and phyllosilicate ore guides in Central Europe-A function of geodynamics and climate change, *Ore Geology Reviews*, 119, 103304.

Duan, Z. et al. (2023). Mechanical and microscopic properties of soil according to the rate of increase in pore water pressure, *Soil and Tillage Research*, 225, 105530.

Ellouze, S. et al. (2017). Numerical analysis of the installation effects on the behaviour of soft clay improved by stone columns, *Geomechanics and Geoengineering*, 12(2), 73–85.

Etezad, M., Hanna, A. M., & Ayadat, T. (2015). Bearing capacity of a group of stone columns in soft soil, *International Journal of Geomechanics*. 15(2), 4014043.

Farah, R. E., & Nalbantoglu, Z. (2020). Behavior of geotextile-encased single stone column in soft soils, *Arabian Journal for Science and Engineering*, 45, 3877–3890.

Grizi, A., Al-Ani, W. & Wanatowski, D. (2022) 'Numerical analysis of the settlement behavior of soft soil improved with stone columns', *Applied Sciences*. MDPI, 12(11), p. 5293.

Hájková, P. (2018) 'Kaolinite claystone-based geopolymer materials: Effect of chemical composition and curing conditions', Minerals, 8(10), 17–19. https://doi.org/10.3390/min8100444

Hameed, M. A., Abdel-Aleem, O. A., & Hassaballah, M. (2023) 'A secure data hiding approach based on least-significant-bit and nature-inspired optimization techniques, *Journal of Ambient Intelligence and Humanized Computing*, 14(5), 4639–4657.

Harbi, R., Derabla, R., & Nafa, Z. (2017). Improvement of the properties of a mortar with 5% of kaolin fillers in sand combined with metakaolin, brick waste and glass powder in cement, *Construction and Building Materials*, 152, pp. 632–641. https://doi.org/10.1016/j.conbuildmat.2017.07.062.

Hasan, M. et al. (2019). Shear strength of soft clay reinforced with encased lime bottom ash column (ELBAC), *International Journal of GEOMATE*, 16(57), 62–66. https://doi.org/10.21660/2019.57.4644.

Hasan, M., Ali, I., & Hyodo, M. (2019). Strength of soft clay reinforced with 10mm single crushed coconut shell (CCS) column, *International Journal of GEOMATE*, 17(63), 353–359. https://doi.org/10.21660/2019.63.81631.

Hasan, M. et al. (2018). The undrained shear strength of soft clay reinforced with group encapsulated lime bottom ash columns, *GEOMATE Journal*, 14(46), 46–50. https://doi.org/10.21660/2018.46.45208

Hasan, M. et al. (2016). Undrained shear strength of soft clay mixed with different percentages of lime and silica fume, *Jurnal Teknologi*, 78(5), 23–30. https://doi.org/10.11113/jt.v78.9606.

Hasan, M., & Samadhiya, N. K. (2016). Experimental and numerical analysis of geosynthetic-reinforced floating granular piles in soft clays, *International Journal of Geosynthetics and Ground Engineering*, 2, 1–13. https://doi.org/10.1007/s40891-016-0062-6

Hasan, M. (2015). Strength of Soft Clay Reinforced with Group Crushed Polypropylene (PP) Columns, *The Electronic Journal of Geotechnical Engineering*, 20, 12291–122308.

Hasan, M. (2013). Strength and Compressibility of Soft Clay Reinforced with Bottom Ash Column. Thesis Paper, Universitiy of Technology Malaysia, Malaysia.

He, H., Wang, Y. & Wang, J. (2019). Effects of Aggregate Micro Fines (AMF), Aluminum Sulfate and Polypropylene Fiber (PPF) on Properties of Machine-Made Sand Concrete, *Applied Sciences*, 9(11), 2250. https://doi.org/10.3390/app9112250

Head, K. H. (1980). Manual of soil laboratory testing. Pentech press London.

Hegde, A., & Sitharam, T. G. (2015). Use of bamboo in soft-ground engineering and its performance comparison with geosynthetics: experimental studies, *Journal of Materials in Civil Engineering*. American Society of Civil Engineers, 27(9), 4014256.

Hong, A. N. W. (2019). Undrained Shear Strength of Soft Clay Reinforced with Encapsulated Polypropylene Column', *Final Year Project Report*. Universiti Malaysia Pahang, Malaysia.

Hoque, M. I., Hasan, M., Islam, M. S., et al. (2023). Machine Learning Methods to Predict and Analyse Unconfined Compressive Strength of Stabilised Soft Soil with Polypropylene Columns, *Cogent Engineering*, 10(1), 2220492.

Hoque, M. I., Hasan, M., & Datta, S. D. (2019). Effect Of Waste Plastic Strip on The Shear Strength and Permeability Characteristics of Black Cotton Soil. *Journal of Applied Science and Engineering*, 27(2). https://doi.org/10.6180/jase.202402_27(2).0003

Hoque, M. I., Hasan, M., & Mim, N. J. (2023). Shear Strength of Soft Clay Reinforced with Single Encased Stone Dust Columns, *Jurnal Teknologi*, 85(5), 27–34.

Hugher, J. M. O., & Withers, N. J. (1974). Reinforcing of soft cohesive soils with stone columns', *Ground engineering*, 7(3).

Ismail, N., & Ani, F. N. (2015). Solid waste management and treatment in Malaysia. Applied Mechanics and Materials, *Trans Tech Publ*, 699, 969–974.

Jagadeesh, P. et al. (2022). Effect of natural filler materials on fiber reinforced hybrid polymer composites: An Overview, *Journal of Natural Fibers*, 19(11), 4132–4147.

Jala, S. K., Rawat, S., & Gupta, A. K. (2023). Effect of underreamed pervious concrete columns on load-carrying capacity of loose cohesionless soils. *International Journal of Geomechanics*, 23(3), 4022304.

Jones, C. J. F. P. (2013), *Earth reinforcement and soil structures*, Elsevier, PP 56-60

Kalantari, B. et al. (2015). Flow-induced crystallization of polypropylene in the presence of graphene nanoplatelets and relevant mechanical properties in nanocompsoite fibres, *Composites Part A: Applied Science and Manufacturing*, 76, 203–214.

Kalantari, B., & Rezazade, R. K. (2015). Compressibility behaviour of peat reinforced with precast stabilized peat columns and FEM analysis, *Geomech. Eng*, 9(4), 415–426.

Kaniraj, S. R., Huong, H. L., & Yee, J. H. S. (2011). Electro-osmotic consolidation studies on peat and clayey silt using electric vertical drain, *Geotechnical and Geological Engineering*, 29(3), 277–295.

Kasprzhitskii, A. et al. (2018). Mid-infrared spectroscopic assessment of plasticity characteristics of clay soils , Minerals, 8(5), 1–18. https://doi.org/10.3390/min8050184.

Kassim, A. M. H. (2017). Shear Strength of Soft Clay Reinforced with Polypropylene Column. *M.Sc. Engineering Thesis*, University Malaysia Pahang, Malaysia.

Kelesoglu, M. K., & Durmus, C. (2022). Numerical plane-strain modelling of stone columns: Installation process, single and group column behaviour, *KSCE Journal of Civil Engineering*, 26(8), 3402–3415.

Kirsch, K., & Kirsch, F. (2017). Ground improvement by deep vibratory methods. *Taylor & Francis*.

Kumar, A., & Srivastava, A. (2017). Preparation and mechanical properties of jute fiber reinforced epoxy composites, *Industrial Engineering & Management*, 6(4), 1000234.

Kumar, J., Mukherjee, S., & Pallepati, R. R. (2022). Bearing Capacity of Circular Foundations on Weak Cohesive Soils Reinforced with Stone Columns, *International Journal of Geomechanics*, 22(11), 4022186.

Kumar, P., & Mir, F. A. (2017). Improvement in Subgrade Characteristics of Soil Reinforced with Jute Fiber, *International Journal of Innovative Research in Science, Engineering and Technology*, 6(2), 2220–2224. https://doi.org/10.15680/IJIRSET.2017.0602133.

Kumari, N., & Mohan, C. (2021). Basics of clay minerals and their characteristic properties, Clay Clay Miner, 24(1).

Li, L.Y., Rajesh, S., & Chen, J.F. (2021). Centrifuge model tests on the deformation behavior of geosynthetic-encased stone column supported embankment under undrained condition, *Geotextiles and Geomembranes*, 49(3), 550–563.

Lima, B. T., Almeida, M. S. S., & Hosseinpour, I. (2022). Field measured and simulated performance of a stone columns-strengthened soft clay deposit, *International Journal of Geotechnical Engineering*, 16(6), 776–785.

Ling, J. et al. (2019). Analysis of airfield composite pavement responses using full-scale accelerated pavement testing and finite element method, *Construction and Building Materials*, 212, 596–606. https://doi.org/10.1016/j.conbuildmat.2019.03.336

Liu, J. et al. (2018). Experimental study on unconfined compressive strength of organic polymer reinforced sand, International Journal of Polymer Science. https://doi.org/10.1155/2018/3503415

Liu, Z. bin, Liu, S. yu., & Cai, Y. (2015). Engineering property test of kaolin clay contaminated by diesel oil, Journal of Central South University, 22(12), pp. 4837–4843. https://doi.org/10.1007/s11771-015-3035-3.

Liu, Z., Liu, S., & Cai, Y. (2015). Engineering property test of kaolin clay contaminated by diesel oil, *Journal of Central South University*, 22(12), 4837–4843

Lyu, H. et al. (2020). Analysis of compressibility and mechanical behavior of red clay considering structural strength, *Arabian Journal of Geosciences*, 13, 1–11.

Maakaroun, T., Najjar, S. S., & Sadek, S. (2009). Effect of Sand Columns on the Load Response of Soft Clays', in Contemporary Topics in Ground Modification, Problem Soils, and Geo-Support, *Reston, VA: American Society of Civil Engineers*, 217–224. https://doi.org/10.1061/41023(337)28.

Maddah, H. A. (2016). Polypropylene as a promising plastic: A revie, *American Journal of Polymer Science*, 6(1), 1–11.

Malakar, S., & Sultana, P. (2021). Study of Bearing Capacity of Shallow Foundation on Bamboo Geotextile-Reinforced Clayey Bed, *Indian Geotechnical Conference*, 1–12.

Manzoor, S. O., & Yousuf, A. (2020). Stabilisation of soils with lime : a review. *Journal of Materials and Environmental Science*, 11(9), 1538–1551.

Marto, A. (1996) Volumetric Compression of a Silt Under Periodic Loading: An Experimentally Based Effective Stress Volumetric Compression Model for Isotropically and Anisotropically Consolidated Silt Subjected to Undrained Two-way Cyclic Loading with Drainage Periods.

Marto, A. et al. (2016). Bearing capacity of soft clay installed with singular and group of encased bottom ash columns, *Jurnal Teknologi*, 78(7–3), 105–110.

Mathew, A., & Sasikumar, A. (2017). Performance of Soft Soil Reinforced With Bamboo and Geonet. *International Research Journal of Engineering and Technology*, 04(11), 646–649.

Maxim, L.D., Niebo, R., & McConnell, E.E. (2016). Bentonite toxicology and epidemiology-a review, *Inhalation toxicology*, 28(13), 591–617.

Mirabi, M., Hadadkazarji, M. & Abbasi, M. (2021). Recycling of construction and demolition gypsum wastes as stabilizer of soft clay soil and effects of drying-rewetting frequency on the treated soil stability, *Environmental Resources Research*, 9(2), 117-132. https://doi.org/10.22069/IJERR.2021.15541.1250.

Mirzababaei, M. et al. (2018). Effect of fiber reinforcement on shear strength and void ratio of soft clay. *Geosynthetics International*, 25(4), 471–480.
https://doi.org/10.1680/jgein.18.00023.

Mohamad, N. O. et al. (2016). Challenges in construction over soft soil-case studies in Malaysia, *IOP conference series: materials science and engineering*, 12002.

Mohamad, N. O. et al. (2016). Challenges in Construction over Soft Soil - Case Studies in Malaysia, *IOP Conference Series: Materials Science and Engineering*, 136(1). https://doi.org/10.1088/1757-899X/136/1/012002.

Mohanty, P., & Samanta, M. (2015). Experimental and numerical studies on response of the stone column in layered soil, *International Journal of Geosynthetics and Ground Engineering*, 1, 1–14.

Mohapatra, S. R., Rajagopal, K., & Sharma, J. (2016). Direct shear tests on geosynthetic-encased granular columns, *Geotextiles and Geomembranes*. Elsevier, 44(3), 396–405.

Mokhtari, M., & Kalantari, B. (2012). Soft Soil Stabilization using Stone Column-A Review., *Electronic Journal of Geotechnical engineering*, 17, 1459–1466.

Moradi, R. et al. (2018). Bearing capacity of soft soil model treated with end-bearing bottom ash columns, *Environmental Earth Sciences*, 77(3), 100. https://doi.org/10.1007/s12665-018-7287-8.

Mousavi, S. E., & Wong, L. S. (2016). Permeability characteristics of compacted and stabilized clay with cement, peat ash and silica sand. *Civil Engineering Infrastructures Journal (Ceij)*, 49(1), 149-164. https://doi.org/10.7508/CEIJ.2016.01.011

Najjar, S. S. et al. (2020). Drained triaxial response of clay reinforced with sand columns, *Proceedings of the Institution of Civil Engineers-Ground Improvement*, 173(3), 170–186.

Namikawa, T. (2016). Conditional Probabilistic Analysis of Cement-Treated Soil Column Strength, *International Journal of Geomechanics*, 16(1). https://doi.org/10.1061/(ASCE)GM.1943-5622.0000481.

Noor Muneerah PG Haji Jeludin, D. K. et al. (2016). Experimental observations of settlement of footings supported on soft clay reinforced with granular columns: laboratory model study, *Journal of Geotechnical and Geoenvironmental Engineering*, 142(1), 4015063.

Oyegbile, B. O., & Oyegbile, B. A. (2017). Applications of geosynthetic membranes in soil stabilization and coastal defence structures. *International Journal of Sustainable Built Environment*, 6(2), 636–662. https://doi.org/10.1016/j.ijsbe.2017.04.001.

Ozbakkaloglu, T., Gu, L., & Gholampour, A. (2017). Short-term mechanical properties of concrete containing recycled polypropylene coarse aggregates under ambient and elevated temperature, *Journal of materials in Civil Engineering*, 29(10), 4017191.

Pham, B. T. et al. (2018). Prediction of shear strength of soft soil using machine learning methods, *Catena* , 66(2), 181–191. https://doi.org/10.1016/j.catena.2018.04.004.

Pham, B. T. et al. (2020). A novel hybrid soft computing model using random forest and particle swarm optimization for estimation of undrained shear strength of soil, *Sustainability*, 12(6), 1–16. https://doi.org/10.3390/su12062218.

Podin, Y. et al. (2006). Sentinel surveillance for human enterovirus 71 in Sarawak, Malaysia: lessons from the first 7 years, *BMC public health*, 6, 1–10.

Powrie, W. (2018). Soil mechanics: concepts and applications. CRC Press.

Prakash, K. G. et al. (2022). An embankment stability analysis using finite element method constructed over soft consolidating soil improved from lime columns and prefabricated vertical drains. *Engineered Science*, 17, 309-318.

Rathod, D., Abid, M. S., & Vanapalli, S. K. (2021). Performance of polypropylene textile encased stone columns, *Geotextiles and Geomembranes*, 49(1), 222–242. https://doi.org/10.1016/j.geotexmem.2020.10.025.

Rehman, W. U. et al. (2023). Exfoliation characteristics of Swat vermiculite clay and its application in the preparation of lightweight composite panels, *Construction and Building Materials*, 366, 130200.

Romanello, M. et al. (2021). The 2021 report of the Lancet Countdown on health and climate change: code red for a healthy future, *The Lancet*, 398(10311), 1619–1662.

Roshan, M. J. et al. (2023). Application of self-sensing cement-stabilized sand for damage detection, *Construction and Building Materials*, 403, 133080.

Saadi, N., Ismail, Z., & Alias, Z. (2016). A review of construction waste management and initiatives in Malaysia, *Journal of Sustainability Science and Management*, 11(2), 101-114.

Saberian, M. et al. (2023). Mechanical properties of polypropylene fibre reinforced recycled concrete aggregate for sustainable road base and subbase applications, *Construction and Building Materials*, 405, 133352. https://doi.org/10.1016/j.conbuildmat.2023.133352.

Salimnezhad, A., Soltani-Jigheh, H., & Soorki, A. A. (2021). Effects of oil contamination and bioremediation on geotechnical properties of highly plastic clayey soil, *Journal of Rock Mechanics and Geotechnical Engineering*, 13(3), 653–670.

Santos Jr, O. F., Lacerda, W. A., & Ehrlich, M. (2020). Effects of cyclic variations of pore pressure on the behaviour of a gneiss residual soil, *Geotechnical and Geological Engineering*. *Springer*, 38(5), 5201–5212.

Sany, S. B. T. et al. (2019). The west coast of Peninsular Malaysia, *World seas: An environmental evaluation*, pp- 437–458.

Sasikumar, J. (2016). A study on the effect of salt solu-tions on certain geotechnical properties of two clays. I*nternational Journal of Scientific Research in Science, Engineering and Technology*, 2(5), 33–136.

Schofield, A. N., & Wroth, P. (1968). Critical state soil mechanics, McGraw-hill London.

Sexton, B. G. et al. (2016). Stone column settlement performance in structured anisotropic clays: the influence of creep. *Journal of Rock Mechanics and Geotechnical Engineering*, 8(5), 672–688.

Shehata, H. F., Sorour, T. M., & Fayed, A. L. (2021). Effect of stone column installation on soft clay behavior, *International Journal of Geotechnical Engineering*, 15(5), 530–542. https://doi.org/10.1080/19386362.2018.1478245.

Sobhan, K., Das, B. M., & Zahid Reza, R. M. (2013). Characterization of soft organic subgrade using Piezocone penetration testing. Geotechnical and Geophysical Site Characterization 4 - *Proceedings of the 4th International Conference on Site Characterization 4*, ISC -4(2), 1543–1549.

Spagnoli, G. et al. (2018). Statistical variability of the correlation plasticity index versus liquid limit for smectite and kaolinite, *Applied Clay Science*, 156, 152–159.

Subramani, T., & Udayakumar, D. (2016). Experimental study on stabilization of clay soil using coir fibre, *International Journal of Application or Innovation in Engineering Management Decision*, 5, 192–204.

Sun, J. et al. (2023). Experimental Investigation of Mechanical Properties of Clay-Cement Slurry Containing Graphene Oxide. Applied Sciences, 13(14), 8452.

Taylor, D. W. (1948) Fundamentals of soil mechanics. LWW.

Thakur, A., Rawat, S., & Gupta, A. K. (2021a). Experimental and numerical modelling of group of geosynthetic-encased stone columns, *Innovative Infrastructure Solutions*, 6, 1–17.

Thakur, A., Rawat, S., & Gupta, A. K. (2021b). Experimental study of ground improvement by using encased stone columns, *Innovative Infrastructure Solutions*. 6, 1–13.

Tomar, A., Sharma, T., & Singh, S. (2020). Strength properties and durability of clay soil treated with mixture of nano silica and Polypropylene fiber, *Materials Today: Proceedings*, 26, 3449–3457.

Tsige, D., Korita, M., & Beyene, A. (2022). Deformation analysis of cement modified soft clay soil using finite element method (FEM), *Heliyon*, 8(6), 09613. https://doi.org/10.1016/j.heliyon.2022.e09613.

Valipour, A. et al. (2017). Hybrid SWARA-COPRAS method for risk assessment in deep foundation excavation project: An Iranian case study, *Journal of civil engineering and management*, 23(4), 524–532.

Wang, B. et al. (2022). Sensitivity analysis of factors affecting the bearing capacity of suction bucket foundation in soft clay, *Sustainability*, 14(15), 9615. https://doi.org/10.3390/su14159615

Wang, Y. X. et al. (2017). Laboratory Investigation on Strength Characteristics of Expansive Soil Treated with Jute Fiber Reinforcement. *International Journal of Geomechanics*, 17(11). https://doi.org/10.1061/(ASCE)GM.1943-5622.0000998.

Xiao, Y. et al. (2016). Influence of particle breakage on critical state line of rockfill material, *International Journal of Geomechanics*, 16(1), 4015031.

Yahaya, S. et al. (2017a). Chemical composition and particle size analysis of kaolin. *Traektoriâ Nauki Path of Science*, 3(10), 1001–1004.

Yahaya, S. et al. (2017b). Chemical Composition and Particle Size Analysis of Kaolin. P*ath of Science*, 3(10), 1001–1004. https://doi.org/10.22178/pos.27-1.

Yin, S. et al. (2015). Fiber preparation and mechanical properties of recycled polypropylene for reinforcing concrete. *Journal of Applied Polymer Science*, 132(16).

Yusuf, N. (2015). Strength of Soft Clay Reinforced with Group Crushed Polypropylene (PP) Columns. UMP.

Zaidi, A., Khan, M. K., & Hussain, S. M. A. (2016). Enhancement in Engineering Properties of Soil Reinforced with Jute Fiber, I*nternational Journal of Emerging Technologies in Engineering Research*, 4(4), 96–98.

Zaini, M. S. I., & Hasan, M. (2023). Effect of Optimum Utilization of Silica Fume and Lime On the Stabilization of Problematic Soils. *International Journal of Integrated Engineering*, 15(1), 352–366.

Zaini, M. S. I., Hasan, M. & Jusoh, W. N. B. W. (2023). Utilization of bottom ash waste as a granular column to enhance the lateral load capacity of soft kaolin clay soil, *Environmental Science and Pollution Research.* 1–27.

Zhang, L., & Zhao, M. (2015). Deformation analysis of geotextile-encased stone columns, *International Journal of Geomechanics*. 15(3), 4014053.

Zhang, T. et al. (2017). Preparation and rheological properties of attapulgite gel for aqueous suspensions', *7th International Conference on Education, Management, Computer and Medicine*, 547–559.

Zhang, X. et al. (2020). Performance evaluation of a MICP-treated calcareous sandy foundation using shake table tests', Soil Dynamics and Earthquake Engineering,129, 105959.

Zukri, A., & Nazir, R. (2018). Sustainable materials used as stone column filler: A short review', *IOP Conference Series: Materials Science and Engineering*, 12001.

APPENDICES

Appendix A: Sieve analysis test result

Sample: Kaolin S300

Test Method: BS1377: Part 4: 1990: 3.3

Dated Test: 06.01.2022

Mass of Sample = 500gm

Sieve size (mm)	Mass of Soil Retained (gm)	Percentage Retained (%)	Cumulative Percent Retained (%)	Percent Passing (%)
1.20	0	0.0	0.0	100.0
1.00	0	0.0	0.0	100.0
0.60	0	0.0	0.0	100.0
0.30	0	0.0	0.0	100.0
0.150	0	0.0	0.0	100.0
0.125	1.0	0.20	0.20	99.80
0.105	3.50	0.70	0.90	99.10
0.088	7.50	1.50	2.40	97.60
0.074	80.00	16.00	18.40	81.60
0.063	116.00	23.20	41.60	58.40
0.053	147.00	29.40	71.00	29.00
0.044	83.00	16.60	87.60	12.40
0.037	62.00	12.40	100	0
0.022	0	0	100	0
0.010	0	0	100	0

Sample: Polypropylene

Test Method: BS1377: Part 2: 1990: 9.3

Dated Test: 05.02.2022

Weight of Sample Used = 500gm

Sieve size (mm)	Mass of Soil Retained (gm)	Percentage Retained (%)	Cumulative Percent Retained (%)	Percent Passing (%)
9.5	0	0.0	0.0	100.0
4.75	0	0.0	0.0	100.0
3.35	278.45	55.70	55.70	44.30
2.36	120.35	24.00	79.70	21.30
1.20	70.70	14.15	93.85	6.15
1.00	30.50	6.15	100.0	0.0
0.60	0	0.0	100.0	0.0
0.30	0	0.0	100.0	0.0
0.15	0	0.0	100.0	0.0
0.063	0	0.0	100.0	0.0

Appendix B: Hydrometer test result

Sample: Kaolin S300

Test Method: BS 1377: Part 2: 1990: 9.6

Dated Test: 18.02.2022

Meniscus Correction, $C_m = 0$

Reading in Dispersant, $R_o' = 1.0005$

Dry Mass of Soil, m = 50gm

Particle Density = 2.62

Date	Time	Elapsed Time, t (min)	Temp. T (ºC)	Hydrometer Reading, R_h'	True Reading R_h	Effective Depth, H_R (mm)	Modified Reading R_d	Particle Diameter D (mm)	Percentage Finer, K (%)
12.01.22	8.30 am	0	26.3						
12.01.22	8.31 am	0.5	26.3	1.0090	1.0090	83.976	0.0085	0.0528	2.8
12.01.22	8.32 am	1	26.3	1.0085	1.0085	82.044	0.0080	0.0369	2.6
12.01.22	8.34 am	2	26.3	1.0080	1.0080	80.112	0.0075	0.0258	2.4
12.01.22	8.38 am	4	26.3	1.0075	1.0075	78.18	0.0070	0.0180	2.3
12.01.22	8.46 am	8	26.3	1.0070	1.0070	76.248	0.0065	0.0126	2.1
12.01.22	9.00 am	16	26.2	1.0060	1.0060	72.384	0.0055	0.0087	1.8
12.01.22	9.30 am	30	26.1	1.0050	1.0050	68.52	0.0045	0.0062	1.5
12.01.22	10.30 am	60	26.2	1.0035	1.0035	62.724	0.0030	0.0042	1.0
12.01.22	12.30 pm	120	26.2	1.0030	1.0030	60.792	0.0025	0.0029	0.8
12.01.22	4.30 pm	240	26.3	1.0025	1.0025	58.86	0.0020	0.0021	0.7
13.01.22	4.30 pm	1440	26.3	1.0005	1.0005	51.132	0.0000	0.0008	0.0

Appendix C: Atterberg limit test result

Sample: Kaolin S300

Test Method: BS 1377: Part 2: 1990: 4.3 & 5.3

Dated Test: 10.01.2022

Liquid Limit

Test	1		2		3	
Cone Penetration (mm)	18.50	18.50	22.50	22.50	27.50	27.50
Average Penetration (mm)	18.50		22.50		27.50	
Container No.	A	B	C	D	E	F
Container Weight (gm)	10.50	9.50	15.00	15.50	14.65	15.10
Wet Soil + Container (gm)	22.75	23.55	27.05	27.80	27.05	26.15
Wet Soil, W_w (gm)	12.25	14.05	12.05	12.30	12.40	11.05
Dry Soil + Container (gm)	19.58	19.92	23.90	24.60	23.75	23.20
Dry Soil, W_d (gm)	9.08	10.42	8.90	9.10	9.10	8.10
Moisture Loss, $W_w - W_d$ (gm)	3.17	3.63	3.15	3.20	3.30	2.95
Moisture Content, $(W_w - W_d)/W_d$ (%)	34.91	34.84	35.39	35.16	36.26	36.42
Average Moisture Content (%)	34.87		35.28		36.34	
Liquid Limit (%)	35.50					

Plastic Limit:

Container No.	G	H
Container Weight (gm)	23.10	23.50
Wet Soil + Container (gm)	40.40	40.10
Wet Soil, W_w (gm)	17.30	16.60
Dry Soil + Container (gm)	36.90	36.80
Dry Soil, W_d (gm)	13.80	13.30
Moisture Loss, $W_w - W_d$ (gm)	3.50	3.30
Moisture Content, $(W_w - W_d)/W_d$ (%)	25.36	24.81
Average Moisture Content (%)	25.10	

Plastic Index (PI) = LL – PL

= 35.50 – 25.10

= 10.40 %

Linier Shrinkage:

Sample Initial Length (mm)	140
Oven-dried Length (mm)	120
Liner Shrinkage	14.29 %

Appendix D: Relative density test result

Sample: Polypropylene

Test Method: BS1377: Part 2: 1990: 9.3

Dated Test: 04.03.2022

Mould Diameter = 15.10 cm

Mould Height = 15.10 cm

Volume of the Mould = 2702.72cm^3

Minimum Density Determination (0% Relative Density)

Test Sample No.	1	2
Mass of Mould, m_1 (gm)	9300	9300
Mass of Mould + Soil, m_2 (gm)	10850	10850
Mass of Soil, $m_a = m_2 - m_1$ (gm)	1550	1550
Minimum Density of soil, $\rho_a = m_a/V$ (gm/cm^3)	0.57	0.57
Average Minimum Density (gm/cm^3)	0.57	

Maximum Density Determination (100% Relative Density)

Test Sample No.	1				2			
Gauge Reading (cm)	2.10	2.16	2.21	2.26	2.12	2.18	2.23	2.27
Average Gauge Reading (cm)	2.21				2.23			
Gauge Reading + Plate Thickness (cm)	3.44				3.45			
Mass of Mould, m_3 (gm)	9300				9300			
Mass of Mould + Soil, m_4 (gm)	10850				10850			
Mass of Polypropylene, $m_b = m_4 - m_3$ (gm)	1550				1550			
Volume of Polypropylene, V_s (cm^3)	2087.00				2085.81			
Maximum density of Polypropylene, $\rho_b = m_b/V_s$ (gm/cm^3)	0.74				0.74			
Average Maximum Density (gm/cm^3)	0.74							

Appendix E: Sacrifice gravity test result

Sample: Kaolin S300

Test Method: BS 1377: Part 2: 1990: 8.3

Dated Test: 04.01.2022

Specimen Reference	1	2	3
Mass of Bottle	20.85	27.25	27.70
Mass of Bottle + Stopper, m_1 (gm)	27.20	33.65	32.80
Mass of Bottle + Stopper + Dry Soil, m_2 (gm)	37.40	43.40	42.80
Mass of Bottle + Stopper + Soil + Water, m_3 (gm)	84.00	89.35	89.48
Mass of Bottle + Stopper + Water, m_4 (gm)	77.70	83.30	83.28
Mass of Dry Soil, $m_2 - m_1$ (gm)	10.20	9.75	10.00
Mass of Water in Full Bottle, $m_4 - m_1$ (gm)	50.50	49.65	50.48
Mass of Water Used, $m_3 - m_2$ (gm)	46.60	45.95	46.68
Particle Density, ρ_s (Mg/m^3)	2.62	2.64	2.63
Average Particle Density, ρ_s (Mg/m^3)	2.63		

Appendix F: Standard compaction test result

Sample: Kaolin S300

Test Method: BS 1377: Part 4: 1990: 3.3

Dated Test: 14.01.2022

Water Content	5%		10%		15%		20%		25%		30%	
Mass of Mould + Base, m_1 (gm)	5580		5580		5580		5580		5580		5580	
Mass of Mould + Base + Compacted Specimen, m_2 (gm)	7070		7220		7340		7460		7330		7294	
Mass of Compacted Specimen, $m_2 - m_1$ (gm)	1490		1640		1760		1880		1750		1714	
Bulk Density, ρ (gm/cm^3)	1.57		1.72		1.85		1.97		1.84		1.8	
Moisture Content Container No.	A	B	C	D	E	F	G	H	I	J	K	L
Container Weight (gm)	14.25	15.05	14.95	14.65	14.20	13.70	15.20	14.65	13.30	14.15	24.57	23.57
Wet Soil + Contain (gm)	31.65	34.75	35.60	36.85	37.80	34.45	37.80	36.20	40.40	35.70	31.60	32.60
Wet Soil, W_w (gm)	17.40	19.70	20.65	22.20	23.60	20.75	22.60	21.55	27.10	21.55	7.03	9.03
Dry Soil + Contain (gm)	30.75	33.75	33.65	34.75	34.70	31.70	33.95	32.55	34.95	31.35	30.05	30.61
Dry Soil, W_d (gm)	16.50	18.70	18.70	20.10	20.50	18.00	18.75	17.90	21.65	17.20	5.48	7.04
Moisture Loss, $W_w - W_d$ (gm)	0.90	1.00	1.95	2.10	3.10	2.75	3.85	3.65	5.45	4.35	1.55	1.99
Moisture Content, $(W_w - W_d)/W_d$ (%)	5.45	5.35	11.50	10.45	15.59	15.83	20.53	21.51	25.17	25.29	28.28	28.27
Average Moisture Content, W_{avg} (%)	5.40		10.97		15.76		21.02		25.23		28.28	
Dry Density, γ_d (kN/m^3)	1.48		1.55		1.60		1.63		1.47		1.40	

Appendix G: Falling head test result

Sample: Kaolin S300

Test Method: ASTM D 2434

Dated Test: 26.03.2022

Diameter = 100 mm

Length, L = 150mm

Area, A = 7850.00 mm^2

Manometer Tube	Diameter (m)	Start Level, h_1 (m)	End Level, h_2 (m)	Time, t (s)
T1	0.0200	1.0000	0.4530	7200
T2	0.0110	1.0000	0.5430	1800
T3	0.0040	1.0000	0.4510	360
T4	0.0038	1.0000	0.3940	360

Manometer Tube	h_1/h_2	$\log_{10}(h_1/h_2)$	Time, t (s)	Area Manometer Tube, a (mm^2)	A*t	K (m/s)
T1	2.208	0.792	7200	3.14E+02	565200000.00	2.53E-11
T2	1.842	0.611	1800	9.50E+01	141300000.00	2.36E-11
T3	2.217	0.796	360	1.26E+01	28260000.00	2.04E-11
T4	2.538	0.931	360	1.13E+01	28260000.00	2.15E-11
Average						2.27E-11

Permeability $K = 3.84\ x\ \frac{aL}{At}\ x\ \log_{10}\left(\frac{h_1}{h_2}\right)\ x\ 10^{-5}$

Appendix H: Constant head permeability test result

Sample: Polypropylene

Test Method: ASTM D 2434

Dated Test: 25.03.2022

Length of Soil Specimen = 21.4 cm

Diameter of Soil Specimen =7.42 cm

Area of Permeameter = 43.22 cm^2

Volume of Soil Specimen = 924.89 cm^3

Dry Mass of Soil + Pan = 1850 gm

Dry Mass of Soil = 1520 gm

Dry Density of Soil = 1.64 gm/cm^3

Trial Number	Constant Head, h (cm)	Elapsed Time, t (s)	Outflow Volume, Q (cm^3)	Water Temperature, T	K_T (cm/s)	K_{20} (cm/s)
1	60	66	1000	25	0.00974	0.00865
2	70	74	1000	25	0.00744	0.00666
3	80	81	1000	25	0.00595	0.00528
4	90	162	1000	25	0.00264	0.00234
Average K_{20}						0.00573

K_{20} = 5.73E-03 m/s

Permeability, K = $\frac{q}{Ai\ x\ 60}$ and $q = \frac{Q}{t}$

Appendix I: Unconfined compression test (UCT)

Reference: BS 1377: Part 7: 1990: Clause 8.0

Sample Height	100	mm
Sample Diameter	50	mm
Rate of Axial Strain	2%	per minute
Area Replacement Ratio	0%	

Sample Details		1	2	3	4
Initial Bulk Density	Mg/cm^3	1.77	1.79	1.78	1.76
Initial Dry Density	Mg/cm^3	1.48	1.49	1.48	1.47
Initial Moisture Content	%	20	20	20	20

Conditions at Failure		1	2	3	4
Maximum Corrected Deviator Stress	kPa	12.56	12.80	12.40	12.84
Shear Strength	kPa	6.28	6.40	6.20	6.42
Axial Strain	%	2.46	2.76	2.45	2.48
Final Density	Mg/cm^3	1.77	1.79	1.78	1.76
Final Moisture Content	%	20	20	20	20

Sample Details		
Initial Bulk Density	1.77	Mg/cm^3
Initial Dry Density	1.48	Mg/cm^3
Initial Moisture Content	20	%

Conditions at Failure		
Maximum Corrected Deviator Stress	12.84	kPa
Shear Strength	6.42	kPa
Axial Strain	2.76	%
Final Density	1.77	Mg/cm^3
Final Moisture Content	20	%

Samples Reinforced with Single Column

Sample Height	100	mm
Sample Diameter	50	mm
Rate of Axial Strain	2	% per minute
Area Replacement Ratio	4%	(1 column 10mm diameter)
Column Penetration Ratio	0.60	(60 mm penetration height)

Sample Details		1	2	3	4
Initial Bulk Density	Mg/cm^3	0.54	0.55	0.54	0.55
Initial Dry Density	Mg/cm^3	0.45	0.46	0.45	0.46
Initial Moisture Content	%	20	20	20	20

Conditions at Failure		1	2	3	4
Maximum Corrected Deviator Stress	kPa	16.43	18.02	19.79	19.49
Shear Strength	kPa	8.22	9.01	9.90	9.50
Axial Strain	%	2.63	2.42	2.43	2.41
Final Density	Mg/cm^3	0.54	0.55	0.54	0.55
Final Moisture Content	%	20	20	20	20

Sample Details		
Initial Bulk Density	0.54	Mg/cm^3
Initial Dry Density	0.45	Mg/cm^3
Initial Moisture Content	20	%

Conditions at Failure		
Maximum Corrected Deviator Stress	19.79	kPa
Shear Strength	9.90	kPa
Axial Strain	2.43	%
Final Density	0.54	Mg/cm^3
Final Moisture Content	20	%

Samples Reinforced with Single Column

Sample Height	100	mm
Sample Diameter	50	mm
Rate of Axial Strain	2%	per minute
Area Replacement Ratio	4%	(1 column 10mm diameter)
Column Penetration Ratio	0.80	(80 mm penetration height)

Sample Details		1	2	3	4
Initial Bulk Density	Mg/cm^3	0.54	0.54	0.55	0.55
Initial Dry Density	Mg/cm^3	0.45	0.45	0.46	0.46
Initial Moisture Content	%	20	20	20	20

Conditions at Failure		1	2	3	4
Maximum Corrected Deviator Stress	kPa	18.40	18.24	19.86	20.38
Shear Strength	kPa	9.20	9.12	9.93	10.19
Axial Strain	%	2.74	2.78	2.80	2.86
Final Density	Mg/cm^3	0.54	0.54	0.55	0.55
Final Moisture Content	%	20	20	20	20

Sample Details		
Initial Bulk Density	0.55	Mg/cm^3
Initial Dry Density	0.46	Mg/cm^3
Initial Moisture Content	20	%

Conditions at Failure		
Maximum Corrected Deviator Stress	20.38	kPa
Shear Strength	10.19	kPa
Axial Strain	2.86	%
Final Density	0.56	Mg/cm^3
Final Moisture Content	20	%

Samples Reinforced with Single Column

Sample Height	100	mm
Sample Diameter	50	mm
Rate of Axial Strain	2%	per minute
Area Replacement Ratio	4%	(1 column 10mm diameter)
Column Penetration Ratio	1.0	(100 mm penetration height)

Sample Details		1	2	3	4
Initial Bulk Density	Mg/cm^3	0.54	0.54	0.54	0.53
Initial Dry Density	Mg/cm^3	0.45	0.45	0.45	0.44
Initial Moisture Content	%	20	20	20	20

Conditions at Failure		1	2	3	4
Maximum Corrected Deviator Stress	kPa	16.78	16.02	19.44	19.62
Shear Strength	kPa	8.39	8.01	9.72	9.81
Axial Strain	%	2.72	2.75	2.67	2.69
Final Density	Mg/cm^3	0.54	0.54	0.54	0.53
Final Moisture Content	%	20	20	20	20

Sample Details		
Initial Bulk Density	0.54	Mg/cm^3
Initial Dry Density	0.45	Mg/cm^3
Initial Moisture Content	20	%

Conditions at Failure		
Maximum Corrected Deviator Stress	19.62	kPa
Shear Strength	9.81	kPa
Axial Strain	2.69	%
Final Density	0.53	Mg/cm^3
Final Moisture Content	20	%

Samples Reinforced with Single Column

Sample Height	100	mm
Sample Diameter	50	mm
Rate of Axial Strain	2%	per minute
Area Replacement Ratio	10.24%	(1 column 16mm diameter)
Column Penetration Ratio	0.60	(60 mm penetration height)

Sample Details		1	2	3	4
Initial Bulk Density	Mg/cm^3	0.54	0.54	0.54	0.55
Initial Dry Density	Mg/cm^3	0.45	0.45	0.45	0.46
Initial Moisture Content	%	20	20	20	20

Conditions at Failure		1	2	3	4
Maximum Corrected Deviator Stress	kPa	16.58	17.70	19.50	19.52
Shear Strength	kPa	8.29	8.85	9.75	9.76
Axial Strain	%	2.52	2.76	2.72	2.74
Final Density	Mg/cm^3	0.54	0.54	0.55	0.55
Final Moisture Content	%	20	20	20	20

Sample Details		
Initial Bulk Density	0.55	Mg/cm^3
Initial Dry Density	0.46	Mg/cm^3
Initial Moisture Content	20	%

Conditions at Failure		
Maximum Corrected Deviator Stress	19.52	kPa
Shear Strength	9.76	kPa
Axial Strain	2.74	%
Final Density	0.55	Mg/cm^3
Final Moisture Content	20	%

Samples Reinforced with Single Column

Sample Height	100	mm
Sample Diameter	50	mm
Rate of Axial Strain	2%	per minute
Area Replacement Ratio	10.24%	(1 column 16mm diameter)
Column Penetration Ratio	0.80	(80 mm penetration height)

Sample Details		1	2	3	4
Initial Bulk Density	Mg/cm^3	0.55	0.54	0.54	0.53
Initial Dry Density	Mg/cm^3	0.46	0.45	0.45	0.44
Initial Moisture Content	%	20	20	20	20

Conditions at Failure		1	2	3	4
Maximum Corrected Deviator Stress	kPa	20.66	21.24	23.56	23.52
Shear Strength	kPa	10.33	10.62	11.78	11.76
Axial Strain	%	2.55	2.54	2.54	2.52
Final Density	Mg/cm^3	0.55	0.54	0.54	0.53
Final Moisture Content	%	20	20	20	20

Sample Details		
Initial Bulk Density	0.54	Mg/cm^3
Initial Dry Density	0.45	Mg/cm^3
Initial Moisture Content	20	%

Conditions at Failure		
Maximum Corrected Deviator Stress	23.56	kPa
Shear Strength	11.78	kPa
Axial Strain	2.54	%
Final Density	0.54	Mg/cm^3
Final Moisture Content	20	%

Samples Reinforced with Single Column

Sample Height	100	mm
Sample Diameter	50	mm
Rate of Axial Strain	2%	per minute
Area Replacement Ratio	10.24%	(1 column 16mm diameter)
Column Penetration Ratio	1.00	(100 mm penetration height)

Sample Details		1	2	3	4
Initial Bulk Density	Mg/cm^3	0.54	0.53	0.53	0.53
3Initial Dry Density	Mg/cm^3	0.45	0.44	0.44	0.44
Initial Moisture Content	%	20	20	20	20

Conditions at Failure		1	2	3	4
Maximum Corrected Deviator Stress	kPa	16.85	18.85	20.64	19.72
Shear Strength	kPa	8.44	9.43	10.32	9.86
Axial Strain	%	2.66	2.74	2.76	2.78
Final Density	Mg/cm^3	0.54	0.53	0.53	0.53
Final Moisture Content	%	20	20	20	20

Sample Details		
Initial Bulk Density	0.53	Mg/cm^3
Initial Dry Density	0.44	Mg/cm^3
Initial Moisture Content	20	%

Conditions at Failure		
Maximum Corrected Deviator Stress	20.64	kPa
Shear Strength	10.32	kPa
Axial Strain	2.78	%
Final Density	0.52	Mg/cm^3
Final Moisture Content	20	%

Samples Reinforced with Group Column

Sample Height	100	mm
Sample Diameter	50	mm
Rate of Axial Strain	2%	per minute
Area Replacement Ratio	12%	(3 column 10mm diameter)
Column Penetration Ratio	0.60	(60 mm penetration height)

Sample Details		1	2	3	4
Initial Bulk Density	Mg/cm^3	0.53	0.54	0.53	0.54
Initial Dry Density	Mg/cm^3	0.44	0.45	0.44	0.45
Initial Moisture Content	%	20	20	20	20

Conditions at Failure		1	2	3	4
Maximum Corrected Deviator Stress	kPa	16.78	19.20	19.48	20.28
Shear Strength	kPa	8.39	9.60	9.74	10.14
Axial Strain	%	2.76	2.46	2.74	2.92
Final Density	Mg/cm^3	0.53	0.54	0.53	0.54
Final Moisture Content	%	20	20	20	20

Sample Details		
Initial Bulk Density	0.54	Mg/cm^3
Initial Dry Density	0.45	Mg/cm^3
Initial Moisture Content	20	%

Conditions at Failure		
Maximum Corrected Deviator Stress	20.28	kPa
Shear Strength	10.14	kPa
Axial Strain	2.92	%
Final Density	0.54	Mg/cm^3
Final Moisture Content	20	%

Samples Reinforced with Group Column

Sample Height	100	mm
Sample Diameter	50	mm
Rate of Axial Strain	2%	per minute
Area Replacement Ratio	12%	(3 column 10mm diameter)
Column Penetration Ratio	0.80	(80 mm penetration height)

Sample Details		1	2	3	4
Initial Bulk Density	Mg/cm^3	0.54	0.54	0.55	0.55
Initial Dry Density	Mg/cm^3	0.45	0.45	0.46	0.46
Initial Moisture Content	%	20	20	20	20

Conditions at Failure		1	2	3	4
Maximum Corrected Deviator Stress	kPa	18.98	21.78	23.80	23.40
Shear Strength	kPa	8.49	10.89	11.90	11.70
Axial Strain	%	2.52	2.84	2.86	2.76
Final Density	Mg/cm3	0.54	0.54	0.55	0.54
Final Moisture Content	%	20	20	20	20

Sample Details		
Initial Bulk Density	0.54	Mg/cm^3
Initial Dry Density	0.45	Mg/cm^3
Initial Moisture Content	20	%

Conditions at Failure		
Maximum Corrected Deviator Stress	23.80	kPa
Shear Strength	11.90	kPa
Axial Strain	2.86	%
Final Density	0.54	Mg/cm^3
Final Moisture Content	20	%

Samples Reinforced with Group Column

Sample Height	100	mm
Sample Diameter	50	mm
Rate of Axial Strain	2%	per minute
Area Replacement Ratio	12%	(3 column 10mm diameter)
Column Penetration Ratio	1.0	(100 mm penetration height)

Sample Details		1	2	3	4
Initial Bulk Density	Mg/cm^3	0.53	0.54	0.53	0.53
Initial Dry Density	Mg/cm^3	0.44	0.45	0.44	0.44
Initial Moisture Content	%	20	20	20	20

Conditions at Failure		1	2	3	4
Maximum Corrected Deviator Stress	kPa	15.64	18.36	19.80	20.32
Shear Strength	kPa	7.82	9.18	9.90	10.16
Axial Strain	%	2.55	2.48	2.74	2.76
Final Density	Mg/cm^3	0.53	0.54	0.53	0.53
Final Moisture Content	%	20	20	20	20

Sample Details		
Initial Bulk Density	0.53	Mg/cm^3
Initial Dry Density	0.44	Mg/cm^3
Initial Moisture Content	20	%

Conditions at Failure		
Maximum Corrected Deviator Stress	20.32	kPa
Shear Strength	10.16	kPa
Axial Strain	2.76	%
Final Density	0.53	Mg/cm^3
Final Moisture Content	20	%

Samples Reinforced with Group Column

Sample Height	100	mm
Sample Diameter	50	mm
Rate of Axial Strain	2%	per minute
Area Replacement Ratio	30.72%	(3 column 16mm diameter)
Column Penetration Ratio	0.60	(60 mm penetration height)

Sample Details		1	2	3	4
Initial Bulk Density	Mg/cm^3	0.55	0.56	0.55	0.56
Initial Dry Density	Mg/cm^3	0.46	0.47	0.46	0.47
Initial Moisture Content	%	20	20	20	20

Conditions at Failure		1	2	3	4
Maximum Corrected Deviator Stress	kPa	14.44	13.88	15.64	15.94
Shear Strength	kPa	7.22	6.94	7.82	7.97
Axial Strain	%	2.70	2.52	2.56	2.54
Final Density	Mg/cm^3	0.55	0.56	0.55	0.56
Final Moisture Content	%	20	20	20	20

Sample Details		
Initial Bulk Density	0.56	Mg/cm^3
Initial Dry Density	0.47	Mg/cm^3
Initial Moisture Content	20	%

Conditions at Failure		
Maximum Corrected Deviator Stress	15.94	kPa
Shear Strength	7.97	kPa
Axial Strain	2.54	%
Final Density	0.56	Mg/cm^3
Final Moisture Content	20	%

Samples Reinforced with Group Column

Sample Height	100	mm
Sample Diameter	50	mm
Rate of Axial Strain	2%	per minute
Area Replacement Ratio	30.72%	(3 column 16mm diameter)
Column Penetration Ratio	0.80	(80 mm penetration height)

Sample Details		1	2	3	4
Initial Bulk Density	Mg/cm^3	0.55	0.55	0.56	0.55
Initial Dry Density	Mg/cm^3	0.46	0.46	0.47	0.46
Initial Moisture Content	%	20	20	20	20

Conditions at Failure		1	2	3	4
Maximum Corrected Deviator Stress	kPa	15.04	14.00	15.04	16.22
Shear Strength	kPa	7.52	7.00	7.52	8.11
Axial Strain	%	2.67	2.52	2.56	2.54
Final Density	Mg/cm^3	0.55	0.55	0.56	0.55
Final Moisture Content	%	20	20	20	20

Sample Details		
Initial Bulk Density	0.55	Mg/cm^3
Initial Dry Density	0.46	Mg/cm^3
Initial Moisture Content	20	%

Conditions at Failure		
Maximum Corrected Deviator Stress	16.22	kPa
Shear Strength	8.11	kPa
Axial Strain	2.54	%
Final Density	0.55	Mg/cm^3
Final Moisture Content	20	%

Samples Reinforced with Group Column

Sample Height	100	mm
Sample Diameter	50	mm
Rate of Axial Strain	2%	per minute
Area Replacement Ratio	30.72%	(3 column 16mm diameter)
Column Penetration Ratio	1.00	(100 mm penetration height)

Sample Details		1	2	3	4
Initial Bulk Density	Mg/cm^3	0.54	0.53	0.53	0.54
Initial Dry Density	Mg/cm^3	0.45	0.44	0.44	0.45
Initial Moisture Content	%	20	20	20	20

Conditions at Failure		1	2	3	4
Maximum Corrected Deviator Stress	kPa	14.44	14.46	15.66	15.06
Shear Strength	kPa	7.22	7.23	7.83	7.53
Axial Strain	%	2.70	2.48	2.48	2.52
Final Density	Mg/cm^3	0.54	0.53	0.53	0.54
Final Moisture Content	%	20	20	20	20

Sample Details		
Initial Bulk Density	0.54	Mg/cm^3
Initial Dry Density	0.45	Mg/cm^3
Initial Moisture Content	20	%

Conditions at Failure		
Maximum Corrected Deviator Stress	15.06	kPa
Shear Strength	7.53	kPa
Axial Strain	2.52	%
Final Density	0.54	Mg/cm^3
Final Moisture Content	20	%

Appendix J: Mohr-Coulomb Failure Criterion

Sample: Control

Angle of Internal Friction: 32.30^0

Apparent of Cohesion: 1.37 kPa

Cell Pressure: 100, 200 and 400 kPa

Back Pressure: 50, 100 and 200 kPa

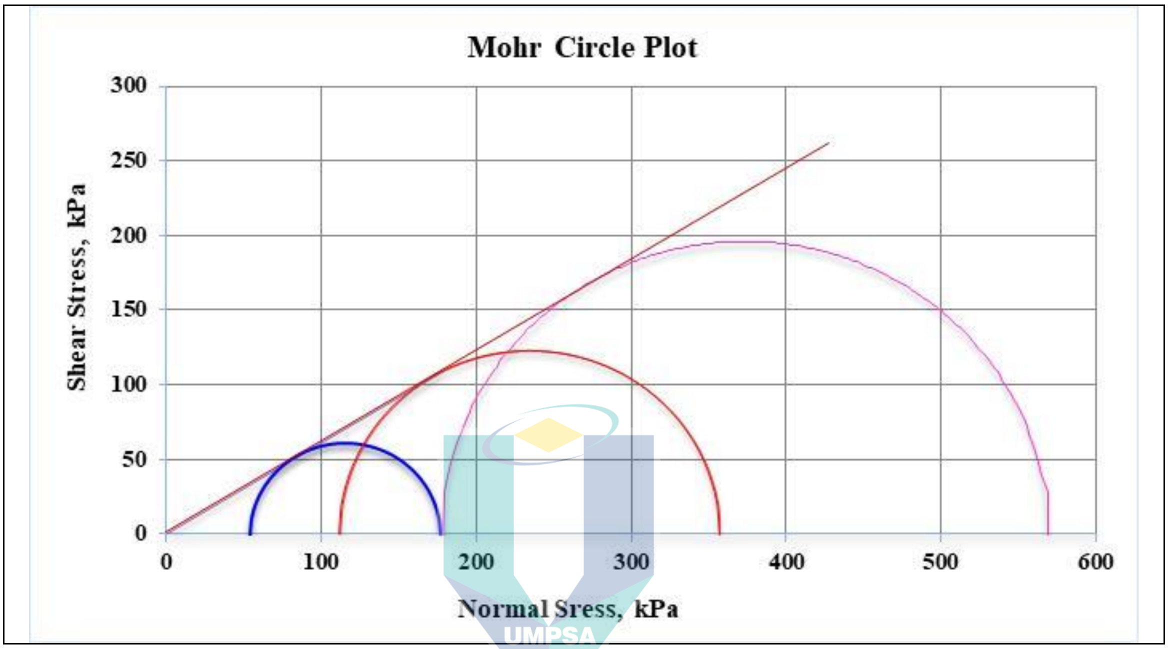

Sample: S1060

Angle of Internal Friction: 31.20^0

Cell Pressure: 100, 200 and 400 kPa

Apparent of Cohesion: 4.96 kPa

Back Pressure: 50, 100 and 200 kPa

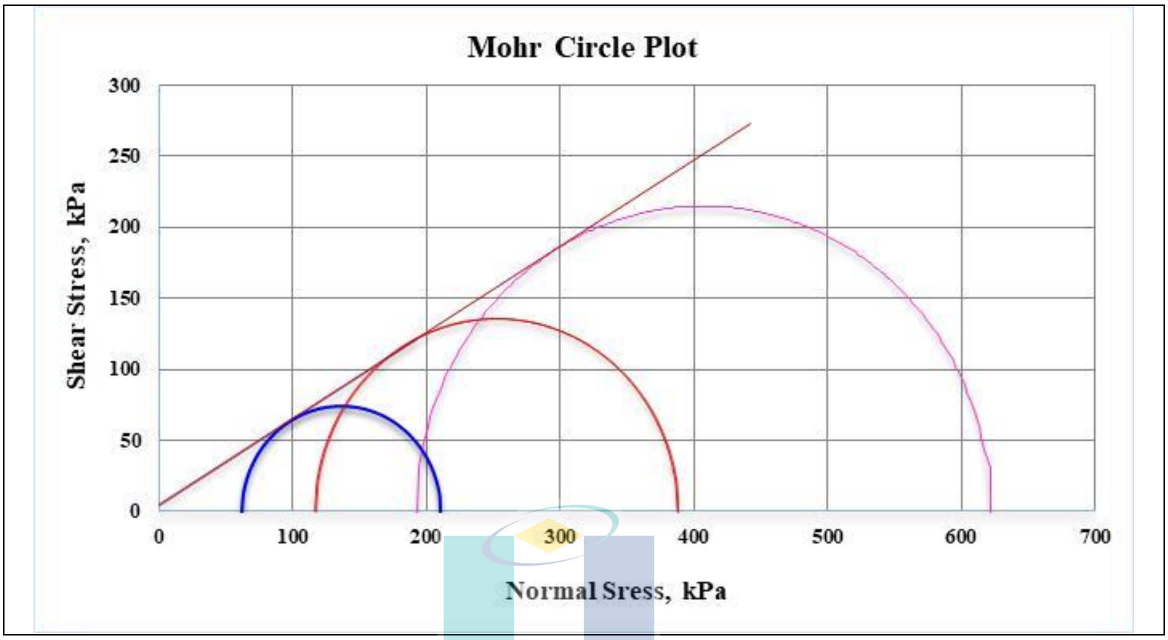

Sample: S1080

Angle of Internal Friction: 30.2^0

Cell Pressure: 100, 200 and 400 kPa

Apparent of Cohesion: 7.31 kPa

Back Pressure: 50, 100 and 200 kPa

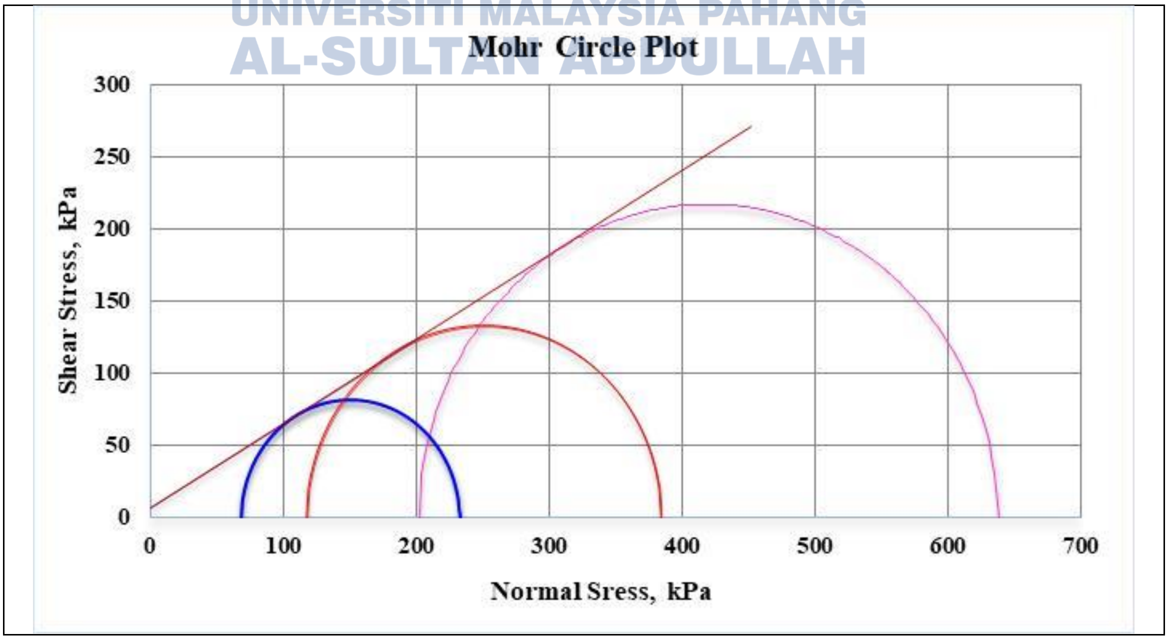

Sample: S10100

Angle of Internal Friction: 31.00^0

Apparent of Cohesion: 5.55 kPa

Cell Pressure: 100, 200 and 400 kPa

Back Pressure: 50, 100 and 200 kPa

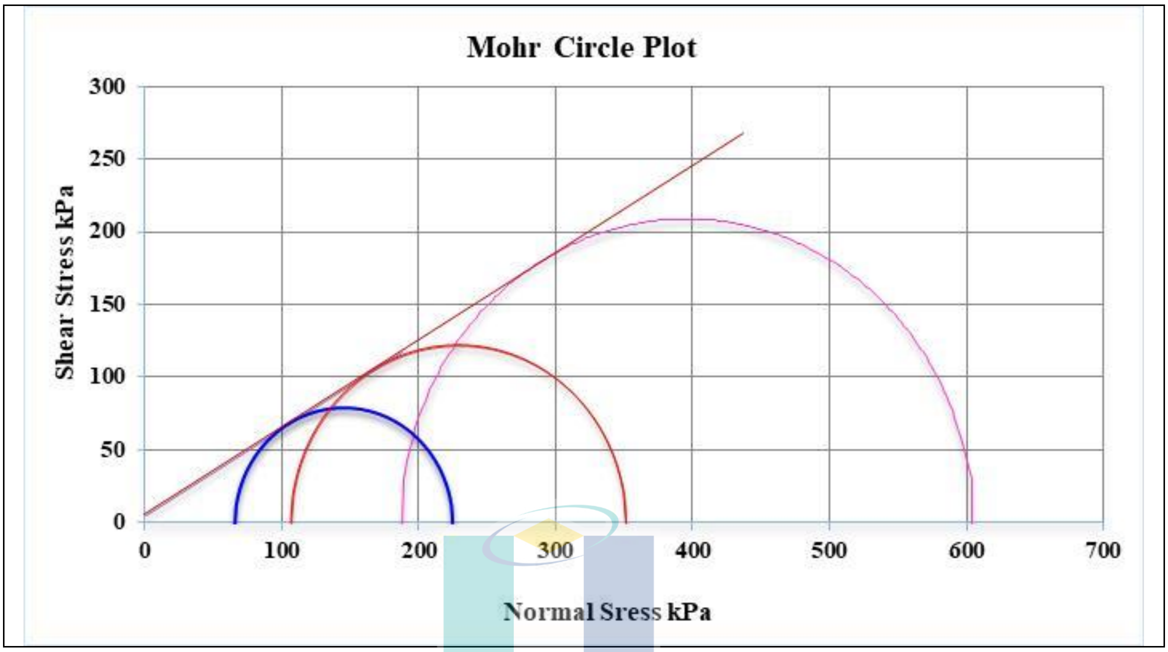

Sample: S1660

Angle of Internal Friction: 30.0^0

Apparent of Cohesion: 9.86 kPa

Cell Pressure: 100, 200 and 400 kPa

Back Pressure: 50, 100 and 200 kPa

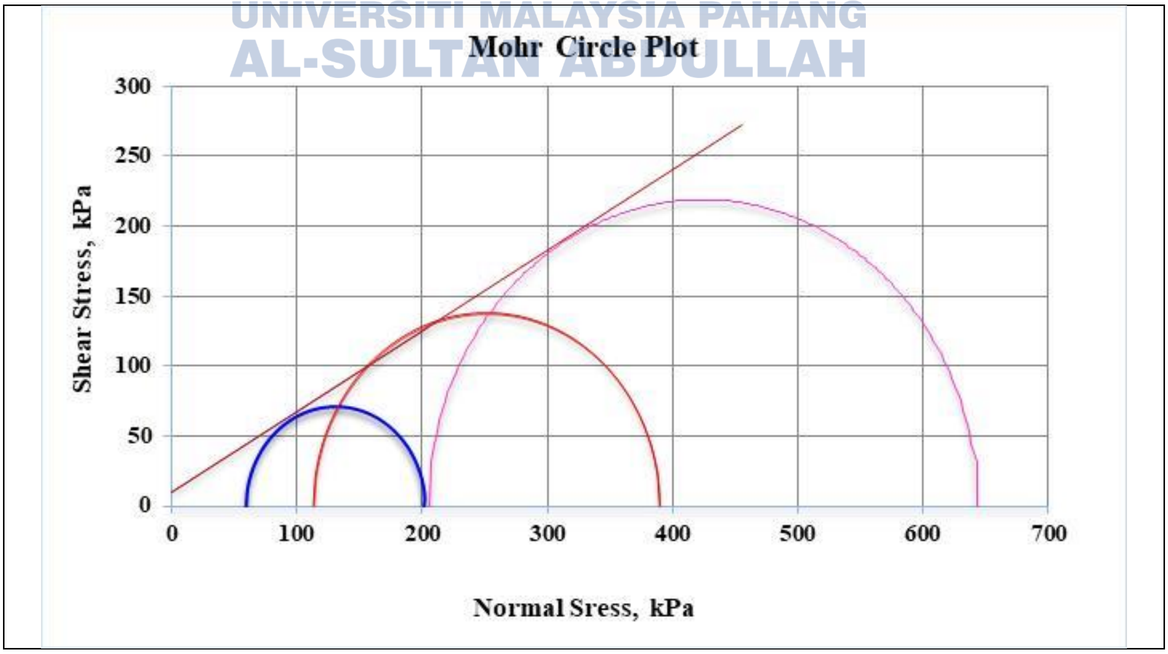

Cell Pressure: 100, 200 and 400 kPa

Sample: S1680

Back Pressure: 50, 100 and 200 kPa

Angle of Internal Friction: 29.00^0

Apparent of Cohesion: 14.38 kPa

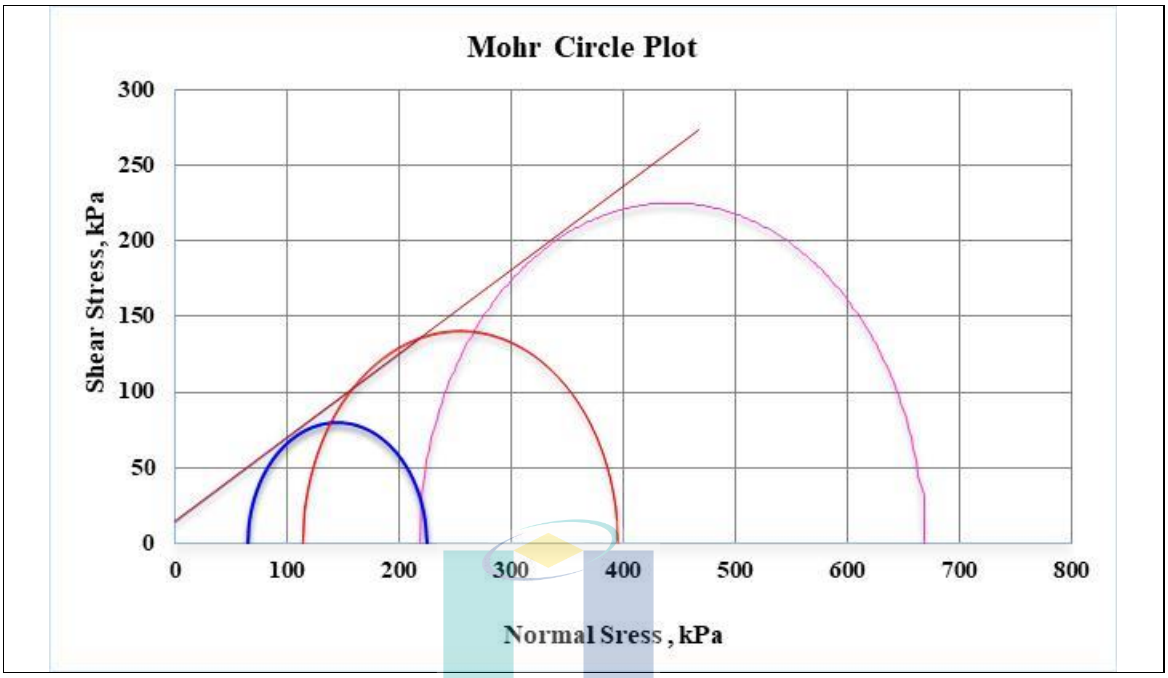

Sample: S16100

Angle of Internal Friction: 31.20^0

Cell Pressure: 100, 200 and 400 kPa

Apparent of Cohesion: 6.73 kPa

Back Pressure: 50, 100 and 200 kPa

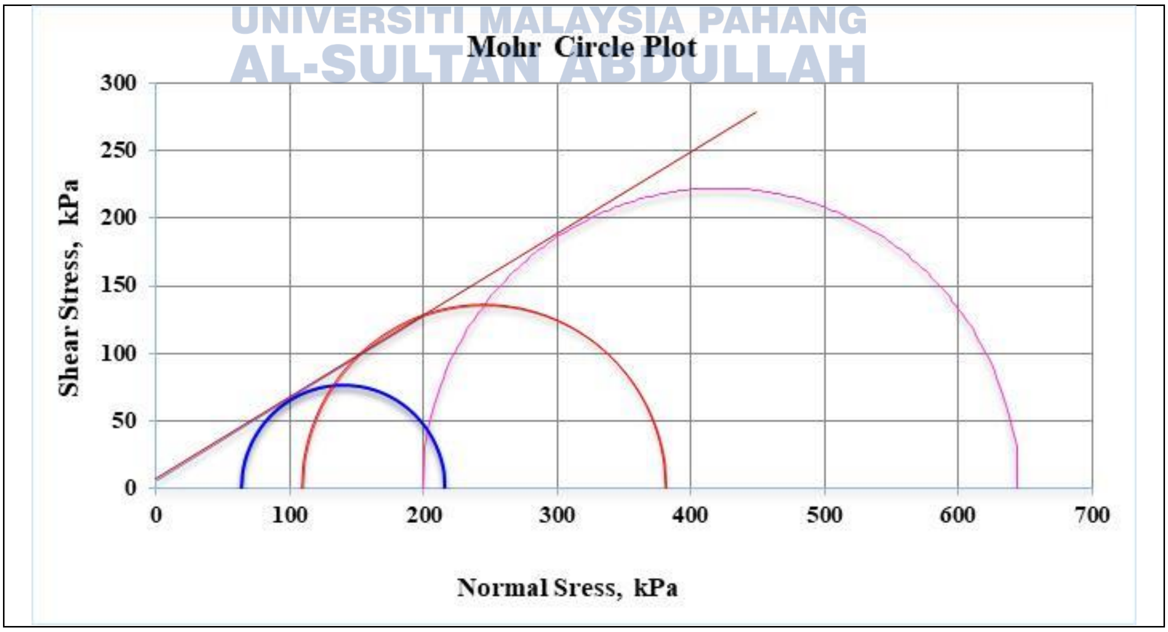

Sample: G1060

Angle of Internal Friction: 30.60^0

Apparent of Cohesion: 6.01 kPa

Cell Pressure: 100, 200 and 400 kPa

Back Pressure: 50, 100 and 200 kPa

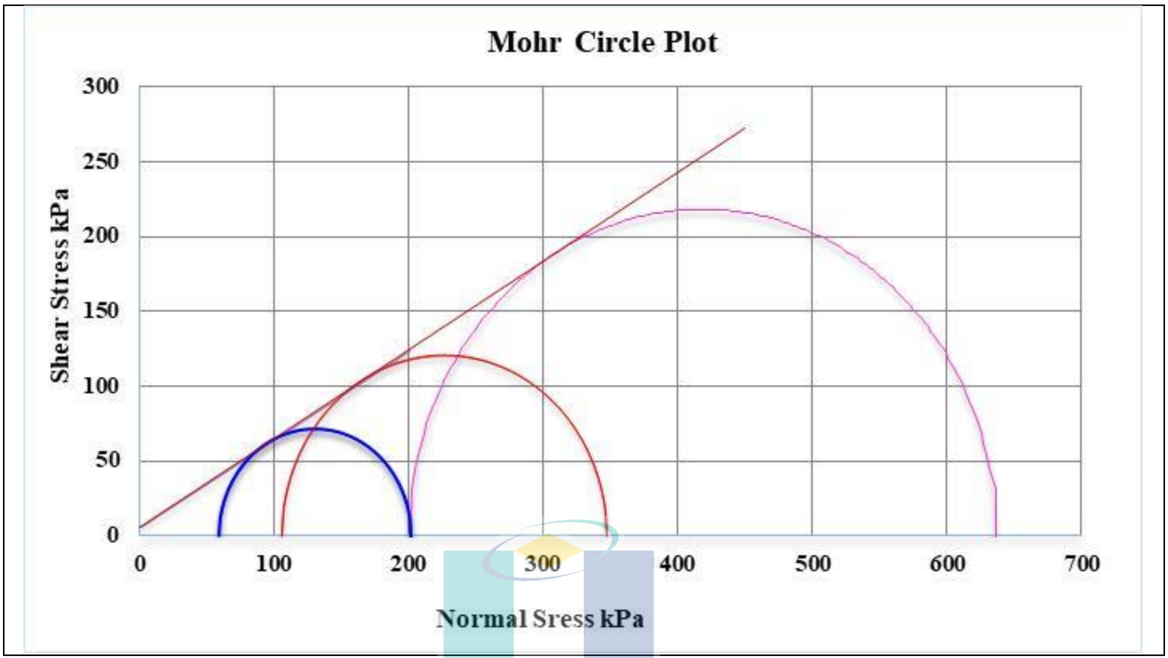

Sample: G1080

Angle of Internal Friction: 31.00^0

Apparent of Cohesion: 13.86 kPa

Cell Pressure: 100, 200 and 400 kPa

Back Pressure: 50, 100 and 200 kPa

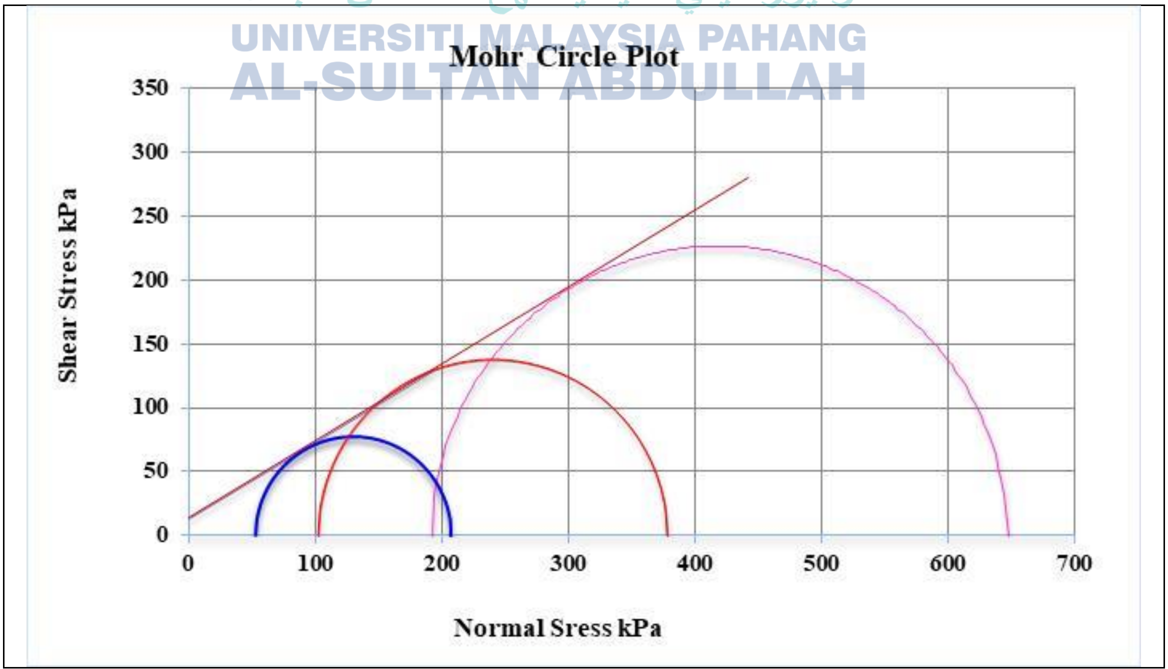

Sample: G10100

Angle of Internal Friction: 29.90^{0}

Apparent of Cohesion: 7.40 kPa

Cell Pressure: 100, 200 and 400 kPa

Back Pressure: 50, 100 and 200 kPa

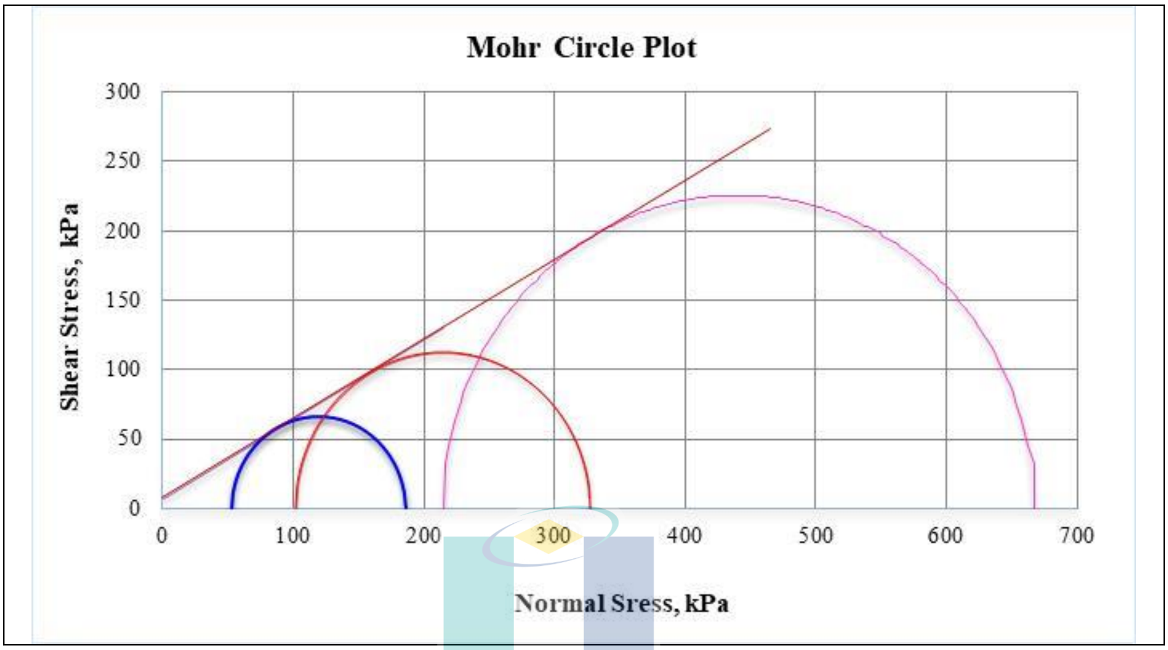

Sample: G1660

Angle of Internal Friction: 30.90^{0}

Apparent of Cohesion: 4.08 kPa

Cell Pressure: 100, 200 and 400 kPa

Back Pressure: 50, 100 and 200 kPa

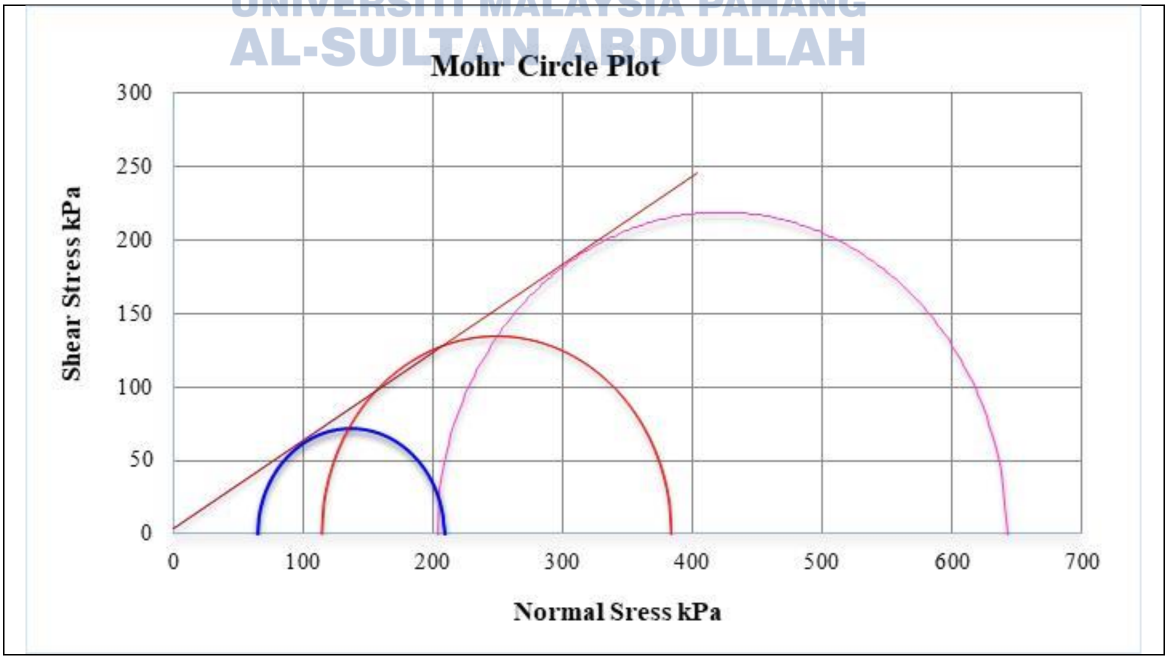

Sample: G1680

Angle of Internal Friction: 31.90^0

Apparent of Cohesion: 5.90 kPa

Cell Pressure: 100, 200 and 400 kPa

Back Pressure: 50, 100 and 200 kPa

Sample: G16100

Angle of Internal Friction: 32.00^0

Apparent of Cohesion: 2.70 kPa

Cell Pressure: 100, 200 and 400 kPa

Back Pressure: 50, 100 and 200 kPa

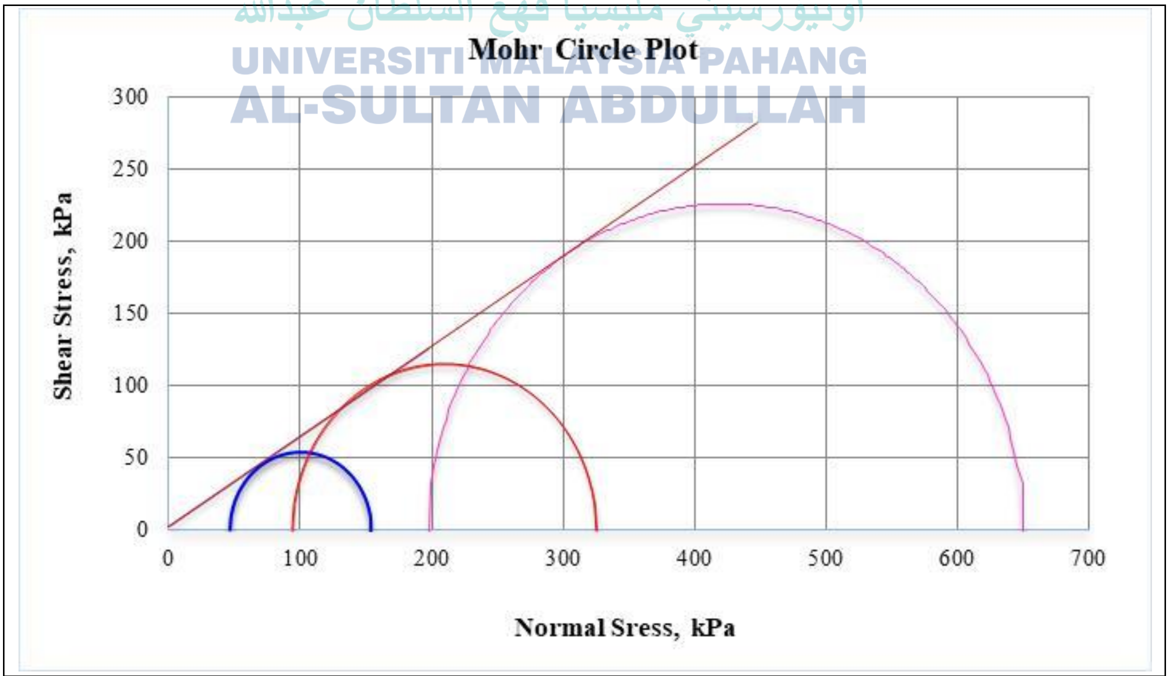

Appendix K: Shear strength by direct shear small shear box

Shear Strength By Direct Shear Small Shear Box

Client	Md Ikramul Hoque	**Lab Ref**	
Project		**Job**	210323-A
Borehole		**Sample**	1

Test Details			
Standard	BS 1377 Part 7 :1990 Clause 4	**Particle Density**	2.65 Mg/m^3
Sample Type	Core sample	**Single or Multi Stage**	Single Stage
Lab. Temperature	28.0 deg.C	**Location**	
Sample Description			
Variations from procedure	None		

Specimen Details			
Specimen Reference	A	**Description**	
Depth within Sample	0.00mm	**Orientation within Sample**	
Initial Height	20.000 mm	**Area**	3600.00 mm^2
Preparation		**Initial Moisture Content***	1161.8 %
Bulk Density	2.22 Mg/m^3	**Dry Density**	0.18 Mg/m^3
Initial Voids Ratio	14.0473	**Degree of Saturation**	219.18 %
Dry or Submerged	Dry		
Comments			

* Calculated from initial and dry weights of whole specimen

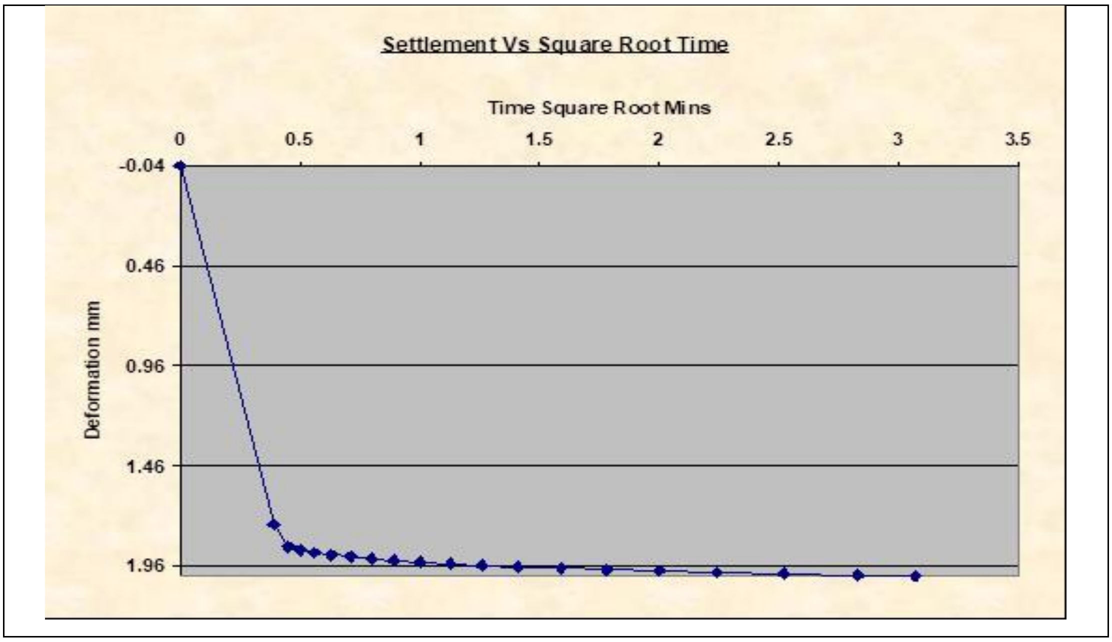

Rates of Horizontal Displacement	Stage 1: 0.4464mm/min

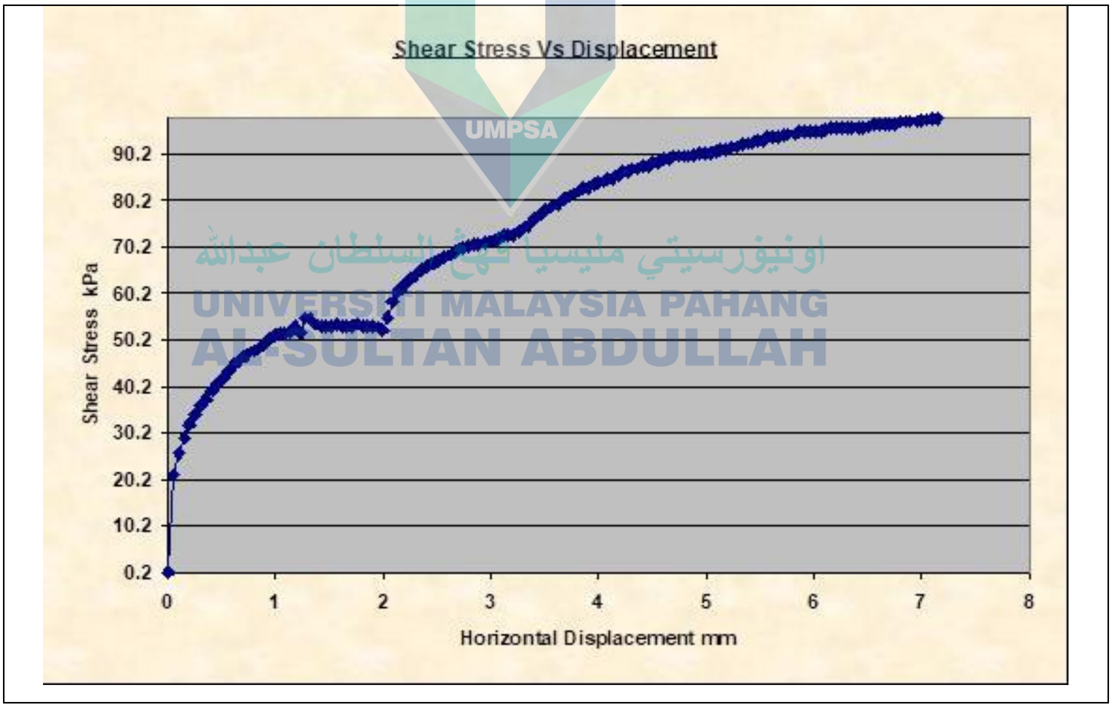

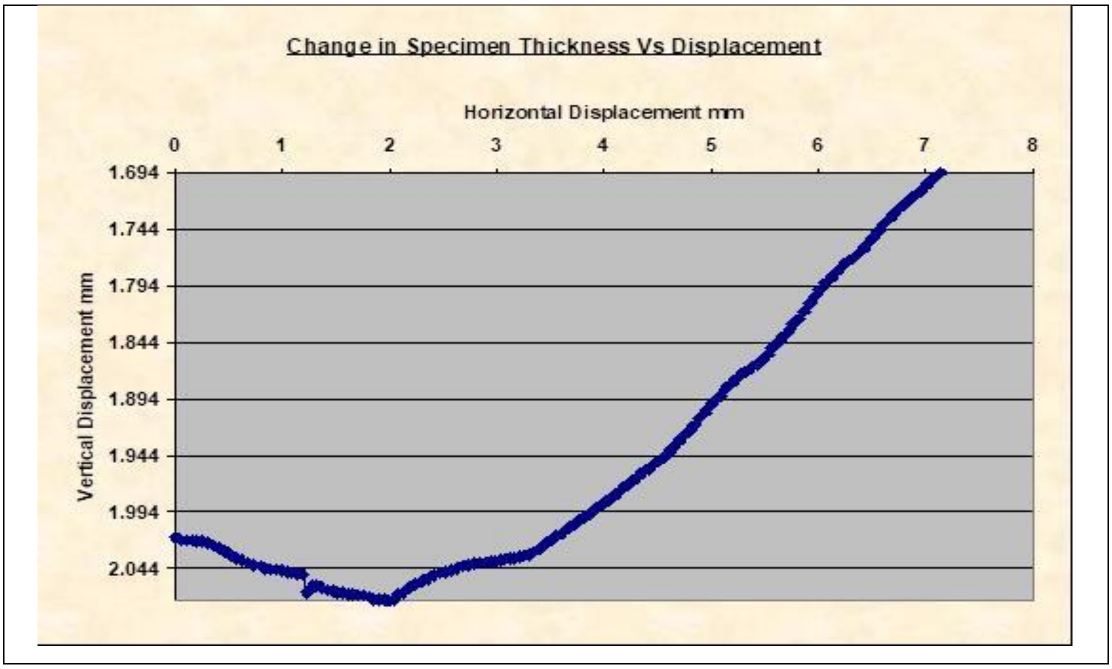

Conditions at Failure	
Applied Normal Stress	136.2 kPa
Maximum Shear Stress	97.4 kPa
Horizontal Deformation	7.000 mm
Residual Shear Stress	0.0 kPa
Vertical Deformation	1.706 mm
Cumulative Horizontal Displacement	7.146 mm

Tested By and Date:	
Checked By and Date:	
Approved By and Date:	

Shear Strength By Direct Shear

Small Shear Box

Client	Md Ikramul Hoque	**Lab Ref**	
Project		**Job**	210323-B
Borehole		**Sample**	2

Test Details			
Standard	BS 1377 Part 7 :1990 Clause 4	**Particle Density**	2.65 Mg/m^3
Sample Type	Core sample	**Single or Multi Stage**	Single Stage
Lab. Temperature	28.0 deg.C	**Location**	
Sample Description			
Variations from procedure	None		

Specimen Details			
Specimen Reference	B	**Description**	
Depth within Sample	0.00mm	**Orientation within Sample**	
Initial Height	20.000 mm	**Area**	3600.00 mm^2
Preparation		**Initial Moisture Content***	1021.2 %
Bulk Density	2.22 Mg/m^3	**Dry Density**	0.20 Mg/m^3
Initial Voids Ratio	12.3707	**Degree of Saturation**	218.76 %
Dry or Submerged	Dry		
Comments			

* Calculated from initial and dry weights of whole specimen

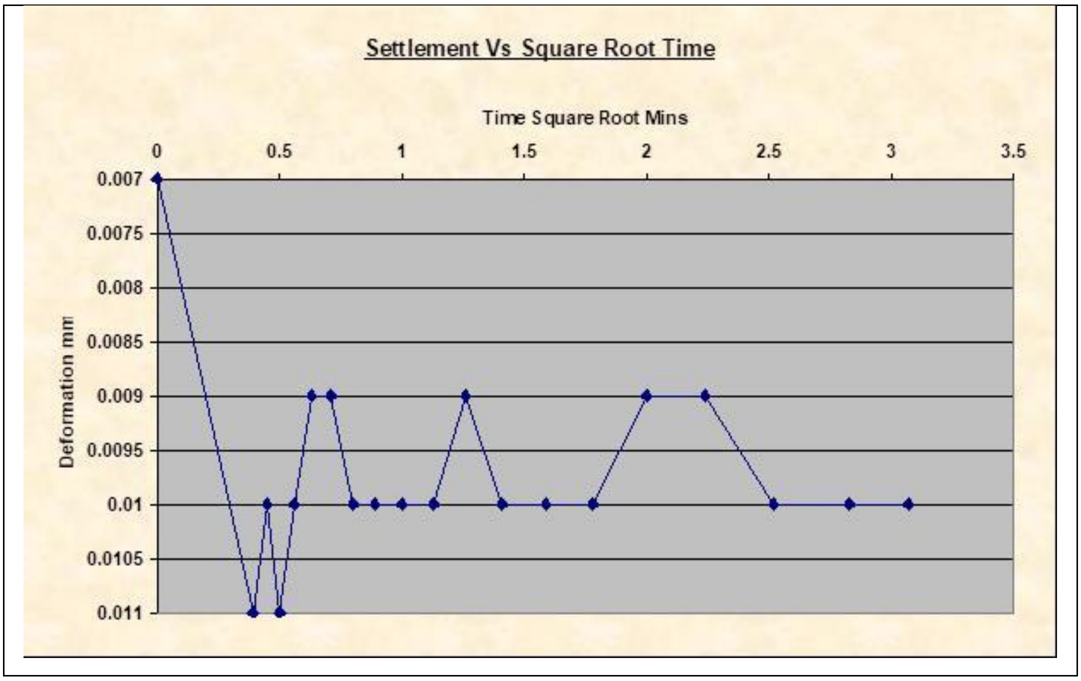

Rates of Horizontal Displacement	Stage 1: 0.0286mm/min

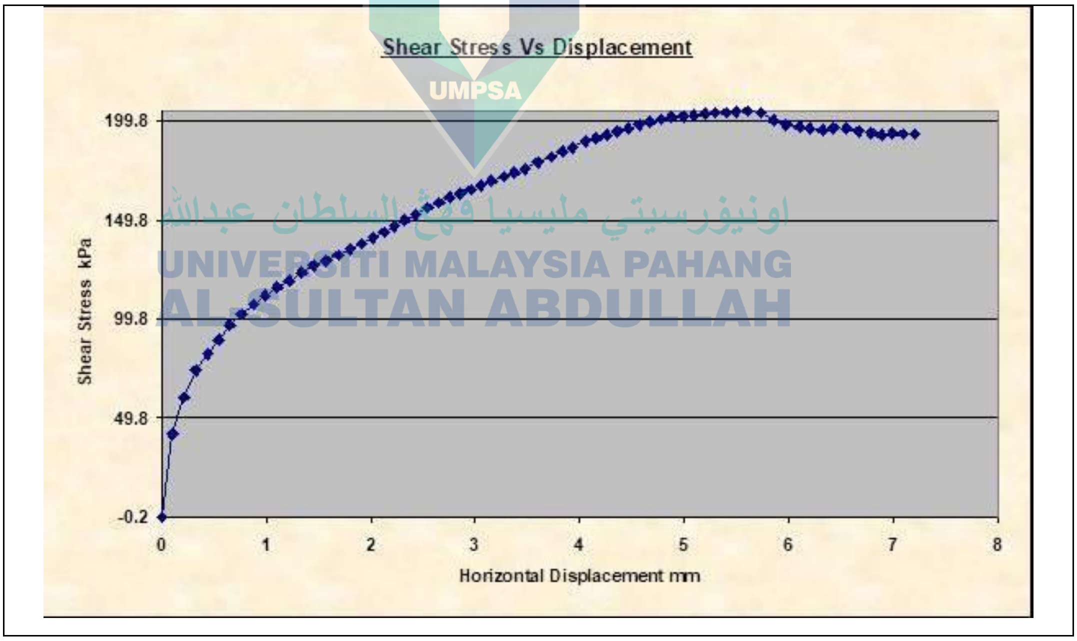

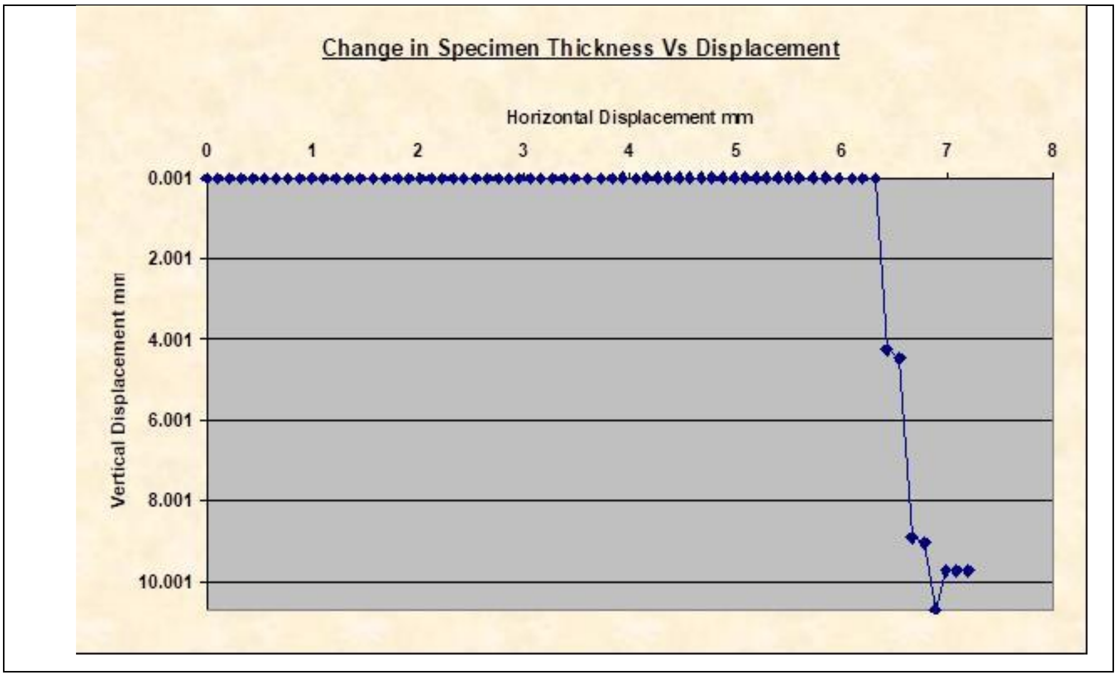

Conditions at Failure	
Applied Normal Stress	272.5 kPa
Maximum Shear Stress	204.2 kPa
Horizontal Deformation	5.732 mm
Residual Shear Stress	0.0 kPa
Vertical Deformation	0.001 mm
Cumulative Horizontal Displacement	7.205 mm

Tested By and Date:	
Checked By and Date:	
Approved By and Date:	

Shear Strength By Direct Shear

Small Shear Box

Client	Md Ikramul Hoque	**Lab Ref**	
Project		**Job**	210323-C
Borehole		**Sample**	3

Test Details			
Standard	BS 1377 Part 7 :1990 Clause 4	**Particle Density**	2.65 Mg/m^3
Sample Type	Core sample	**Single or Multi Stage**	Single Stage
Lab. Temperature	0.0 deg.C	**Location**	
Sample Description			
Variations from procedure	None		

Specimen Details			
Specimen Reference	C	**Description**	
Depth within Sample	0.00mm	**Orientation within Sample**	
Initial Height	20.000 mm	**Area**	3600.00 mm^2
Preparation		**Initial Moisture Content***	236.4 %
Bulk Density	2.57 Mg/m^3	**Dry Density**	0.76 Mg/m^3
Initial Voids Ratio	2.4691	**Degree of Saturation**	253.68 %
Dry or Submerged	Dry		
Comments			

* Calculated from initial and dry weights of whole specimen

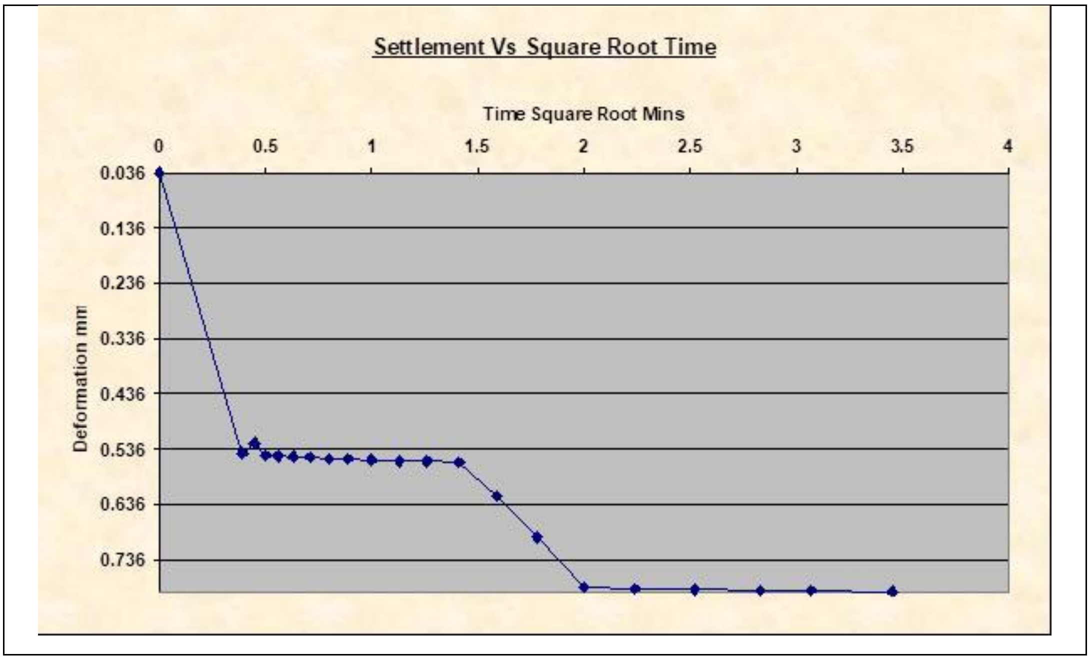

Rates of Horizontal Displacement	Stage 1: 0.0286mm/min

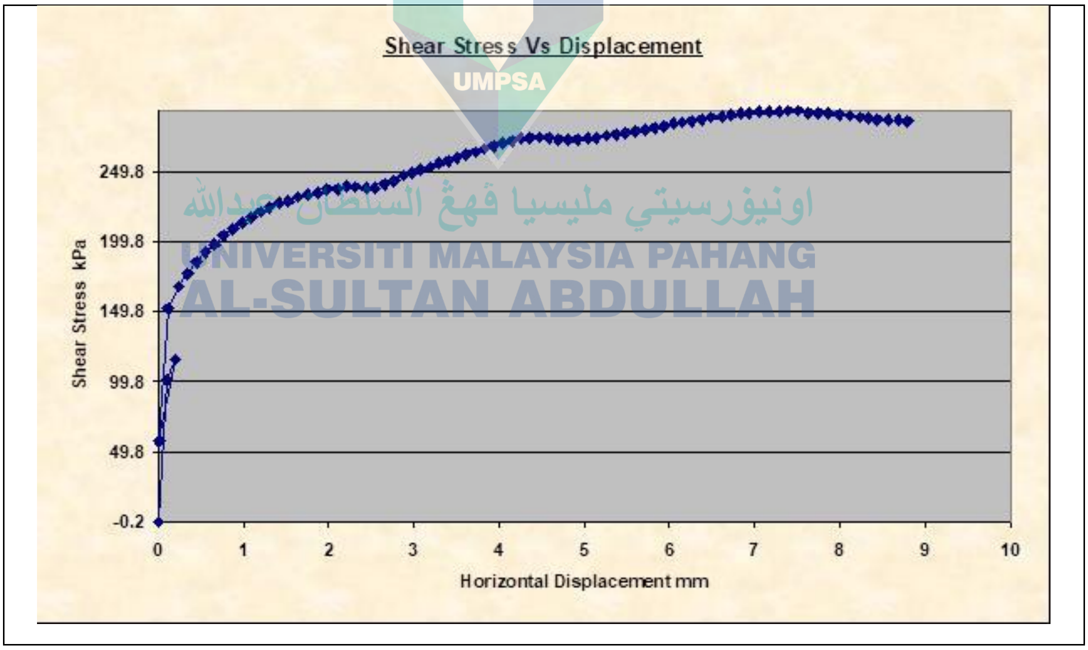

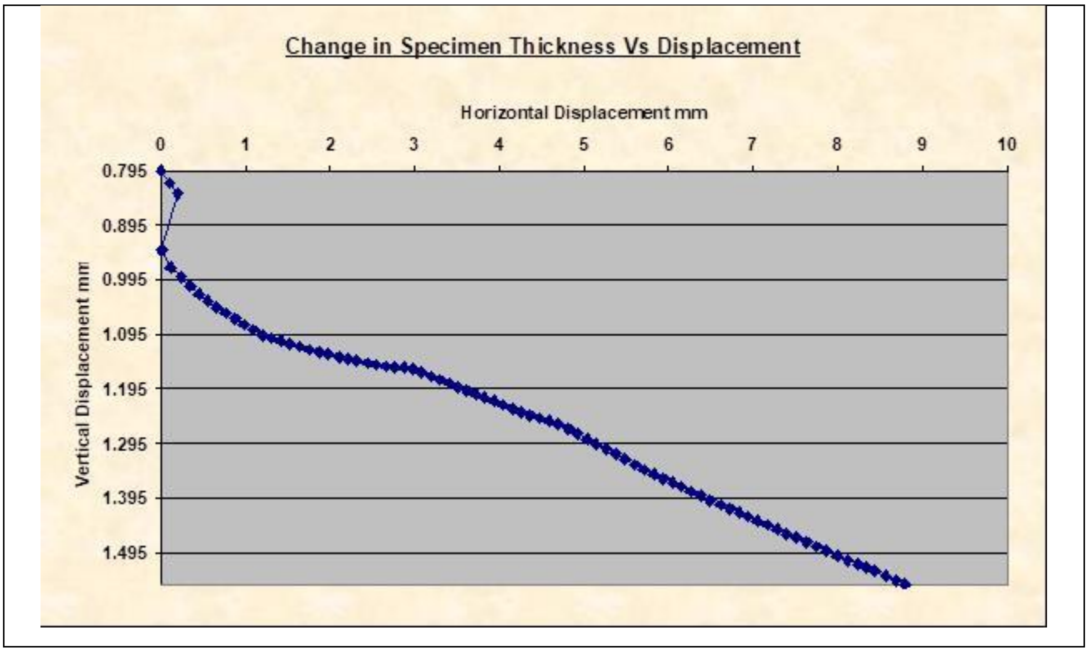

Conditions at Failure	
Applied Normal Stress	408.80 kPa
Maximum Shear Stress	275.7 kPa
Horizontal Deformation	7.090 mm
Residual Shear Stress	0.0 kPa
Vertical Deformation	1.553 mm
Cumulative Horizontal Displacement	7.090 mm

Tested By and Date:	
Checked By and Date:	
Approved By and Date:	

Appendix L: Consolidated Undrained Triaxial Compression Test

Your Company Name Here

Consolidated Undrained Triaxial Compression Test

BS 1377 : Part 8 : 1990

Date:
Date:
Checked by:
Approved by:
Filename: D:\UMP PhD\CU Test Results\[BH00 Report Final.xlsx]Report
Date: 5/17/2023

Specimen Details

		Specimen 1	Specimen 2	Specimen 3
Job Ref.				
Job Location				
Borehole		BH00	BH00	BH00
Sample No.		S37	S38	S39
Depth	m		0	0
Date		21/10/2022	25/10/2022	26/10/2022
Disturbed / Undisturbed				

Description of Specimen

Initial Specimen Conditions

		Specimen 1	Specimen 2	Specimen 3
Height	mm	100.00	100.00	100.00
Diameter	mm	50.00	50.00	50.00
Area	mm^2	1963.50	1963.50	1963.50
Volume	cm^3	196.35	196.35	196.35
Mass	g	360.00	360.00	360.00
Dry Mass	g	330.00	330.00	330.00
Density	Mg/m^3	1.83	1.83	1.83
Dry Density	Mg/m^3	1.68	1.68	1.68
Moisture Content	%	9.09	9.09	9.09
Degree of Saturation	%	43.21	43.21	43.21
Specific Gravity (assumed/measured)		2.60	2.60	2.60

Final Specimen Conditions

		Specimen 1	Specimen 2	Specimen 3
Moisture Content	%			
Density	Mg/m^3	0.00	0.00	0.00
Dry Density	Mg/m^3			

Sketch of Failure of the Specimen

Specimen 1 Specimen 2 Specimen 3

Your Company Name Here

Consolidated Undrained Triaxial Compression Test

BS 1377 : Part 8 : 1990

Specimen Details

		Specimen 1	Specimen 2	Specimen 3
Job Ref.		0		
Job Location		0		
Borehole		BH00	BH00	BH00
Sample No.		S37	S38	S39
Depth	m	0	0	0
Date		21/10/2022	25/10/2022	26/10/2022

Test Setup

	Specimen 1	Specimen 2	Specimen 3
Date started			
Date Finished			
Top Drain Used			
Base Drain Used			
Side Drains Used			
Pressure System Number			
Cell Number			

Saturation

		Specimen 1	Specimen 2	Specimen 3
Cell Pressure Incr.	kPa	50.00	49.90	50.00
Back Pressure Incr.	kPa	27.00	43.00	48.00
Differential Pressure	kPa	33.00	17.90	13.00
Final Cell Pressure	kPa	150.00	249.90	450.00
Final Pore Pressure	kPa	113.60	229.20	434.50
Final B Value		0.56	0.86	0.97

Consolidation

		Specimen 1	Specimen 2	Specimen 3
Effective Pressure	kPa	50.00	101.00	201.00
Cell Pressure	kPa	100.00	200.00	400.00
Back Pressure	kPa	50.00	99.00	199.00
Excess Pore Pressure	kPa	-3.70	-2.90	-2.50
Pore Pressure at End	kPa	52.50	99.20	198.50
Consolidated Volume	cm^3	186.67	180.42	178.93
Volumetric Strain		0.016428185	0.027043608	0.029578203
Consolidated Height	mm	98.36	97.30	97.04
Consolidated Area	mm^2	1898.98	1857.30	1847.34
Vol. Compressibility	m^2/MN	0.85267	0.63433	0.37599
Consolidation Coef.	$m^2/yr.$			

Date:
Date:
Checked by:
Approved by:
Filename: D:\UMP PhD\CU Test Results\[BH00 Report Final.xlsx]Report
Date: 5/17/2023

Your Company Name Here

Consolidated Undrained Triaxial Compression Test

BS 1377 : Part 8 : 1990

Specimen Details

		Specimen 1	Specimen 2	Specimen 3
Job Ref.		0		
Job Location		0		
Borehole		BH00	BH00	BH00
Sample No.		S37	S38	S39
Depth	m	0	0	0
Date		21/10/2022	25/10/2022	26/10/2022

Consolidation Stage

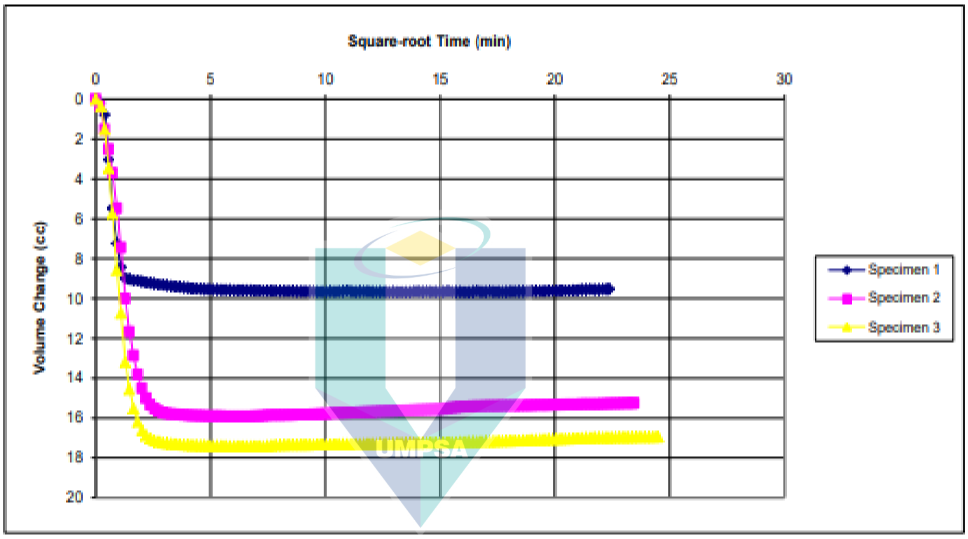

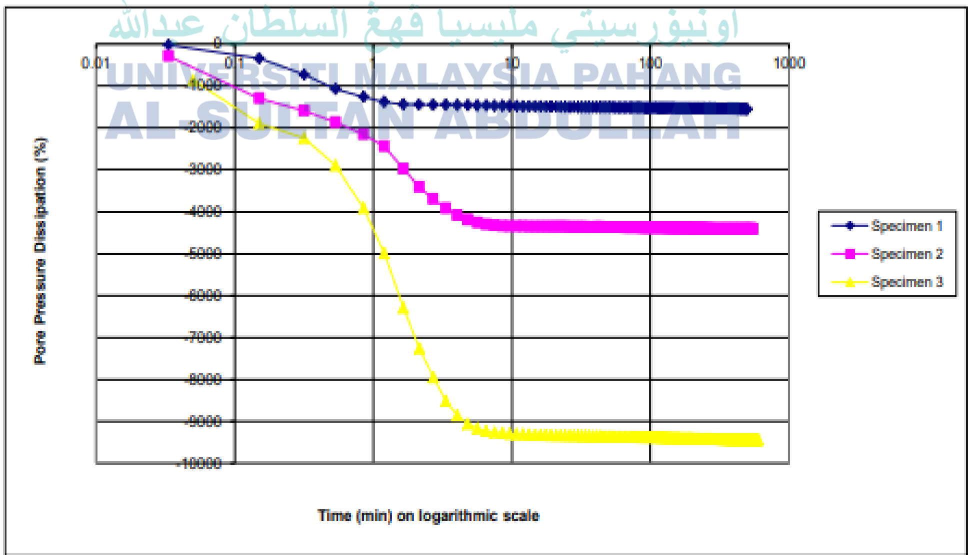

Date:
Date:
Checked by:
Approved by:
Filename: D:\UMP PhD\CU Test Results\[BH00 Report Final.xlsx]Report
Date: 5/17/2023

Your Company Name Here

Consolidated Undrained Triaxial Compression Test

BS 1377 : Part 8 : 1990

Specimen Details

		Specimen 1	Specimen 2	Specimen 3
Job Ref.		0		
Job Location		0		
Borehole		BH00	BH00	BH00
Sample No.		S37	S38	S39
Depth	m	0	0	0
Date		21/10/2022	25/10/2022	26/10/2022

Shearing

		Specimen 1	Specimen 2	Specimen 3
Initial Cell Pressure	kPa	100	200	400
Initial Pore Pressure	kPa	52.6	99.4	198.7
Rate of Strain	%/hour	60.00012	60.00012	60.00012
Max Deviator Stress				
Axial Strain		16.969	17.949	17.484
Axial Stress	kPa	122.86	195.71	391.10
Cor. Deviator stress	kPa	122.86	195.71	391.10
Effective Major Stress	kPa	175.86	287.91	568.60
Effective Minor Stress	kPa	53.00	92.20	177.50
Effective Stress Ratio		3.318	3.123	3.171
s'	kPa	114.43	190.05	373.05
t'	kPa	61.43	97.85	195.55
Shear Resistance Angle	degs	31.03	31.03	31.03
Cohesion c'	kPa	1.63	1.63	1.63
Max Effective Priciple Stress Ratio				
Axial Strain		14.512	13.478	12.005
Axial Stress	kPa	119.75	193.79	366.78
Cor. Deviator stress	kPa	119.75	193.79	366.78
Effective Major Stress	kPa	170.75	282.59	530.78
Effective Minor Stress	kPa	51.00	88.80	164.00
Effective Stress Ratio		3.348	3.182	3.236
s'	kPa	110.87	185.70	347.39
t'	kPa	59.87	96.90	183.39

Checked by: Date:

Approved by: Date:

Filename: D:\UMP PhD\CU Test Results\[BH00 Report Final.xlsx]Report

Date: 5/17/2023

Your Company Name Here

Consolidated Undrained Triaxial Compression Test

BS 1377 : Part 8 : 1990

Specimen Details

		Specimen 1	Specimen 2	Specimen 3
Job Ref.			0	
Job Location			0	
Borehole		BH00	BH00	BH00
Sample No.		S37	S38	S39
Depth	m	0	0	0
Date		21/10/2022	25/10/2022	26/10/2022

Shearing Stage

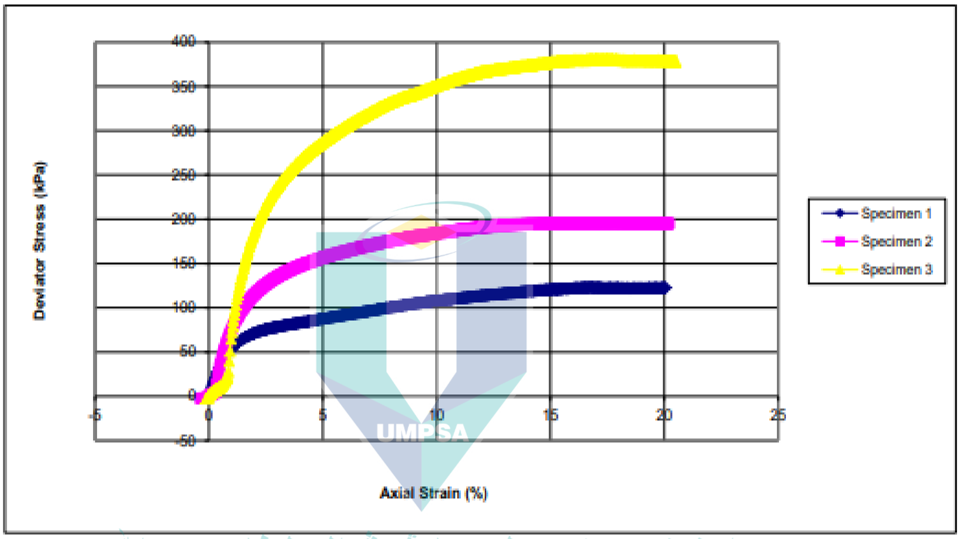

Date:
Date:
Checked by:
Approved by:
Filename: D:\UMP PhD\CU Test Results\[BH00 Report Final.xlsx]Report
Date: 5/17/2023

Your Company Name Here

Consolidated Undrained Triaxial Compression Test

BS 1377 : Part 8 : 1990

Sample Details

		Specimen 1	Specimen 2	Specimen 3
Job Ref.		0		
Job Location		0		
Borehole		BH00	BH00	BH00
Sample No.		S37	S38	S39
Depth	m	0	0	0
Date		21/10/2022	25/10/2022	26/10/2022

Shearing Stage

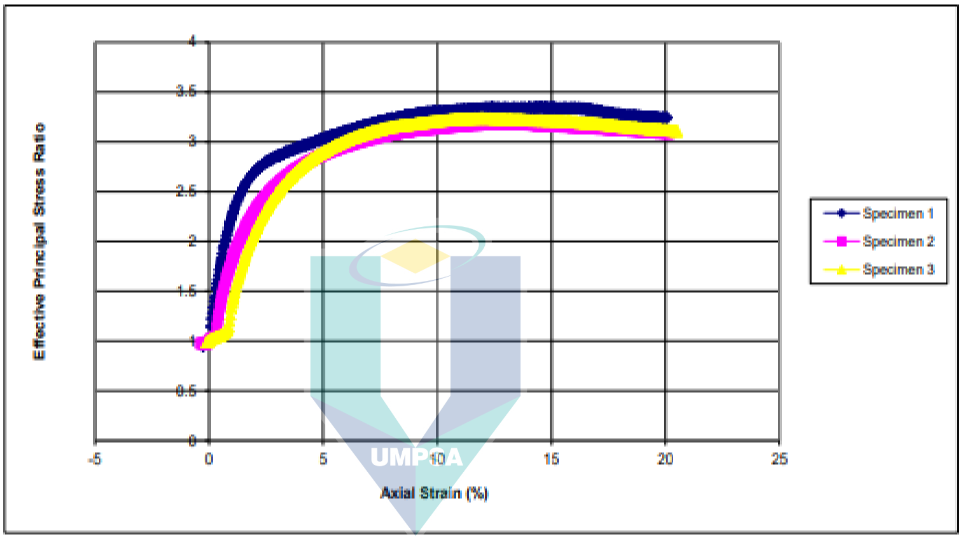

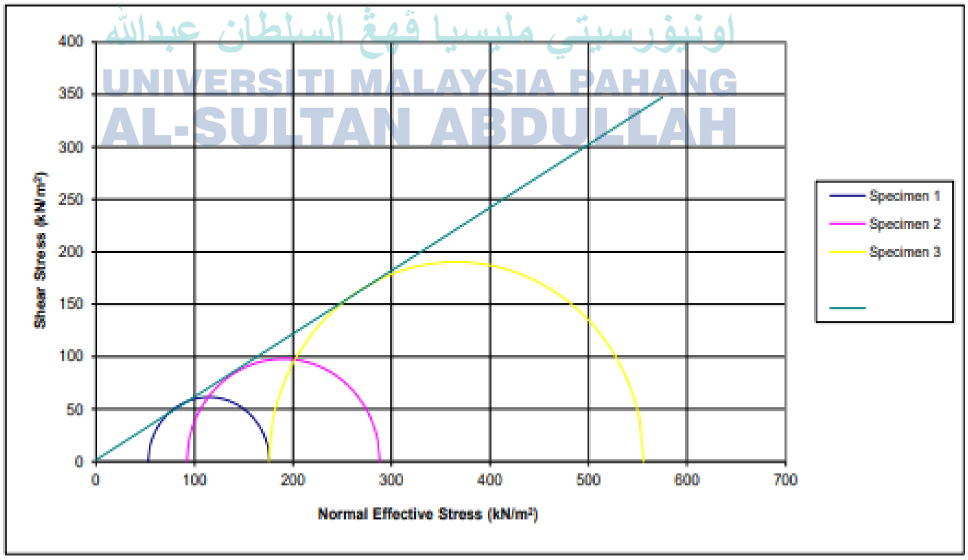

Filename: D:\UMP PhD\CU Test Results\[BH00 Report Final.xlsx]Report

Date: 5/17/2023

Checked by: Date:

Approved by: Date:

Your Company Name Here

Consolidated Undrained Triaxial Compression Test

BS 1377 : Part 8 : 1990

Sample Details

		Specimen 1	Specimen 2	Specimen 3
Job Ref.		0		
Job Location		0		
Borehole		BH00	BH00	BH00
Sample No.		S37	S38	S39
Depth	m	0	0	0
Date		21/10/2022	25/10/2022	26/10/2022

Shearing Stage

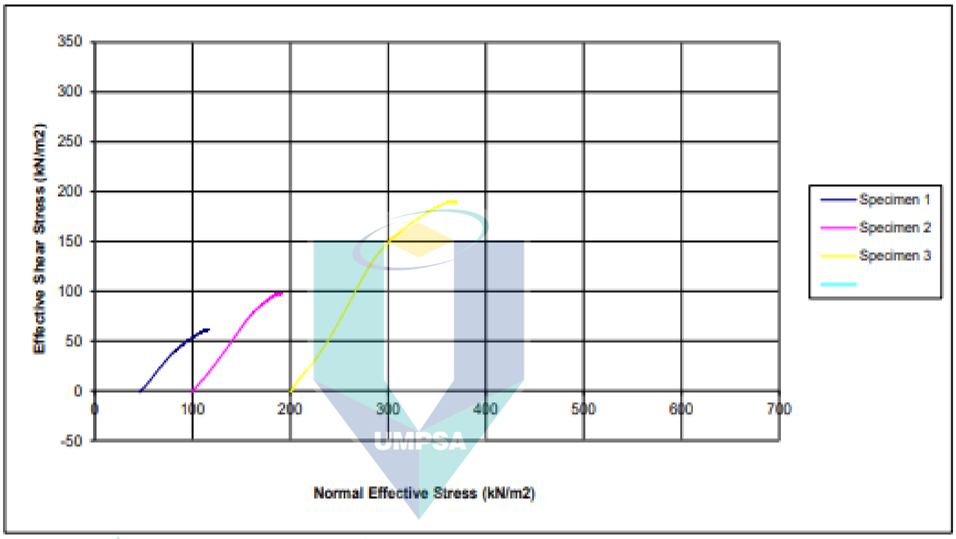

Date:
Date:
Checked by:
Approved by:
Filename: D:\UMP PhD\CU Test Results\[BH00 Report Final.xlsx]Report
Date: 5/17/2023

Your Company Name Here

Consolidated Undrained Triaxial Compression Test

BS 1377 : Part 8 : 1990

Filename: D:\UMP PhD\CU Test Results\[BH01 Report Final.xlsx]Report
Date: 5/17/2023
Checked by:
Date:
Approved by:
Date:

Specimen Details

		Specimen 1	Specimen 2	Specimen 3
Job Ref.				
Job Location				
Borehole		BH01	BH01	BH01
Sample No.		S16	S17	S18
Depth	m		0	0
Date		17/10/2022	18/10/2022	20/10/2022
Disturbed / Undisturbed				

Description of Specimen

Initial Specimen Conditions

		Specimen 1	Specimen 2	Specimen 3
Height	mm	100.00	100.00	100.00
Diameter	mm	50.00	50.00	50.00
Area	mm^2	1963.50	1963.50	1963.50
Volume	cm^3	196.35	196.35	196.35
Mass	g	360.00	360.00	360.00
Dry Mass	g	330.00	330.00	330.00
Density	Mg/m^3	1.83	1.83	1.83
Dry Density	Mg/m^3	1.68	1.68	1.68
Moisture Content	%	9.09	9.09	9.09
Degree of Saturation	%	43.21	43.21	43.21
Specific Gravity (assumed/measured)		2.60	2.60	2.60

Final Specimen Conditions

		Specimen 1	Specimen 2	Specimen 3
Moisture Content	%			
Density	Mg/m^3	0.00	0.00	0.00
Dry Density	Mg/m^3			

Sketch of Failure of the Specimen

Specimen 1 Specimen 2 Specimen 3

Your Company Name Here

Consolidated Undrained Triaxial Compression Test

BS 1377 : Part 8 : 1990

Specimen Details

		Specimen 1	Specimen 2	Specimen 3
Job Ref.			0	
Job Location			0	
Borehole		BH01	BH01	BH01
Sample No.		S16	S17	S18
Depth	m	0	0	0
Date		17/10/2022	18/10/2022	20/10/2022

Test Setup

	Specimen 1	Specimen 2	Specimen 3
Date started			
Date Finished			
Top Drain Used			
Base Drain Used			
Side Drains Used			
Pressure System Number			
Cell Number			

Saturation

		Specimen 1	Specimen 2	Specimen 3
Cell Pressure Incr.	kPa	50.00	50.00	49.90
Back Pressure Incr.	kPa	29.00	41.00	48.00
Differential Pressure	kPa	31.00	20.00	13.00
Final Cell Pressure	kPa	150.00	250.00	450.00
Final Pore Pressure	kPa	115.20	227.60	433.90
Final B Value		0.61	0.83	0.96

Consolidation

		Specimen 1	Specimen 2	Specimen 3
Effective Pressure	kPa	50.00	100.90	201.00
Cell Pressure	kPa	100.00	199.90	400.00
Back Pressure	kPa	50.00	99.00	199.00
Excess Pore Pressure	kPa	-4.20	-2.60	-3.10
Pore Pressure at End	kPa	51.00	99.20	195.90
Consolidated Volume	cm^3	187.16	183.91	180.81
Volumetric Strain		0.015608219	0.0211188	0.02637643
Consolidated Height	mm	98.44	97.89	97.36
Consolidated Area	mm^2	1902.20	1880.56	1859.92
Vol. Compressibility	m^2/MN	0.77014	0.50203	0.33248
Consolidation Coef.	m^2/yr.			

Filename: D:\UMP PhD\CU Test Results\[BH01 Report Final.xlsx]Report
Date: 5/17/2023

Checked by:
Approved by:

Date:
Date:

Your Company Name Here

Consolidated Undrained Triaxial Compression Test

BS 1377 : Part 8 : 1990

Specimen Details

	Specimen 1	Specimen 2	Specimen 3
Job Ref.	0		
Job Location	0		
Borehole	BH01	BH01	BH01
Sample No.	S16	S17	S18
Depth m	0	0	0
Date	17/10/2022	18/10/2022	20/10/2022

Consolidation Stage

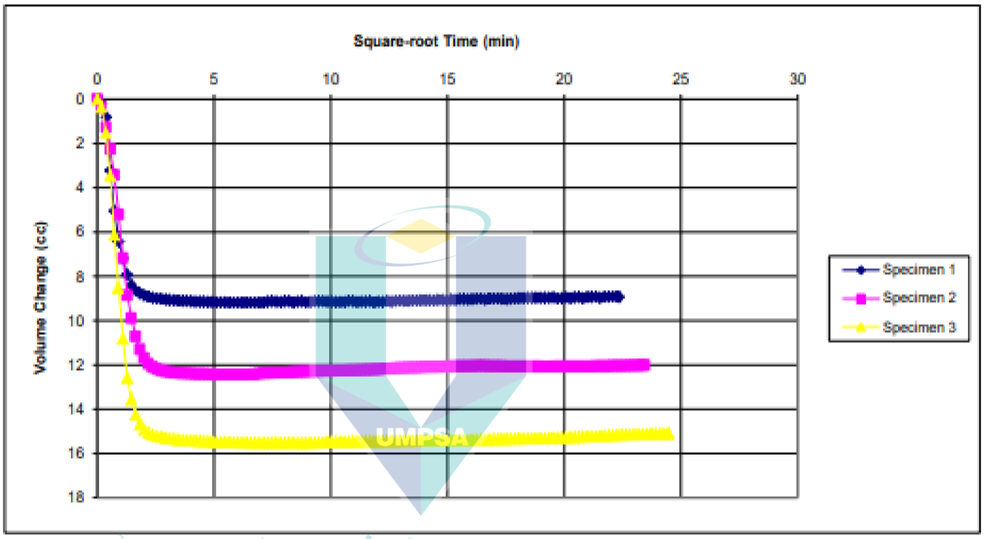

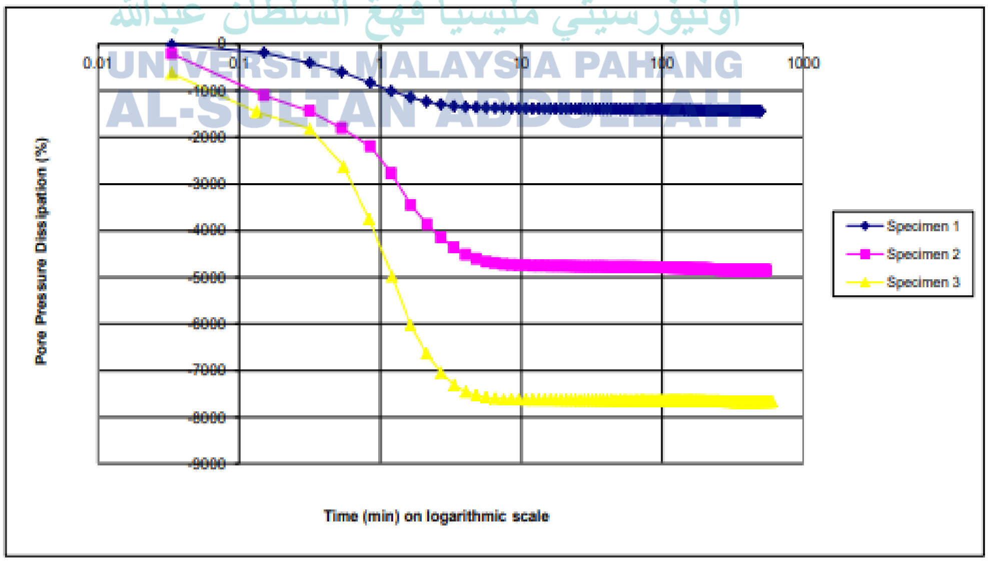

Filename: D:\UMP PhD\CU Test Results\[BH01 Report Final.xlsx]Report
Date: 5/17/2023
Checked by:
Date:
Approved by:
Date:

Your Company Name Here

Consolidated Undrained Triaxial Compression Test

BS 1377 : Part 8 : 1990

Specimen Details

		Specimen 1	Specimen 2	Specimen 3
Job Ref.		0		
Job Location		0		
Borehole		BH01	BH01	BH01
Sample No.		S16	S17	S18
Depth	m	0	0	0
Date		17/10/2022	18/10/2022	20/10/2022

Shearing

		Specimen 1	Specimen 2	Specimen 3
Initial Cell Pressure	kPa	100	199.8	400
Initial Pore Pressure	kPa	51.1	99.4	196.1
Rate of Strain	%/hour	60.00012	60.00012	60.00012
Max Deviator Stress				
Axial Strain		18.957	19.270	19.277
Axial Stress	kPa	148.69	271.31	429.24
Cor. Deviator stress	kPa	148.69	271.31	429.24
Effective Major Stress	kPa	210.79	387.81	621.84
Effective Minor Stress	kPa	62.10	116.50	192.60
Effective Stress Ratio		3.394	3.329	3.229
s'	kPa	136.45	252.15	407.22
t'	kPa	74.35	135.65	214.62
Shear Resistance Angle	degs	31.17	31.17	31.17
Cohesion c'	kPa	4.96	4.96	4.96
Max Effective Priciple Stress Ratio				
Axial Strain		11.406	12.937	13.491
Axial Stress	kPa	136.93	256.02	408.84
Cor. Deviator stress	kPa	136.93	256.02	408.84
Effective Major Stress	kPa	191.13	361.32	586.54
Effective Minor Stress	kPa	54.20	105.30	177.70
Effective Stress Ratio		3.526	3.431	3.301
s'	kPa	122.66	233.31	382.12
t'	kPa	68.46	128.01	204.42

Date:
Date:
Checked by:
Approved by:
Filename: D:\UMP PhD\CU Test Results\[BH01 Report Final.xlsx]Report
Date: 5/17/2023

Filename: D:\UMP PhD\CU Test Results\[BH01 Report Final.xlsx]Report
Date: 5/17/2023
Checked by: Date:
Approved by: Date:

Your Company Name Here

Consolidated Undrained Triaxial Compression Test

BS 1377 : Part 8 : 1990

Specimen Details

		Specimen 1	Specimen 2	Specimen 3
Job Ref.			0	
Job Location			0	
Borehole		BH01	BH01	BH01
Sample No.		S16	S17	S18
Depth	m	0	0	0
Date		17/10/2022	18/10/2022	20/10/2022

Shearing Stage

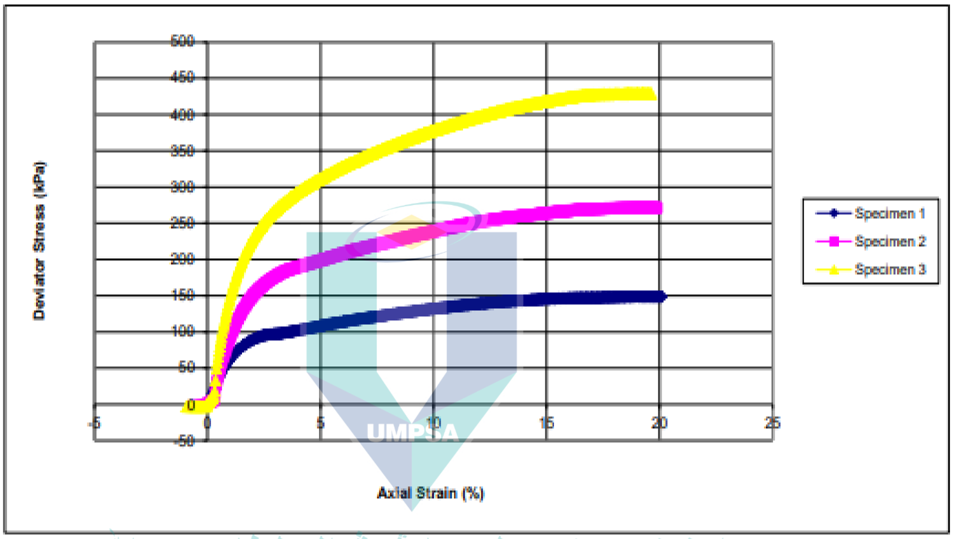

Your Company Name Here

Consolidated Undrained Triaxial Compression Test

BS 1377 : Part 8 : 1990

Sample Details

		Specimen 1	Specimen 2	Specimen 3
Job Ref.		0		
Job Location		0		
Borehole		BH01	BH01	BH01
Sample No.		S16	S17	S18
Depth	m	0	0	0
Date		17/10/2022	18/10/2022	20/10/2022

Shearing Stage

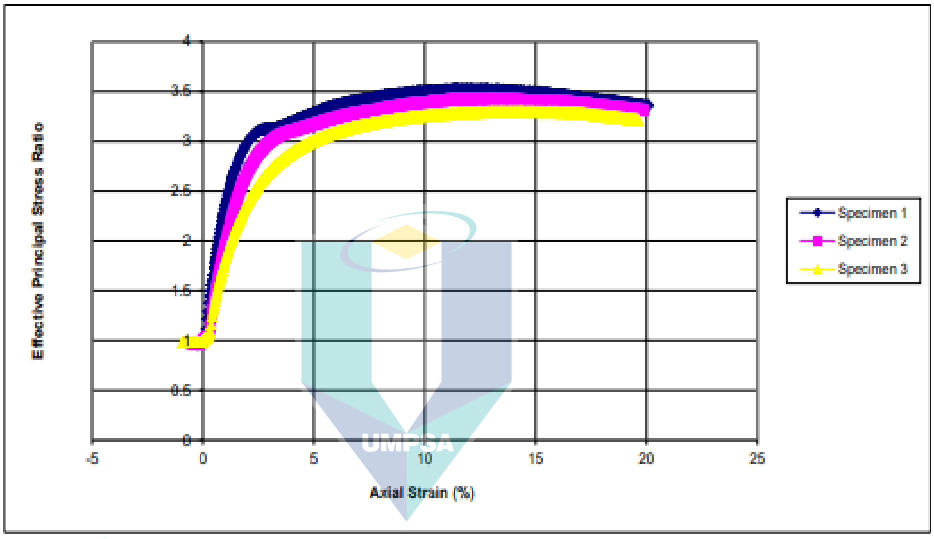

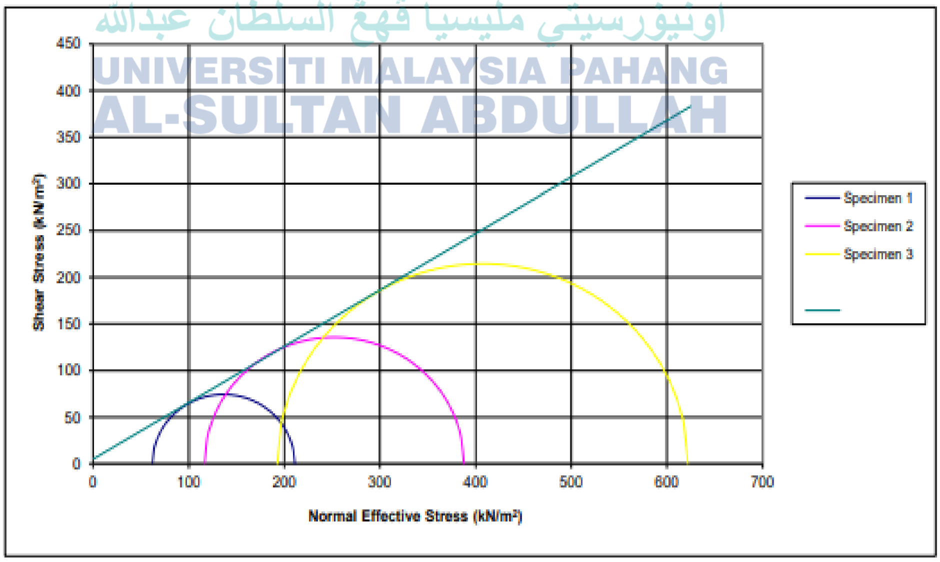

Date:
Date:
Checked by:
Approved by:
Filename: D:\UMP PhD\CU Test Results\[BH01 Report Final.xlsx]Report
Date: 5/17/2023

Your Company Name Here

Consolidated Undrained Triaxial Compression Test

BS 1377 : Part 8 : 1990

Sample Details

	Specimen 1	Specimen 2	Specimen 3
Job Ref.	0		
Job Location	0		
Borehole	BH01	BH01	BH01
Sample No.	S16	S17	S18
Depth m	0	0	0
Date	17/10/2022	18/10/2022	20/10/2022

Shearing Stage

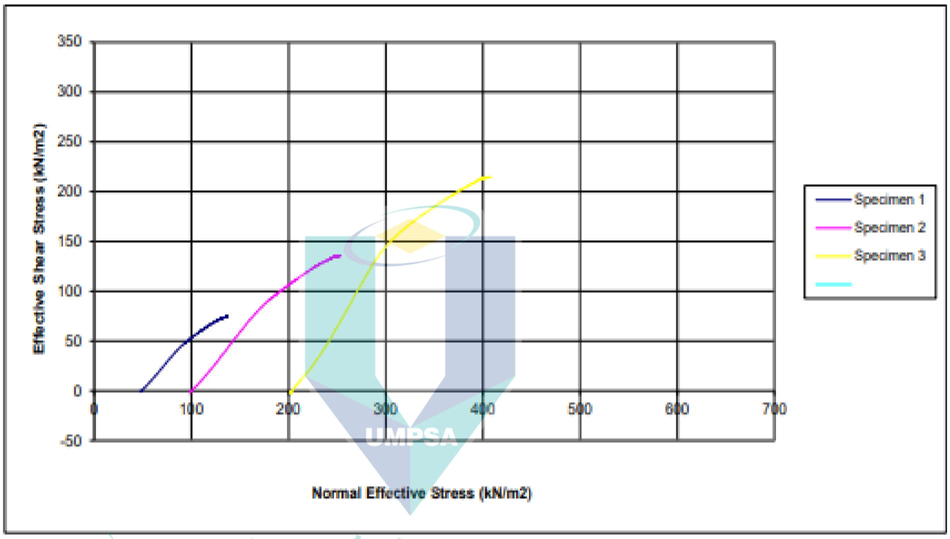

Date :
Date :
Checked by :
Approved by :
Filename: D:\UMP PhD\CU Test Results\[BH01 Report Final.xlsx]Report
Date: 5/17/2023

Your Company Name Here

Consolidated Undrained Triaxial Compression Test

BS 1377 : Part 8 : 1990

Checked by: Date:
Approved by: Date:
Filename: D:\UMP PhD\CU Test Results\[BH02 Report Final.xlsx]Report
Date: 5/17/2023

Specimen Details

		Specimen 1	Specimen 2	Specimen 3
Job Ref.				
Job Location				
Borehole		BH02	BH02	BH 02
Sample No.		S07	S08	S 09
Depth	m		0	0
Date		11.10.2022	10/12/2022	14/10/2022
Disturbed / Undisturbed				

Description of Specimen

Initial Specimen Conditions

		Specimen 1	Specimen 2	Specimen 3
Height	mm	100.00	100.00	100.00
Diameter	mm	50.00	50.00	50.00
Area	mm^2	1963.50	1963.50	1963.50
Volume	cm^3	196.35	196.35	196.35
Mass	g	360.00	360.00	360.00
Dry Mass	g	330.00	330.00	330.00
Density	Mg/m^3	1.83	1.83	1.83
Dry Density	Mg/m^3	1.68	1.68	1.68
Moisture Content	%	9.09	9.09	9.09
Degree of Saturation	%	43.21	43.21	43.21
Specific Gravity (assumed/measured)		2.60	2.60	2.60

Final Specimen Conditions

		Specimen 1	Specimen 2	Specimen 3
Moisture Content	%			
Density	Mg/m^3	0.00	0.00	0.00
Dry Density	Mg/m^3			

Sketch of Failure of the Specimen

Specimen 1 Specimen 2 Specimen 3

Your Company Name Here

Consolidated Undrained Triaxial Compression Test

BS 1377 : Part 8 : 1990

Specimen Details

		Specimen 1	Specimen 2	Specimen 3
Job Ref.			0	
Job Location			0	
Borehole		BH02	BH02	BH 02
Sample No.		S07	S08	S 09
Depth	m	0	0	0
Date		11.10.2022	10/12/2022	14/10/2022

Test Setup

	Specimen 1	Specimen 2	Specimen 3
Date started			
Date Finished			
Top Drain Used			
Base Drain Used			
Side Drains Used			
Pressure System Number			
Cell Number			

Saturation

		Specimen 1	Specimen 2	Specimen 3
Cell Pressure Incr.	kPa	50.00	50.00	50.00
Back Pressure Incr.	kPa	0.00	38.00	47.00
Differential Pressure	kPa	60.00	23.00	14.00
Final Cell Pressure	kPa	150.00	250.00	430.00
Final Pore Pressure	kPa	85.30	224.90	413.60
Final B Value		0.29	0.77	0.94

Consolidation

		Specimen 1	Specimen 2	Specimen 3
Effective Pressure	kPa	51.00	101.00	190.90
Cell Pressure	kPa	100.00	200.00	379.90
Back Pressure	kPa	49.00	99.00	189.00
Excess Pore Pressure	kPa	-3.30	-2.80	-3.30
Pore Pressure at End	kPa	50.90	95.90	187.30
Consolidated Volume	cm^3	191.96	184.92	184.00
Volumetric Strain		0.007450998	0.019407605	0.020967709
Consolidated Height	mm	99.25	98.06	97.90
Consolidated Area	mm^2	1934.24	1887.28	1881.16
Vol. Compressibility	m^2/MN	0.72575	0.46467	0.28032
Consolidation Coef.	m^2/yr.			

Date:
Date:
Checked by:
Approved by:
Filename: D:\UMP PhD\CU Test Results\[BH02 Report Final.xlsx]Report
Date: 5/17/2023

Your Company Name Here

Consolidated Undrained Triaxial Compression Test

BS 1377 : Part 8 : 1990

Specimen Details

		Specimen 1	Specimen 2	Specimen 3
Job Ref.		0		
Job Location		0		
Borehole		BH02	BH02	BH 02
Sample No.		S07	S08	S 09
Depth	m	0	0	0
Date		11.10.2022	10/12/2022	14/10/2022

Consolidation Stage

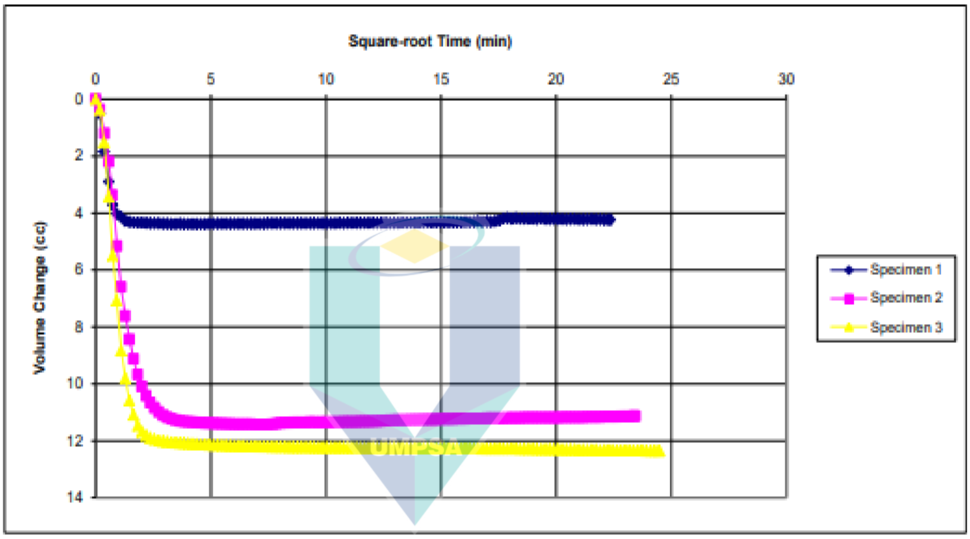

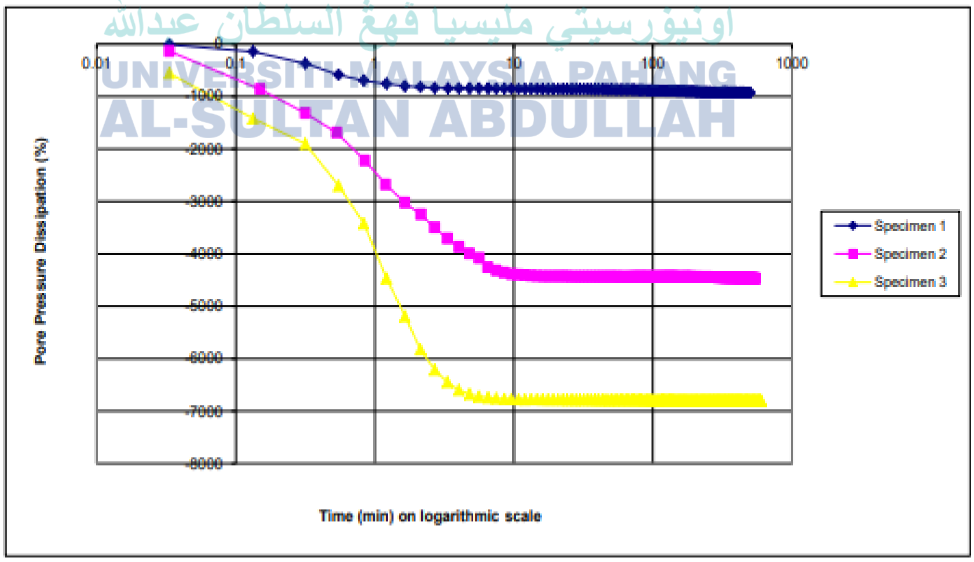

Date:
Date:
Checked by:
Approved by:
Filename: D:\UMP PhD\CU Test Results\[BH02 Report Final.xlsx]Report
Date: 5/17/2023

Your Company Name Here

Consolidated Undrained Triaxial Compression Test

BS 1377 : Part 8 : 1990

		Specimen 1	Specimen 2	Specimen 3
Specimen Details				
Job Ref.		0		
Job Location		0		
Borehole		BH02	BH02	BH 02
Sample No.		S07	S08	S 09
Depth	m	0	0	0
Date		11.10.2022	10/12/2022	14/10/2022
Shearing				
Initial Cell Pressure	kPa	100	200	379.9
Initial Pore Pressure	kPa	51	96	187.5
Rate of Strain	%/hour	60.00012	60.00024	60.00012
Max Deviator Stress				
Axial Strain		17.351	16.949	20.120
Axial Stress	kPa	164.08	266.67	435.25
Cor. Deviator stress	kPa	164.08	266.67	435.25
Effective Major Stress	kPa	233.18	384.27	637.65
Effective Minor Stress	kPa	69.10	117.60	202.40
Effective Stress Ratio		3.375	3.268	3.150
s'	kPa	151.14	250.94	420.02
t'	kPa	82.04	133.34	217.62
Shear Resistance Angle	degs	30.24	30.24	30.24
Cohesion c'	kPa	7.32	7.32	7.32
Max Effective Priciple Stress Ratio				
Axial Strain		8.485	9.827	11.268
Axial Stress	kPa	147.14	249.89	404.24
Cor. Deviator stress	kPa	147.14	249.89	404.24
Effective Major Stress	kPa	206.04	356.39	583.74
Effective Minor Stress	kPa	58.90	106.50	179.50
Effective Stress Ratio		3.498	3.346	3.252
s'	kPa	132.47	231.44	381.62
t'	kPa	73.57	124.94	202.12

Date:
Date:
Checked by:
Approved by:
Filename: D:\UMP PhD\CU Test Results\[BH02 Report Final.xlsx]Report
Date: 5/17/2023

Your Company Name Here

Consolidated Undrained Triaxial Compression Test

BS 1377 : Part 8 : 1990

Specimen Details

		Specimen 1	Specimen 2	Specimen 3
Job Ref.		0		
Job Location		0		
Borehole		BH02	BH02	BH 02
Sample No.		S07	S08	S 09
Depth	m	0	0	0
Date		11.10.2022	10/12/2022	14/10/2022

Shearing Stage

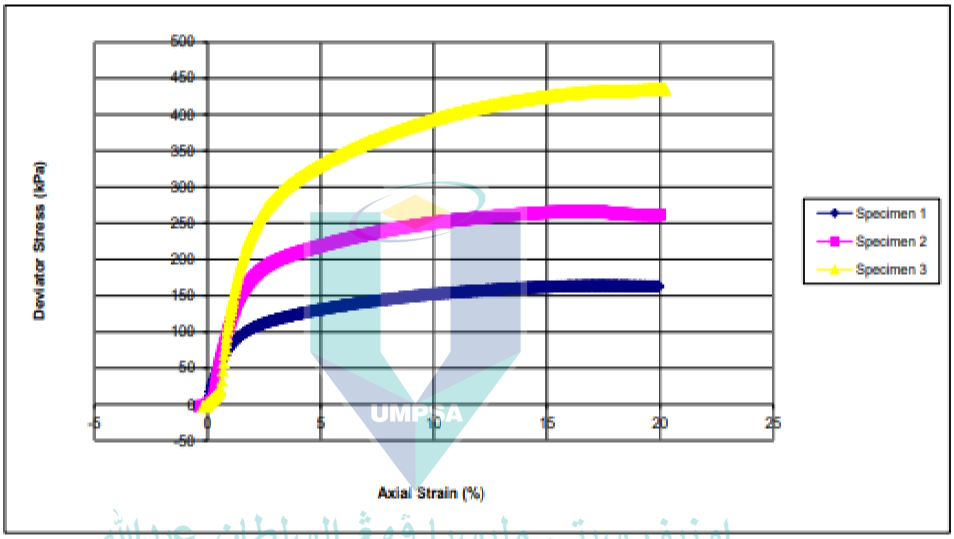

Date:
Date:
Checked by:
Approved by:
Filename: D:\UMP PhD\CU Test Results\[BH02 Report Final.xlsx]Report
Date: 5/17/2023

Your Company Name Here

Consolidated Undrained Triaxial Compression Test

BS 1377 : Part 8 : 1990

Date:
Date:
Checked by:
Approved by:
Filename: D:\UMP PhD\CU Test Results\[BH02 Report Final.xlsx]Report
Date: 5/17/2023

Sample Details

		Specimen 1	Specimen 2	Specimen 3
Job Ref.			0	
Job Location			0	
Borehole		BH02	BH02	BH 02
Sample No.		S07	S08	S 09
Depth	m	0	0	0
Date		11.10.2022	10/12/2022	14/10/2022

Shearing Stage

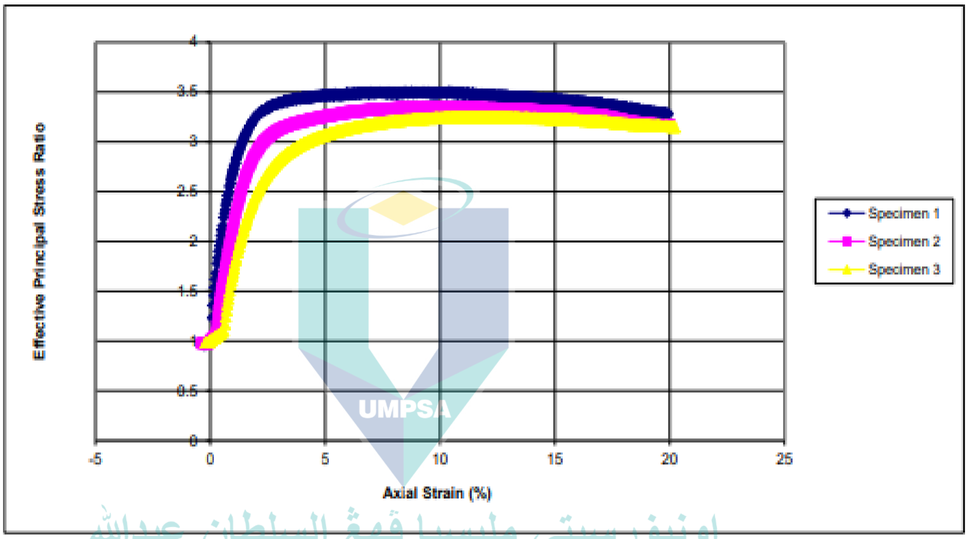

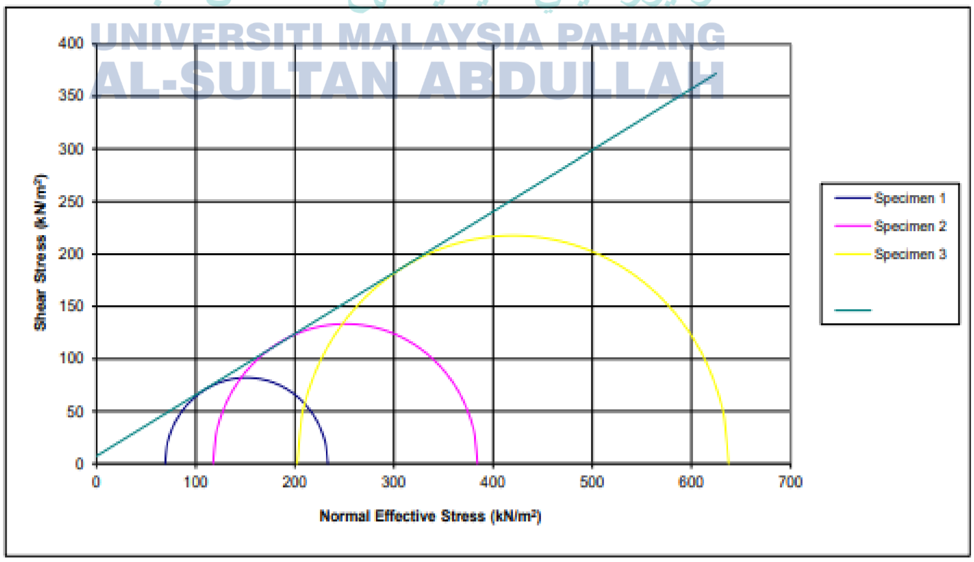

Your Company Name Here

Consolidated Undrained Triaxial Compression Test

BS 1377 : Part 8 : 1990

Sample Details

		Specimen 1	Specimen 2	Specimen 3
Job Ref.		0		
Job Location		0		
Borehole		BH02	BH02	BH 02
Sample No.		S07	S08	S 09
Depth	m	0	0	0
Date		11.10.2022	10/12/2022	14/10/2022

Shearing Stage

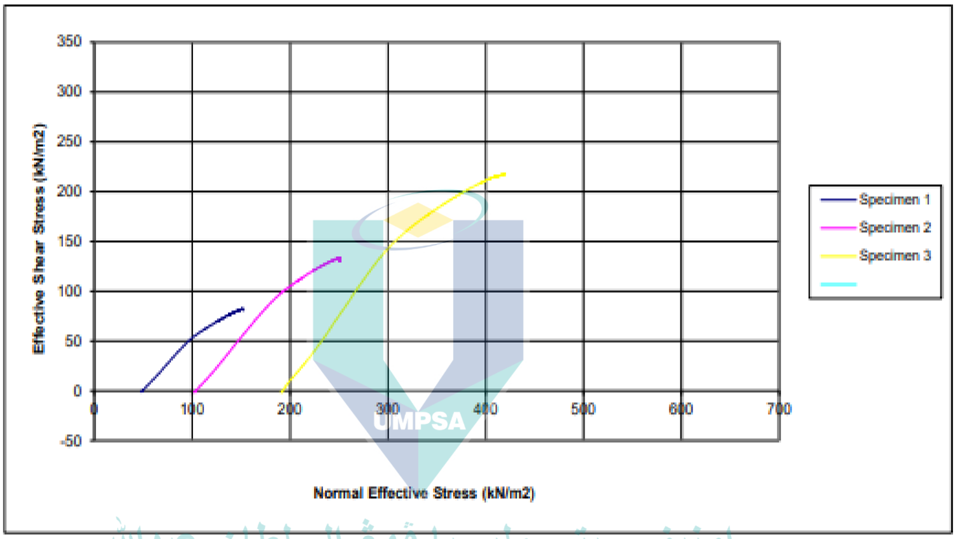

Date:
Date:
Checked by:
Approved by:
Filename: D:\UMP PhD\CU Test Results\[BH02 Report Final.xlsx]Report
Date: 5/17/2023

Date:
Date:
Checked by:
Approved by:
Filename: D:\UMP PhD\CU Test Results\[BH09 Report Final.xlsx]Report
Date: 5/17/2023

Your Company Name Here

Consolidated Undrained Triaxial Compression Test

BS 1377 : Part 8 : 1990

Specimen Details

		Specimen 1	Specimen 2	Specimen 3
Job Ref.				
Job Location				
Borehole		BH 09	BH 09	BH 09
Sample No.		S 25	S 26	S 27
Depth	m		0	0
Date		28/10/2022	11/1/2022	11/2/2022
Disturbed / Undisturbed				

Description of Specimen

Initial Specimen Conditions

		Specimen 1	Specimen 2	Specimen 3
Height	mm	100.00	100.00	100.00
Diameter	mm	50.00	50.00	50.00
Area	mm^2	1963.50	1963.50	1963.50
Volume	cm^3	196.35	196.35	196.35
Mass	g	360.00	360.00	360.00
Dry Mass	g	330.00	330.00	330.00
Density	Mg/m^3	1.83	1.83	1.83
Dry Density	Mg/m^3	1.68	1.68	1.68
Moisture Content	%	9.09	9.09	9.09
Degree of Saturation	%	43.21	43.21	43.21
Specific Gravity (assumed/measured)		2.60	2.60	2.60

Final Specimen Conditions

		Specimen 1	Specimen 2	Specimen 3
Moisture Content	%			
Density	Mg/m^3	0.00	0.00	0.00
Dry Density	Mg/m^3			

Sketch of Failure of the Specimen

Specimen 1 Specimen 2 Specimen 3

Your Company Name Here

Consolidated Undrained Triaxial Compression Test

BS 1377 : Part 8 : 1990

Specimen Details

		Specimen 1	Specimen 2	Specimen 3
Job Ref.		0		
Job Location		0		
Borehole		BH 09	BH 09	BH 09
Sample No.		S 25	S 26	S 27
Depth	m	0	0	0
Date		28/10/2022	11/1/2022	11/2/2022

Test Setup

	Specimen 1	Specimen 2	Specimen 3
Date started			
Date Finished			
Top Drain Used			
Base Drain Used			
Side Drains Used			
Pressure System Number			
Cell Number			

Saturation

		Specimen 1	Specimen 2	Specimen 3
Cell Pressure Incr.	kPa	50.00	49.70	50.00
Back Pressure Incr.	kPa	36.00	44.00	49.00
Differential Pressure	kPa	24.00	16.80	12.00
Final Cell Pressure	kPa	150.00	249.80	450.00
Final Pore Pressure	kPa	121.50	230.20	434.90
Final B Value		0.71	0.89	0.98

Consolidation

		Specimen 1	Specimen 2	Specimen 3
Effective Pressure	kPa	50.90	101.20	201.10
Cell Pressure	kPa	99.90	200.20	400.10
Back Pressure	kPa	49.00	99.00	199.00
Excess Pore Pressure	kPa	-3.10	-2.40	-3.10
Pore Pressure at End	kPa	49.60	99.20	196.60
Consolidated Volume	cm^3	187.18	183.57	181.23
Volumetric Strain		0.01557084	0.021701095	0.025661719
Consolidated Height	mm	98.44	97.83	97.43
Consolidated Area	mm^2	1902.35	1878.28	1862.72
Vol. Compressibility	m^2/MN	0.67406	0.50312	0.32306
Consolidation Coef.	m^2/yr.			

Checked by: Date:
Approved by: Date:
Filename: D:\UMP PhD\CU Test Results\[BH09 Report Final.xlsx]Report
Date: 5/17/2023

Your Company Name Here

Consolidated Undrained Triaxial Compression Test

BS 1377 : Part 8 : 1990

Specimen Details

		Specimen 1	Specimen 2	Specimen 3
Job Ref.		0		
Job Location		0		
Borehole		BH 09	BH 09	BH 09
Sample No.		S 25	S 26	S 27
Depth	m	0	0	0
Date		28/10/2022	11/1/2022	11/2/2022

Consolidation Stage

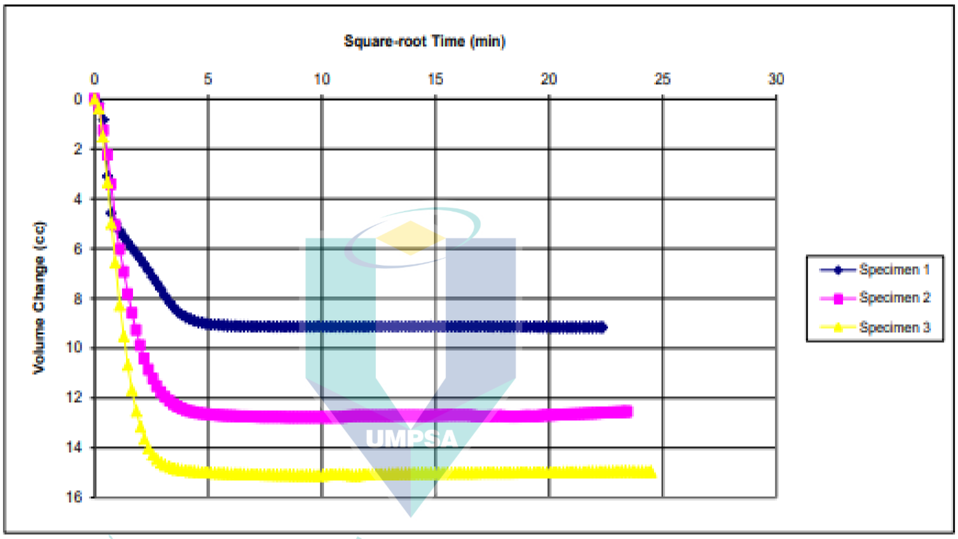

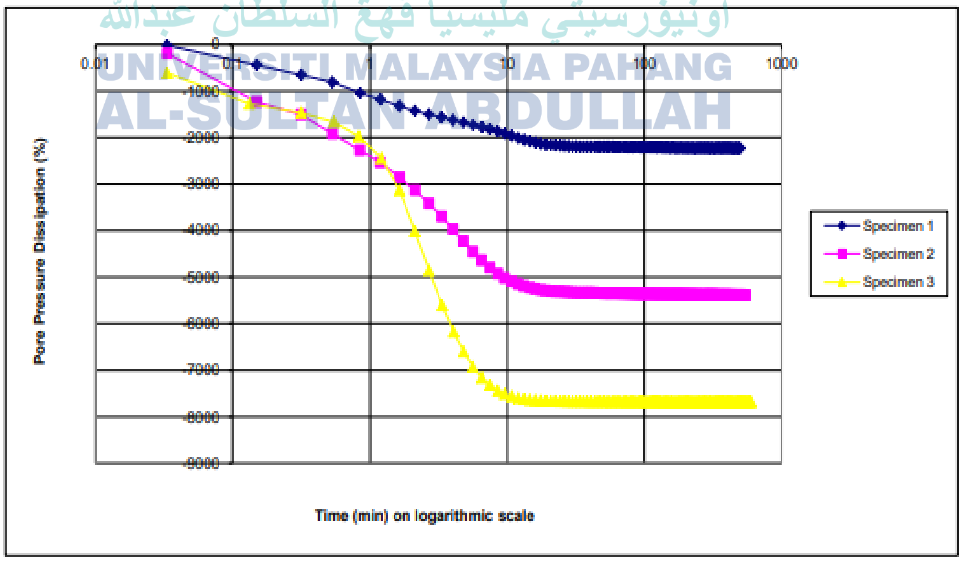

Date:
Date:
Checked by:
Approved by:
Filename: D:\UMP PhD\CU Test Results\[BH09 Report Final.xlsx]Report
Date: 5/17/2023

Your Company Name Here

Consolidated Undrained Triaxial Compression Test

BS 1377 : Part 8 : 1990

		Specimen 1	Specimen 2	Specimen 3
Specimen Details				
Job Ref.			0	
Job Location			0	
Borehole		BH 09	BH 09	BH 09
Sample No.		S 25	S 26	S 27
Depth	m	0	0	0
Date		28/10/2022	11/1/2022	11/2/2022
Shearing				
Initial Cell Pressure	kPa	100.1	200	400
Initial Pore Pressure	kPa	49.8	99.3	197
Rate of Strain	%/hour	60	60.00012	60.00012
Max Deviator Stress				
Axial Strain		19.779	19.440	19.952
Axial Stress	kPa	143.80	231.18	367.00
Cor. Deviator stress	kPa	143.80	231.18	367.00
Effective Major Stress	kPa	210.60	337.78	553.40
Effective Minor Stress	kPa	66.80	106.60	186.40
Effective Stress Ratio		3.153	3.169	2.969
s'	kPa	138.70	222.19	369.90
t'	kPa	71.90	115.59	183.50
Shear Resistance Angle	degs	28.69	28.69	28.69
Cohesion c'	kPa	7.66	7.66	7.66
Max Effective Priciple Stress Ratio				
Axial Strain		8.318	12.660	11.861
Axial Stress	kPa	128.68	220.41	344.47
Cor. Deviator stress	kPa	128.68	220.41	344.47
Effective Major Stress	kPa	183.08	318.71	512.67
Effective Minor Stress	kPa	54.40	98.30	168.20
Effective Stress Ratio		3.365	3.242	3.048
s'	kPa	118.74	208.51	340.43
t'	kPa	64.34	110.21	172.23

Checked by: Date:
Approved by: Date:
Filename: D:\UMP PhD\CU Test Results\[BH09 Report Final.xlsx]Report
Date: 5/17/2023

Your Company Name Here

Consolidated Undrained Triaxial Compression Test

BS 1377 : Part 8 : 1990

Specimen Details

		Specimen 1	Specimen 2	Specimen 3
Job Ref.		0		
Job Location		0		
Borehole		BH 09	BH 09	BH 09
Sample No.		S 25	S 26	S 27
Depth	m	0	0	0
Date		28/10/2022	11/1/2022	11/2/2022

Shearing Stage

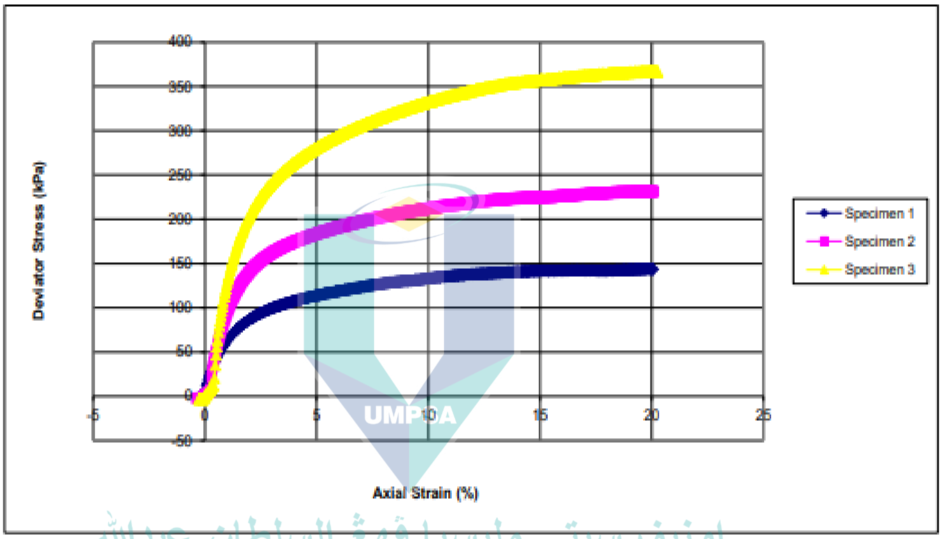

Date:
Date:
Checked by:
Approved by:
Filename: D:\UMP PhD\CU Test Results\[BH09 Report Final.xlsx]Report
Date: 5/17/2023

Your Company Name Here

Consolidated Undrained Triaxial Compression Test
BS 1377 : Part 8 : 1990

Sample Details

		Specimen 1	Specimen 2	Specimen 3
Job Ref.		0		
Job Location		0		
Borehole		BH 09	BH 09	BH 09
Sample No.		S 25	S 26	S 27
Depth	m	0	0	0
Date		28/10/2022	11/1/2022	11/2/2022

Shearing Stage

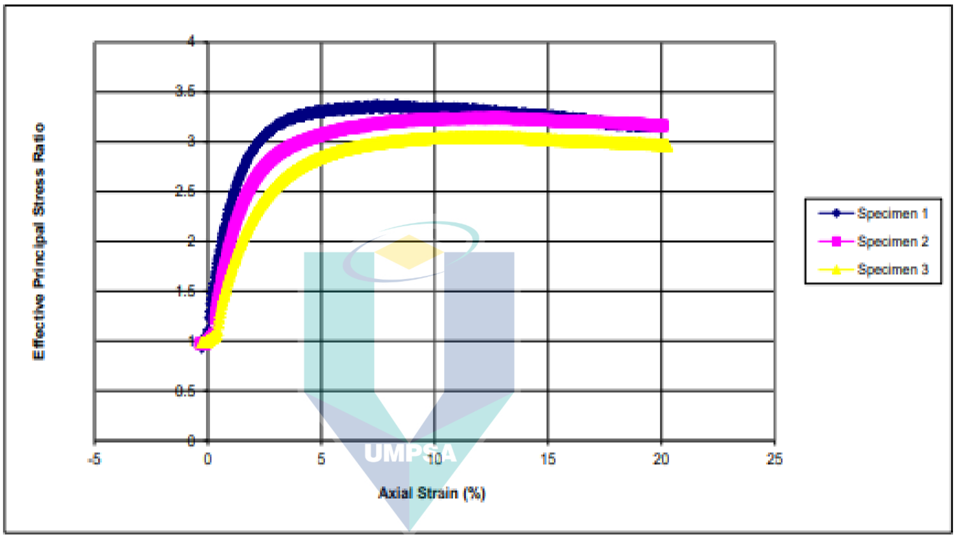

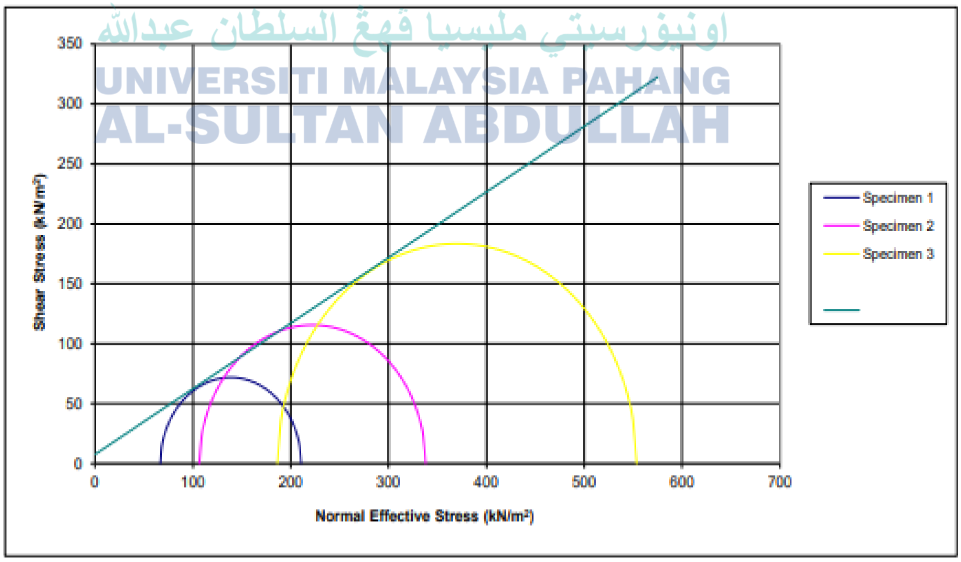

Filename: D:\UMP PhD\CU Test Results\[BH09 Report Final.xlsx]Report
Date: 5/17/2023
Checked by:
Date:
Approved by:
Date:

Your Company Name Here

Consolidated Undrained Triaxial Compression Test

BS 1377 : Part 8 : 1990

Sample Details

		Specimen 1	Specimen 2	Specimen 3
Job Ref.		0		
Job Location		0		
Borehole		BH 09	BH 09	BH 09
Sample No.		S 25	S 26	S 27
Depth	m	0	0	0
Date		28/10/2022	11/1/2022	11/2/2022

Shearing Stage

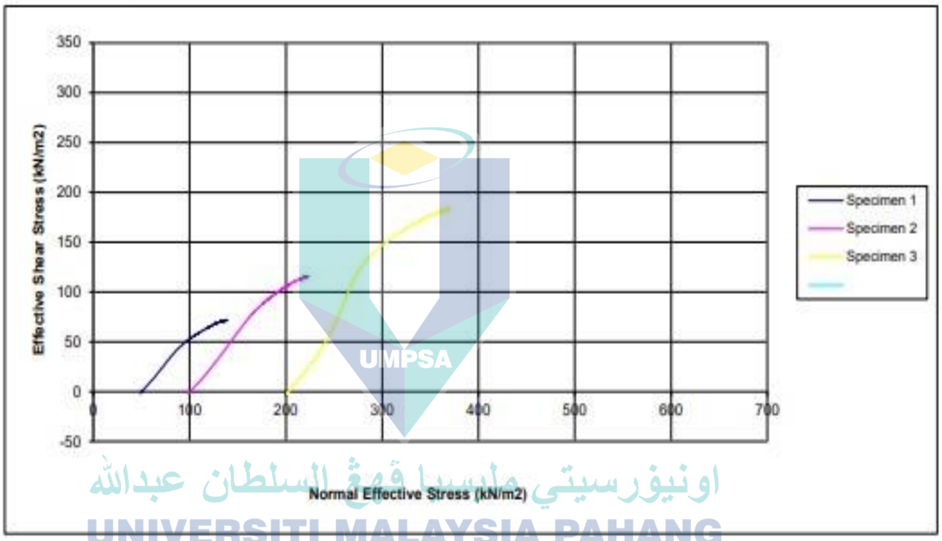

Date:
Date:
Checked by:
Approved by:
Filename: D:\UMP PhD\CU Test Results\[BH09 Report Final.xlsx]Report
Date: 5/17/2023